Compatibilisation of blends of incompatible mesogens

by

Antoine J. Herbaut

UNIVERSITY OF BIRMINGHAM

A thesis submitted to

The University of Birmingham

For a degree of

DOCTOR OF PHILOSOPHY

School of Chemistry

College of Engineering and Physical Sciences

University of Birmingham

September 2016

Abstract

Controlling the morphology of blends of materials is crucial for organic optoelectronic devices. However, the blends are often made of incompatible materials, resulting in an undesirable macrophase separation.

This thesis focusses on the addition of a third component into the immiscible blend of small molecules to control their morphology.

After introducing the concept of organic solar cells and the liquid crystalline state of matter, the available methods to control the morphology of blends in these two fields will be reviewed.

Model compounds based on triphenylene derivatives was first studied. After preparing two incompatible triphenylenes based on the immiscibility of their pendent chains, the introduction of tailor-made compatibilisers was shown to have a tremendous effect on the morphology by suppressing the macrophase separation between the incompatible materials to a reproducible micro-segregation.

Our research was then focussed on incompatible functional materials showing high promises for solar cell application: the hexa-*peri*-hexabenzocoronene and the perylene diimide family. By applying the same concept as in the triphenylene derivatives, the incompatibility between hexa-*peri*-hexabenzocoronene and perylene diimide was introduced by the immiscibility of their pendent chains. The synthesis of a tailor-made functional dyad was successfully carried out and preliminary results of its effect on the compatibilisation of hexa-*peri*-hexabenzocoronene and perylene diimide was investigated.

Acknowledgements

Firstly, I would like to thank my supervisor Dr Etienne Baranoff for giving me the opportunity to join his group for my PhD and for his help and support throughout this exciting project.

I am grateful to all the analytical services for their support and assistance, Dr Neil Spencer and Dr Cécile Le Duff for NMR, Dr. Chi Tsang and Peter Ashton for mass spec. I am very grateful to the University of Leeds and University College London for their help in doing high temperature NMR. I am also taking the opportunity to thank the EPSRC for the financial support and the School of Chemistry for the facilities.

I would like to thank all the Baranoff group, past and present. A special thank goes to Yanouk, François and Tom for all the fun we had in and out the lab. The PhD would not had been the same without your friendship. Chiara, thank you for taking your precious time to help for the AFM! I am not forgetting to thank all my friends in France.

I am especially grateful to Cynthia and Fatima for spending time reading and correcting drafts of my thesis. The writing up would have been even more difficult without your precious support, advice and corrections! Cynthia thanks for our discussions that always cheered me up.

Special thanks must go to my family; thanks to my parents and my sister for their support over the years.

Table of contents

Abbreviations

A	Acceptor
AFM	Atomic force microscopy
AP	Atmospheric pressure chemical ionisation
aq.	Aqueous
BHJ	Bulk heterojunction
br	Broad
°C	Degrees Celsius
cat.	Catalytic
conc.	Concentrated
d	Doublet
D	Donor
DCC	*N,N*'-Dicyclohexylcarbodiimide
DCM	Dichloromethane
DDQ	2,3-Dichloro-5,6-dicyanobenzoquinone
DIO	1,8-Diiodooctane
DMAP	4-dimethylaminopyridine
DME	1,2-dimethoxyethane
DMF	*N,N*-dimethylformamide
DMSO	Dimethylsulfoxide
DSC	Differential scanning calorimetry

eq.	Equivalent
ES	Electrospray
EtOAc	Ethyl acetate
EtOH	Ethanol
FGI	Functional group interconversion
FRET	Förster resonance energy transfer
g	gram(s)
h	hour(s)
HOMO	Highest occupied molecular orbital
HPLC	High-performance liquid chromatography
HRMS	High resolution mass spectrometry
Hz	Hertz
i-Pr	Isopropoxy
IR	Infrared spectroscopy
ITO	Indium tin oxide
J	Coupling constant (in Hz)
L	Litre
LESA	Liquid extraction sample analysis
LUMO	Lowest unoccupied molecular orbital
m	Multiplet
M	Molar concentration
MALDI	Matrix assisted laser desorption

MeOH	Methanol
Mesyl, Ms	Methanesulfonyl
min	Minute(s)
mol	Mole(s)
m.p.	Melting point (°C)
MS	Mass spectrometry
m/z	mass/charge
NMR	Nuclear magnetic resonance
NPhth	Phthalimido
OSC	Organic solar cell
P3HT	Poly-3-hexylthiophene
PCBM	[6,6]-Phenyl-C_{61}-butyric acid methyl ester
PCE	Power conversion efficiency
POM	Polarised optical microscopy
ppm	Part(s) per million
PTCDA	Perylene-3,4-9,10-tetracarboxylic dianhydride
PPV	Polyphenylenevinylene
rt	Room temperature
s	Singlet
SEM	Scanning electron microscopy
SVA	Solvent vapour annealing
t	Triplet

T	Temperature
THF	Tetrahydrofuran
TLC	Thin layer chromatography
TMS	Trimethylsilyl
Tosyl, Ts	4-toluenesulfonyl
UV	Ultraviolet
w	weak
Å	Ångström
δ	Chemical shift
ε	Molar extinction coefficient ($M^{-1}.cm^{-1}$)
λ	Wavelength (nm)
µ	Micro

Chapter 1:

Introduction

1.1 Optoelectronics – General background

Optoelectronics is a field of research and technology than covers all electronic devices based on light interaction. Solar cells, which convert solar energy to an electric current and light emitting diodes (LED) are amongst the most known and widely used optoelectronics in commercial applications.

The industrial applications of optoelectronics rely mostly on inorganic semiconductors, such as silicon. However, high manufacturing costs are required to obtain high efficiency devices. Moreover, the difficulty to build devices on flexible substrates limits their wide application.

A growing interest in organic components for optoelectronic application has emerged in the past decades. The large database of organic semi-conductors, their generally easier purification and the promise of low processing costs have attracted both academics and industrials. Typical examples of commercial organic based optoelectronics devices are OLEDs. OLEDs are used in displays for mobile phones or large screen TVs.

Solar cells are particular devices of interest. Due to increasing energy consumption and the environmental issues encountered with fossil fuels, obtaining renewable sources of energy is one of the biggest challenges of the 21st century. Among all the available technologies, solar cells are of particular interest. Indeed, the sun is a clean, unlimited and abundant source of energy. Although advances have been made in this field, solar photovoltaics only represented 0.3% of the global electricity production in 2015, while non-renewable (including fossil fuels and nuclear power) still represents 80%.[1]

1.2 Organic solar cells

Solar cells are optoelectronic devices which convert solar radiation to an electric current. They are usually composed of a photo active layer sandwiched between two electrodes. A short history of solar cell technology, with an emphasis on the promising advancements of organic solar cells will be presented. The next section will focus solely on the architecture of the active layer.

1.2.1 History of solar cells

In 1839 A. E. Becquerel was the first to report on the photovoltaic effect, where an electric current is generated when a device is illuminated – the example being an electrolytic cell containing silver chloride between two metal electrodes.[2] This observation has been the basis of all devices generating energy from solar radiation.

While observations of photovoltaic currents in inorganic materials such as selenium have been published since the late 19th century,[3,4] the first inorganic solar cell was built by Bell Laboratories in 1954 from silicon.[5] Silicon-based solar cells, also called first generation, are still largely used for commercial applications due to their high efficiencies. Indeed, a maximum confirmed power conversion efficiency (PCE) of *ca.* 26% has been reached for crystalline silicon.[6] However, obtaining electronic grade silicon monocrystals requires a high cost of manufacturing, which restricts their wide use. Efforts towards the use of less energy demanding multi-crystalline silicon have been developed, but their efficiencies are lower than crystalline silicon (21%[6]).

Second generation solar cells aim at avoiding the use of silicon wafers. They are typically composed of thin films of amorphous silicon, Copper-Indium-Gallium-Selenide (CIGS), or Cadmium Telluride (CdTe). While the manufacturing cost is slightly decreased compared to

the first generation and flexible devices can be manufactured, the low availability of such metals and the possible environmental impact of cadmium are the main drawbacks of this generation. Furthermore, efficiencies are still lower than the first generation solar cells (amorphous silicon: 10%, CIGS: 21%, CdTe: 21%[6]).

The first purely organic based solar cell (OSC) was developed by Pochettino in 1906 and relied on the use of anthracene as the photovoltaic active material.[7] OSCs, also called 3rd generation, were composed of one single active component until the mid-1980s. Typical materials are generally based on tetracene **1**, phthalocyanine **2** or merocyanine **3** (Figure 1.1) and efficiency up to 1% had been obtained.[8]

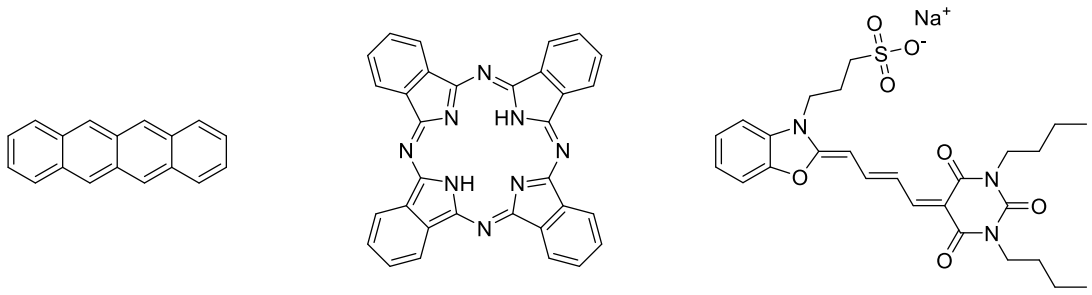

1 Tetracene **2** Phthalocyanine **3** Merocyanine

Figure 1.1: Typical examples of single component organic solar cells.

In order to improve the device efficiency, another OSC architecture emerged in 1986 and was based on using a binary mixture of components as the photovoltaic active layer. C. G. Tang built the first bilayer structure, which was based on copper phthalocyanine **4** and a perylene derivative **5** as shown in Figure 1.2.[9] Even if the PCE is in the same range as the single component devices, Tang claimed that the presence of two components facilitate the charge generation. This new bilayer architecture constituted a major breakthrough in OSCs.

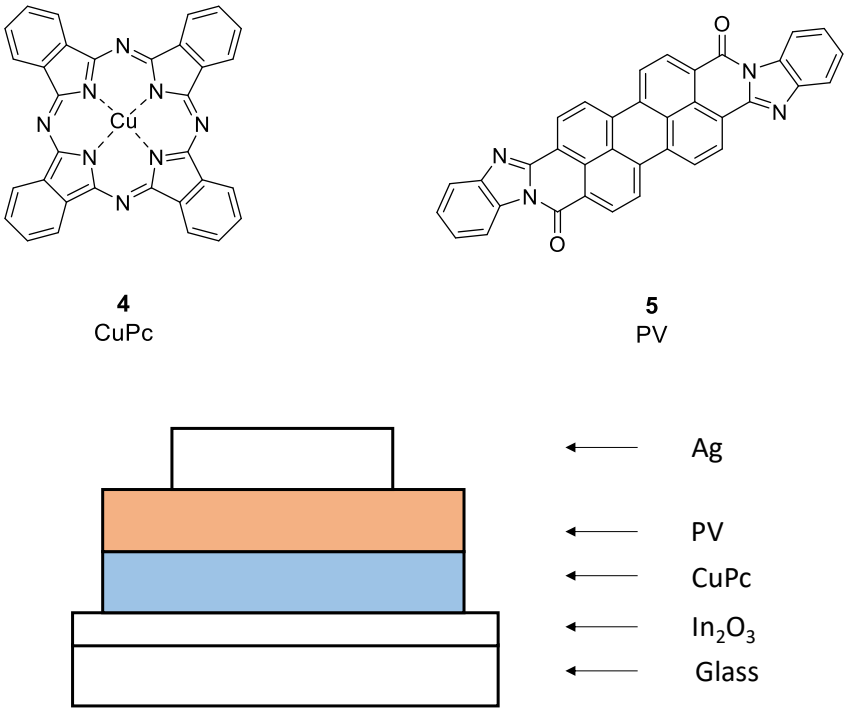

Figure 1.2: Top: chemical structures of CuPc 4 and PV 5 used in Tang's bilayer OSCs. Bottom: architecture of Tang's OSC.

A tremendous variety of binary mixtures has indeed been used since then. Polymers, such as poly(*p*-phenylene vinylene) derivatives **6** (PPV) or poly(3-hexylthiophene) **7** (P3HT) (Figure 1.3) are by far the most common. However, polymer-based technology suffers from poor control of the molecular weight and batch to batch variations. An alternative to polymers is the use of small molecules. Indeed, the high variety of organic molecules, the easy tuning of their optical/electrical properties, and their lower batch-to-batch variation are advantages over polymers. A large variety of electron donor [10] and acceptor [11,12] small-molecules have shown their potential in OSCs. Due to their self-assembly, liquid crystalline compounds are of great interest in optoelectronic devices.[13] Substantial improvement on PCE has been observed in the past three decades. Recently, the 10% efficiency barrier has been crossed, the best efficiency to date being 11.2%.[6] However, 1st generation solar cells are still more efficient therefore, still more widely utilised in commercial applications.

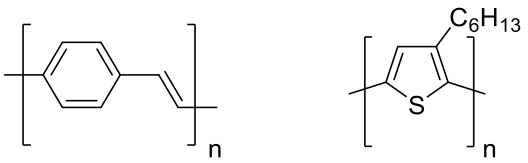

6 PPV **7** P3HT

Figure 1.3: Examples of polymer used in OSCs.

1.2.2 Working principle of organic solar cells

The working principle of OSCs can be divided into four steps. (1) A photon is absorbed by the active layer and generates an electron-hole pair called an exciton. (2) The exciton is traveling until (3) the electron and the hole dissociate into free charges, (4) which migrate towards their respective electrode, creating an electric current.

The low efficiency of OSCs compared to their inorganic analogues is related to the type of exciton involved. In organic materials, due to their low dielectric constant, strongly bound electron/hole pair excitons are generated. These so-called Frenkel excitons have a binding energy one to two orders of magnitude higher than the exciton in inorganic materials. The dissociation of the exciton into free charges is therefore more difficult, limiting the efficiency of OSCs.

The binary mixture of two compounds described by Tang aims at facilitating the exciton dissociation. Indeed, the two components have different electron affinities and ionisation energies. In other term, each of these components have different HOMO and LUMO energies. The component with the highest ionisation potential is referred as the electron donor (D) while the electron acceptor (A) has the highest electron affinity. The difference between the HOMO and LUMO level of the donor and the acceptor allows the exciton electron to be transferred from one component to the other, as schematised in Figure 1.4.

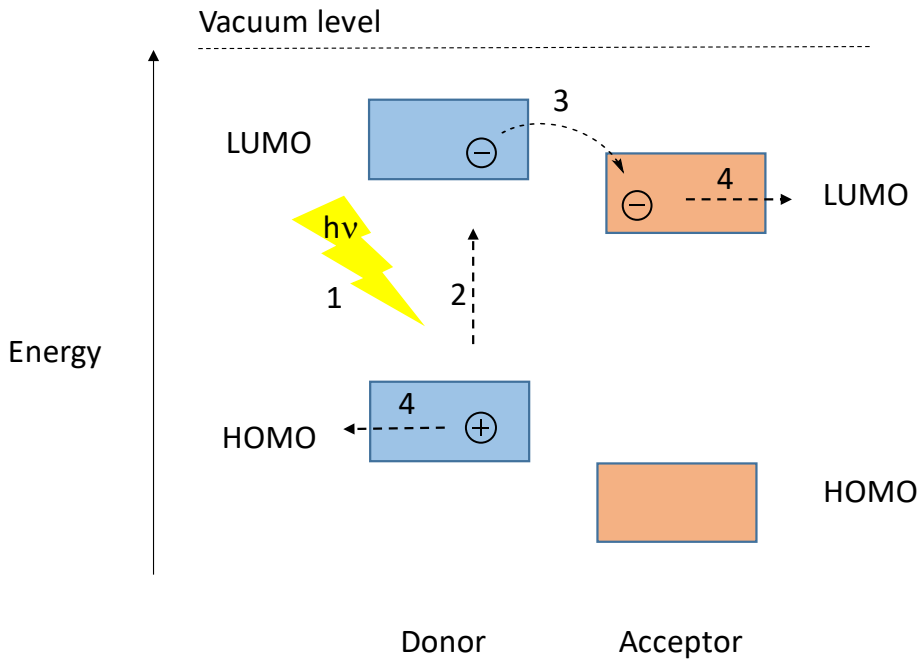

Figure 1.4: Working principle of organic solar cells. (1) Absorption of the photon, (2) Generation of the exciton, (3) Charge separation, (4) Free charge diffusion to the electrodes.

It was shown that the interface area between the electron donor and acceptor is where the exciton has the most chance to generate charges and therefore generate current.[9] Controlling the morphology, *i.e.* the organisation of the photoactive components in the binary blend, has therefore been extensively studied.

1.2.3 Morphology of the active layer

A bilayer structure (also called flat heterojunction) has a minimum interfacial area between the donor and acceptor. As the exciton dissociation occurs at the interface, the obvious strategy would be to enhance the area to increase the charge splitting probability. Shortly after the use of a bilayer structure in OSCs, the concept of bulk heterojunctions (BHJs) was described on polymer:polymer[14] and polymer:fullerene binary mixtures[15]. A BHJ, as shown in Figure 1.5, is made of an interpenetrating network of the donor and acceptor materials. The increased interface area inducing higher levels of interaction between the two components is observed which results in an improvement of the photovoltaic properties.

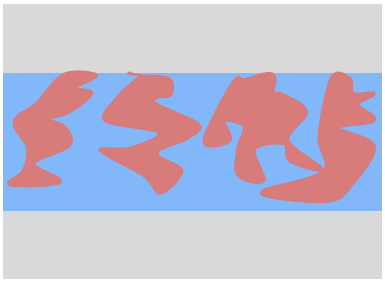

Figure 1.5: Schematic representation of a bulk heterojunction.

J. J. M. Halls and-co-workers have studied the morphology on a MEH-PPV:CN-PPV blends by transmission electron microscopy (TEM).[14] By changing the MEH-PPV:CN-PPV ratio from 1:10 to 7:1, 10 to 100 nm sized domains of MEH-PPV into a CN-PPV matrix are observed. Photoluminescence studies have shown that efficient emission quenching is observed for that ratio, and was attributed to charge generation.

The same year, A. J. Heeger and co-workers have also introduced the concept of bulk-heterojunction on MEH-PPV:PCBM systems.[15] By changing the ratio of the two components and the solvent used for film preparation, an improvement of the photovoltaic properties was observed. It was attributed to the formation of interpenetrating domains into the blend. However, no morphological study of the blend was investigated.

The ideal BHJ morphology was shown to be a trade-off between low interfacial and ideal mixing between the electron acceptor and donor materials. Indeed, low interfacial area, *i.e.* the bilayer structure, results in poor charge creation. However, an ideal mixture, with a maximum interfacial area, leads to an efficient charge generation but poor charge transport to the electrode due to charge trapping.

It is widely accepted that the size of the electron acceptor and donor domains in BHJ has to be commensurate with the exciton travel distance (L_D) and its lifetime. In organic materials,

the exciton travel distance is in the order of 1 to 100 nm.[16] A theoretical study towards the ideal BHJ developed by A.B. Walker and co-workers showed that the morphology of the active layer which lead to the best performance relies on highly ordered domains with a width of two times the exciton travel distance, as schematised in Figure 1.6.[17] Nano-sized segregation between the two materials is then required, and is generally situated in the 10 to 20 nm range.[18]

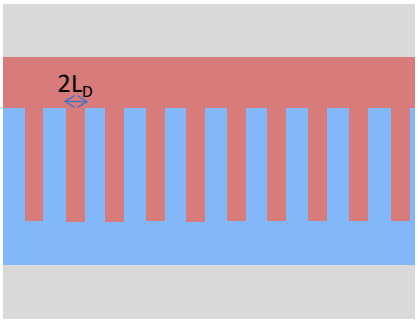

Figure 1.6: Schematic representation of an ideal BHJ.

Mixing two materials is therefore a common and successful strategy to obtain functional devices especially in organic solar cell technology. While numerous studies have shown that the bulk heterojunction is the architecture of choice, controlling the morphology, *i.e.* changing the organisation of the donor and acceptor in the active layer, is not trivial. Indeed, when two materials are mixed together, the favoured organisation is a bilayer structure. As a simple analogy, mixing water and oil results in a macrophase separation, where a layer of oil sits on the layer of water (Figure 1.7).

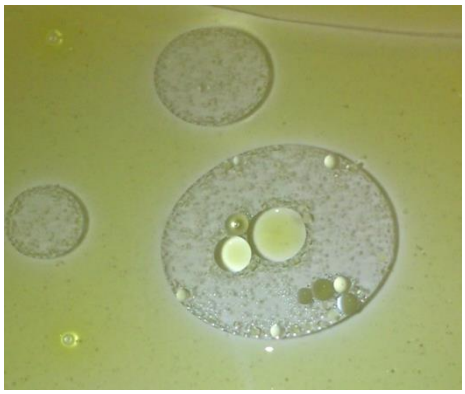

Figure 1.7: Macrophase separation between oil and water.

This favoured macrophase separation can be explained by thermodynamics. The Gibbs free energy of mixing $\Delta_{mix}G$ can be decomposed into an enthalpic $\Delta_{mix}H$ and entropic $\Delta_{mix}S$ factors, as described in equation (1).

$$\Delta_{mix}G = \Delta_{mix}H - T\Delta_{mix}S \qquad (1)$$

The entropy is related to the order in the film, *i.e.* the number of microscopic configurations in the macroscopic system. An increase of the number of microscopic configurations leads to a positive $\Delta_{mix}S$ and is often interpreted as an increase of disorder. Therefore, mixing two components is entropically favoured.

The enthalpic factor is related to the intermolecular forces between the two components. In the example of water (A) and oil (B), mixing interactions the two components would results in breaking H-bonds and Keesom dipole/dipole between AA (Figure 1.8). In an ideal mixing, the resulting AB intermolecular forces are dipole/induced dipole type (Debye forces). As the Debye forces are less energetic than H-Bonding and Keesom forces, mixing water and oil is therefore endothermic ($\Delta_{mix}H$ is positive). The enthalpic factor dominates the entropy factor. The Gibbs energy of mixing, $\Delta_{mix}G$, is therefore positive. Hence, the mixing results in macrophase separation between oil and water.

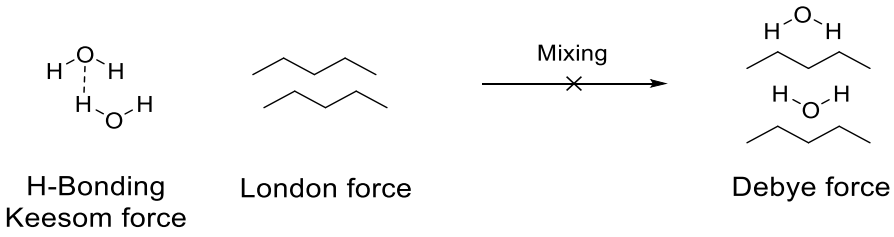

Figure 1.8: Mixing of water and oil.

In the case of an electron acceptor (A) and donor (D) blends, an additional enthalpically favoured force has to be taken into account. Due to their difference in potential, A and D are coulombically bonded. Despite this interaction, most of the electron donor and acceptor does not mix and the $\Delta_{mix}G$ remains positive. Indeed, the difference in shape between the two materials does not allow an efficient coulombic bonding.

In this thesis, the term "incompatible" will be therefore used to describe two materials that do not mix.

The following section will review the available strategies to control the morphology in organic solar cell technology, in order to supress the macrophase separation of incompatible materials and develop an ideal bulk heterojunction.

1.2.3.1 Morphology control in polymer-based organic solar cells

The morphology control of the active layer in organic solar cell has been successfully achieved by either physical or chemical methods. This section reviews the main techniques to obtain an optimal bulk-heterojunction for the poly(3-hexylthiophene):[6,6]-phenyl-C_{61}-butyric acid methyl ester (P3HT:PCBM, **7**:**8**) systems (Figure 1.9), the most studied system for organic solar cells. Most of the techniques described can nevertheless be applied to other polymer:fullerene based organic solar cells. Although numerous strategies are available to improve the efficiency of OSCs, such as enhancing the photon absorption, adding an additional

layer to increase the charge migration to the electrode or changing the electrodes,[19] only the morphology of the active layer will be discussed.

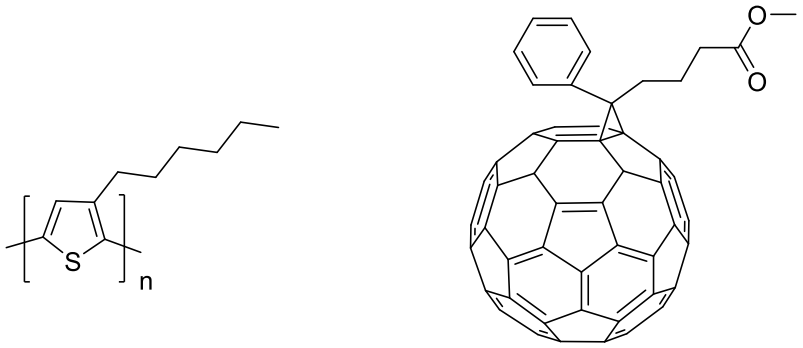

7 **8**
PCBM

Figure 1.9: Structure of P3HT **7** and PCBM **8**.

Compared to inorganic-based solar cells, OSCs appears to be highly promising because of their low-cost and easy manufacturing. Solution-process appears to be the most viable technique in order to fulfil those promises. Solution-process techniques have been widely studied and a large choice of methods are available and used as a way to control the morphology.[20]

A simple method of deposition is drop-casting. A solution of the active component is dropped onto the substrate. The desired thin film is created as the solvent evaporates. The organisation of the active components can be tuned by changing the solvent, which affects the rate of evaporation and the solubility of the components. The morphology is therefore altered. While drop-casting is a simple procedure and does not require any special instrument, the poor control of the film thickness precludes its use for OSCs. Spin-coating is therefore preferred. A solution of the component is dropped onto the substrate, which is spun to obtain a uniform film. For this method, the choice of the solvent, the spinning speed and the concentration of the active components are important parameters to control the film deposition and the subsequent organisation of the blend.[21]

A less common method is the dip-coating, where the substrate is dipped into a solution of the desired component and gradually withdrawn to allow deposition onto the substrate.[20] Zone-casting, which allows the deposition of a solution onto the substrate *via* a nozzle was proved to be an efficient method to induce different morphologies. [22]

Post-treatment of the thin film was also shown to be an efficient method for morphology control. The most common method relies on a thermal treatment, called annealing, where the thin film is heated. Thermal reorganization of the active layer is observed. Cross section scanning electron microscopy shows that a bilayer structure of P3HT:PCBM rearranges into more nano-segragated domains upon thermal annealing at 150 °C during 30 s.[23] C. J. Hawker and M. L. Chabinyc also demonstrated that the reorganisation of PCBM occurs only in amorphous P3HT. It has been shown that thermal annealing induces a controlled dispersion of PCBM and enhances the crystallization of P3HT.

Solvent vapour annealing (SVA) allows the reorganization of a binary thin film by placing it in a saturated atmosphere of solvent. The morphology is altered by the controlled solubilisation of the thin film. The choice of the solvent is therefore crucial in order to obtain the desired morphology. For example, M. Dadmun and co-workers studied the effect of carbon disulphide as an annealing solvent on a P3HT:PCBM thin film.[24] It was shown by atomic force microscopy that the morphology of the blend is altered from the bilayer structure to small aggregates of PCBM into a crystalline P3HT matrix. The PCE was increased by 105% (from 1.69% to 3.46%) when the sample was solvent annealed for 5 s. They also demonstrated that the time of exposure has to be controlled to avoid the formation of larger aggregates - leading to a decrease of the efficiency. The PCE was indeed decreased by 16% (from 3.46 % to 2.89%) when the film was left for 120 s in a carbon disulphide saturated atmosphere.

Although these physical methods induce a change of the morphology in the active layer, the resulting organisation was shown to be meta-stable and long-term use of the device can result in the thermodynamically favoured macrophase separation.[19] This phenomenon is accelerated by the high-operating temperature of OSCs.[19]

Chemical methods have also been introduced to control the morphology and rely on adding a third component into the binary mixture.

Water and oil are taken as a simple example. The macrophase separation can be suppressed by adding soap into the blend, as observed in Figure 1.10. Indeed, smaller droplets of oil, therefore smaller domains are obtained. The large domains are suppressed and micelles of oil are obtained. The soap acts as a chemical agent to change the morphology in a mixture of water and oil. This principle is the basis of all detergents.

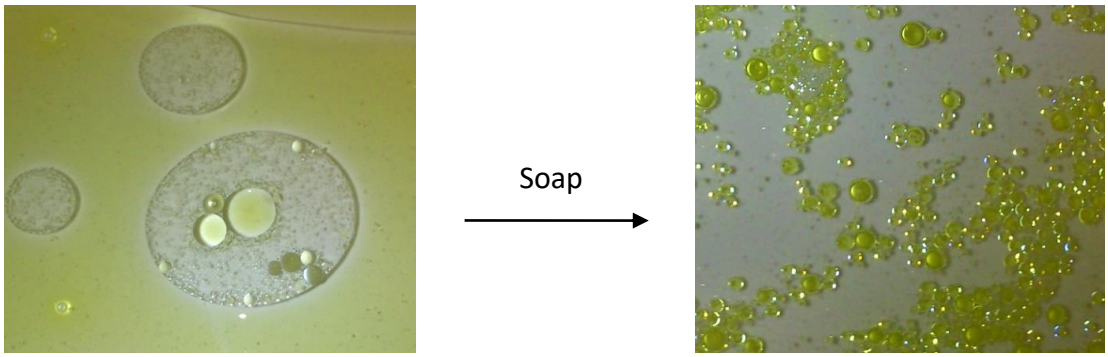

Figure 1.10: Macrophase separation suppression on adding soap into an oil and water binary mixture.

Based on this analogy, ternary blends of organic solar cells have emerged. This strategy was used and described for a wide range of organic compounds to change the organisation of binary mixtures based on polymer:fullerene or all polymeric active layers.[25–33]

Purely structural volatile processing additives have shown to improve the efficiency of organic solar cells. 1,8-diiodooctane **9** (DIO) is by far the most common (Figure 1.11). The action

mechanism of DIO in polymer:fullerene systems relies on its selective solubility. Fullerenes are soluble in DIO, unlike P3HT. Due to the high boiling point of DIO (bp=167 °C), slow polymer crystallization occurs while the fullerene derivatives are still in solution. Reorganization of the active layer occurs and nano-domains, the ideal morphology in BHJ, are obtained. P. Lugli and co-workers have for example shown a 32% increase of the PCE (PCE from 3.7% to 4.9%) when adding 2.5 vol% DIO into a 1:0.75 blend of P3HT:PCBM blend.[34] Likewise, alkanedithiols **10** have been used (Figure 1.11).[35]

9
DIO

10
n = 1, 2, 4, 5

Figure 1.11: Examples of volatile processing additives.

Non-volatile and purely structural additives have also been employed (Figure 1.12). These types of additives act as a nucleating agent to force the crystallisation of one of the components to smaller crystalline domains, therefore adopting a more optimal BHJ morphology for charge generation to occur. As an example, Y. L. Loo has shown an increase of the PCE by 79% (PCE from 1.01% to 1.81%) by adding 5% of **11** into a 1:0.8 blend of P3HT:PCBM.[36] Likewise, a 16% efficiency improvement (PCE from 1.80% to 2.09%) have been obtained on adding 1.6% of **12** to the binary blend.[28]

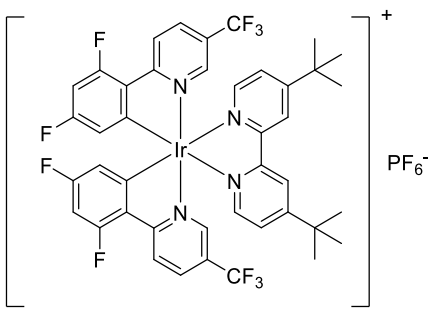

11

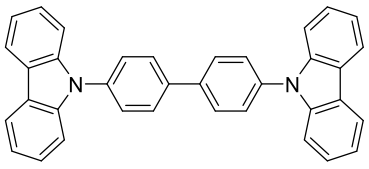

12

Figure 1.12: Examples of non-volatile structural additive for polymeric solar cells.

However, the aforementioned additives are purely structural, and do not participate to the charge generation process, necessary to create an electric current. Moreover, long term stability issues have been raised due to the meta-stable nature of the morphology.[19]

Diblock-copolymers have successfully been used as a third compound for ternary OSCs. A small amount of these, introduced into the blend of incompatibles allows for the change of interfacial energy between the electron donor and acceptor and alters the morphology of the mixture. C. Brochon, G. Hadziioannou and co-workers have shown a 62% increase in efficiency (PCE from 2.7% to 4.3%) on adding 8% **13** into a P3HT:PCBM binary system (Figure 1.13).[37] Co-polymers containing liquid crystalline moieties, such as **14** (Figure 1.13) can also successfully increase the efficiency: Y. Chen and co-workers have shown an increase of the PCE by 24% on adding 10% of **14** (PCE from 3.24% to 4.03%).[38] By the self-assembly of the co-polymer into the ternary mixture, higher ordering of P3HT is obtained, which facilitates the charge transport. Moreover, macrophase separation between P3HT and PCBM was reduced, and the formation of nano-segregated domains was observed.

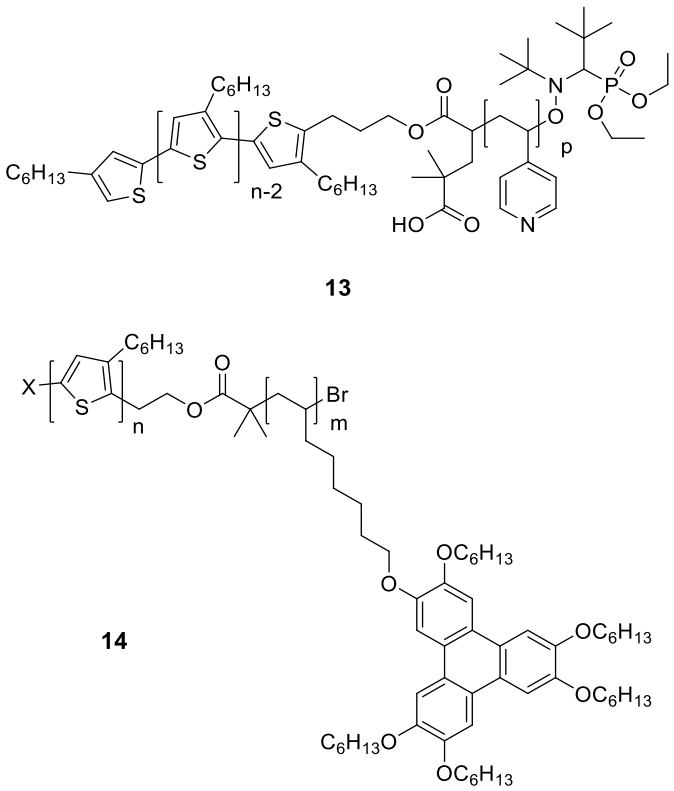

Figure 1.13: Examples of diblock-copolymers used in ternary OSCs.

Functional third components, *i.e.* dyads composed of covalently-bonded electron donor and acceptor moieties have also been employed. F. Wudl and co-workers designed a diblock-copolymer composed on a polythiophene moiety covalently linked to a C_{60}-containing block **15** (Figure 1.14).[39] The addition of 5 wt% of this functional diblock-copolymer into a 1:0.7 w/w mixture of P3HT:PCBM was proved to induce a controlled phase separation between the two incompatible components. Moreover, the efficiency was increased by 34% compared to the binary P3HT:PCBM mixture (PCE from 2.6% to 3.5%). **15** was inferred to be located at the interface between the electron donor and the electron acceptor.

Simpler functional components, based on oligothiophene/C_{60} based components have recently been designed and their morphological impact on P3HT:PCBM system studied. The advantages over functional diblock-copolymer are numerous. Indeed, small molecules are easier to purify and better solution-processability is observed compared to polymers. Kim et

Al. developed a small molecule compatibiliser **16** (Figure 1.15).[40] Presumably located at the interface between P3HT and PCBM, its effect is similar to the functional diblock copolymer and alters the morphological organization of the blend by suppressing the macrophase separation. Their work was shortly followed by R. Raja and co-workers with the use of **17a** and **17b**[41] (Figure 1.15).

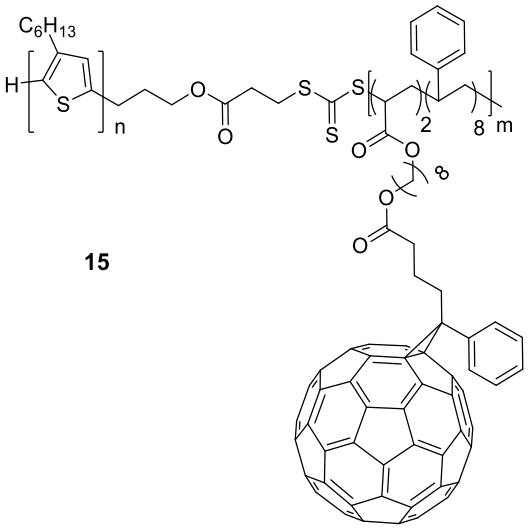

Figure 1.14: Example of a polymeric functional compatibiliser.

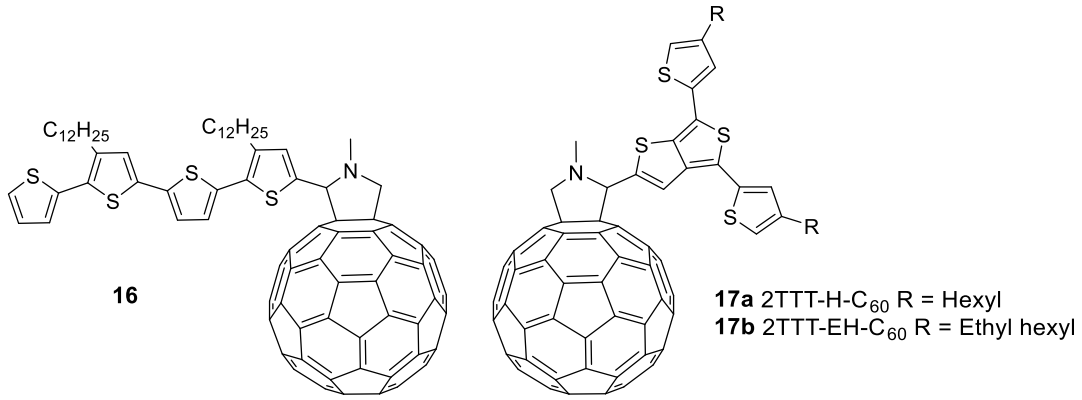

Figure 1.15: Examples of small-molecule functional compatibiliser.

Strategies to control the morphology in polymer:fullerene OSCs are therefore numerous. However, the limited control of the polymer molecular weight and the difficulty of its purification is considered as a drawback towards highly efficient OSCs. Moreover, fullerene derivatives, the most common type of electron acceptor used in polymer-based OSCs, show

limited absorption of sun light, especially in the visible-near IR region, and tuning of their HOMO and LUMO levels is difficult due to the limited functionalization of such derivatives.[12]

1.2.3.2 Morphology control in small molecule organic solar cells

While the physical methods applied to the polymer:fullerene can still be applied in small molecule OSCs, chemical methods which rely on adding a third compound are more limited. DIO have also been employed in small-molecule organic solar cells and also show an improvement of their efficiency compared to processing without any additives. [42–46]

Another type of additive, primary used as a light-harvesting compound to enhance the absorption of thin films, was proved to have an effect on the morphology of the blend. While the incorporation of the third component improves the absorption of light and facilitates the charge splitting due to their HOMO and LUMO energies, the morphology has also been studied. As an example, the incorporation of **19** into a BDT6T:$PC_{71}BM$ (**18**:**20**) binary mixture (Figure 1.16) results in smaller BDT6T and PCBM domains, therefore increasing the PCE by 13% when 15% of **19** in **20** was added.[31]

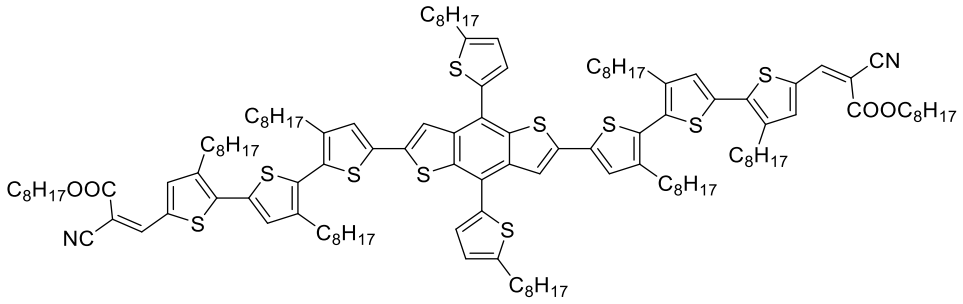

18

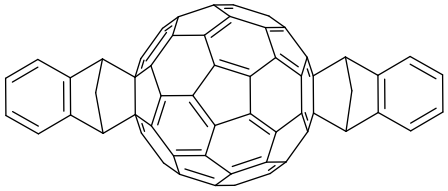

19
ICBA

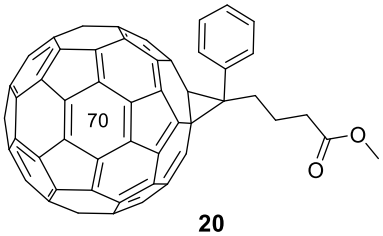

20
$PC_{71}BM$

Figure 1.16: Examples of light-harvesting components with proven effect on the morphology of small molecule OSCs.

To our knowledge, no morphological studies have been investigated on ternary all small-molecule blends of a donor:functional component:acceptor.

Liquid crystalline components have received a lot of attention in the field of optoelectronic devices, including solar cells.[13] One major advantage over both crystalline and amorphous small molecules used in OSCs is their self-assembly into well-organized structures. Their self-assembly could be a considerable advantage for charge transport. Moreover, numerous available techniques are available to study their morphology in both solution and in thin film forms. After a brief introduction about the liquid crystalline state, with an emphasis on discotic materials, examples of morphology control using liquid crystals will be presented.

1.3 Liquid crystals

The self-assembly, *i.e.* the autonomous self-organisation of components into a well-defined structure, is found in numerous fields. Examples in biology include the self-assembly of two strands of DNA, the cell membrane or the folding of proteins. The high potential of

self-assembly has been applied in other fields, such as optoelectronics. One particularly interesting class of self-assembling components are liquid crystals.

1.3.1 Introduction to liquid crystals

A liquid crystal (also called mesogen) is a material which combines the properties of both liquids and solids. A common definition is that it flows like liquids but has some order like crystals. Since their discovery by Friedrich Reinitzer in 1888,[47] this intermediate state of matter between the solid and the liquid phase has been extensively studied and a large family of liquid crystals has been discovered.

A mesogen is usually composed of a rigid core covalently linked to a flexible chain. The self-organisation of mesogens into liquid crystalline phases is based on their intermolecular forces: Van der Waals forces, hydrogen bonding, π-π interaction between two aromatic cores or electrostatic interaction play a crucial role in liquid crystalline phase formation.

There are many ways to categorise liquid crystalline materials. Mesogens can be separated into two mains groups: thermotropic and lyotropic liquid crystals. Thermotropic mesogens are temperature dependent while lyotropic mesogens forms liquid crystalline phases in solution and are solvent and concentration dependent. Lyotropic systems can also be divided into two main classes: chromonic and non-chromonic systems.[48,49]

Mesogens can also be classified by their shapes: rod-like (or calamitic), disc-like (or discotic), or banana-like mesogens can be cited and various self-organisation are obtained.

Liquid crystals have been used in a wide range of application, the most known being liquid crystals displays (LCDs). First fabricated in the late 1960s by Heilmeier and co-workers,[50] this technology is still used in calculators, televisions or smaller screens. The working principle of

LCDs relies on the ability of calamitic liquid crystals to alter their packing upon application of an electric current.

As this thesis focuses on discotic liquid crystals, this family will be discussed in more details in the next section.

1.3.2 Discotic liquid crystals

The discotic liquid crystalline phase (DLC) was first observed in 1977 by S. Chandrasekhar on benzene hexa-n-alkanoates **21a-f** (Figure 1.17).[51]

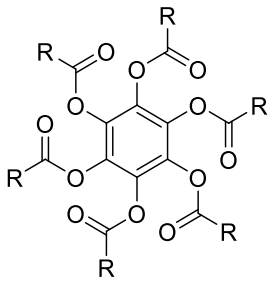

21a-f
R = C_4H_9 to C_9H_{19}

Figure 1.17 : Structure of benzene hexa-n-alkanoates **21a-f**.

DLC's structures are usually composed of a rigid aromatic core surrounded by flexible chains (examples shown in Figure 1.18). Due to the π-π supramolecular interaction between two aromatic cores and the steric interaction of the peripheral chains, a large majority of DLCs self-assembles into 1D columnar aggregates. These columns further self-assemble into 2D lattice and a wide range of structures have been described. 2D lattices can be discriminated between the order in the columns (ordered, disordered, tilted) and the symmetry of the lattice (columnar hexagonal, columnar rectangular, columnar oblique or columnar nematic) (Figure 1.19). It is worth noting that discotic nematic or discotic lamellar mesophases have also been described (Figure 1.19).[52,53]

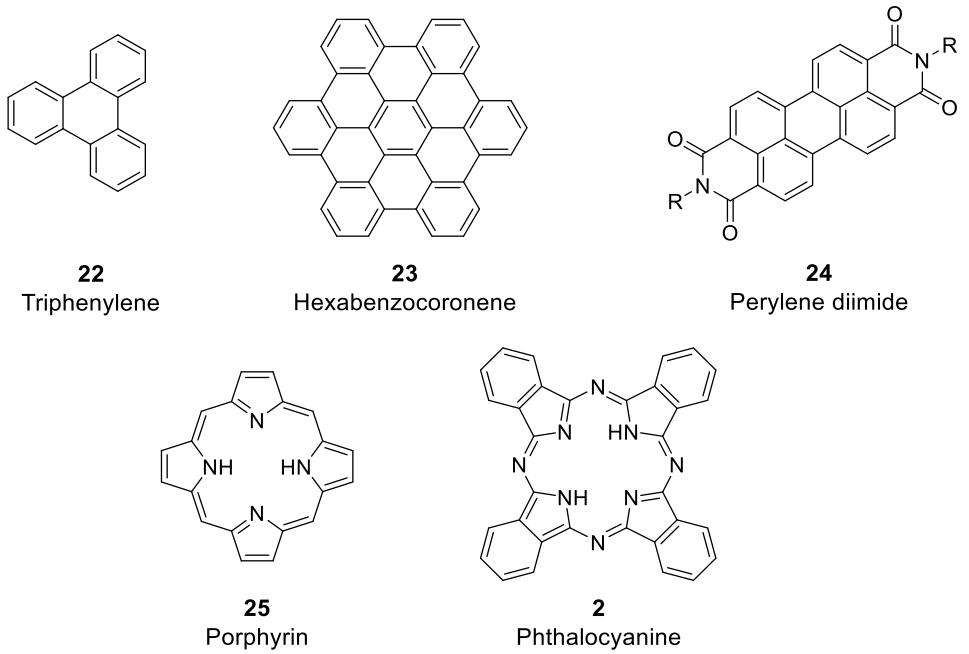

Figure 1.18: Typical examples of DLC aromatic core.

The ability of DLCs to self-assemble into 1D column has raised considerable attention in the optoelectronic field. Indeed, due to π-π stacking, DLCs are considered as excellent 1D charge transport carrier. Their promising properties have been employed for example in photovoltaics, OLEDs ad OFETs. [13,52,53]

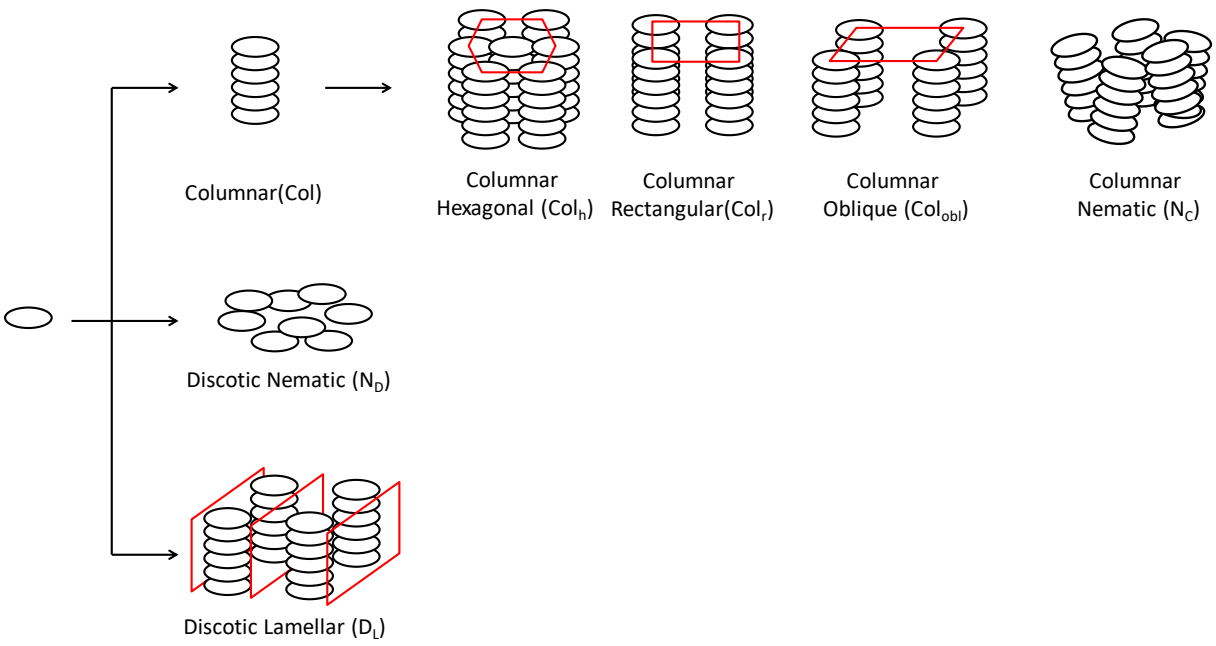

Figure 1.19: Schematic representation of discotic liquid crystal self-assemblies.

1.3.3 Theory of aggregation in lyotropic liquid crystals

Lyotropic liquid crystals can be divided into two groups. On one hand, the chromonic systems are generally discotic liquid crystals and are characterised by their aggregation into columns and their absence of critical micelle concentration. Their aggregation behaviour is generally considered as isodesmic, *i.e.* the energy necessary to add one monomer into the aggregate is constant and independent of the size of the aggregate. On the other hand, non-chromonic systems, such as phospholipids or detergents does have a critical micelle concentration. This section will focus on the aggregation process of chromonic discotic liquid crystals materials.

The thermodynamics of chromonic liquid crystals have been explored by Israelachvili.[54] Based on the law of mass action, the average number molecules in the aggregate and the bond energy between two monomers in the aggregate can be calculated. However, this theory only applies to diluted systems and approximate the aggregation as isodesmic. As an example V. R. Horowitz and co-workers investigated the aggregation of **26** by UV-Visible spectroscopy based on this theory.[55]

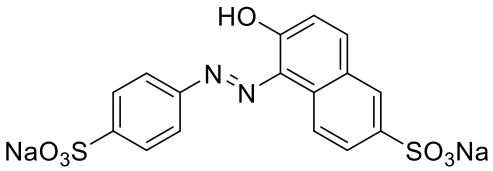

26

Figure 1.20: Sunset yellow CFC **26**.

The theoretical considerations are presented in the Appendix.

1.3.4 Characterisation of liquid crystalline phases

Due to their self-assembly and orientational order, mesogens are typically studied by polarized optical microscopy (POM), differential scanning calorimetry (DSC), and small and

wide angle X-ray scattering. This section briefly describes the different methods and the information that can be extracted.

The POM is the first characterisation conducted when working on liquid crystals, as only a small amount of the component is needed. The sample is deposited onto a substrate (typically on glass) and the film is viewed in transmission mode under crossed polarized light whilst being heated or cooled. Phase changes can therefore be observed and phase transition temperatures estimated. Indeed, while crystalline phases are hard to deform and show birefringence under polarised light due to their high anisotropy, an isotropic phase shows no birefringence and is easy to deform under pressure or shearing. A mesogenic phase, due to its combined properties of liquid and solid, shows birefringence and easy deformation under shearing.

Differential scanning calorimetry measures the enthalpy difference between the sample and a reference when heated or cooled. A phase transition involves an exothermic or endothermic process, which is recorded by the instrument. A precise transition temperature can therefore be extracted from DSC curves. The enthalpy value indicates the type of transition; a large enthalpy points to a high molecular rearrangement of the sample (from crystal to liquid crystal or from liquid crystal to isotropic) while smaller enthalpies are characteristic of liquid crystalline to liquid crystalline phase transitions.

X-ray diffraction provides additional and precise information on the structure of the mesophase. Due to the different packing of the mesophases, characteristic diffraction peaks are observed.[53] The lattice parameters can therefore be extracted. Various X-ray techniques, such as small-angle X-ray scattering (SAXS), wide-angle X-ray scattering (WAXS), one-dimensional or two-dimensional are available.

1.3.5 Compatibiliser in liquid crystals

Controlling the morphology in a binary mixture of mesogens to induce additional properties of the blends was also studied. A few examples of dyads (*i.e.* a molecule composed of two covalently attached components) have been published and were based on the shape-incompatibility between a disc-like and a rod-like mesogens.[56–62]

G. Mehl and co-workers have synthesised a dyad **27** composed of covalently linked disc-like and rod-like moiety (Figure 1.21) They have demonstrated that mixing this dyad with either the disc like or the rod like homologue, respectively **28** and **29** shows a full miscibility over the whole range of composition of temperature. No macrophase separation was observed in any of the studied mixture. Further studies on various rod-like (cyanobiphenyl[56–59], biphenyl[60] or azobenzene[61]) or disc-like (pentakis-methoxyphenylethynyl)benzene derivatives[56–59,61]) with tailor-made compatibiliser also show complete mixing. However, no study of ternary blend composed of the rod-like, the disc-like and the dyad were reported.

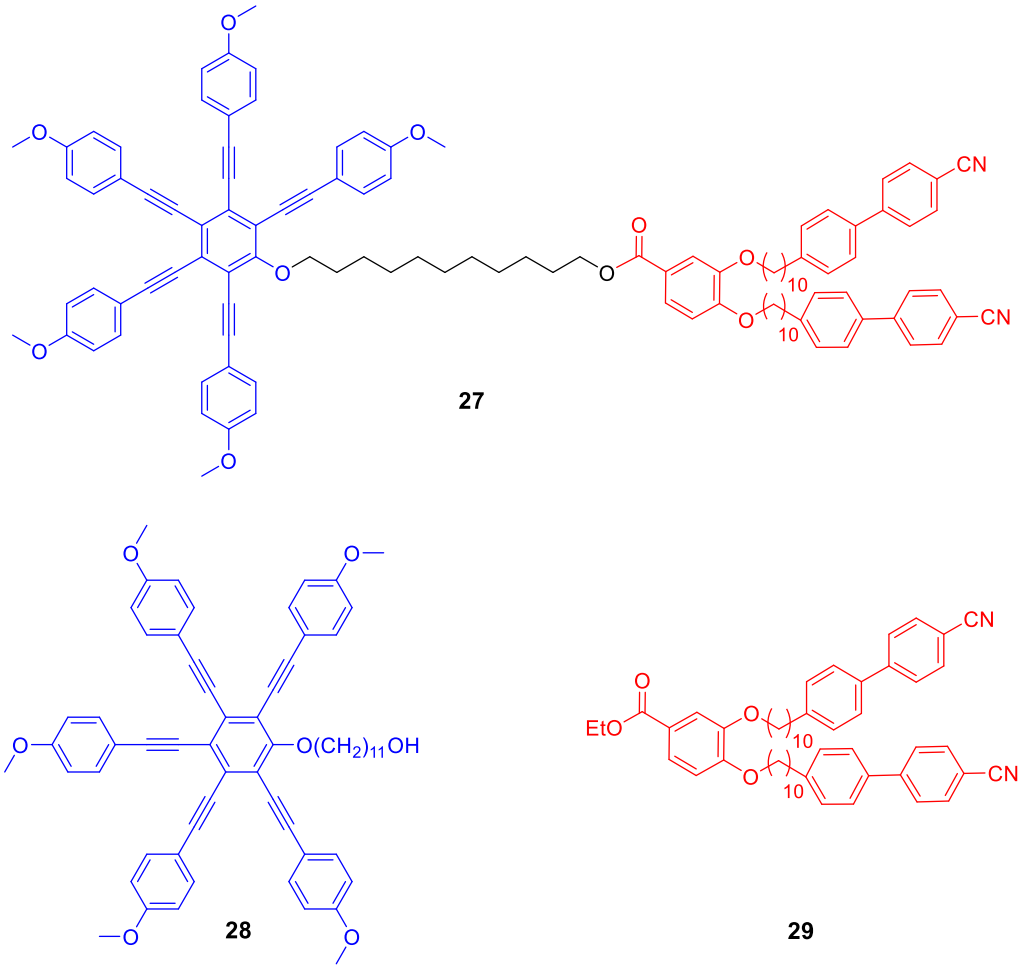

Figure 1.21: Structure of the dyad **25**, the disc-like **26** and the rod-like **27** mesogens.[56]

Date and Bruce have also designed a dyad **30** composed of a covalently linked rod-like and disc-like moiety.[62] While their corresponding disc-like **31** and rod-like **32** shows a total macrophase separation over the whole range of temperature and composition, the addition of **30** into the binary mixture leads to a single nematic phase from 20 mol% of **30**. Unfortunately, no further details on the morphology were given.

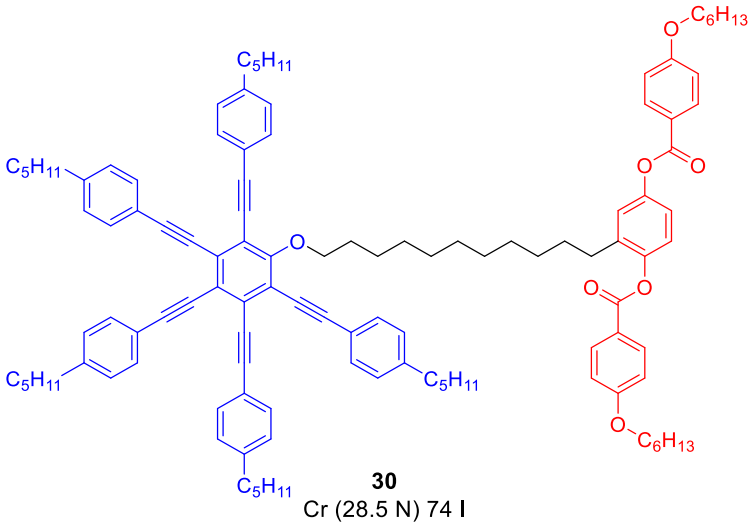

30
Cr (28.5 N) 74 I

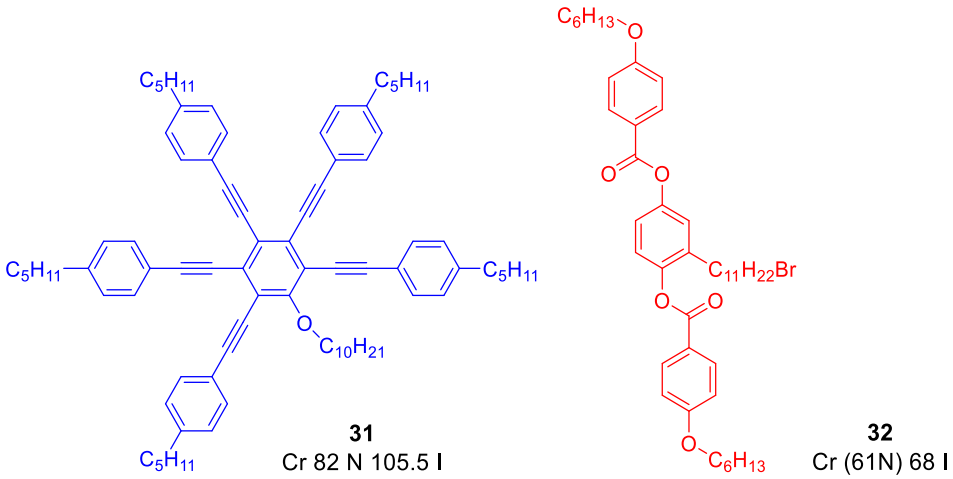

31
Cr 82 N 105.5 I

32
Cr (61N) 68 I

Figure 1.22: Structure of the dyad **30**, the disc-like **31** and the rod-like **32** mesogens.[62]

1.4 Aims and objectives

Controlling the morphology of the active area in solar cell technology is one of the crucial parameters for high efficiency devices. However, mixing an electron acceptor and donor material leads to the thermodynamically favoured bilayer structure, which is the least efficient morphology. The so-called bulk-heterojunction, where a controlled nanoscale blend of the two materials is preferred.

Although numerous physical and chemical methods to suppress the bilayer structure show great promise, the morphology control of small molecules-based solar cells are scarce and rely solely on meta-stable organisation of the blend.

The aim of this thesis is to provide a strategy to control the morphology of small molecule organic solar cells by adding a third component into the blend. Based on the numerous examples of polymeric or oligomeric compatibiliser in polymer based organic solar cell, this third component would act as a functional compatibilising agent. The goal of this strategy applied to small molecules will suppress the macrophase separation and lead to a micro to nano segregated interpenetrated architecture as presented in Figure 1.23.

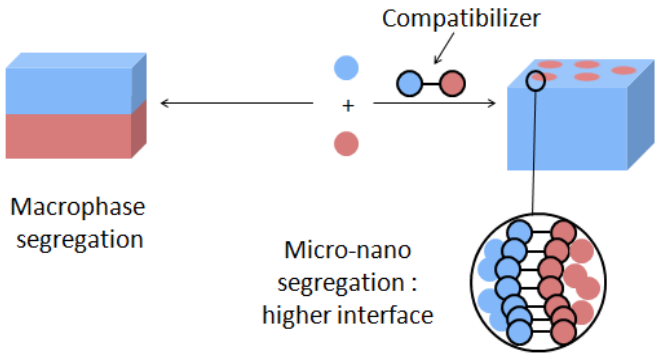

Figure 1.23: Schematic representation of the macrophase segragation and the expected effect of the compatibiliser on a mixture of incompatible materials.

Liquid crystalline compounds were the chosen family of small molecule. Indeed, the high potential of mesogens in optoelectronics and the successful strategy to control the morphology in the liquid crystal field by adding functional compatibiliser show promise for their application in small molecules OSCs.

To prove the concept of compatibilising materials, two non-miscible discotic mesogens will be synthesised. Their immiscibility will be introduced by the incompatibility of their surrounding chains. In the scope of this thesis, alkoxy and ethylene glycol-based chains will be the chosen incompatible moieties. A tailor-made compatibiliser will be designed and the effect of this third component on the morphology of the incompatible binary mixture will be investigated.

Chapter two:

Incompatible model materials based on triphenylene derivatives

2.1 Aims and objectives

To prove the concept of compatibilising a mixture of two incompatible materials, we initially focused our research on model compounds that are easily functionalisable and widely described in the literature. We have therefore chosen the triphenylene derivatives. The peripheral chains are used as a way to introduce incompatibility between the two triphenylenes. Indeed, linear alkyl chains are immiscible with ethylene glycol-based aliphatic chains. The hydrophobic 2,3,6,7,10,11-hexahexyloxytriphenylene TP6 and three hydrophilic ethylene glycol-based triphenylenes TP6EOnM (n = 2, 3, 4) are therefore chosen as the incompatible materials (Figure 2.1).

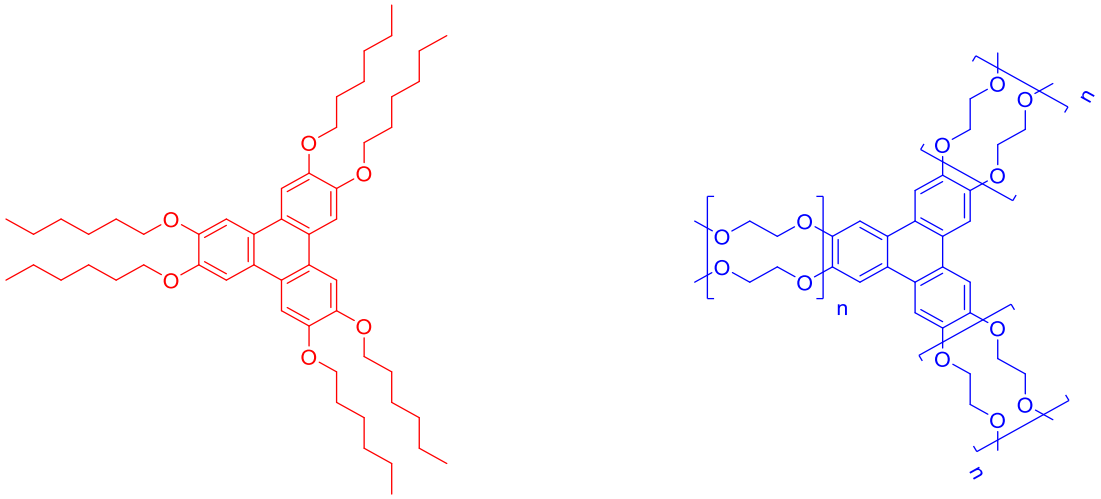

TP6 **TP6EOnM**
n = 2, 3, 4

Figure 2.1: Target incompatible compounds.

This chapter focusses on the synthesis of TP6 and TP6EOnM (n = 2, 3, 4) and their full mesogenic characterisation. The incompatibility between TP6 and TP6EO2M will then be discussed.

2.2 Introduction to triphenylene derivatives

The triphenylene molecule is a flat polycyclic aromatic composed of three fused annulated benzene rings to form a fourth ring (Figure 2.2). It was first discovered and isolated from the pyrolysis of benzene by Schmidt and Shultz in 1880.[63]

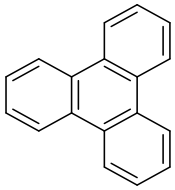

22

Figure 2.2: Chemical structure of triphenylene.

Since the first synthesis by the aldol trimerisation of cyclohexanone by C. Mannich more than a century ago, this polyaromatic hydrocarbon has received a lot of attention (Scheme 2.1).[64]

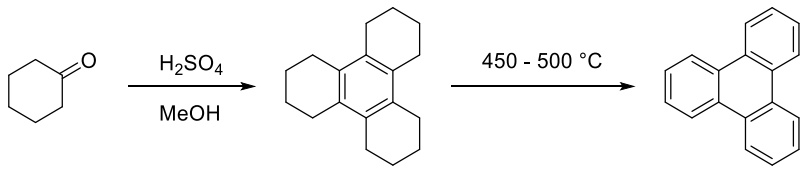

33 **22**

Scheme 2.1: Synthesis of the triphenhylene core **22** *via* aldol trimerisation by C. Mannich.[64]

Triphenylene derivatives have been widely studied for their supramolecular and physical properties. Due to the π-π stacking of the aromatic core and their aggregation into liquid crystalline phases, triphenylenes, and discotic liquid crystals in general,[13] has been for example used as one-dimensional charge transport materials,[65,66] electroluminescent material for light emitting diodes (LEDs),[67–69] sensors,[70,71] in solar cells[72] or self-assembled monolayers (SAMs)[73]. Their properties can be easily tuned by changing the surrounding chains and a large family has already been reviewed.[74–76] The most common triphenylene derivatives are the hexa-substituted ethers. Symmetrical hexasubstituted esters, thio- or seleno-ethers,

as well as unsymmetrical oligomeric and polymeric triphenylene or hepta-substituted triphenylenes have also been synthesised.[75,77]

Numerous routes to the synthesis of triphenylene derivatives are available. Scheme 2.2 summarises the most common methods.

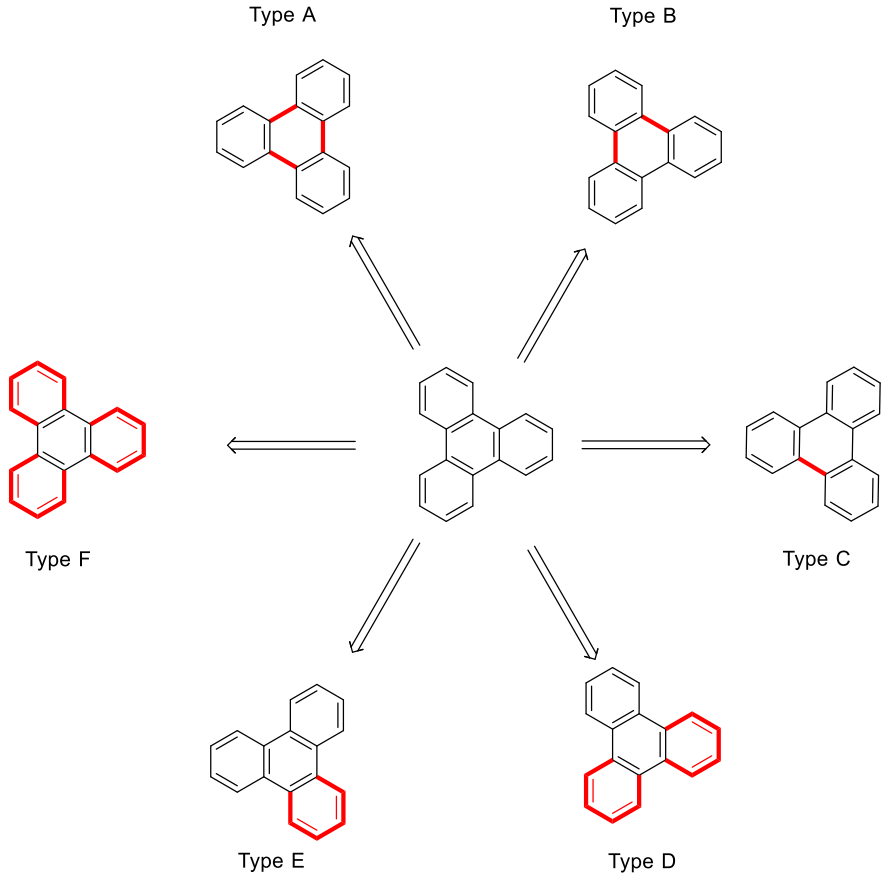

Scheme 2.2: Main synthetic pathways towards triphenylenes. The formed carbon carbon bonds are highlighted in red.

Type A synthesis is by far the most common method towards hexasubstituted symmetrical triphenylenes. The triphenylene core is generated *via* oxidative trimerisation of disubstituted benzene derivatives, easily available from 1,2-dihydroxybenzene (or catechol) *via* a *Williamson* type ether synthesis.

Type B offers an interesting alternative towards unsymmetrical triphenylenes. First described by R. J. Bushby[78] an oxidative cyclisation between a tetrasubstituted biphenyl **34** and a

disubstituted phenyl **35** leads to the corresponding triphenylene **36** (Scheme 2.3). It is worth noting that the biphenyl-phenyl coupling can also be achieved out *via* a double Suzuki coupling or an intramolecular/intermolecular Diels-Alder [4+2], but the synthesis of the precursors are more synthetically demanding.[79]

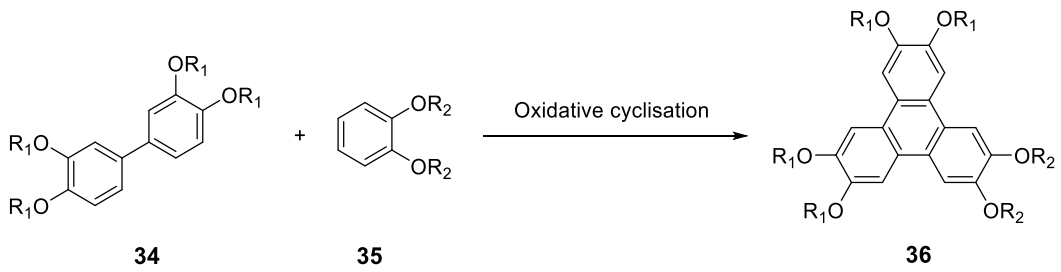

Scheme 2.3: Oxidative cyclisation of a biphenyl and phenyl derivative.

Other less common methods and more demanding syntheses of triphenylenes can be achieved by the oxidative cyclisation of terphenyl derivatives (Scheme 2.2, type C), from naphthalene (Scheme 2.2, type D), phenanthrene (Scheme 2.2, type E) or by functionalisation of benzene (Scheme 2.2, type F).

The pathways A, B and C presented in Scheme 2.2 usually involve an oxidative cyclodehydrogenation coupling step to form a new C-C bond, called the *Scholl* reaction. The *Scholl* reaction is a subcategory of a *Friedel-Crafts* reaction where the coupling of two arenes using a Lewis acid is achieved. The *Scholl* reaction can be performed using various inorganic oxidants, the most commons being $FeCl_3$[80], $VOCl_3$[81], $MoCl_5$[82], $SbCl_5$[83] as well as organic oxidants: chloranil:H_2SO_4[84] or 2,3-dichloro-5,6-dicyano-1,4-benzoquinone (DDQ) with acids[85,86].

The mechanism of the *Scholl* reaction is still debated.[87] The oxidative cyclodehydrogenation of *o*-terphenyl **37** will be taken as an example. Two different mechanisms can be found in the

literature and are based on either an arenium (Scheme 2.4) or a radical cation (Scheme 2.5) intermediate.

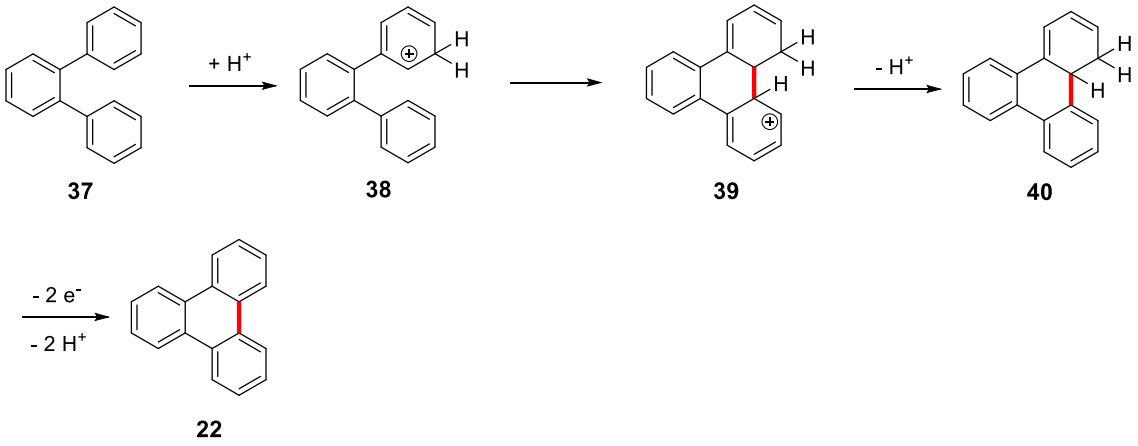

Scheme 2.4: Arenium cation based mechanism of the *Scholl* reaction.

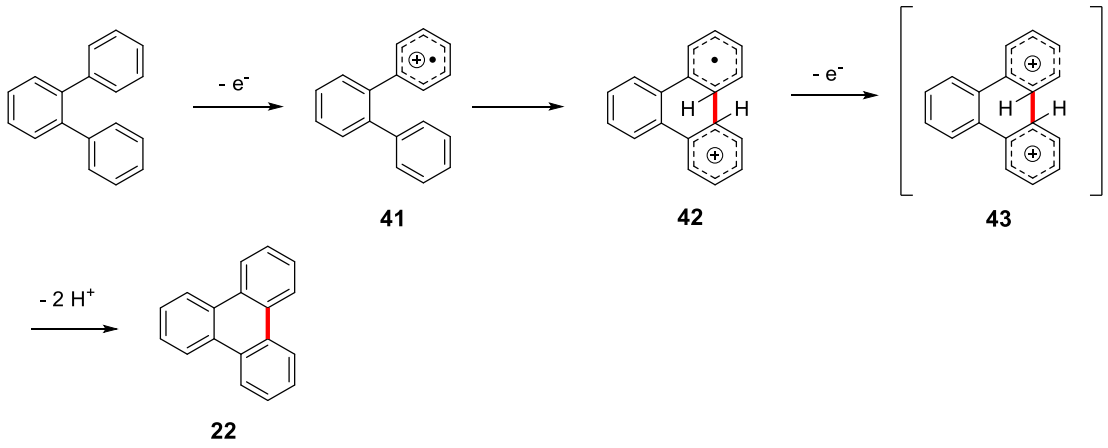

Scheme 2.5: Radical cation based mechanism of the *Scholl* reaction as suggested by R. Rathore and co-workers.[88]

B.T. King and co-workers have investigated the two different *Scholl* mechanisms *via* computational calculations on *o*-terphenyl and oligophenylbenzene (n= 3, 4, 6).[89–91] It was suggested that the radical cation pathway is energetically disfavoured compared to the arenium cation pathway. The proposed mechanism relies on the formation of a cation *via* protonation (**38**), followed by a C-C bond formation (**39**), dehydrogenation (**40**) and oxidative

rearomatisation (**22**) (Scheme 2.4). Nevertheless, the influence of the solvent was not considered in the computational calculations.

However, R. Rathore and co-workers provide experimental mechanistic facts towards the radical cation mechanism on *o*-terphenyl derivatives **37**.[88] The suggested mechanism is first based on the formation of a radical cation (**41**) by oxidation, an electrophilic attack (**42**), the formation of a dicationic intermediate (**43**) and finally a dehydrogenation step (**22**) (Scheme 2.5). It was demonstrated that no conversion of the terphenyl was observed when reacted with solely acidic solutions in dichloromethane (Brönsted or Lewis acid) suggesting the radical pathway. Moreover, the protonation of **37** to **38** must occur on the unfavourable *meta* position. In this article, X-ray crystallography evidence of a dicationic intermediate **1'c** from octamethoxytetraphenylene was also shown pointing again to a radical cation mechanism.

H. Butenschön, D.T. Gryko and co-workers summarise this divergence on the *Scholl* mechanism by suggesting different mechanism depending on the electronic structure of the starting materials and the conditions of the reaction.[87]

2.3 Incompatible triphenylene derivatives – Synthesis and characterisation

2.3.1 2,3,6,7,10,11-Hexahexyloxytriphenylene (TP6)

2.3.1.1 Synthesis of TP6

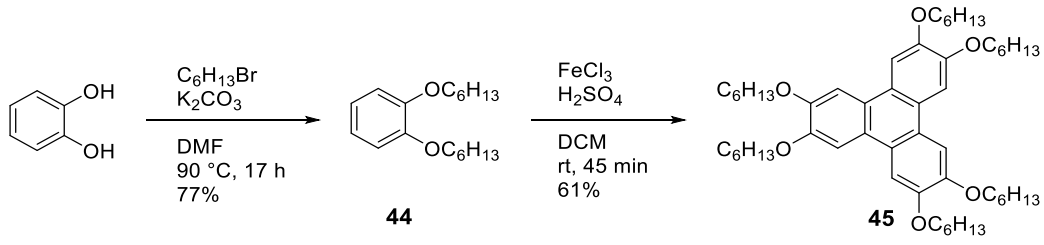

Scheme 2.6: Synthesis of TP6, **45**.

The synthesis of 2,3,6,7,10,11-hexaxyloxytriphenylene, commonly named TP6 was carried out in two steps following the literature with modifications.[92] A *Williamson* type reaction between catechol and an excess of 1-bromohexane using potassium carbonate as a base resulted in the corresponding di-alkylated benzene **44**. **44** was trimerized *via* the oxidative dehydrogenative *Scholl* reaction to afford **45** (called TP6 thereafter) in a satisfactory 47% overall yield on a multi gram scale.

2.3.1.2 Characterisation of TP6

The mesogenic properties of TP6 has been extensively studied in the literature.[93–99] TP6 shows a thermotropic discotic liquid crystalline state from 69 °C to 99 °C as shown by the POM (Figure 2.3), the DSC curve (Figure 2.4) and the X-ray diffraction (Figure 2.5). This mesogenic phase is columnar hexagonal, as indicated by the fan-shaped structure on the POM (Figure 2.3, left). The X-ray diffraction pattern of TP6 at room temperature shows multiple peaks, which is indicative of a crystalline phase (Figure 2.5, bottom). However, above 70 °C, only one diffraction peak is observed (Figure 2.5, top). All these experiments are in agreement with the literature.

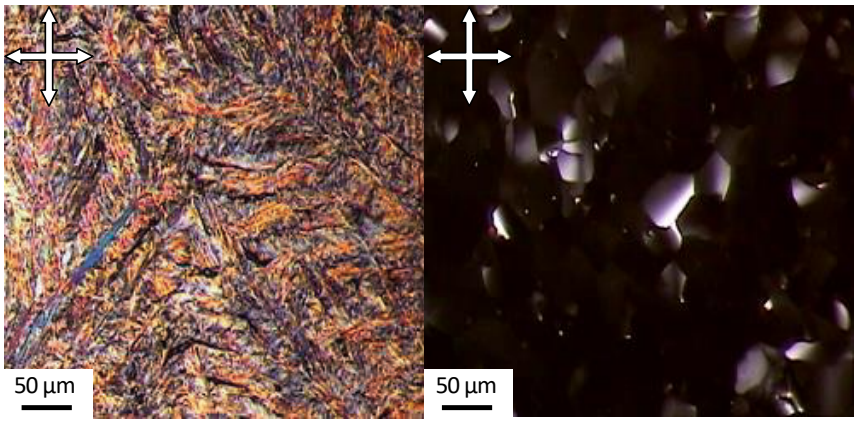

Figure 2.3: POM images of TP6 on heating stage. Left: at room temperature. Right: at 70 °C.

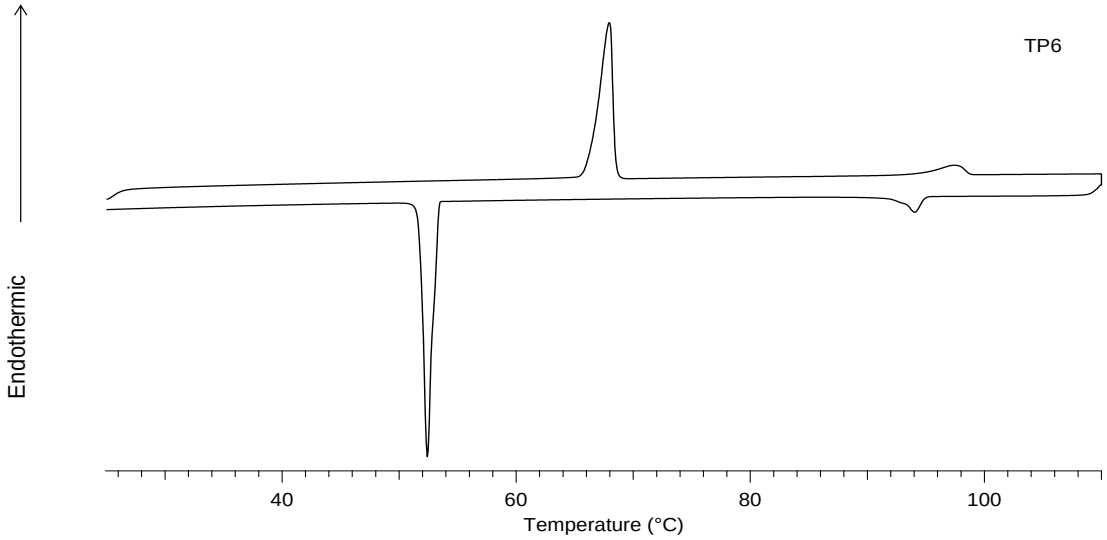

Figure 2.4: DSC curves of TP6 on 2nd heating/cooling cycle.

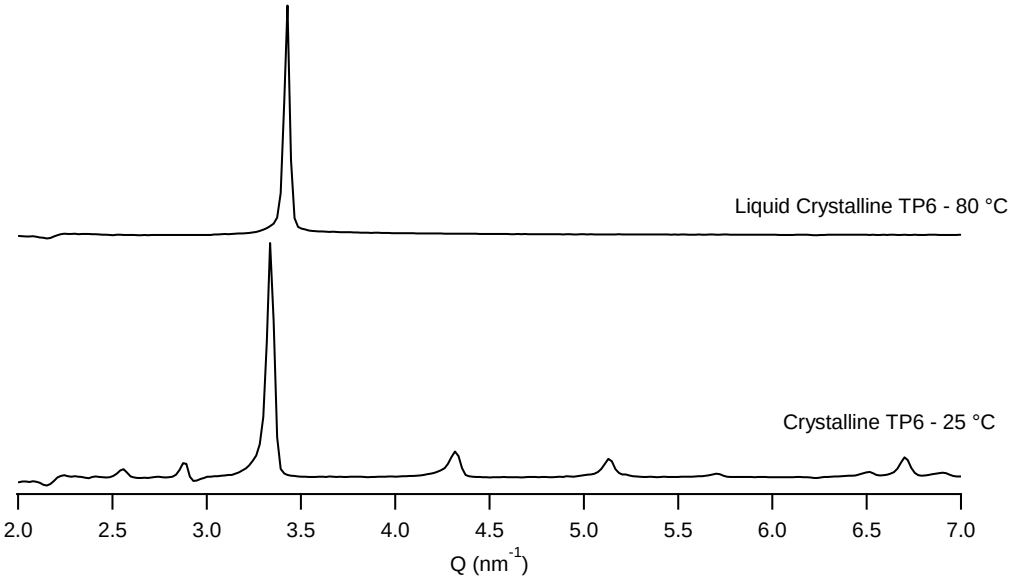

Figure 2.5: X-ray diffraction pattern of TP6: top: at 80 °C phase: bottom at 25 °C.

2.3.1.3 Aggregation of TP6 in solution

The UV-visible spectroscopy of TP6 was carried out in DCM at different dilutions in micro molar concentrations (Figure 2.6). TP6 shows a maximum absorption at 280 nm. The peaks located at 260 and 270 nm corresponds to vibrational levels. An additional broad peak at 315 nm is observed.

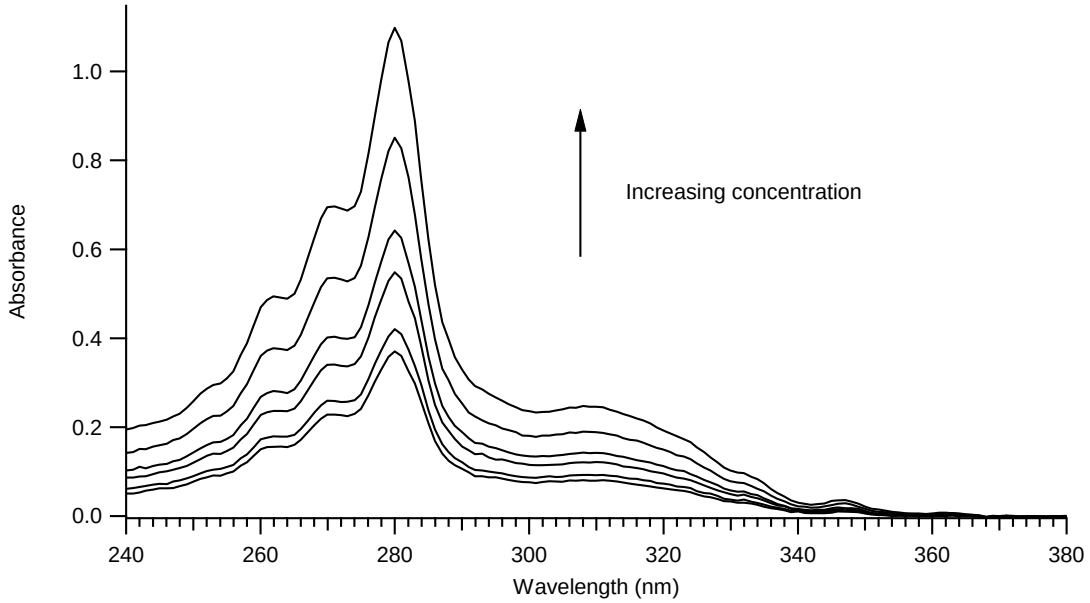

Figure 2.6: Absorption spectra of TP6 in DCM. Concentrations from 3.22 to 9.49 µM.

TP6 obeys the Beer Lambert law, as the concentration increases linearly with the concentration (Figure 2.7). A molar extinction coefficient of ε = 1.16 x 10^5 $M^{-1}.cm^{-1}$ was calculated at 280 nm. The constant molar extinction coefficient suggests that TP6 does not aggregate in DCM. These results are in accordance with the literature.[100,101]

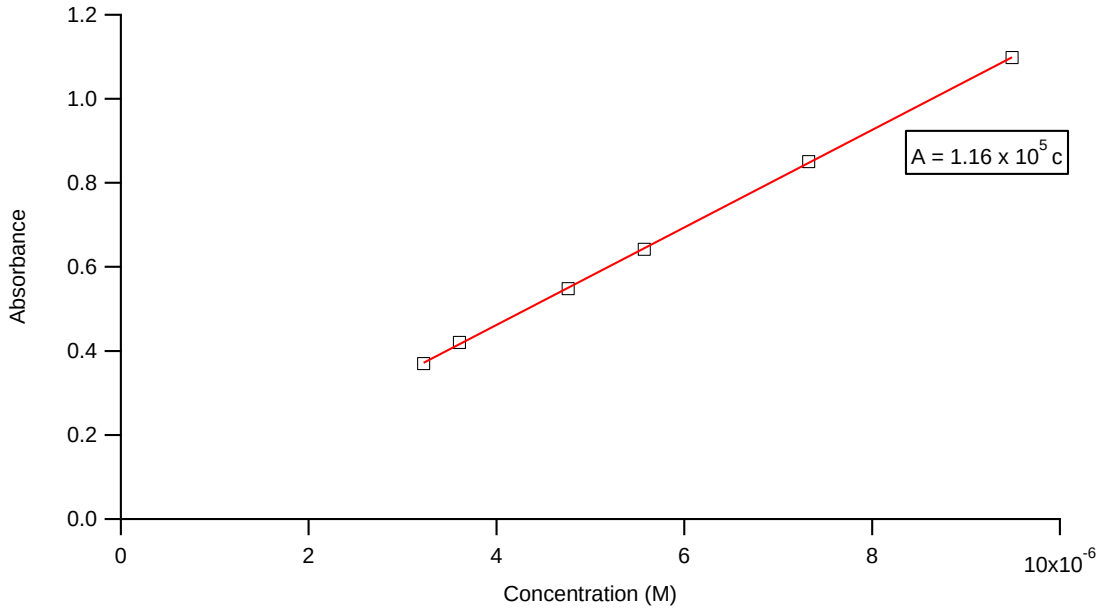

Figure 2.7: Absorbance at 280 nm *vs* concentration in DCM of TP6.

2.3.2 Ethylene glycol-based triphenylenes - TP6EOnM (n = 2, 3, 4)

2.3.2.1 Synthesis of TP6EOnM (n = 2, 3, 4)

The synthesis of triphenylene derivatives *via* the direct functionalization of catechol followed by trimerisation is unfortunately limited to the synthesis of alkoxy-substituted triphenylenes.[92] An alternative strategy was therefore used (Scheme 2.7). Hexasubstituted triphenylene, such as ethylene glycol based triphenylene **49a-c**, can also be obtained from the 2,3,5,6,10,11-hexahydroxytriphenylene building block **47**. **47** is derived from 2,3,5,6,10,11-hexamethoxytriphenylene **46** by functional group interconversion (FGI) which is easily synthesised *via* the *Scholl* type reaction of veratrole.

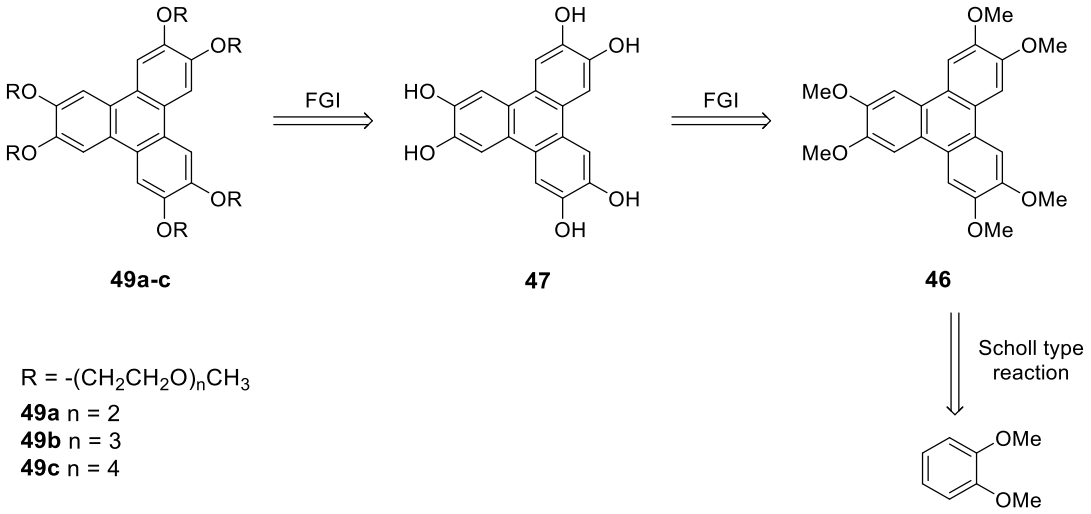

Scheme 2.7: Alternative retrosynthesis to hexasubstituted triphenylenes.

The synthesis of TP6EOnM (n = 2, 3, 4) **49a-c** was therefore carried out following this strategy (Scheme 2.8).[92] **46** was synthesised *via* oxidative cyclodehydrogenation using iron(III) chlroride as the oxidant in a 78% yield. The cleavage of the methyl groups was carried out using a 1:1 mixture of glacial acetic acid and hydrobromic acid. **47** was then substituted with the mesyl-activated ethylene glycol monomethyl chains **48a-c** *via* a *Williamson* type ether synthesis to obtain the desired TP6EOnM derivatives. Due to the high hydrophilicity of the

ethylene glycol chains, purification of these derivatives is tedious and leads to poor yields, respectively 30%, 35% and 30% for **49a**, **49b** and **49c**.

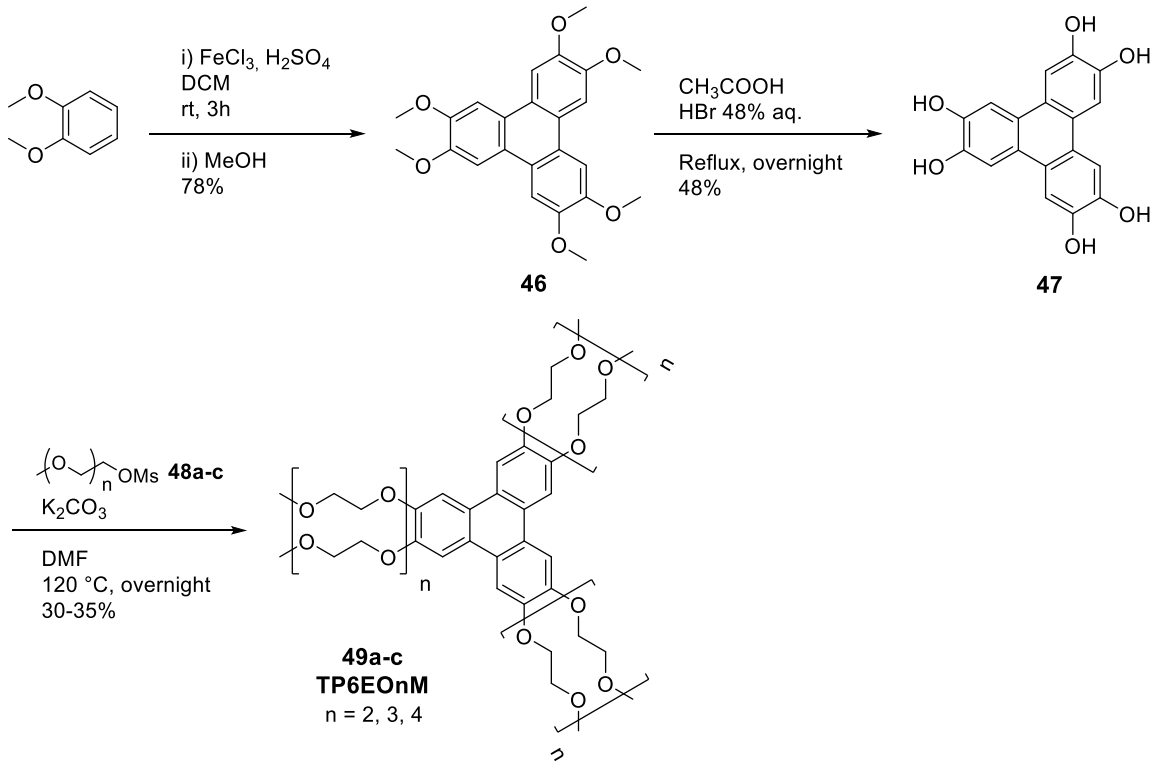

Scheme 2.8: Synthesis of TP6EOnM derivatives (n = 2, 3, 4).

2.3.2.2 Characterisation of TP6EOnM (n = 2, 3, 4) derivatives.

The characterisation of TP6EOnM was carried out by POM and X-ray diffraction. At room temperature, TP6EO2M forms needle-like crystals, as shown by POM (Figure 2.8). At 52 °C, a Cr-I transition is observed. TP6EO2M does not show any thermotropic properties, as no liquid crystalline phases could be observed on heating the neat sample.

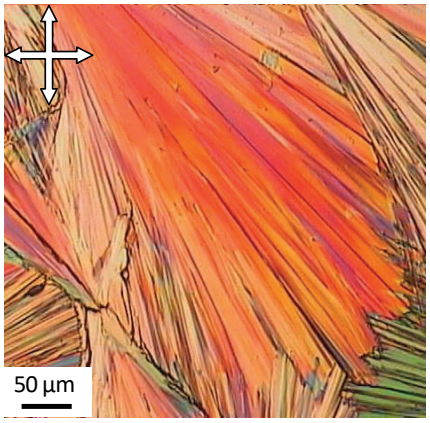

Figure 2.8: POM image of TP6EO2M at room temperature on cooling: needle-like crystalline phase.

The X-ray diffraction pattern at room temperature shows multiple diffraction peaks, indicative of a crystalline arrangement and therefore confirms our hypothesis (Figure 2.9). Above 60 °C, no diffraction peaks are observed. The results are in accordance with the literature.[92,102,103]

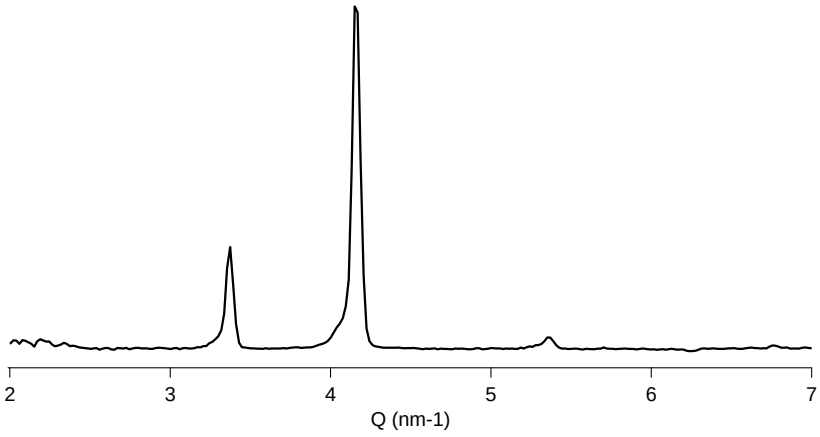

Figure 2.9: X-ray diffraction pattern of crystalline TP6EO2M at 25 °C.

However, TP6EO3M and TP6EO4M are liquid at room temperature. Indeed, the increased chain lengths induce more flexibility and less π-π interaction between the aromatic cores, therefore decreasing their melting point.

2.3.2.3 Aggregation of TP6EOnM (n = 2, 3, 4) in solution

The work presented in this section has been published.[104]

The absorption spectra of TP6EO2M and its homologues TP6EO3M and TP6EO4M were compared. At a concentration of 2.5 x 10^{-6} M (Figure 2.10), the absorption bands are identical: the maximum absorption is located at 276 nm and a broad absorption band located at 306 nm which are respectively attributed to the S_0-S_4 and S_0-S_3 transitions.[105] However, the absorbance is highly dependent on the length of the surrounding chains, indicating the aggregation of TP6EOnM in water.

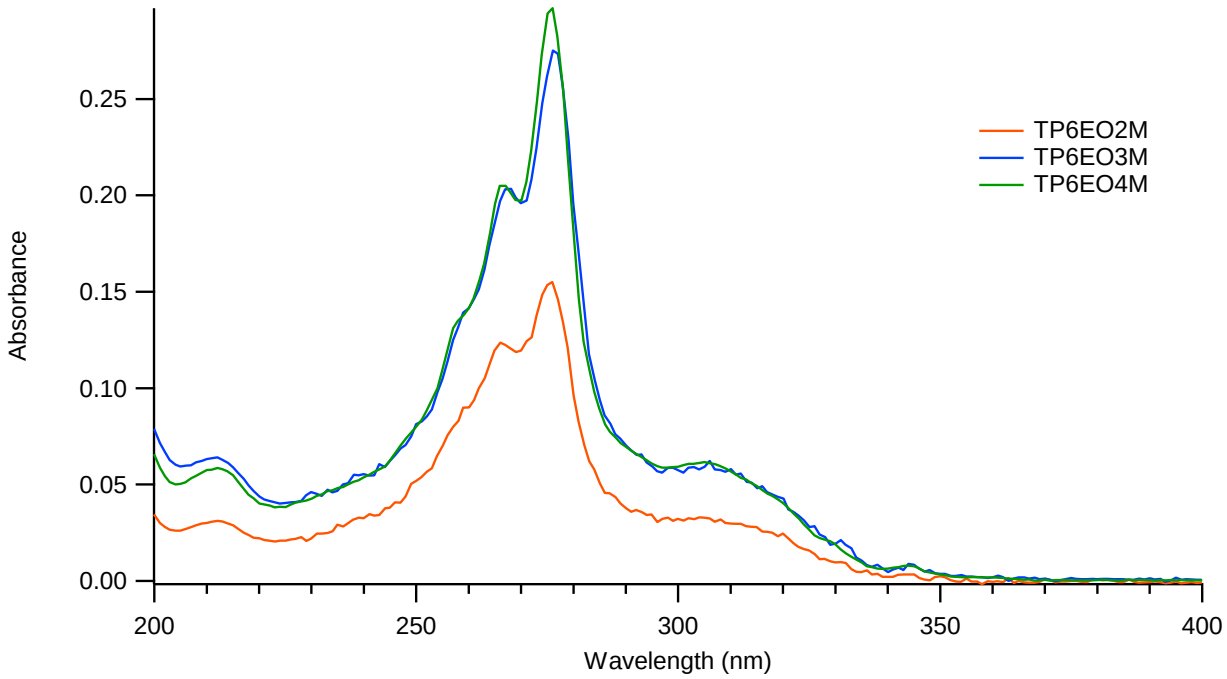

Figure 2.10: Absorption spectra of TP6EO2M (Red), TP6EO3M (blue) and TP6EO4M (green) in water at 2.5 x 10^{-6} M.

Whilst TP6EOnM does not show any thermotropic properties, they behave as chromonic liquid crystals in aqueous solvents. Theoretical studies as well as experimental studies on the chromonic properties of TP6EO2M have been investigated.[106–114] However, limited studies in low concentration was provided.[114]

TP6EOnM derivatives have the same aromatic core and therefore the same photophysical properties. We have therefore decided to study the aggregation process in diluted TP6EOnM (n = 2, 3, 4) solutions by UV-visible spectroscopy: the absorbance spectra of a wide range of concentration will be recorded and the effect of the concentration on the molar extinction coefficient ε will be presented. Using the theory of aggregation described in section 1.3.3 and in the appendix, the effect of the chain length will be discussed.

The aggregation of TP6EOnM in aqueous solution has been investigated at low concentration (from 10^{-7} to 10^{-4} M). Due to the very low concentration, extra care on the purity of the samples is needed. Although all the TP6EOnM derivatives are NMR grade pure, analytical HPLC of TP6EO2M reveals the presence of impurities with close retention times (33.4min, 34.6 min and 34.8 min, Figure 2.11). The side-products have been determined by mass spectrometry and have been ascribed to respectively the 2-monohydroxy **50**, the 2-methoxy 3,5,6,10,11-hexahydroxytriphenylene **51** and TP6EO2M. Similar HPLC chromatogram were obtained for TP6EO3M and TP6EO4M. TP6EOnM were nevertheless obtained in HPLC pure grade by purifying by preparative HPLC on reverse C_{18} phase.

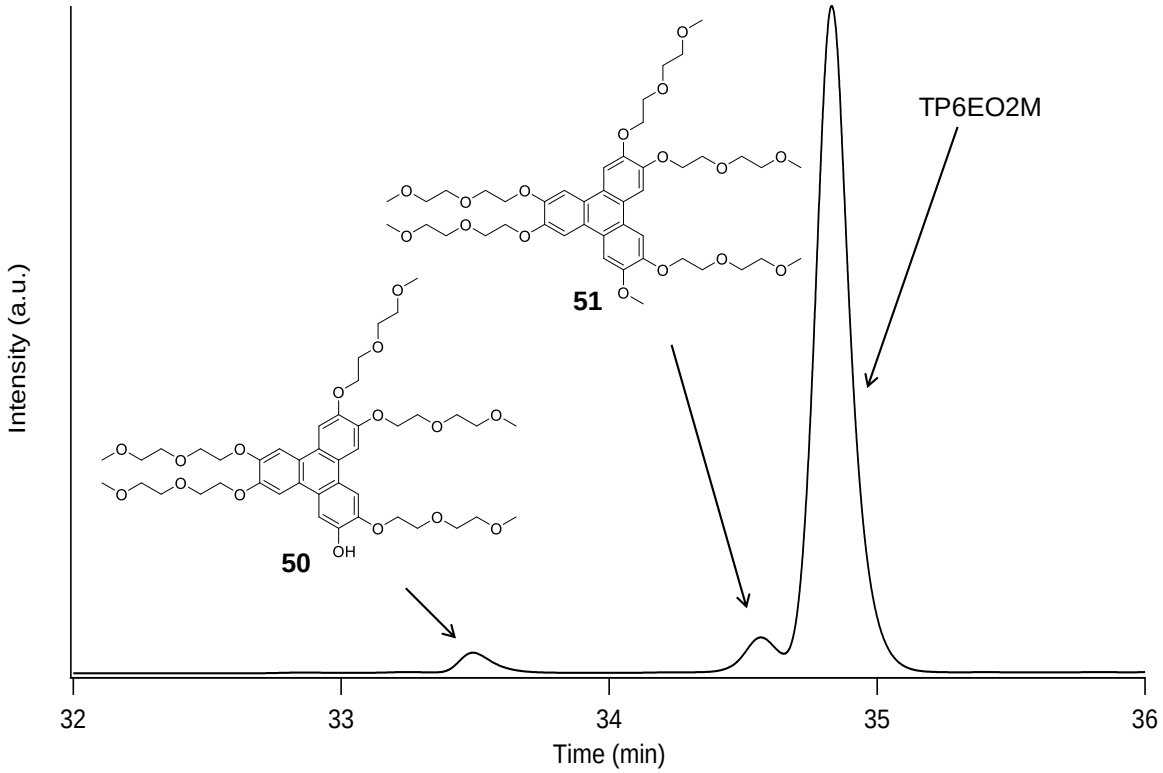

Figure 2.11: Analytical reverse phase C18-HPLC chromatograph of TP6EO2M (retention time = 34.8 min) using H_2O:MeOH gradient (0-100% MeOH over 60 min) after purification by column chromatography. Detection wavelength = 254 nm.

To observe the effect of the impurity on the aggregation behaviour, the aggregation of two different TP6EO2M grades was first investigated by UV-Visible spectroscopy: the technical grade TP6EO2M which contains a small fraction of **51** and the HPLC grade TP6EO2M (Figure 2.12). All the molar extinction coefficients were calculated at λ_{max} = 276 nm. While both grades behave similarly at concentration above 4 x 10^{-6} M, drastic change at low concentration is observed (< 2 x 10^{-6} M). Technical grade TP6EO2M has an abnormal behaviour as the molar extinction coefficient decreases dramatically as the concentration decreases, indicating the formation of longer aggregates. This behaviour is reproducible and error in dilution or measurement can be excluded. The impurity **51** is considered as less hydrophilic than TP6EO2M as it contains one methoxy group instead of one ethylene glycol based chain. At high dilution, the more hydrophobic impurity is strongly aggregating due to the disfavoured

interaction with the solvent molecules. However, at higher concentration when longer aggregates are in solution, the methoxy group is less accessible by the water molecules as ethylene glycol-based chains are predominant in the aggregate. The impact of the impurity is therefore greatly reduced. It is therefore essential that the TP6EOnM derivatives has to be HPLC pure to avoid any abnormal behaviour of the aggregation in very dilute solutions.

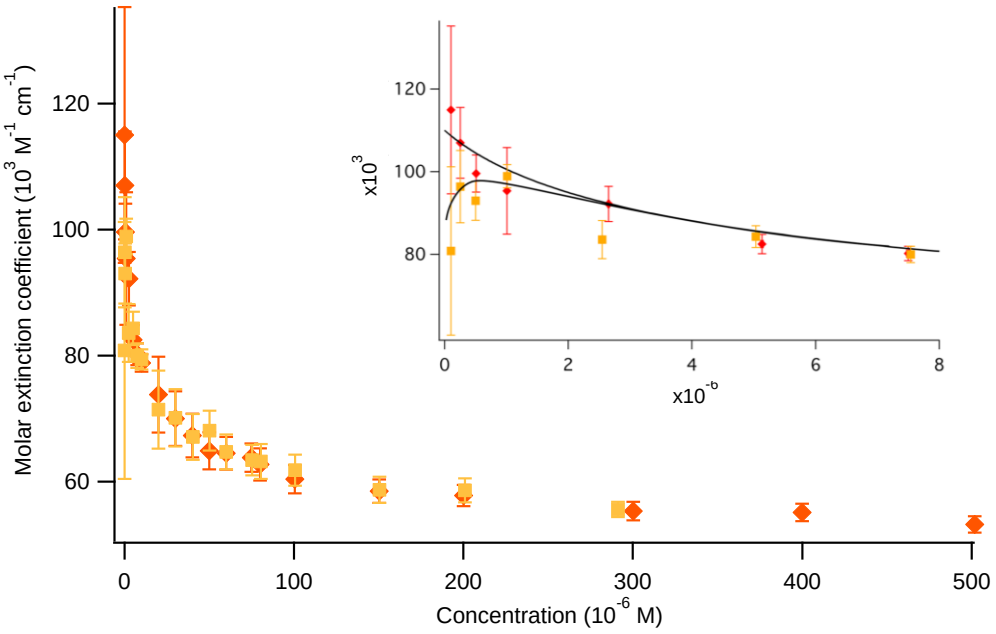

Figure 2.12: Molar extinction coefficient at 276 nm as a function of the concentration in water for HPLC grade TP6EO2M (red diamonds) and technical grade TP6EO2M (orange squares).

The extinction coefficients were calculated at λ_{max} = 276 nm and plotted versus the concentration for the HPLC grade TP6EOnM (n = 2, 3, 4) derivatives (Figure 2.13). Compared to the hydrophobic TP6 (see section 2.3.1.3), no linear behaviour is observed as the molar extinction coefficient increases as the concentration decreases. The TP6EOnM derivatives are therefore aggregating in solution and are chromonic liquid crystals, which is in accordance with the previous literature on TP6EO2M.[109]

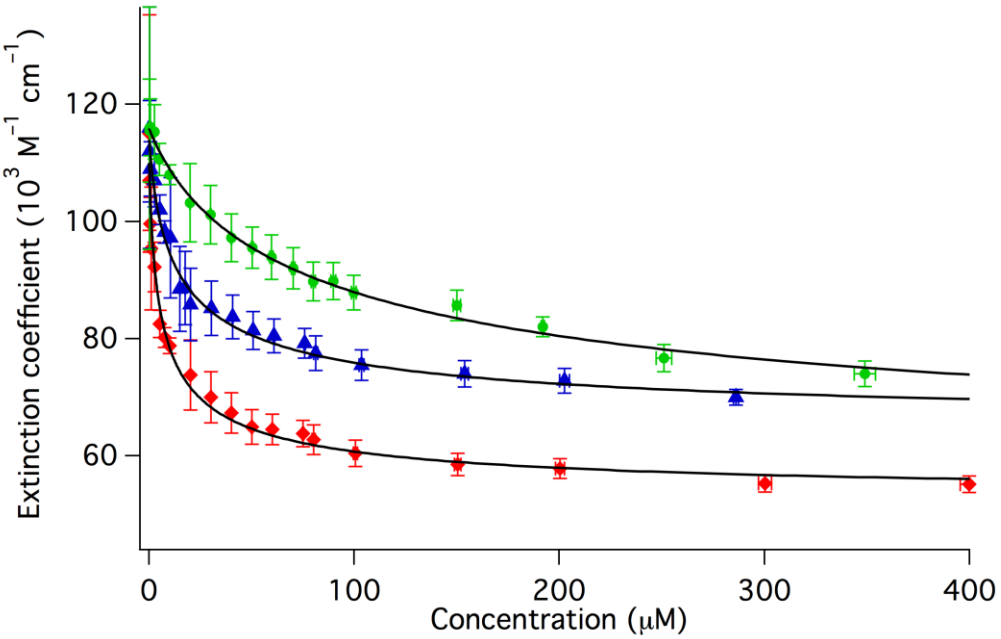

Figure 2.13: Molar extinction coefficient at 276 nm as a function of the concentration in water for HPLC grade TP6EO2M (red diamonds), TP6EO3M (blue triangles) and TP6EO4M (green circles).

By using the theory of aggregation described by Israelachvili (see Appendix), the bond energy α between two molecules in the aggregate, the absorption coefficient of the monomer ε_{mono} and the coupling constant of the exciton β can be extracted by fitting with the experimental study. Results are summarised in Table 2.1. As the chain length increases, the value of α decreases, indicating that the formation of aggregates is less favourable. The α value for TP6EO2M are in accordance with the literature, in both NMR aggregation study[114] (α = 14 kT) and simulation study[106] (α = 14.7 kT). This means that for a given concentration, as the length of the peripheral chains increases, the size of the aggregate decreases. Indeed, longer ethylene glycol-based chains increases the hydrophilicity of TP6EOnM derivatives. TP6EO4M is therefore interacting more with the water molecules than its homologues TP6OE3M and TP6EO2M, hence disfavouring the aggregation process.

At very low concentration (*ca.* 10^{-7} M), the experimental molar extinction coefficient of the TP6EOnM derivatives are similar. This suggest that the triphenylene core does not aggregate

in this range of concentration. This is supported by the fitting parameters ε_{mono} calculated using the isodesmic model

The isodesmic model shows its limitation at low concentration. Indeed, the experimental molar extinction coefficient decreases faster than the fitting curve. This shows that the isodesmic model is not adapted to high diluted solutions. The assumption that the energy of adding one monomer into the aggregate does not depend on the size of the aggregate is therefore verified experimentally.

	α (kT)	**β**	**ε_{mono} (10^3 M^{-1} cm^{-1})**
TP6EO2M	12.6 ± 0.2	-28600 ± 1000	110 ± 2
TP6EO3M	11.4 ± 0.2	-24600 ± 800	114 ± 2
TP6EO4M	9.3 ± 0.2	-29800 ± 1000	116 ± 2

Table 2.1: Fitting parameters for the molar exticntion coefficent of TP6EOnM (n = 2, 3, 4) in water.

To conclude, the aggregation study of TP6EOnM (n = 2, 3, 4) was carried out experimentally by UV-Visible spectroscopy and the results fitted using an isodesmic aggregation model. As the chain length increases, the bond energy between two aromatic cores decreases. Therefore, at a given concentration, smaller aggregates are observed as the chain length increases. At very dilute solution, the isodesmic model does deviate from the experimental value. It has therefore been shown that the isodesmic model does not apply to very small aggregates and that the energy of dimerization is higher than the energy to add a monomer to a larger aggregate. These results could be used in the context of solar cell. Indeed, a high absorption coefficient is needed to absorb the solar radiations. The use of long flexible chains in the dye could therefore be of use, as smaller aggregates are formed and high absorption coefficients are reached.

2.4 Investigation of the compatibility between TP6 and TP6EO2M

Two triphenylene derivatives types were successfully synthesised: the hydrophobic TP6 and the hydrophilic TP6EOnM (n = 2, 3, 4) derivatives. We believe that the immiscibility of the surrounding chains will induce the incompatibility between the two triphenylene analogues. Investigation on the compatibility of TP6 and TP6EO2M will be discussed in this section.

In order to investigate the mixing behaviour of a TP6 and TP6EO2M over the full composition range, contact study was investigated (Figure 2.14). Over the clearing point of both of the materials (Figure 2.14a), macrophase separation between TP6 and TP6EO2M is clearly seen. On cooling down from the isotropic state, no new phases were observed and the transition temperatures are in agreement with the transition temperatures of the pristine materials, *i.e.* 92 °C and 55,5 °C for TP6 (Figure 2.14b and c respectively), and 41 °C for TP6EO2M (Figure 2.14d). This experiment therefore indicates that TP6 and TP6EO2M does not mix together over the whole range of composition. Is should be noted that at room temperature, TP6EO2M crystals are orienting (Figure 2.14d) and is due to surface effect.

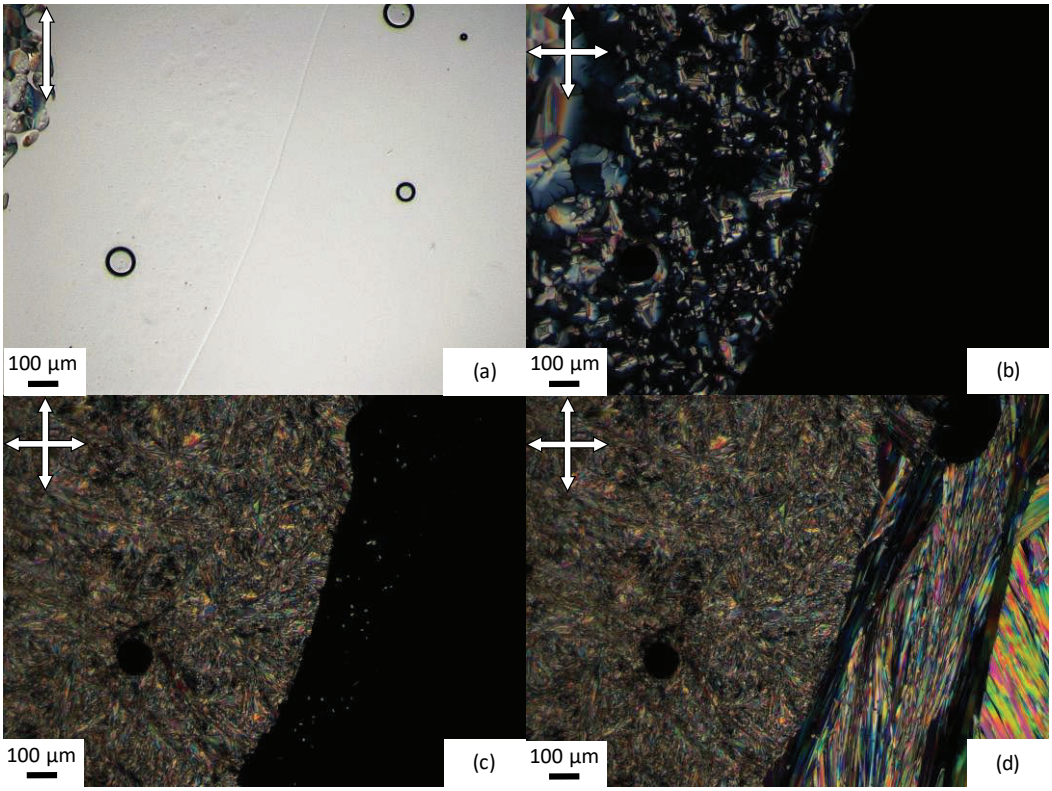

Figure 2.14: POM images of a contact sample of TP6 (left) and TP6EO2M (right) on cooling (2 °C/min): at (a) 98 °C; (b) 92 °C; (c) 55.5 °C; (d) 41 °C.

An equimolar TP6:TP6EO2M blend was also prepared and studied by POM (Figure 2.15), DSC (Figure 2.16) and X-ray diffraction (Figure 2.17). As expected by the polarity difference of the pendent chains of the two triphenylene derivatives, the TP6 and TP6EO2M macrophase separate. Indeed, two relatively large distinct domains can be observed in the POM images over the whole range of temperature (Figure 2.15). In the isotropic state (Figure 2.15a), two liquid immiscible phases are clearly seen. Upon cooling (Figure 2.15b), one of the isotropic phase becomes liquid crystalline then crystalline. At room temperature (Figure 2.15c), two different crystalline phases are observed. The DSC curve of this binary mixture (Figure 2.16) can be described as the sum of the contribution from the pure TP6 and the pure TP6EO2M. The two domains are therefore composed exclusively of pure TP6 and pure TP6EO2M and the components are not interacting with each other.

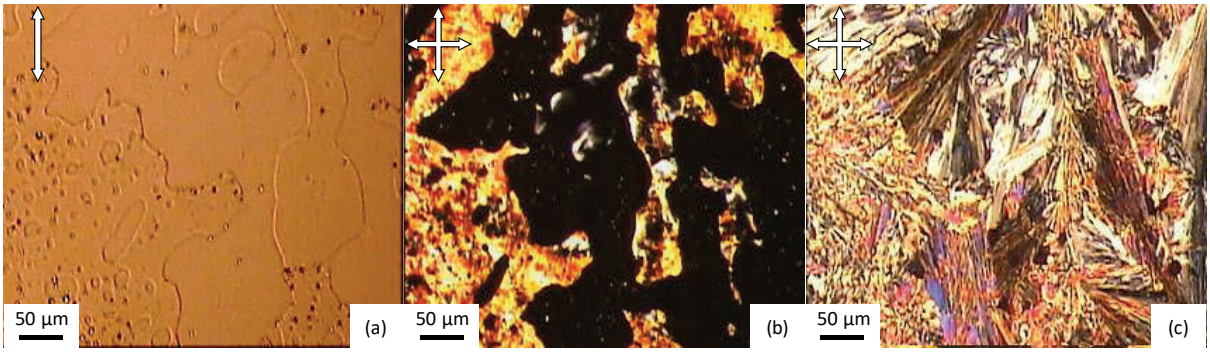

Figure 2.15: TP6: TP6EO2M equimolar mixture: (a), (b) and (c) POM images on cooling at 90 °C, 50 °C, 25 °C.

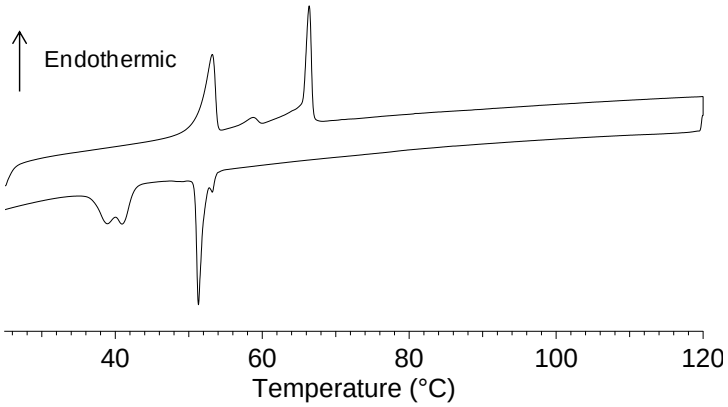

Figure 2.16: DSC curves on 2nd heating/cooling cycle.

The X-ray diffraction pattern supports this result (Figure 2.17). Indeed, at room temperature (Figure 2.17 f), the diffraction pattern of the binary mixture is composed of the diffraction peaks of both the crystalline TP6 phase (highlighted in red) and the crystalline TP6EO2M (highlighted in blue). On heating above the transition temperature of TP6EO2M (T = 60 °C) (Figure 2.17 e), the X-ray diffractogram consists exclusively of the diffraction pattern of crystalline TP6 while above the Cr-Col_h transition temperature of TP6 (Figure 2.17 d) the main peak corresponds to the pure TP6 Col_h phase (highlighted in green).

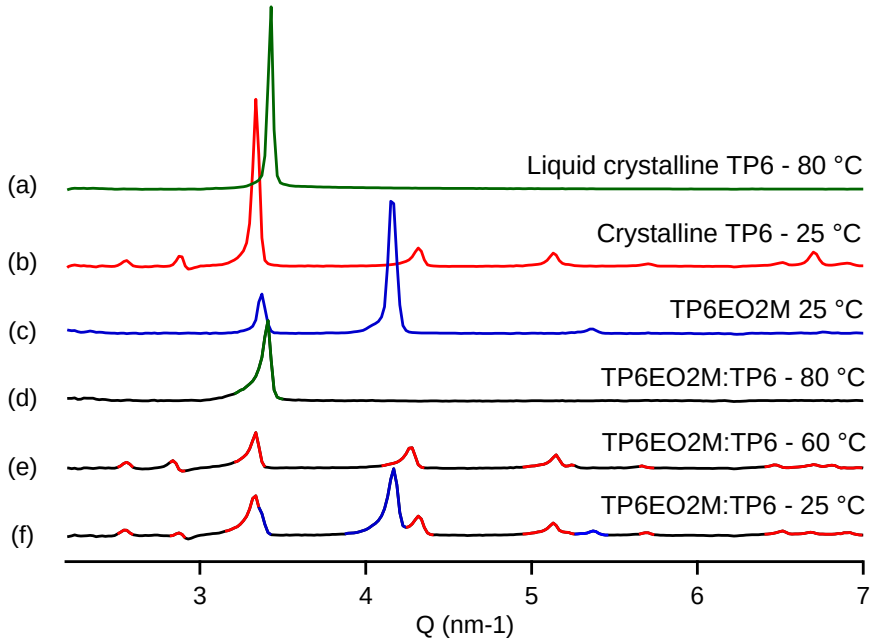

Figure 2.17: SAXS pattern of (a) TP6 at 80 °C (Col_h phase), (b) TP6 at 25 °C (Cr phase), (c) TP6EO2M at 25 °C (Cr phase) and a TP6:TP6EO2M equimolar mixture at (d) 80 °C, (e) 60 °C and (f) 25 °C.

To conclude, a triphenylene derivative composed of a hydrophobic hexyloxy pendant chain, TP6, and triphenylene derivatives composed of ethylene glycol based motifs, TP6EOnM (n = 2, 3, 4) were prepared and their full characterisation and aggregation studied. No mixing was observed over the whole range of composition. More specifically, mixing the hydrophobic TP6 and the hydrophilic TP6EO2M in an equimolar ratio results in a large macrophase separation: no miscibility is observed across the whole range of temperature and the two domains are composed of the pure materials. TP6 and TP6EO2M are therefore fully incompatible and are considered as a perfect binary mixture to control the morphology by adding a third compound.

Chapter three:

Compatibilisation of model compounds: morphology control of TP6:TP6EO2M

3.1 Aims and objectives

As discussed in the previous chapter, the hydrophobic TP6 and the hydrophilic TP6EO2M does not mix and are considered to be incompatible. This chapter focuses on the synthesis of tailor-made compatibilisers to suppress their incompatibility.

As a first simple compatibiliser, a surfactant composed of an aliphatic alkyl chain covalently linked to an ethylene glycol monomethyl ether chain was designed and its effect on the equimolar TP6:TP6EO2M blend discussed. Our efforts focussed next on a design and effect of functional compatibilisers based on a covalently linked hydrophobic and hydrophilic moieties.

3.2 C6E3M as a compatibiliser

3.2.1 Synthesis of C6E3M

As an obvious surfactant-like compatibiliser based on the pendent chains of TP6 and TP6EO2M, the compound C6E3M, **52** presented in Figure 3.1 was designed.

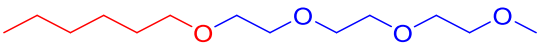

Figure 3.1: Structure of C6E3M, **52**.

Composed of an hexyloxy moiety covalently linked to a triethylene glycol monomethyl ether aliphatic chain, this surfactant can be synthesised easily on a multi-gram scale. Derived from the well-known class of CnEm surfactant, with n defining the number of carbon atoms in the hydrophobic tail and m the number of ethylene glycol motifs, this non-ionic class of material has been studied and used for its surfactant, wetting and foaming properties.[115,116]

We therefore decided to base our first study on C6E3M as a compatibiliser. Unlike the CnEm family a terminal methyl group was added at the end of the ethylene glycol moiety to avoid

any H-bonding and facilitate our study. Previously reported in the literature, C6E3M has displayed interesting properties as a lithium cation based ionic liquid.[117]

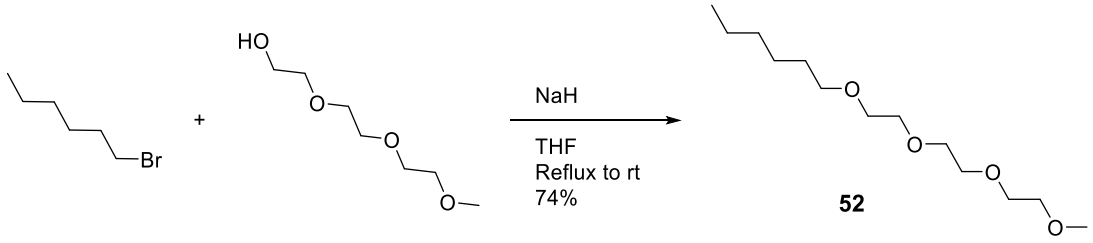

Scheme 3.1: Synthesis of C6E3M, **52**.

The synthesis of **52** (called C6E3M here) was carried out *via* the *Williamson* reaction between 1-bromohexane and the deprotonated triethylene glycol monomethyl ether (Scheme 3.1). After high vacuum distillation, C6E3M was afforded in a 74% yield as a light yellow liquid.

3.2.2 Effect of C6E3M on the TP6:TP6EO2M mixture

The effect of C6E3M on an equimolar mixture of TP6:TP6EO2M was investigated by POM at two different molar concentrations (TP6:TP6EO2M):C6E3M = 50:50 and 50:150 (*i.e* 50mol% and 150mol% of C6E3M into the equimolar blend of TP6:TP6EO2M).

At 50mol% of C6E3M in the equimolar mixture of the incompatibles, the POM images show two large domains over the all range of temperature (Figure 3.2). It is worth noting that the domains appear smaller than the undoped TP6:TP6EO2M blend (see section 2.4). At room temperature, the two domains are composed respectively of a crystalline component and a liquid matrix containing small crystals. Above 48 °C, the purely crystalline domain melted while at an estimated temperature of 75 °C, the blend is fully isotropic. By comparing the transition temperatures to those from the equimolar undoped TP6:TP6EO2M, (Table 3.1) it is thought that the two domains are composed of a TP6EO2M phase and a C6E3M:TP6 phase. Indeed, the transition temperature of the blend containing C6E3M are closed to the one from

the undoped mixture. The low transition temperature of 75 °C (compared to the Col_h-I transition temperature of 88 °C for pure TP6) can be explained by the compatibility between C6E3M and TP6. Is it worth noticing that the Cr-Col_h transition of TP6 could not be observed in POM.

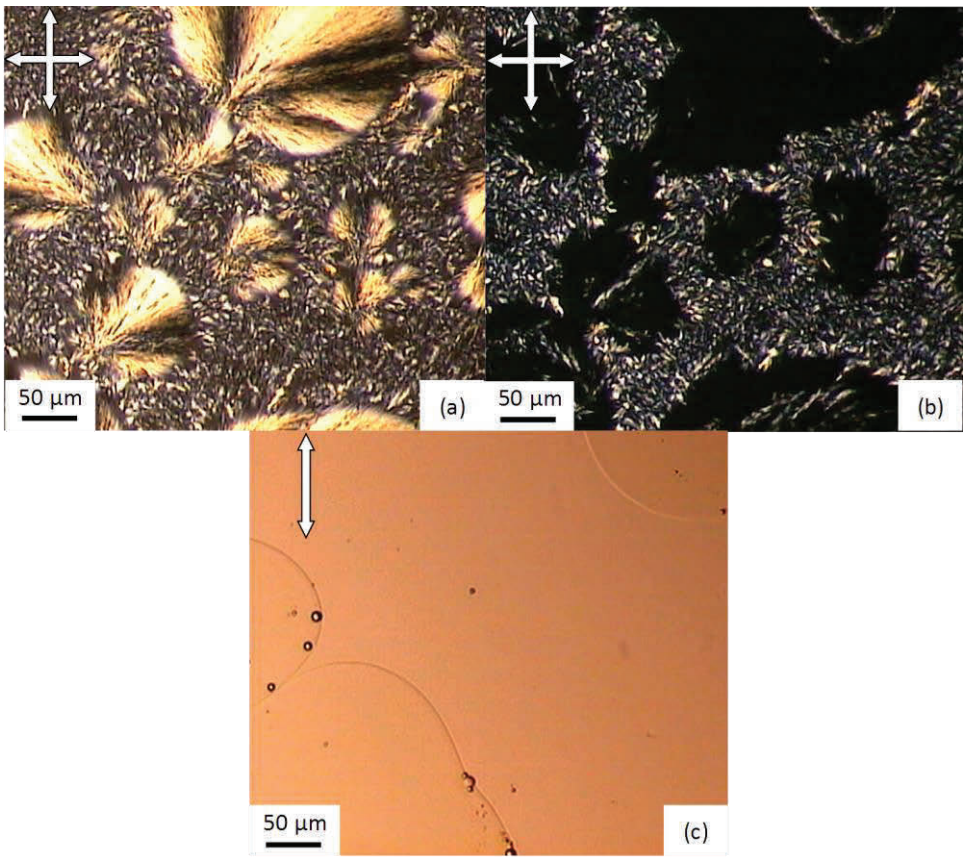

Figure 3.2: POM images of a TP6:TP6EO2M equimolar mixture with 50 mol% C6E3M on heating: (a) at 25 °C; (b) at 55 °C; (c) at 80 °C.

At a molar ratio of (TP6:TP6EO2M):C6E3M = 50:150, the texture of the blend changes dramatically (Figure 3.3). The formation of interpenetrated needle-like crystals into a liquid-like matrix is observed at room temperature. At around 35 °C, these crystals melted. Interestingly, above the clearing point of the mixture (*ca.* 70 °C), only one isotropic phase is observed. The transition temperatures are again lower than the TP6:TP6EO2M binary blend.

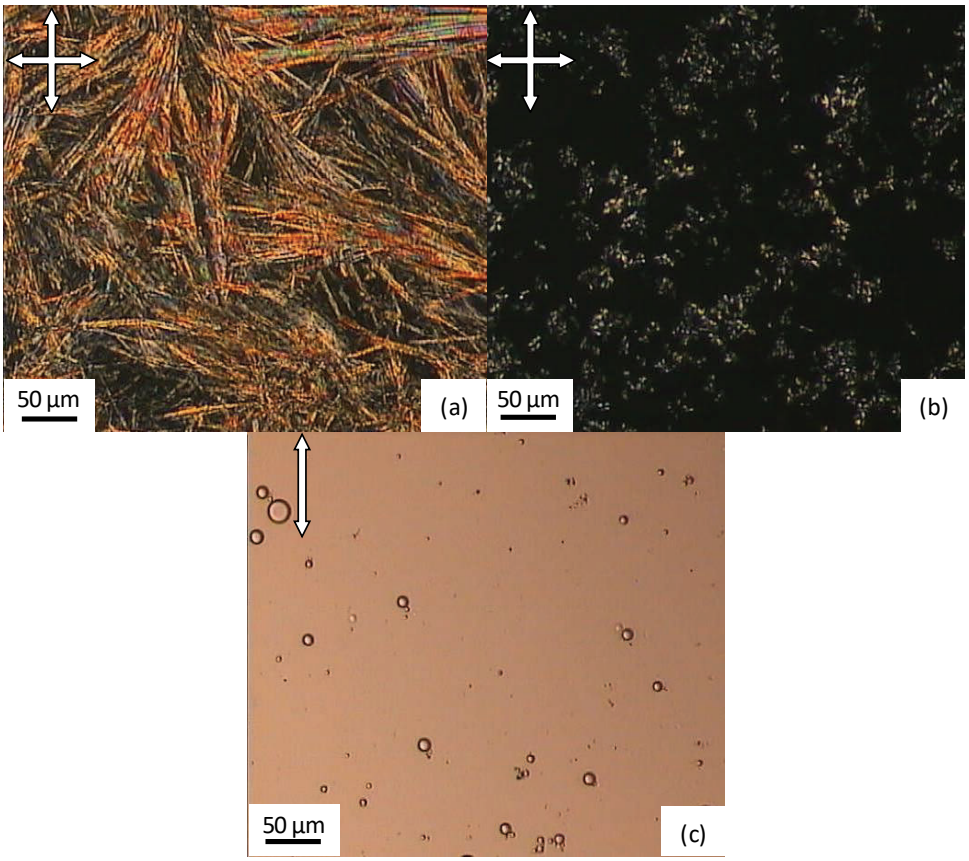

Figure 3.3: POM images of a TP6:TP6EO2M equimolar mixture with 150 mol% C6E3M on heating at: (a) 20 °C; (b) 45 °C; and (c) 80 °C.

C6E3M has unambiguously an impact on the morphology of the TP6:TP6EO2M blend. Indeed, the large macrophase segregation observed is supressed on adding a small amount of C6E3M (50mol%) to obtain smaller domains. The most interesting result is shown with 150mol% C6E3M. Indeed, an interpenetrating crystalline phase into a liquid-like matrix is observed, indicating a micro to nano-phase segregation. Above the clearing point of the blend, one singular isotropic phase is seen. This proves that C6E3M acts as a compatibiliser. The concept of compatibilising a binary triphenylene-based mixture is therefore verified by using C6E3M.

It is worth mentioning that the transition temperatures are only estimated. DSC study and X-ray diffraction would be an interesting characterisation to perform to obtain precisely the transition temperature and the composition of the phases.

TP6: TP6EO2M		TP6:TP6EO2M:C6E3M (50 mol%)		TP6:TP6EO2M:C6E3M (150 mol%)	
2nd heating	**Transition**	**2nd heating**	**Transition**	**2nd heating**	**Transition**
51 (21)	Cr-I (TP6EO2M)	48 [a]	Cr-I	35 [a]	Cr-I
66 (17)	Cr-Col_h (TP6)	75 [a]	X - I	70 [a]	X-I
88	Col_h-I (TP6)				

Table 3.1: Phase transition temperatures (°C) and enthalpies (in brackets, J/g) determined by DSC. Phases were determined by POM and XRD. [a] determined by POM. X: unknown phase.

To conclude, C6E3M has been successfully used as a compatibilising agent to suppress the macrophase separation occurring in TP6:TP6EO2M. Indeed, a micro phase segregation between the two incompatible have been observed when adding 150mol% into the equimolar blend. Despite its beneficial effect, this compatibiliser is only composed of aliphatic chains and is purely acting as a structural additive. Moreover, an high amount of C6E3M is needed. Our efforts focussed next on more complex and functional dyads composed of a triphenylene core.

3.3 Efforts towards the synthesis of TP6-TP6EO2M

As a functional and more complex compatibiliser for the TP6:TP6EO2M equimolar mixture, we targeted an amphiphilic dyad composed of a hydrophobic triphenylene-based moiety covalently linked to a hydrophilic triphenylene-based moiety *via* an alkyl spacer. The attempted synthesis of this compatibiliser, named TP6-TP6EO2M (Figure 3.4) will be described.

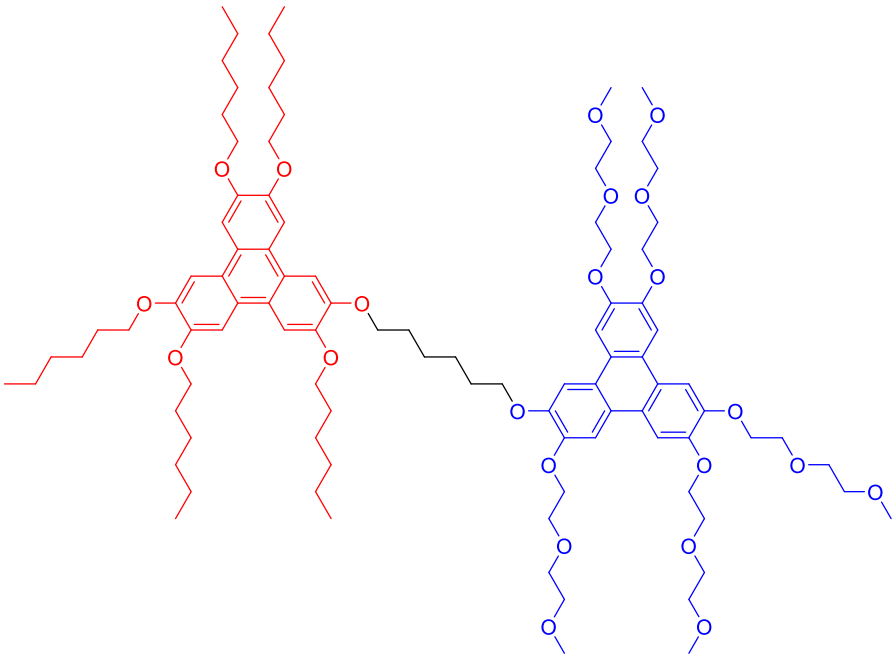

Figure 3.4: Target compatibiliser: TP6-TP6EO2M.

We envisaged that TP6-TP6EO2M could be obtained from a convergent synthesis between the two unsymmetrical hydrophobic and hydrophilic triphenylene derivatives (Scheme 3.2). The key intermediates, which contain a hydroxy group for an easily coupling can be obtained *via* the biphenyl phenyl oxidative coupling between a tetrasubstitued biphenyl and a 1-isopropoxy-2-alkylatedbenzene.[118] The isoproxy group is used as protective group and leads to the desired hydroxyl during the oxidative coupling, following the mechanism described in Scheme 3.3.

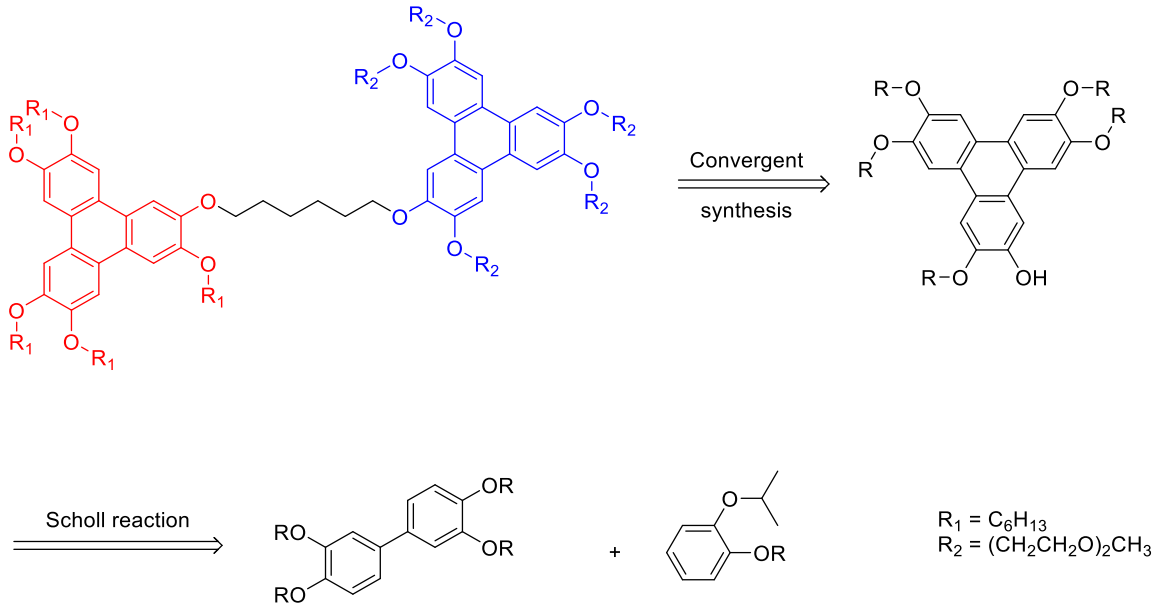

Scheme 3.2: Retrosynthesis of TP6-TP6EO2M.

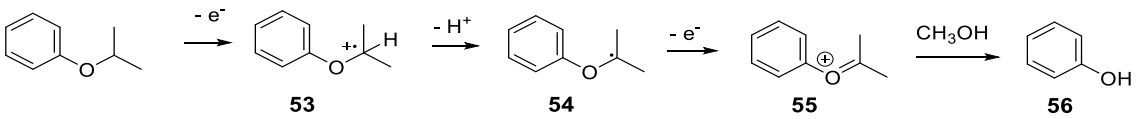

Scheme 3.3: Mechanism of oxidative cleavage of isopropoxy group.[118]

3.3.1 Synthesis of the building blocks

The 3,3',4,4'-tetrasubstituted biphenyls **59a-b** were synthesised *via* a *Suzuki* coupling between the commercially available 1-bromo-3,4-dimethoxybenzene and 3,4-dimethoxyboronic acid affording the biphenyl **57** in an 80% yield (Scheme 3.4). After cleaving the methoxy group using a mixture of acetic acid and a 48% hydrobromic acid solution, **58** was reacted with 1-bromohexane or **48a** under a *Williamson* type reaction to afford the desired 3,3',4,4'-tetrasubstitued biphenyl **59a** or **59b** with a respective overall yield of 47% or 13%. The lower yield observed for **59b** can be explained by the difficulty of purification by column chromatography, due to the high retention of the compounds on silica or alumina.

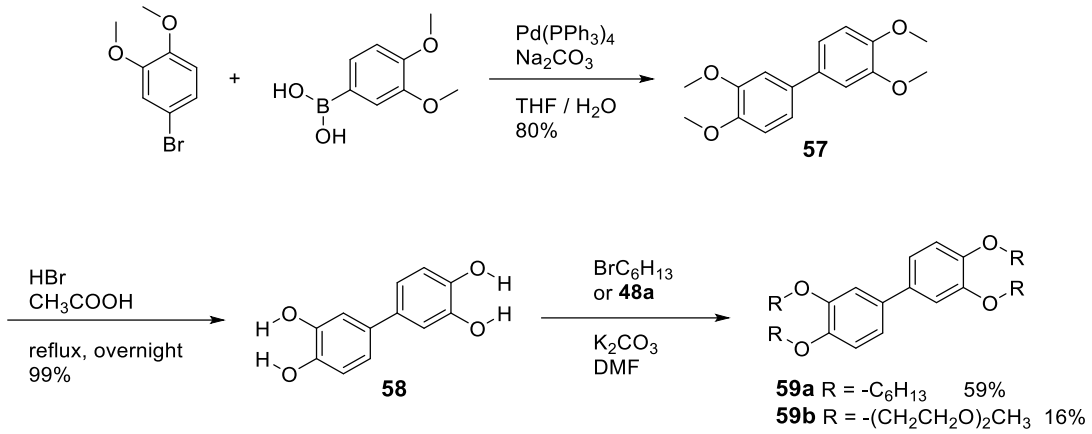

Scheme 3.4: Synthesis of 3,3',4,4'-tetrasubstituted biphenyl **59a-b**.

The synthesis of 1-isopropoxy-2-substituted phenyls **61a-b** were carried out in two steps (Scheme 3.5). The mono-alkylation with the corresponding 1-bromohexane or the mesylated diethyleneglycol monomethyl ether **48a** followed by the subsequent substitution with 2-bromopropane afforded the two mono isopropoxy protected mono-alkylated benzene **61a** and **61b** in a respectively 32% and 4% overall yield.

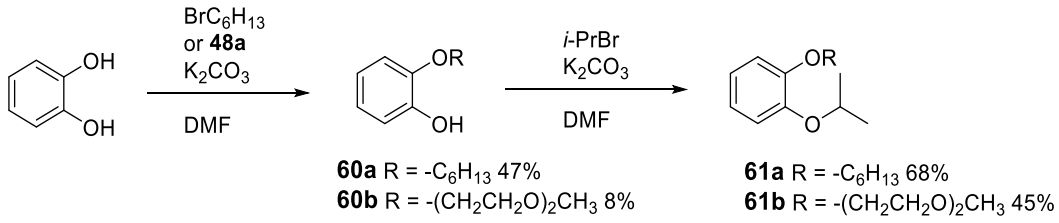

Scheme 3.5: Synthesis of 1-isopropoxy-2-alkylatedbenzene.

Facing a low conversion towards **61b**, we investigated the benefit of a one-pot synthesis (Scheme 3.6). The yield was increased to 22%.

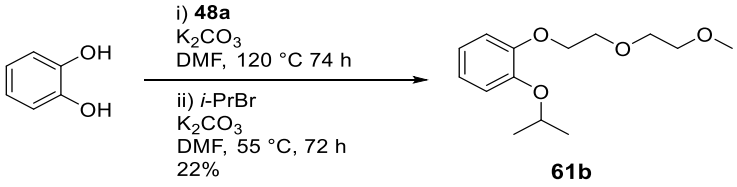

Scheme 3.6: One pot synthesis of 1-isopropoxy-2-(1,4,7-trioxaoctyl)benzene **61b**.

3.3.2 C-C oxidative coupling

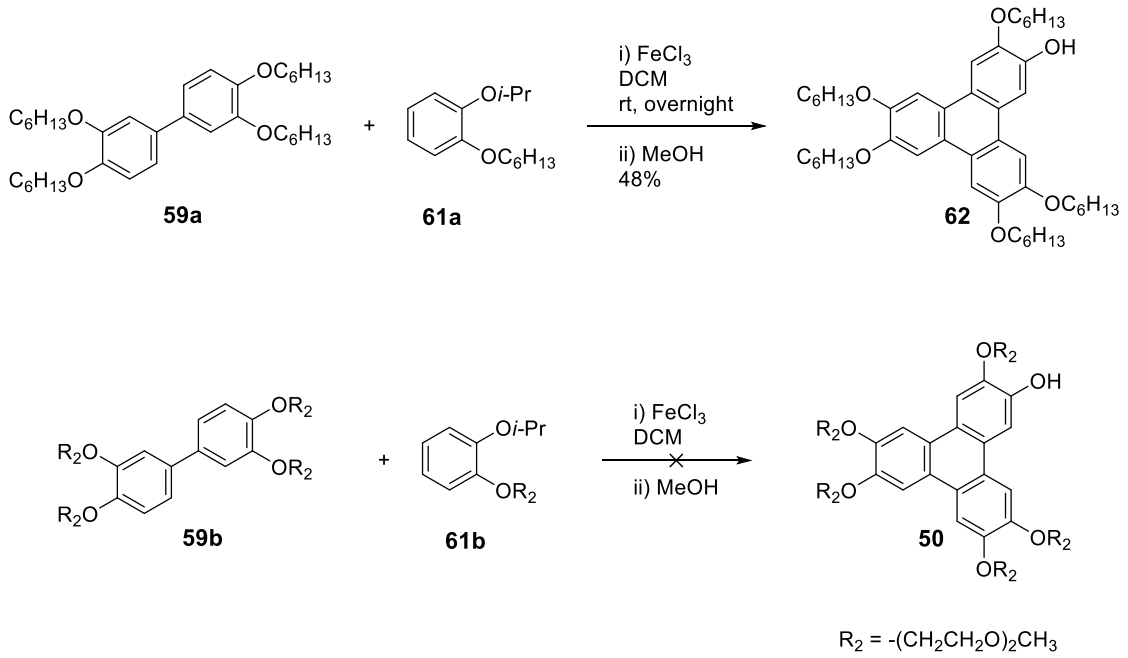

Scheme 3.7: Biphenyl-phenyl oxidative coupling.

While the oxidative coupling of **59a** and **61a** under the *Scholl* conditions (Scheme 3.7) afforded the desired 2-monohydroxy-3,5,6,10,11-pentahexyloxytriphenylene **62** in a satisfactory yield (48%), a similar coupling using the analogues **59b** and **61b** remained unsuccessful. After purification by column chromatography of the crude reaction, the starting materials were recovered. ^{1}H NMR shows that no degradation of either **59b** nor **61b** were observed. Interestingly, the isopropoxy group was not cleaved during the reaction. However, small traces of a new compound (Figure 3.5 and inset) was observed. From the frequency and the integrations of the peaks, it is thought that this compound could be the desired monohydroxy-pentaalkylated triphenylene **50**. Due to the very small quantity of this compound, and the difficulty to isolate it, no further analyses were done.

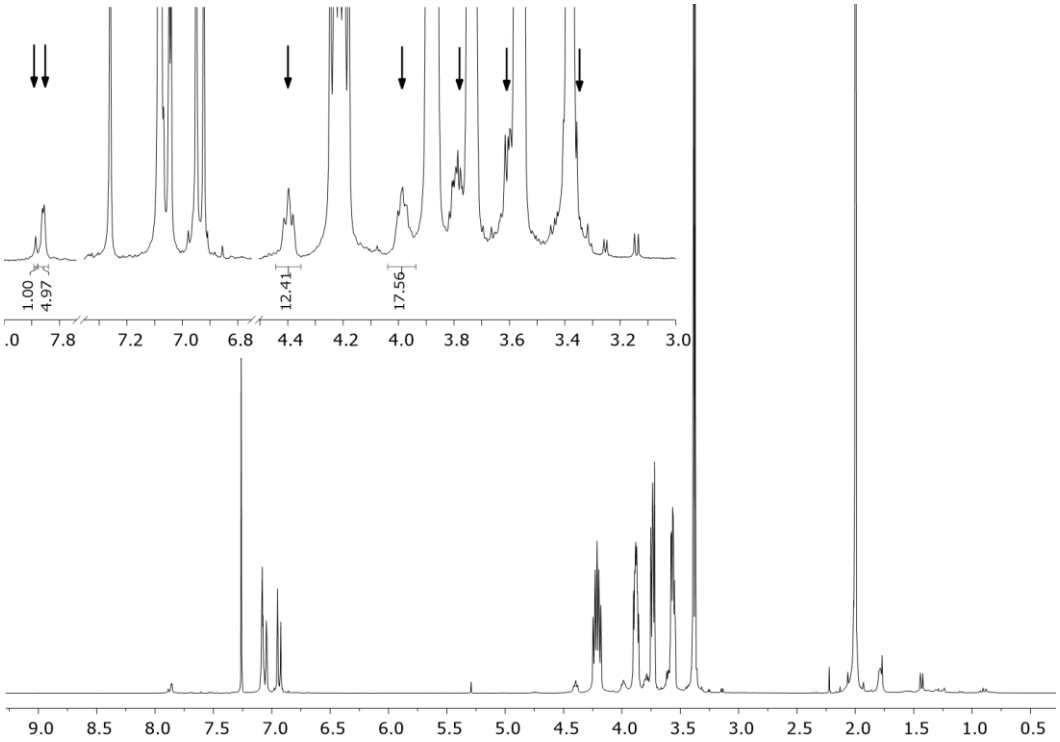

Figure 3.5: ^{1}H NMR spectra of one of the fraction. The new unknown compound is highlighted from black arrows.

To our knowledge, only a few papers have described the C-C oxidative *Scholl* type coupling on intermediates containing an ethylene glycol motif.[119–121] G. W. Buchanan and co-workers have successfully synthesised the tris(n-crown-3)triphenylenes (**64a** n = 9[119], **64b** n = 11[120]) from the trimerisation of benzo-n-crown-3 **63a-b** with $FeCl_3$ and H_2SO_4 (Scheme 3.8 and Scheme 3.9). The yields were nevertheless very low (25% for **64a** and 0.5% for **64b**), and no detailed explanation have been formulated on the poor conversion or the presence of side-products.

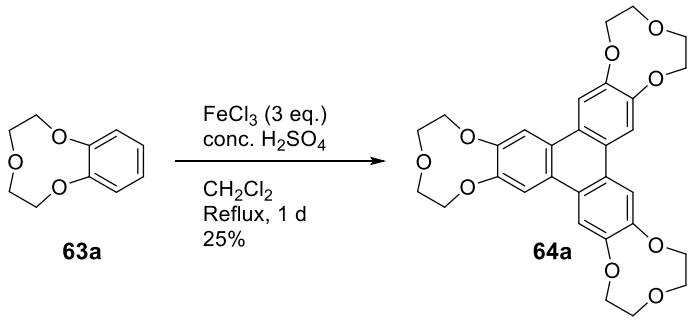

Scheme 3.8: Trimerisation of benzo-9-crown-3 64a.[119]

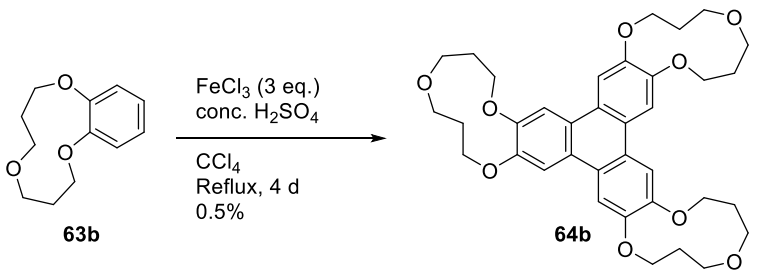

Scheme 3.9: Trimerisation of benzo-11-crown-3 64b.[120]

J. S. Moore and co-workers have also described a *Scholl* type reaction to generate ethylene glycol-based hexa-*peri*-hexabenzocoronene **66** from hexasubstituted benzene **65**, with a satisfactory yield of 45% (Scheme 3.10).[121]

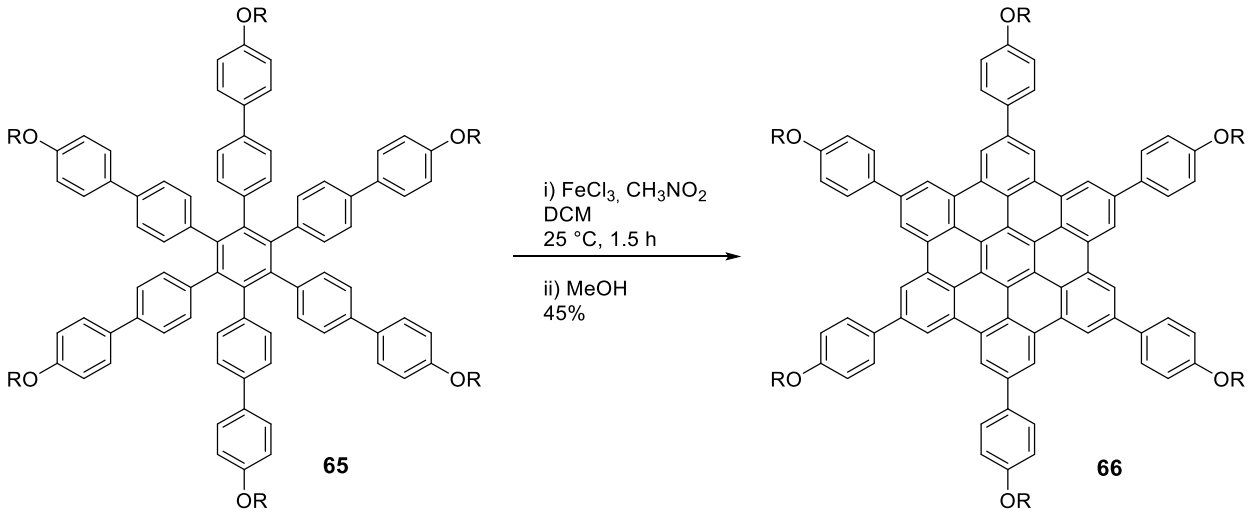

Scheme 3.10: C-C oxidative coupling of hexasubstituted ethylene glycol based benzene.[121]

The failed reaction cannot be explained by the oxidation potential of the starting materials. Indeed, by correlating the oxidation potential with the Hammett constant of the substituent (the more electron donating group the substituent, the easier the aromatic ring will be oxidized) no significant change was obtained between an alkoxy substituent and a $OCH_2CH_2CH_2O$- motif (Table 3.2).

	σ_m	σ_p		σ_m	σ_p
OCH_3	0.12	-0.27	$O(CH_2)_4CH_3$	0.10	-0.34
OCH_2CH_3	0.10	-0.24	$OCH_2CH_2O^-$	-0.12	-0.12
$OCH_2CH_2CH_3$	0.10	-0.25	$OCH_2CH_2CH_2O$-	0	0
$O(CH_2)_3CH_3$	0.10	-0.32			

Table 3.2: Hammett constants.[122]

The cleavage of ether chains by radical reactions, as described in the literature,[123,124] could be excluded, as the starting materials were recovered and no ether degradation were observed on ^{1}H NMR.

A possible explanation for the unsatisfactory *Scholl* type coupling between the ethylene glycol based biphenyl and phenyl might be the poisoning of iron(III) chloride by complexation with the ethylene glycol chains. Indeed, examples of ethylene glycol, polyether (including poly(ethylene oxide)) or polyester iron(III) complexes have been described.[125–127] Additional test reactions (increasing the equivalent of iron(III) chloride, varying the temperature) are nevertheless required to validate this hypothesis.

As an alternative C-C oxidative coupling, DDQ in the presence of an acid was found to be a good oxidant for the oxidative C-C bond formation, including for the synthesis of triphenylene from terphenyl derivatives.[88,128] DDQ with a E_{red} = +0.60 V vs. SCE, is generally used in combination with methanesulfonic acid, with one equivalent per C-C bond formation unlike iron(III) chloride which has to be used in large excess. Test reactions were attempted to verify the viability of this method onto our substrate for the biphenyl-phenyl coupling. The dialkyloxyphenyl derivatives **44** and **67** were reacted with DDQ in a 9:1 mixture of DCM:$MeSO_3H$ at 0 °C for 15 min (Scheme 3.11). The resulting crude ^{1}H NMR spectrum

indicated the consumption of the starting material. However, numerous peaks in the aromatic region were observed. The identification of the products by mass spectrometry (MS ES+) was unsuccessful. This method was abandoned.

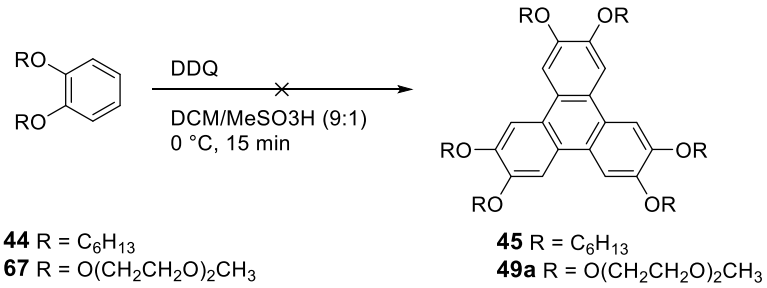

Scheme 3.11: Attempted oxidative cyclodehydrogenation using DDQ as the oxidant.

A recent paper published by L. T. Scott in 2015, suggests that oxidative trimerisation of 1,2-dihexyloxybenzene **44** to the corresponding triphenylene **45** can nevertheless be achieved in high yield.[86] This method differs from the previously described synthesis of triphenylene from *o*-terphenyl as a stoechiometric amount of DDQ in 1,2-dichloroethane is used and the reaction takes place in 10 h. This recent publication presents new reaction conditions (stoechiometry of DDQ, time of reaction) which could have been interesting to investigate.

The synthesis of the building block **50** bearing ethylene-glycol base chains using the biphenyl-phenyl coupling was abandoned due to the poor yield obtained for the synthesis of the building blocks and the difficulties to perform the intermolecular oxidative cyclodehydrogenation. Another routes were therefore investigated.

3.3.3 Alternative synthesis of the hydrophilic moiety

The cleavage of aryl alkyl ethers, especially the aryl methoxy ethers is a well-known procedure.[129] In order to cleave one or multiple alkyloxy chains from the triphenylene core, several methods have been described. Lithium diphenylphosphide Ph_2PLi, despite its toxicity

and its reactivity to air and moisture, is an efficient strategy to afford the 2-hydroxy-3,6,7,10,11-pentapentyloxytriphenylene.[130] B-Bromo-9-borabicyclo[3.3.1]nonane (9-Br-BBN) has also been used but resulted in non-selective cleavage and tedious purification of the desired hydroxy compound.[130] M. Manickam and co-workers have therefore developed a mild and selective synthetic procedure for the preparation of mono- di- or tri- hydroxytriphenylene derivatives by cleavage of the hexyloxy chains from TP6 using B-bromocatecholborane (BCB).[131] We therefore chose BCB as the reagent to cleave one of the chains on TP6EO3M and TP6 as test reactions (Scheme 3.12).

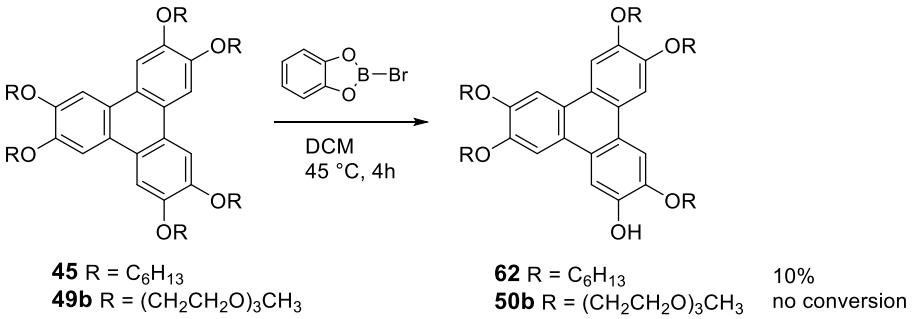

Scheme 3.12: Cleavage of TP6EO3M using B-bromocatecholborane.

After 4 h, ^{1}H NMR revealed that TP6 was successfully cleaved (Figure 3.6), to obtain **62**. The yield is nevertheless much lower than the literature value and the reaction needed to be optimised (NMR yield = 10% versus 68% in the literature). However, **49b** was entirely recovered (Figure 3.7). It can be therefore concluded that the cleavage of one of peripheral chains on triphenylene is not adapted to triphenylene derivatives bearing other surrounding chains than alkoxy. BCB might interact with the numerous ether groups and prevents the cleavage of the desired aryl ether.

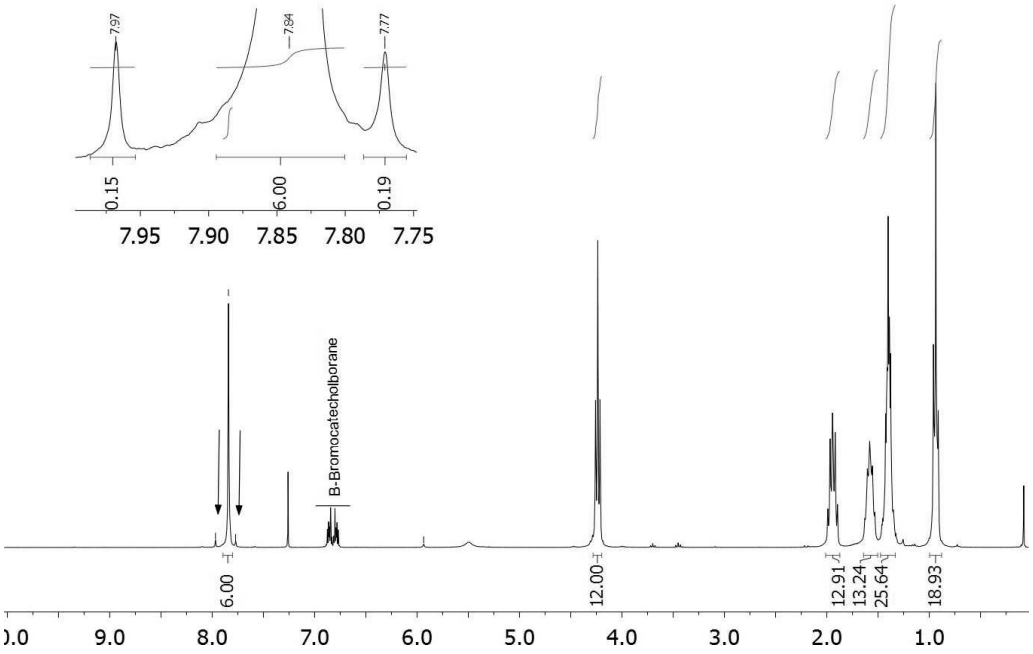

Figure 3.6: ^{1}H NMR spectra - reaction of TP6 with BCB.

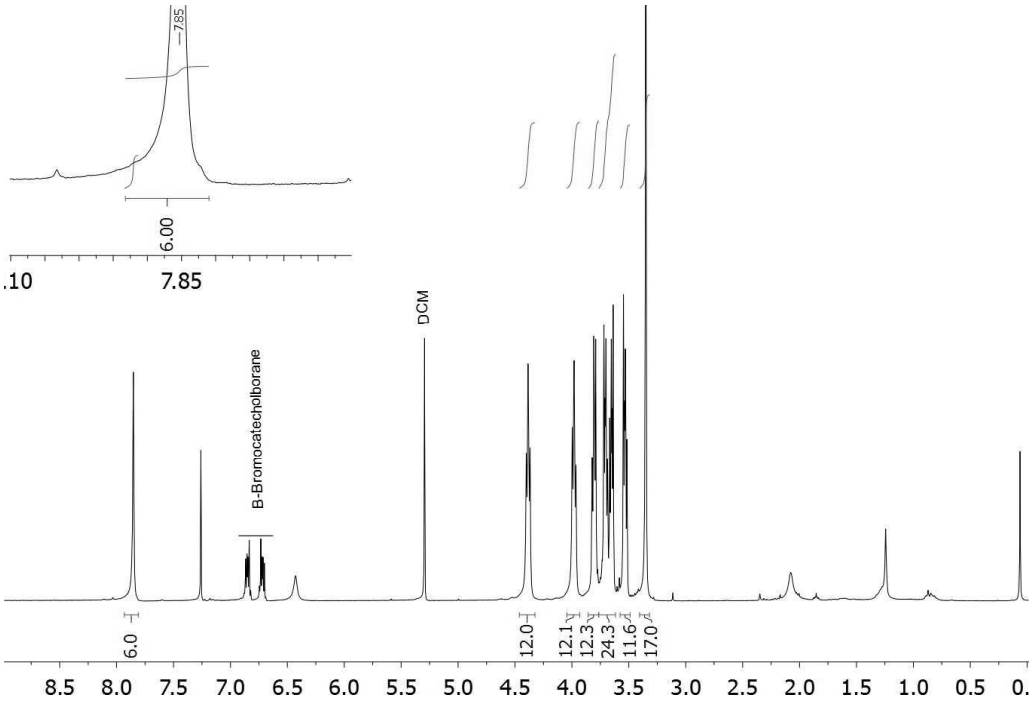

Figure 3.7: ^{1}H NMR spectra – reaction of TP6EO3M with BCB.

A statistical alkylation of **47** with five equivalents of mesylated diethyleneglycol monomethyl ether **48a** was also attempted and the reaction was monitored by HPLC (Scheme 3.13). Even if 5 equivalents of the chains were used, the main product was unfortunately TP6EO2M.

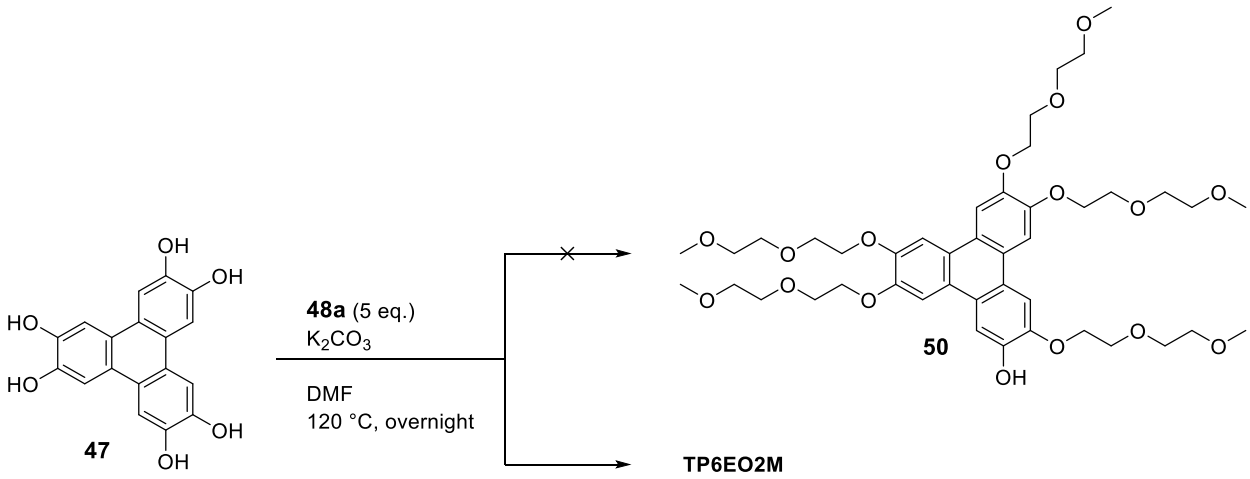

Scheme 3.13: Attempted statistical alkylation of **47** with five eq. of **48a**.

To conclude, the synthesis of the hydrophobic moiety **62** was successfully carried out by the so-called convergent biphenyl-phenyl route in 6 steps in an overall 22% yield. However, the ethylene-glycol based analogue, **50** could not be synthesised. After numerous unsuccessful attempts with the conventional biphenyl-phenyl coupling, the *Scholl* cyclisation using DDQ:$MeSO_3H$ as the oxidant, the cleavage of one chain from TP6EO2M and a statistical *Williamson* type reaction, no acceptable conversion was obtained. Moreover, the ethylene glycol based precursors **59b** and **61b** were obtained in a poor yield. We therefore decided to modify the hydrophilic moiety of TP6-TP6EO2M and design another compatibiliser.

3.4 TP6-Gall as a compatibiliser

The work presented in this section has been published.[132]

3.4.1 Design of TP6-Gall

Due to the unsuccessful synthesis of TP6-TP6EO2M, another compatibiliser, named TP6-Gall was designed (Figure 3.8). Keeping the same hydrophobic moiety as TP6-TP6EO2M (synthesis described in 3.3.1), a new 3,4,5-trialkylatedbenzyl derivative was chosen as the hydrophilic moiety. Derived from the commercially available ethyl or methyl gallate, a large family of

compounds can be obtained by substituting the 3,4,5-trihydroxy positions. The ester in 1 position of the benzyl can be easily converted and offers different linking strategies. The term "gallate" used in this thesis refers to the derivatives obtained from ethyl gallate.

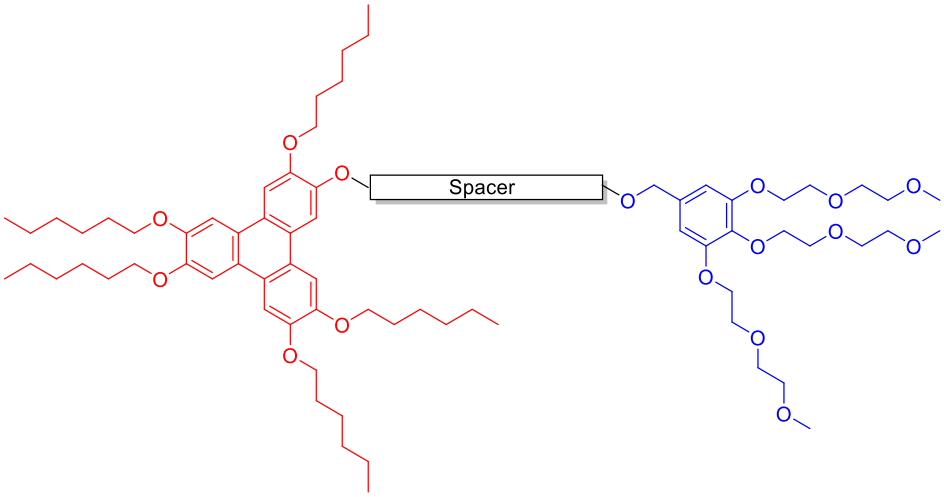

Figure 3.8: Structure of the target compatibiliser TP6-Gall.

The synthesis of TP6-Gall was carried out using a convergent synthesis between **62** and an ethylene glycol based 3,4,5-trialkylylatedbenzyl derivative, following the retrosynthetic scheme shown in Scheme 3.14. The hydrophilic moiety was synthesised from the commercially available ethyl gallate. The synthetic choice of the spacer unit between the two different moieties will be discussed.

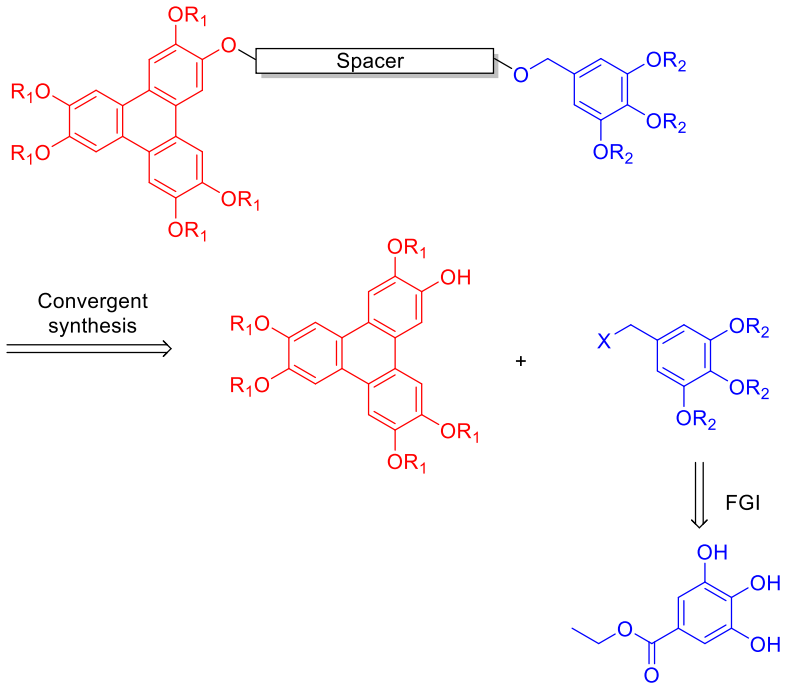

Scheme 3.14: Retrosynthesis of TP6-Gall.

3.4.2 Synthesis of the gallate-based hydrophilic moiety

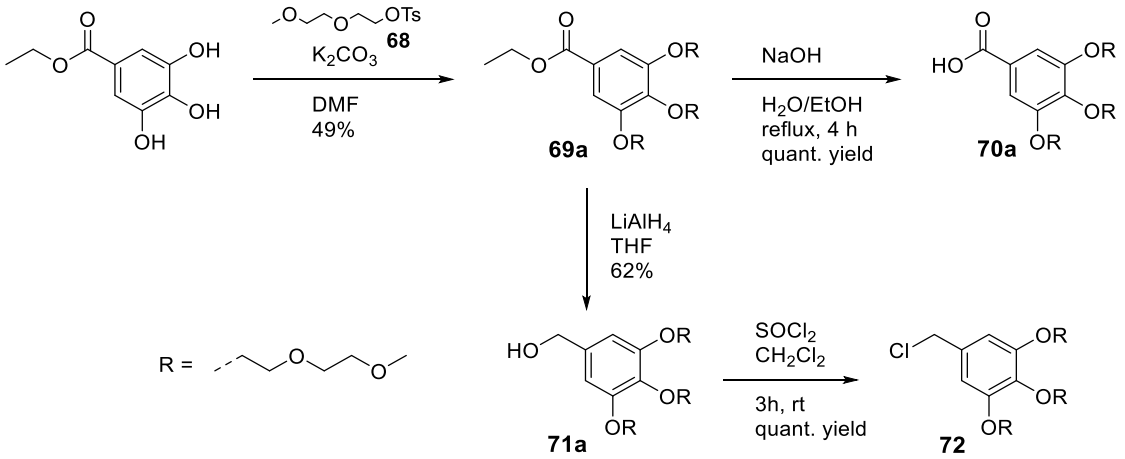

Scheme 3.15: Synthesis of the gallate precursors.

The synthesis of the gallate-based hydrophilic moiety was carried out from ethyl gallate following the literature (Scheme 3.15).[133] A *Williamson* type reaction between ethyl gallate and the tosyl-activated diethylene glycol monomethyl ether **68** afforded **69a** in a 49% yield. The ester group of this gallate derivative can be easily interconverted to a large choice of functional group. Several derivatives of **69a** were therefore synthesised to couple the

hydrophobic and hydrophobic motifs together. The corresponding carboxylic acid **70a** was obtained *via* the base-catalysed hydrolysis of ester. The reduction of **69a** using lithium aluminium hydride afforded the corresponding benzyl alcohol **71a** which could be then converted into a benzyl chloride **72** using thionyl chloride.

3.4.3 Coupling of the two moieties – choice of the spacer

To couple the two different moieties, an alkyl spacer was added to the unsymmetrical triphenylene moiety. The triphenylene **62** was reacted with 1,6-dibromohexane in a *Williamson* type reaction to afford the alkyl bromide **73** (Scheme 3.16).

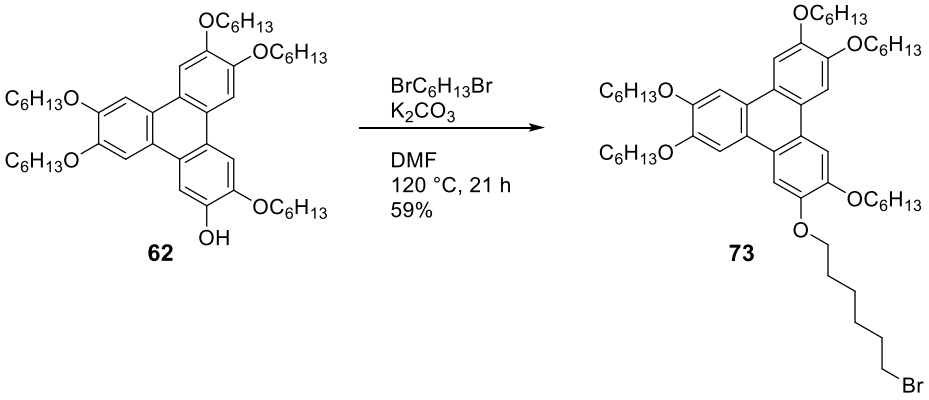

Scheme 3.16: *Williamson* type ether synthesis of **63**.

Unfortunately, the reaction between **73** and the carboxylic acid derivative of **70a** did not afford the desired compound **74** (Scheme 3.17), which can be attributed to the hydrolysis of the ester during the column chromatography.

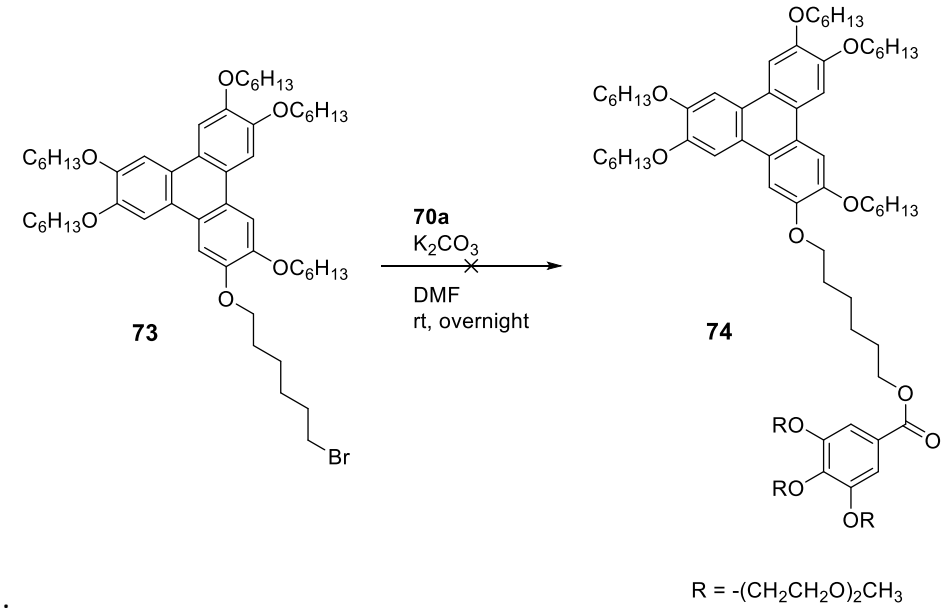

Scheme 3.17: Coupling of the two moieties.

The coupling reaction between **73** and the benzylic alcohol derivative of the gallate **71a**, previously deprotonated using sodium hydride, did not afford the compatibiliser **75** (Scheme 3.18). **73** was recovered and surprisingly the benzylic alcohol **71a** was converted to the benzoic acid **70a** (confirmed by ^{1}H NMR and mass spectrometry).

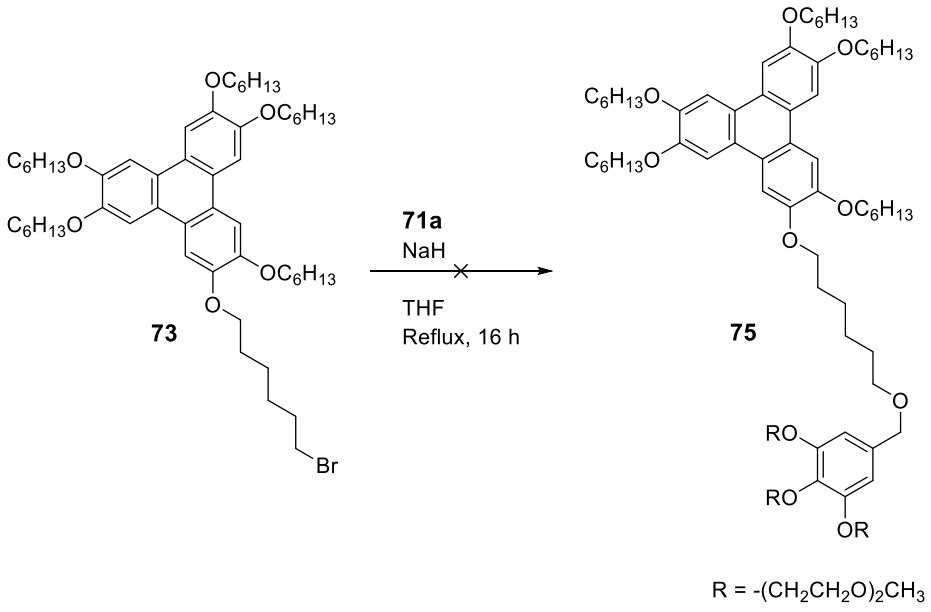

Scheme 3.18: Attempted coupling between **73** and the benzyl alcohol **71a**.

This unusual NaH-promoted oxidation of benzyl alcohols to benzoic acids has been described in the literature.[134–137] S. Ohta and co-workers have observed the oxidation of several aromatic aldehydes or benzyl alcohols to their benzoic acid derivatives in the presence of sodium hydride in tetrahydrofuran under a flux of air.[137] Surprisingly, for the conversion of *o*-chlorobenzyl alcohol to *o*-chlorobenzoic acid, it was claimed that no air flux was required.

In order to prove the degradation of benzyl alcohols to benzoic acid derivatives, a test reaction was performed by reacting two different benzyl alcohols bearing ethylene glycol based and hexyloxy chains (respectively **71a** and **71b**) with sodium hydride under an argon atmosphere (Scheme 3.19).

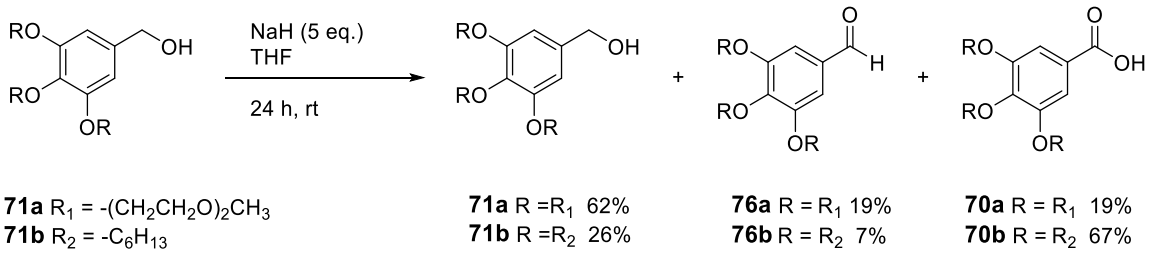

71a R_1 = -$(CH_2CH_2O)_2CH_3$
71b R_2 = -C_6H_{13}

71a R =R_1 62%
71b R =R_2 26%

76a R = R_1 19%
76b R = R_2 7%

70a R = R_1 19%
70b R = R_2 67%

Scheme 3.19: NaH-Promoted oxidation of gallate-based benzyl alcohol derivatives. The yields are determined by ^{1}H NMR.

Under dry conditions and protective atmosphere, **71a** was reacted for 24 h with five equivalents of sodium hydride in dry THF. Its trihexyloxy homologue **71b** (synthesised following the same procedure as **71a**, with a 66% overall yield) was also reacted in the same conditions (Scheme 3.19). ^{1}H NMR of the crude and mass spectrometry indicated the presence of the benzaldehydes **76a** and **76b** (in a respective 19% and 7% yield) and the benzoic acid derivative **70a** and **70b** (in a respective 19% and 67% yield) as shown by ^{1}H NMR (Figure 3.9 and Figure 3.10). It has been assumed that this oxidation was caused by a radical anion.[136] Indeed, even if the reaction was performed under dry conditions, *i.e* flame-drying of the apparatus, reaction under argon, and use of anhydrous THF, the presence of a small

proportion of molecular oxygen cannot be excluded. Moreover, it can be inferred that ageing sodium hydride reacted with molecular oxygen or water present in the atmosphere to produce sodium hydroxide or peroxides.

Is it worth noticing that in the case of the coupling between **73** and **71a**, a quantitative conversion from benzyl alcohol to the benzoic acid derivative is observed and no benzaldehyde derivative was formed as observed by ^{1}H NMR or mass spectrometry. It can be inferred that as the reaction was performed at reflux, unlike the test reaction, the benzaldehyde derivative was formed and was quantitatively converted to the benzoic acid. This hypothesis is in accordance with the proposed mechanism in the literature.[136]

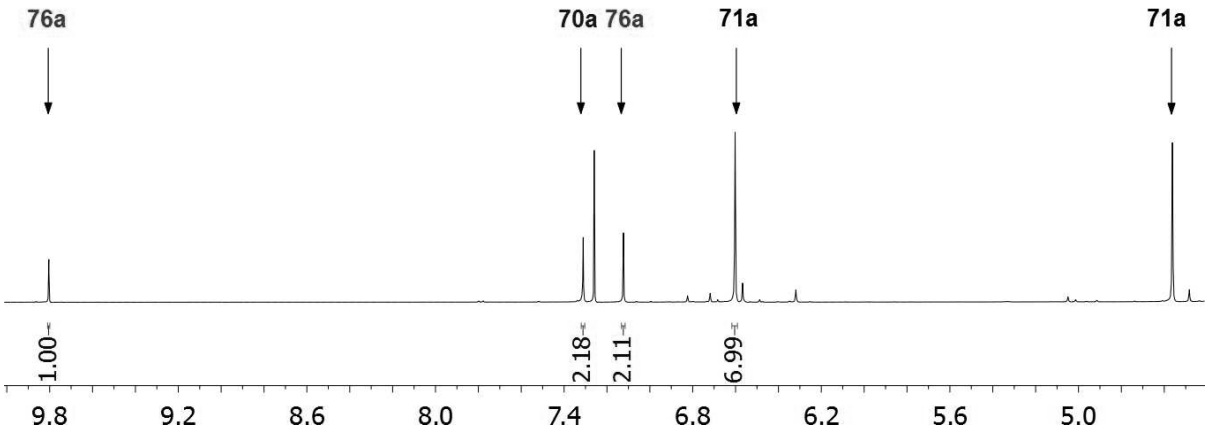

Figure 3.9: Crude ^{1}H NMR ($CDCl_3$) of the NaH-promoted oxidation of **71a** (10-4.5 ppm region).

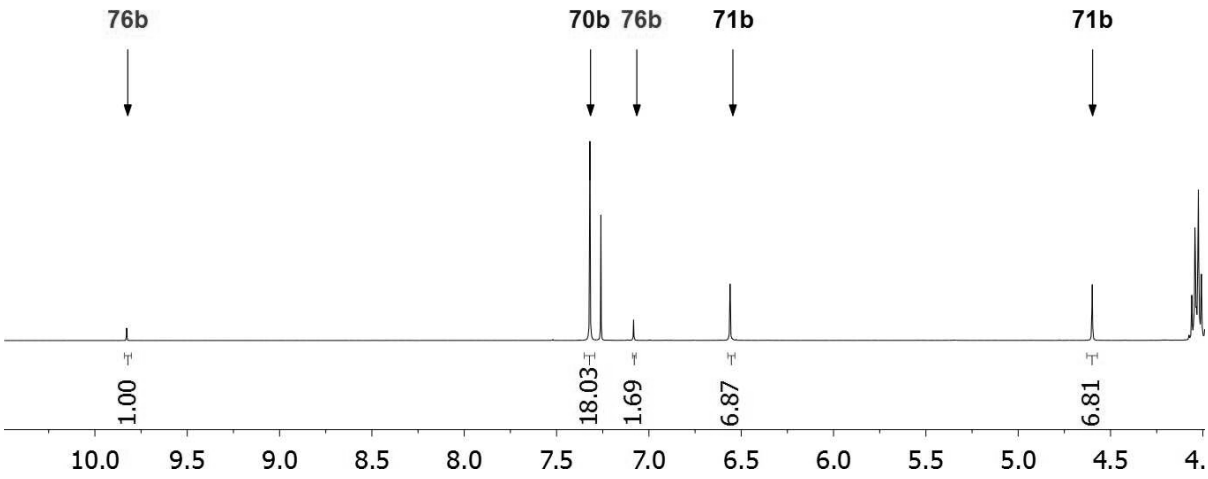

Figure 3.10: Crude ^{1}H NMR ($CDCl_3$) of the NaH-promoted oxidation of **71b** (11-4 ppm region).

To overcome these synthetic issues, another phenyl-based spacer was added to **73** to facilitate the coupling reaction. 1,3-Dihydroxybenzene was chosen as the meta position prevents any unwanted oxidation to benzoquinone derivatives compared to 1,4-dihydroxybenzene. **77** was synthesised *via* a *Williamson* type reaction and was carried out in a 42% yield (Scheme 3.20).

The coupling between **77** and the benzyl chloride derivative **72** was successful and afforded the desired compatibiliser **78** (called TP6-Gall thereafter) (Scheme 3.20).

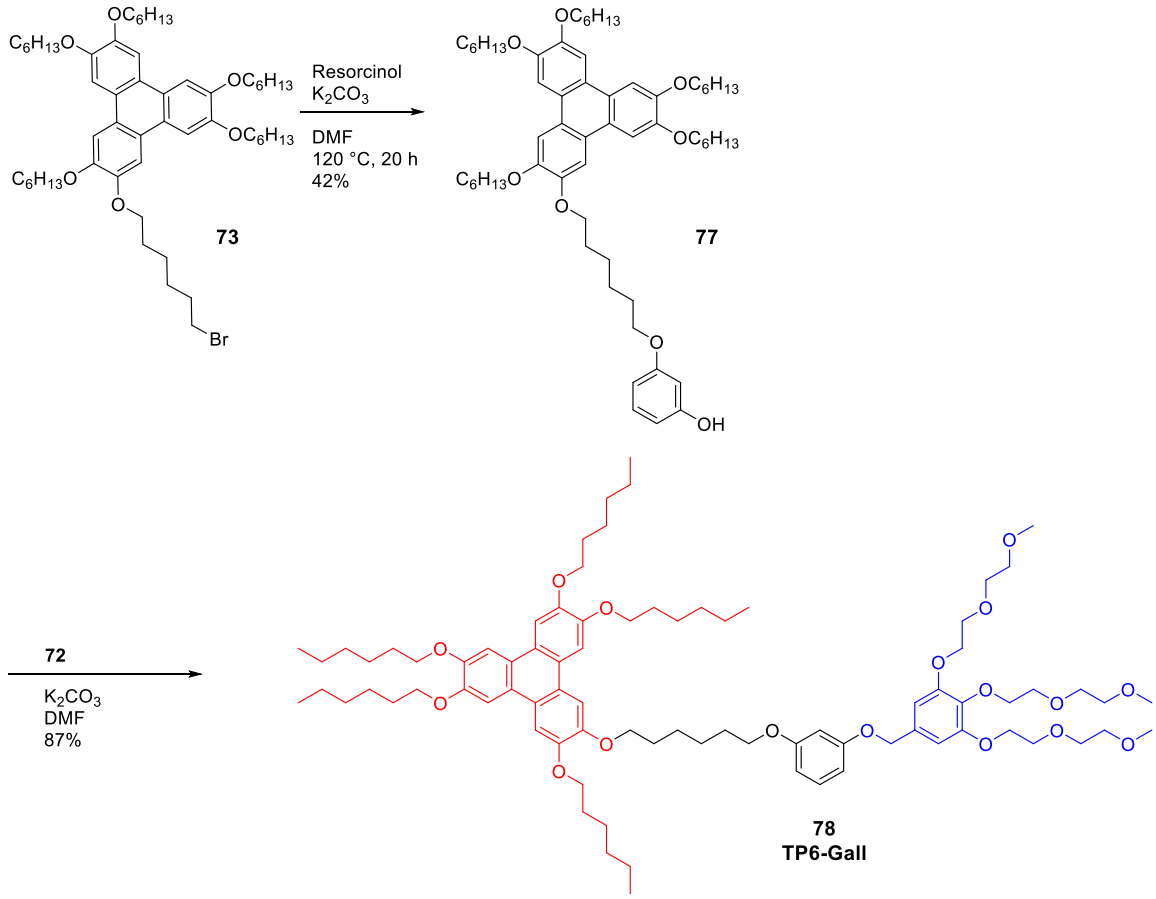

Scheme 3.20: Coupling of the hydrophilic and hydrophobic moieties.

Overall TP6-Gall was obtained in twelve steps with a 5% overall yield by a convergent synthesis between a hydrophobic triphenylene and a hydrophilic gallate moiety. This novel dyad was fully characterised by NMRs, POM, DSC and X-ray diffraction.

3.4.4 Mesogenic properties of TP6-Gall

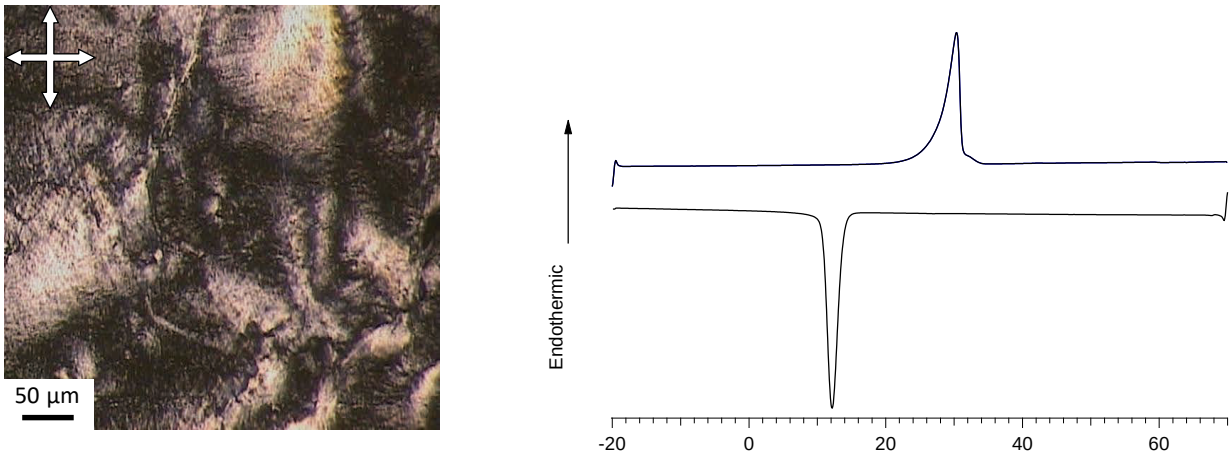

Figure 3.11: left: POM image of TP6-Gall at room temperature on heating; Right: DSC curves of TP6-Gall on 2nd heating/cooling cycle.

TP6-Gall mesogenic properties were investigated. This novel compound shows liquid crystalline properties at room temperature until 30 °C, as shown in the POM (Figure 3.11, left) and the DSC curve (Figure 3.11, right). The X-ray diffraction profile of TP6-Gall at room temperature (Figure 3.12) shows three diffraction peaks with a q-Ratio of $2:\sqrt{5}:\sqrt{6}$ (ascribed to a (200), (210) and (211) planes), and is typical of a cubic lattice. It should be noted that in the case of a cubic lattice, no birefringence should be observed in POM. It is thought that the birefringence observed in TP6-Gall is due to a surface effect and local reorganisation of the mesogen. The calculated lattice parameter a = 33.7 Å, compared to the calculated length of TP6-Gall (*ca.* 35 Å), as shown in the MM2 model (Figure 3.13), is indicative of interpenetration of the surrounding chains.

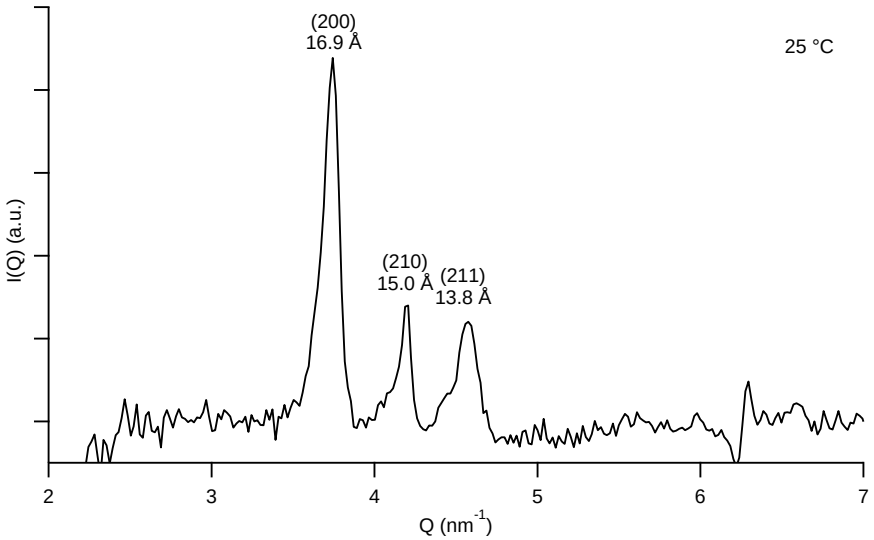

Figure 3.12: SAXS pattern of TP6-Gall at room temperature – cubic mesophase.

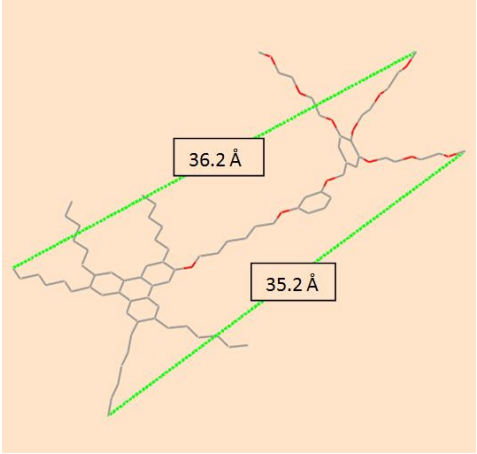

Figure 3.13: MM2 model of TP6-Gall

To conclude, the synthesis of a complex functional compatibiliser, TP6-Gall (Figure 3.14) was successfully achieved and fully characterised. The effect of TP6-Gall on an equimolar blend of TP6:TP6EO2M was investigated and discussed in the next section.

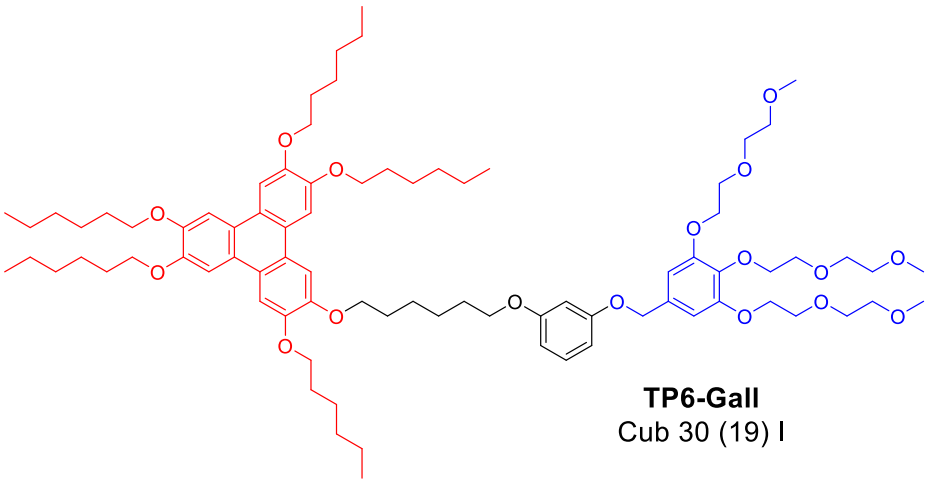

Figure 3.14: Structure of the target compatibiliser TP6Gall and its phase transition (enthalpy (J/g) in parentheses).

3.4.5 Effect of TP6-Gall on the TP6:TP6EO2M mixture

As discussed in section 2.4, an equimolar mixture of TP6 and TP6EO2M results in macrophase separation of the two incompatible materials. The effect of TP6-Gall on this mixture was investigated by POM (Figure 3.15), DSC (Figure 3.16) and X-ray diffraction at different ratio (5mol%, 20mol% and 50mol% of TP6-Gall, Figure 3.17 and Figure 3.18) into the equimolar mixture of TP6:TP6EO2M and is discussed in this section. The POM images of an equimolar TP6:TP6EO2M blends without any compatibiliser are reproduced in Figure 3.15 a, b and c, to allow an easy comparison with the ternary blends.

Upon addition of a small amount of TP6-Gall into the equimolar mixture of the incompatible (5 mol%), no major changes have been observed compared to the TP6:TP6EO2M blend. From the POM pictures (Figure 3.15 d, e and f), two distinct phases are observed from the isotropic state to the crystalline state. However, the domains are smaller and indicates an effect of the compatibiliser even at low concentration. The DSC curve (Figure 3.16b) and the X-ray diffraction pattern (Figure 3.17) do not differ much from the undoped blend. No transition temperature nor diffraction pattern corresponding to TP6-Gall are observed. On studying the

equimolar mixture of TP6:TP6-Gall by POM (Figure 3.19), DSC (Figure 3.20) and X-ray diffraction (Figure 3.18a), it was found that a homogeneous phase was obtained. It is therefore inferred that the two phases observed in the 5 mol% mixture are composed of both pure TP6EO2M and a TP6:TP6-Gall phase. The DSC curve (Figure 3.16b) confirms this hypothesis as a slightly lower clearing point (T = 85 °C) of the ternary mixture is observed compared to the equimolar TP6:TP6EO2M (T = 88 °C), which is indicative of a doping of one of the phases.

At a molar concentration of 20mol% TP6-Gall, tremendous changes are observed. Due to the complexity of the DSC curve of this mixture (Figure 3.16c) the detailed analysis of the phases is precluded. However, POM pictures (Figure 3.15 g, h and i) indicate again smaller domains than the previous mixtures. The isotropic state (Figure 3.15g) is composed of two distinct phases. On cooling from the isotropic phase to 60 °C, one of the phases forms a liquid crystalline state that cannot be determined by X-ray diffraction (Figure 3.18b). Upon further cooling to room temperature, the two domains are composed of a crystalline and a liquid crystalline phase. X-ray diffraction pattern of this mixture (Figure **3.18**c) indicates that the crystalline phase is composed purely of TP6EO2M (highlighted in blue) as the X-ray diffraction pattern fits the pure compound. The additional broad peaks at 3.08 nm^{-1} and 4.35 nm^{-1}, highlighted in green in Figure **3.18**c can be attributed to a TP6:TP6-Gall liquid crystalline phase, with a different ratio than the studied equimolar TP6:TP6-Gall (3.12 nm^{-1} and 4.40 nm^{-1}) blend, based on their similarity.

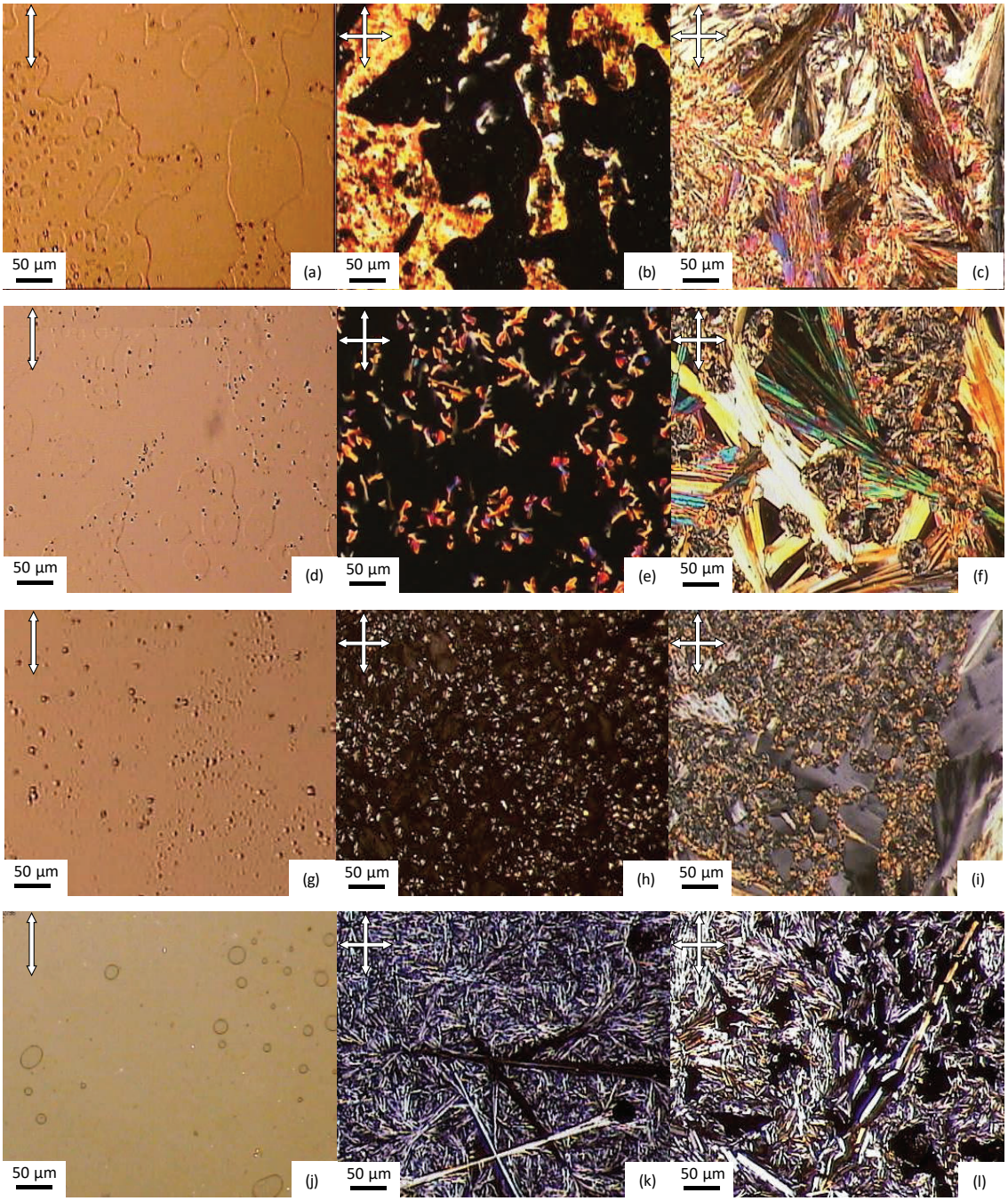

Figure 3.15: POM images of TP6:TP6EO2M mixtures on cooling: First row: with 0mol% TP6-Gall at a) 90 °C; b) 50 °C; and c) 25 °C. Second row: with 5mol% TP6-Gall at d) 85 °C; e) 44 °C; and f) 40 °C. Third row: with 20mol% TP6-Gall at g) 70 °C; h) 50 °C; g) 25 °C. Fourth row: with 50mol% TP6-Gall at j) 70 °C; k) 50 °C; l) 25 °C.

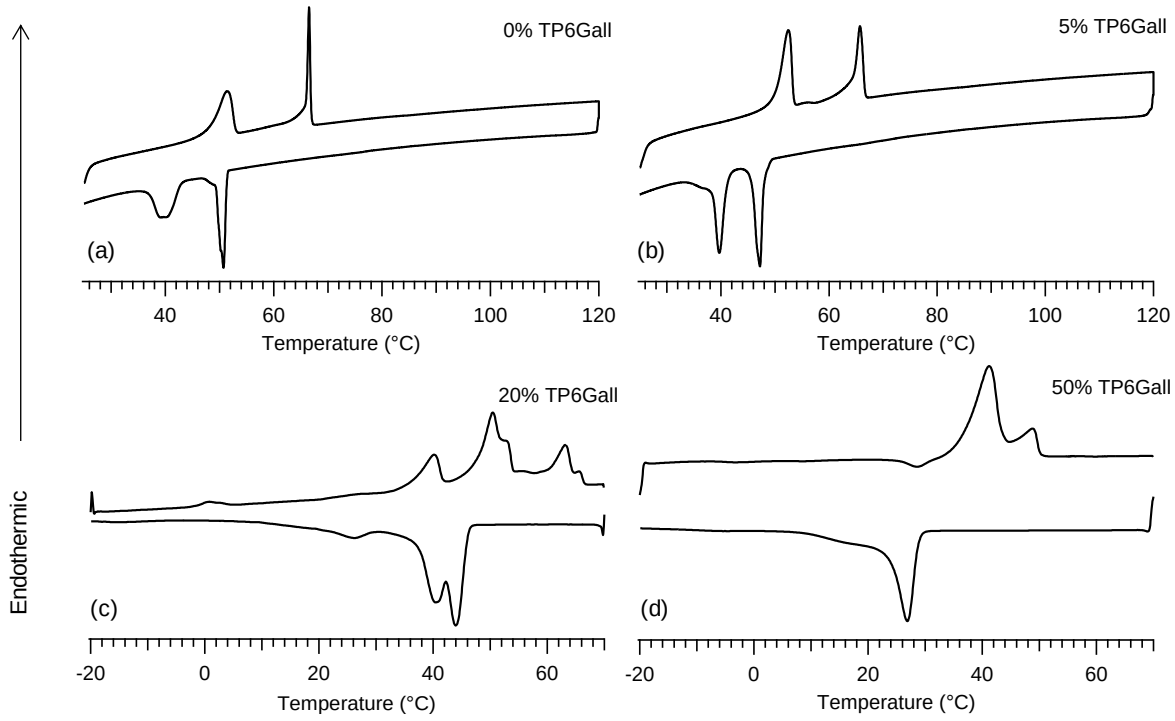

Figure 3.16: DSC curve on 2nd heating/cooling cycle(10 °C/min). Top: (a) with 0mol% TP6Gall and (b) 5mol% TP6Gall. Bottom, from left to right: (c) with 20mol% TP6Gall and (d) 50mol% TP6Gall.

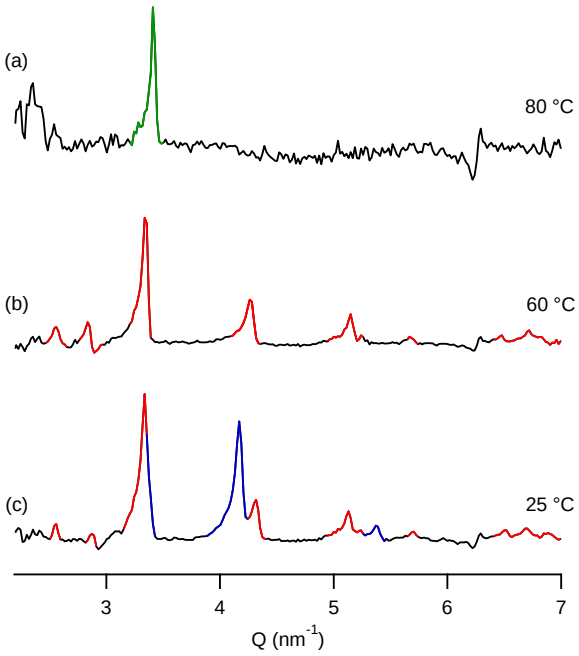

Figure 3.17: X-ray diffraction pattern of a TP6:TP6EO2M equimolar mixture with 5 mol% TP6Gall: (a) at 25 °C, (b) at 60 °C, (c) at 80 °C.

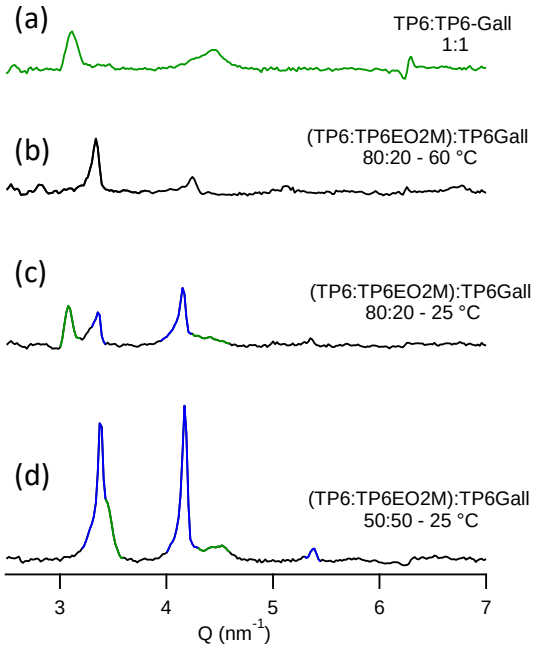

Figure 3.18: X-ray diffraction pattern of (a) TP6:TP6Gall equimolar mixture at 25 °C and (TP6:TP6EO2M):TP6Gall mixture: (b) with 20mol% at 60 °C, (c) with 20mol% TP6Gall at 25 °C, (d) with 50mol% TP6Gall at 25 °C.

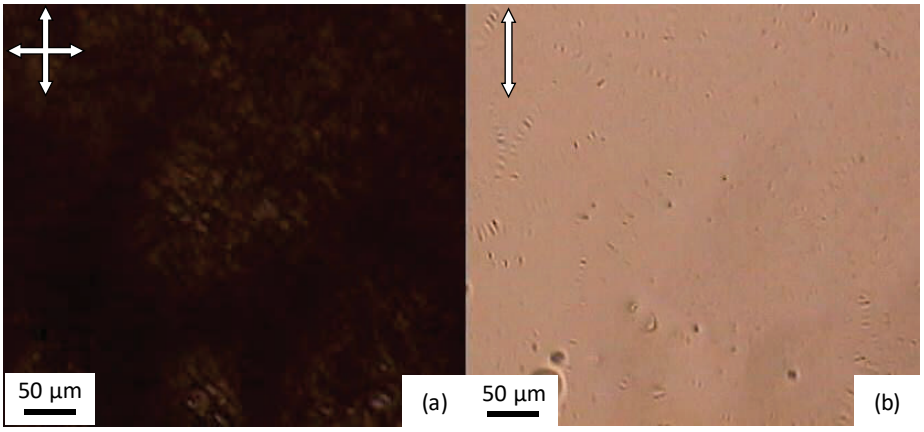

Figure 3.19: POM image of a TP6:TP6Gall equimolar mixture at: (a) 22 °C and (b) 52 °C.

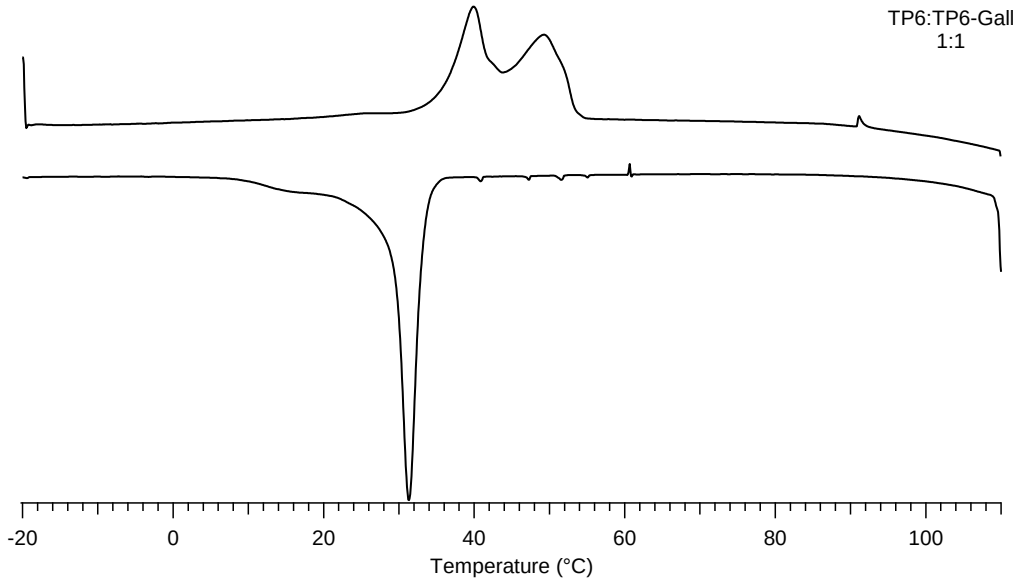

Figure 3.20: DSC curves on 2nd heating/cooling cycle (10 °C/min) of a TP6:TP6Gall equimolar mixture.

Interestingly, at a molar concentration of 50mol% TP6-Gall, the biphasic isotropic phase observed in the previous mixtures is supressed and a single isotropic phase is obtained above 50 °C (Figure 3.15 j). Upon cooling the ternary blend, small crystals are growing into a liquid crystalline phase (Figure 3.15 k and l). It is worth noting that the crystalline domains are very small. Micro-segregation is therefore occurring. From the X-ray diffraction pattern of this mixture (Figure 3.18), we can ascribe the crystalline phase to crystalline TP6EO2M. The additional patterns at 3.49 nm^{-1} and 4.50 nm^{-1} most likely correspond again to a TP6:TP6-Gall

mixture, with both peaks shifted to higher q-value compared to the equimolar TP6:TP6-Gall mixture. The DSC curve (Figure 3.16d) confirms this hypothesis as the transition temperatures of the ternary blend are similar to the TP6:TP6-Gall blend (Figure 3.20). The transition temperature of TP6EO2M is overlapping with the broad and intense first transition peak. It is worth noting that this micro segregation is reproducible over several heating/cooling cycles. We can therefore deduce that this morphology is thermodynamically favoured. As compared to the previous blends, an equimolar mixture of TP6:TP6EO2M with 50mol% of TP6-Gall does not show any sign of macrophase separation. Instead, a micro-phase segregation of the two incompatible materials is observed.

In conclusion, a TP6:TP6EO2M blend can be considered as incompatible as macrophase separation is clearly observed. TP6-Gall has a tremendous effect on the equimolar blend of incompatible, even at low concentration. The most interesting blend is the one composed of 50mol% of TP6-Gall, where a single isotropic phase is obtained. The macrophase separation observed in undoped TP6:TP6EO2M blend is suppressed and a micro-segregation is observed reproducibly upon cooling. We have therefore demonstrated the efficiency of TP6-Gall as a small-molecule compatibiliser on the TP6:TP6EO2M equimolar mixture. TP6-Gall is therefore acting as a compatibilising agent in the TP6:TP6EO2M system.

3.5 Summary

To prove the concept of compatibilising blends of incompatible materials, a model study based on triphenylene derivatives was investigated. Two triphenylenes cores with incompatible pendent chains, *i.e.* TP6 with hexyloxy chains and TP6EO2M with ethylene-glycol based chains, were synthesised and macrophase separate over the all range of temperatures. As a simple compatibiliser, C6E3M was designed and its effect on an

equimolar TP6:TP6EO2M blend was studied. C6E3M has a large effect on the morphology of the blend by suppressing the macrophase segregation between TP6 and TP6EO2M towards micro-segregated phases. However, a high ratio of C6E3M is needed.

Another tailor-made compatibiliser, TP6-TP6EO2M, was designed and its synthesis was attempted. Due to the low yields obtained during the synthesis of the building blocks and the unsuccessful oxidative cyclodehydrogenation of the ethylene glycol based precursors, another amphiphilic dyad was designed. TP6-Gall, composed of the hydrophobic triphenylene moiety and a hydrophilic gallate derivative, was therefore successfully synthesised in 12 steps in a 5% overall yield. This novel amphiphilic dyad shows a cubic liquid crystalline lattice at room temperature. We have demonstrated that TP6-Gall suppresses the macrophase separation to micro-phase segregation on adding 50 mol% of TP6-Gall into an equimolar mixture of the incompatibles. Importantly, this system is reproducible on several heating/cooling cycles, suggesting that the micro-phase segregation morphology is thermodynamically favourable.

In conclusion, this model study proved the high potential of surfactant-like dyads on a mixture of liquid crystalline based incompatible materials.

The next section will be dedicated to the morphology study of another couple of materials based on the incompatibility of their surrounding chains. These components are, unlike TP6 and TP6EO2M, considered as functional due to their electron donor and acceptor properties.

Chapter four:

Incompatible functional materials based on hexa-*peri*-hexabenzocoronene and perylene diimide

4.1 Aims and objectives

As seen in the previous chapter, the use of a compatibiliser as a third component into a mixture of incompatible materials is a very powerful method to control the morphology. In this section, this strategy will be applied on a new binary mixture composed of hexa-*peri*-hexabenzocoronenes (HBCs) and perylene diimides (PDIs). Unlike triphenylene, those materials are considered as functional due to the electron donor and acceptor ability of respectively HBCs and PDIs. Moreover, those derivatives have shown to be excellent candidates to optoelectronic applications. The strategy of incorporating immiscible pendent chains to HBC and PDI will be used to introduce incompatibility between the two materials, as for the triphenylene work described in the previous chapters.

The synthesis of a hydrophobic and electron donor HBC, HBC-PhC12 (Figure 4.1) will be described and its full mesogenic and photophysical properties will be discussed. As a hydrophilic electron acceptor PDI, several designs based on the addition of an ethylene glycol motif on the imide position or on the perylene core will be described (Figure 4.1).

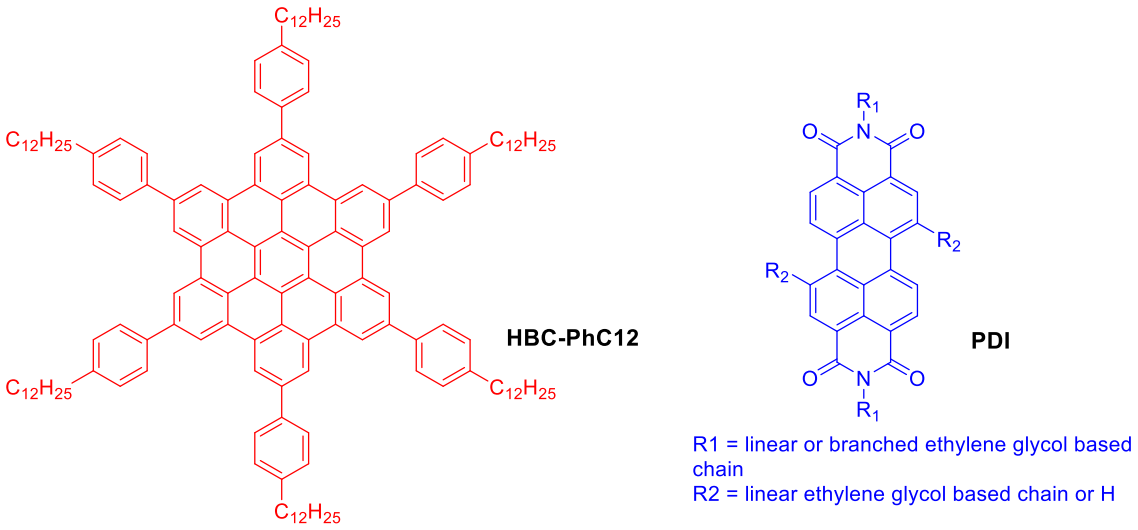

Figure 4.1: Structure of the target incompatible compounds HBC-PhC12 and PDI derivatives

4.2 Literature review on hexa-*peri*-hexabenzocoronene (HBC)

Hexa-peri-hexabenzocoronenes (HBCs) belong to the polyaromatic hydrocarbon family. The HBC core is composed of 13 fused aromatic cores, and is classified as fully benzenoid according to Clar's rule (Figure 4.2). Its unique electronic and liquid properties have received a lot of attention for its application as materials for optoelectronics.

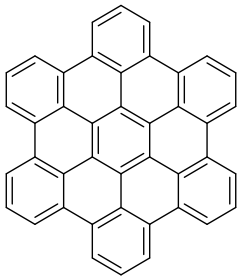

79

Figure 4.2: HBC core.

A short history on the synthesis of HBCs and their properties will be presented in this section.

4.2.1 Synthesis of hexabenzocoronene

The first synthesis of the HBC core has been described in 1959 by Clar and co-workers and was based on the homocoupling of 2:3-7:8-dibenzo-peri-naphthalene **80** (Scheme 4.1).[138] The same year, A. Halleux and co-workers also published the synthesis of this core from the hexaphenylbenzene **82** or the dibenz-1,9:2,3-anthrone **83** (Scheme 4.2).[139] Due to its extended aromatic core and its flat structure, the unsubstituted HBC is highly insoluble and its melting point exceeds 700 °C. Its processing is therefore difficult.

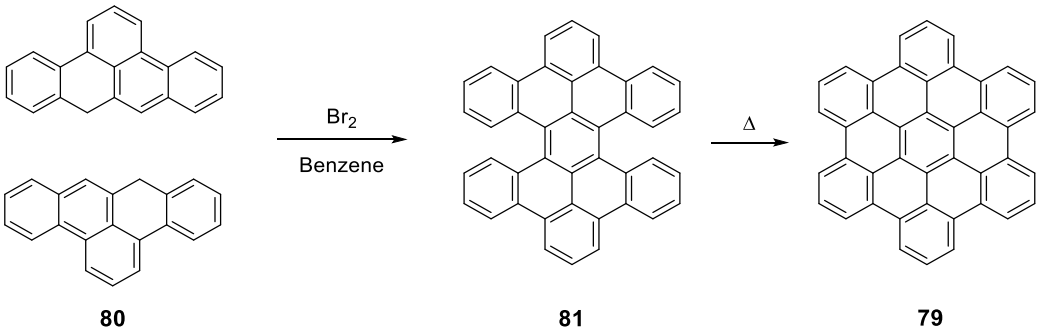

Scheme 4.1: Synthetic pathway towards HBC by Clar.[138]

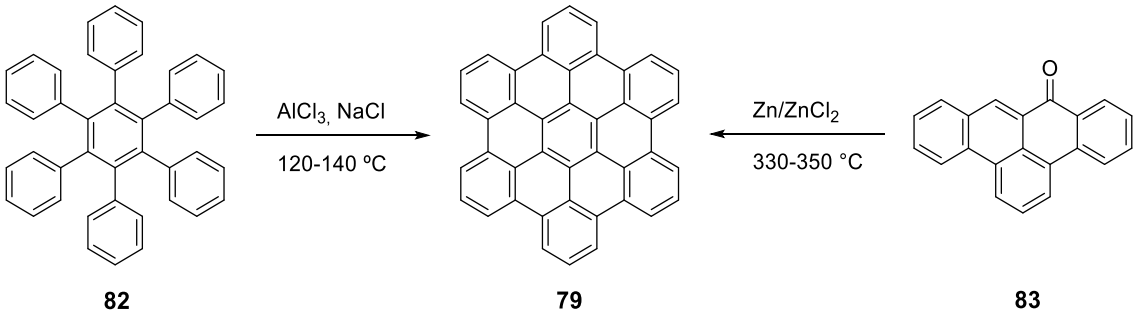

Scheme 4.2: Synthetic routes towards HBC by Halleux**.**[139]

The synthesis and use of substituted HBC, with lower melting point and enhanced solubility have been triggered by H. W. Spiess and co-workers in 1995.[140,141] D_{6h} symmetric HBCs have been successfully prepared following the synthetic route described in Scheme 4.3. Disubstituted acetylene derivatives **84** are trimerised *via* a [2+2+2] cycloaddition using $Co_2(CO)_8$ as the catalyst. The hexaphenylbenzene intermediate **85** is then reacted *via* a *Scholl* type oxidative cyclodehydrogenation, affording the desired D_{6h} symmetric HBCs **86**. Although a mixture of aluminium chloride and a source of copper has been primarily used as reagents for the *Scholl* reaction, iron(III) chloride in a mixture of DCM:CH_3NO_2 is more commonly used.

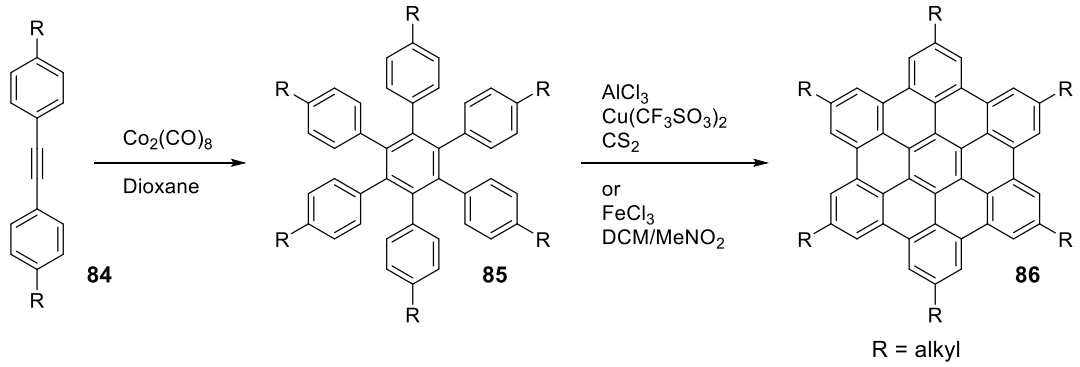

Scheme 4.3: Synthesis of D_6h-symmetric HBC.

Since this first synthetic route was published, numerous strategies towards less symmetric HBCs were designed. C_2 **87a-b**,[142] D_2 **88**,[143] or C_3 **89** [144] symmetric HBCs (Figure 4.3) have been successfully prepared. In this thesis, the C_2 symmetry HBCs will be emphasised.

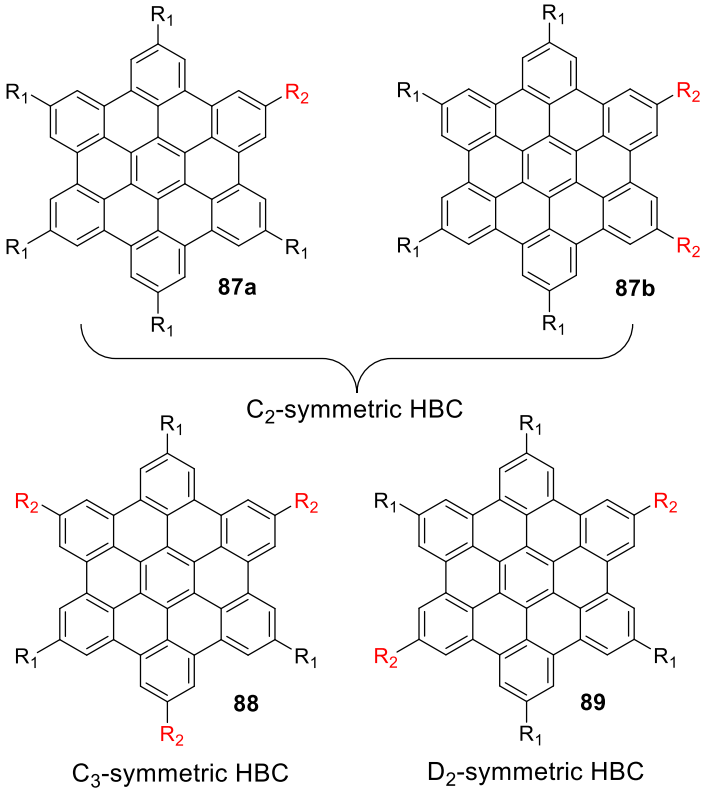

Figure 4.3: Low symmetry hexasubstituted HBC derivatives.

The route towards D_{6h} symmetric HBCs **86** (Scheme 4.3) is unfortunately not applicable to the preparation of less symmetric HBCs. An elegant pathway towards the synthesis of C_2-symmetric HBCs have been described by K. Mullen and co-workers (Scheme 4.4).[142]

Unsymmetrical HBCs are derived from unsymmetrical hexasubstituted benzene derivatives intermediates **94a-b**. These precursors are usually obtained *via* a [4+2] cycloaddition between a tetrasubstituted cyclopentadienone **92** and disubstituted acetylene derivatives **93a-b**. **92** is obtained *via* a double aldol condensation between a diketone **91** and the 1,3-disubstituted propan-2-one **90**. This method was chosen for this project.

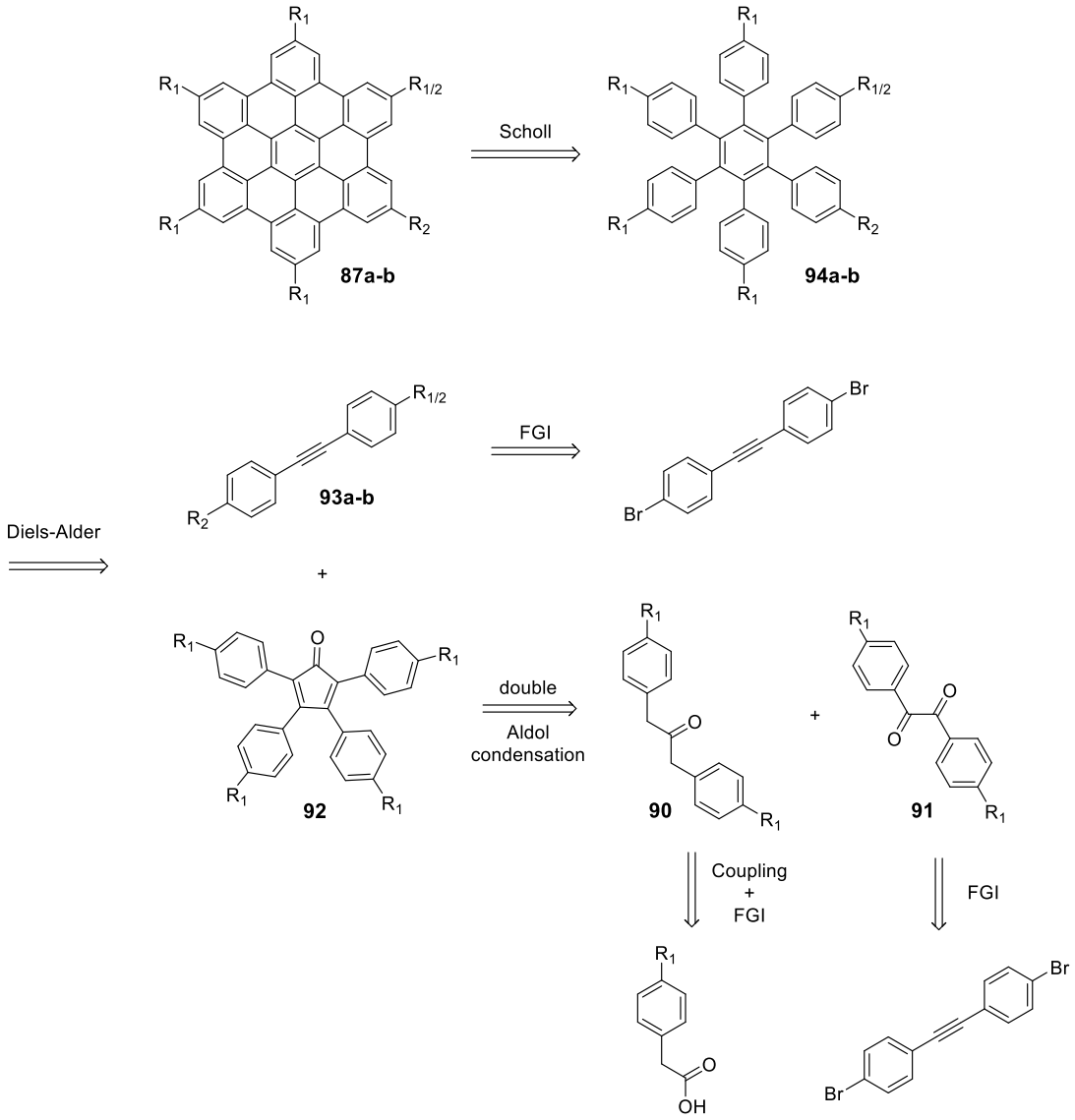

Scheme 4.4: Retrosynthetic route towards C2 or D2 symmetric HBC.

A large library of HBC derivatives has been described in the literature. The most common HBCs are substituted with six alkyl chains. Moverover, higher substituted HBC were published, such

as the dodecylsubstituted HBC **95** [145] or the octadecylsubstituted **96** [146](Figure 4.4).

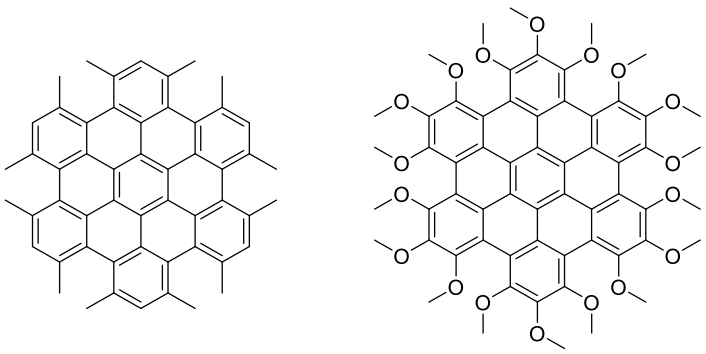

95 **96**

Figure 4.4: Example of dodecylsusbtituted and octadecylsubstituted substituted HBC.

4.2.2 Properties of hexabenzocoronenes

The HBC core properties have been extensively investigated. Crystallography reveals that the unsubstituted HBC core is packing into a monoclinic lattice with an interplanar distance of 3.42 Å.[147] As described above, the main drawback of the unsubstituted HBC core is its high melting point, and therefore its difficulty to be processed.

Due to their planar and large aromatic core surrounded by flexible chains, hexasubstituted HBCs exhibit liquid crystalline properties. HBCs self-assemble into one dimensional columns by π-π stacking interactions between their aromatic core. Due to the extended aromatic core, the charge mobility in HBC is excellent and was shown to be 10 times more efficient than in triphenylene derivatives.[148]

The liquid crystalline properties of HBCs can be tuned by their surrounding flexibles chains. Hexasubstituted HBCs melting point can be lowered by increasing the chain length or by introducing branched alkyl chains. The planarity of the HBC core can also be broken by steric effect, as shown in the 18-fold methoxy-substituted HBC **96** (Figure 4.4).

The application of HBCs as functional materials is vast. HBC can be found in lithium or sodium batteries as an intercalating component[149,150] or as a sensor for detection of volatile organic compounds.[151,152] Application of HBC in solar cell application have also emerged.[153]

To conclude, HBCs are very promising components for optoelectronic devices due to their outstanding electronic properties and their ability to form liquid crystalline 1-dimensional columns. Moreover, the available strategy to change the substituent and the symmetry of HBCs allows a good tunability of their optoelectronic and aggregation properties.

4.3 Literature review on perylene diimide (PDI)

Perylene-3,4-9,10-tetracarboxylic acid diimides **97**, commonly named perylene diimides (PDIs) (Figure 4.5), have also attracted a lot of attention. First prepared by M.Kardos in 1913[154] and used as a pigment for painting,[155] this family of compounds offers high chemical, thermal and photo stability.[156] A relatively large palette of colour can be obtained: from red to violet, burgundy or even black (examples presented in Figure 4.6). PDIs are still currently used in fibre colouring and industrial paints.[157]

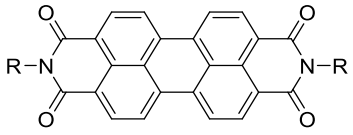

97

Figure 4.5: Structure of the perylene diimide core.

Despite their use in pigmentation, PDIS have been extensively reviewed for their applications in electronics and optics.[156–160]

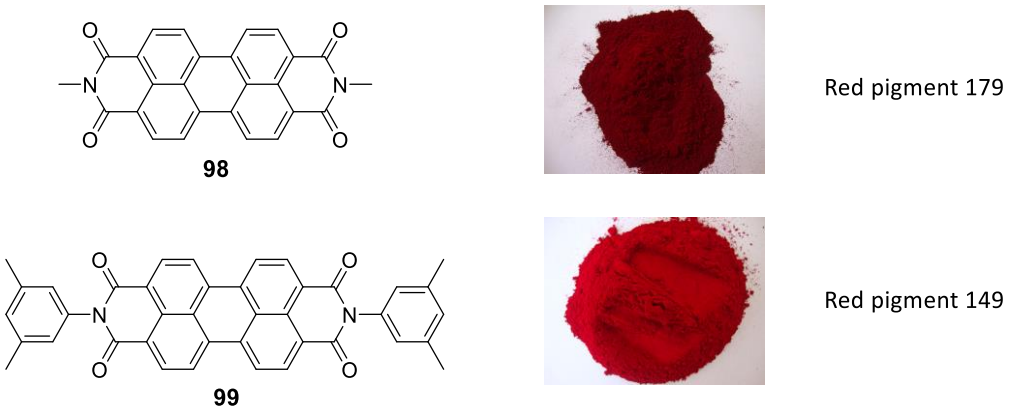

Figure 4.6: Examples of PDI based pigments. Pictures taken from www.honorpigment.com.

Nevertheless, PDIs as presented in Figure 4.6 suffer from poor solubility in organic solvent and have high melting points, and are therefore difficult to handle and study in optoelectronic applications. Strategies to obtain processable PDIs are described in the next section.

4.3.1 Synthesis of PDIs

Soluble and tunable PDIs are usually obtained *via* the functionalisation of the commercially available perylene-3,4-9,10-tetracarboxylic dianhydride (PTCDA) on three different sites, as highlighted in Scheme 4.5. The most common and the first described method relies on the substitution on the imide site. Substituents can also be incorporated in the bay position, *i.e.* at the 1,6,7,12- positions. A quite recent method consists as well in adding substituents in the ortho (2,5,8,11-) positions.

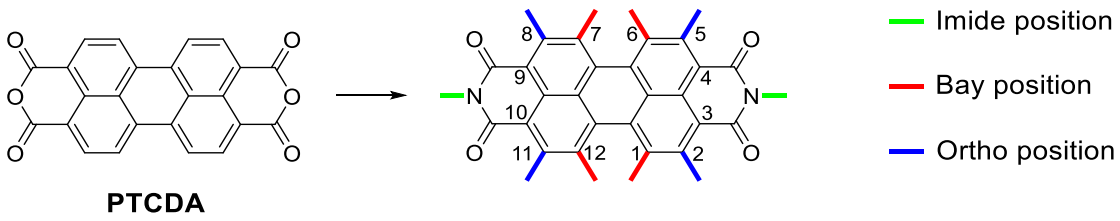

Scheme 4.5: Possible functionalisation of PDI core *via* at the different sites

The substitution of the imide position consists of the incorporation of linear chains, branched chains or bulky groups to increase the solubility of PDI. It is commonly carried out in one step,

by condensation of the corresponding primary amines on PTCDA in high boiling point solvent using a substoechiometric amount of zinc acetate as a catalyst. Typical solvents are imidazole or quinoline. Alternatively, solvent systems such as alcohols, water, carboxylic acid or alcohol:water mixtures such as (n-BuOH:H_2O) has been proposed, but generally offer lower yields.[157]

In order to obtain unsymmetrical PDIs substituted at the imide position, the aforementioned method offers poor yield, even when the primary amine is used in a substoechiometric amount.

Two practical approaches to prepare asymmetrical PDIs have been reported and are described in Scheme 4.6.[161] One possible strategy is based on using the symmetrical PDI **97** as the intermediate (Route A, Scheme 4.6). Hydrolysis of one of the imide position can be carried out affording the resulting perylene monoimide monoanhydride intermediate **100**. **100** is then reacted with a second primary amine to access the desired assymetric N,N'-dialkylated PDI **101**.

Another method relies first on the hydrolysis of PTCDA, affording the monoanhydride potassium salt intermediate **102** (Route B, Scheme 4.6). The monofunctionalisation by imidation of the anhydride, followed by the anhydride regeneration by acidification affords the monoimide monoanhydride PDI derivative **100**, with subsequent imidation leading to the desired compound **101**.

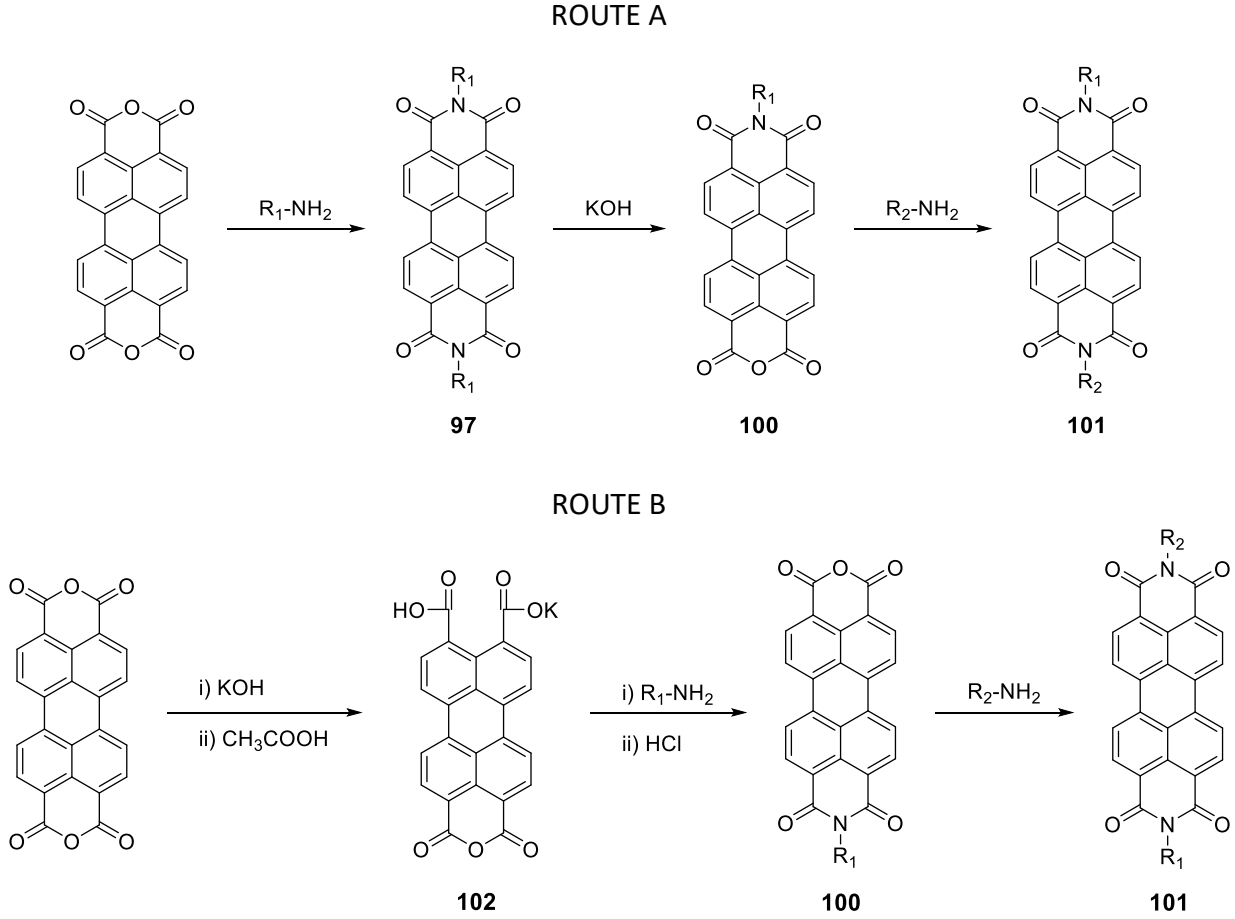

Scheme 4.6: Synthetic routes towards the synthesis of imide-substituted asymmetrical PDIs.

The substitution of the bay positions of PDI is more synthetically demanding. The precursors are typically the 1,7-dibrominated or the 1,6,7,12-tetrachlorinated PTCDA **103** and **104** (Figure 4.7). However, direct substitution on PTCDA bay positions requires challenging purification as mono- di- or tri- halogenated side-products are obtained. Moreover, the bromination or the chlorination leads to regioisomers.[162] As an example, the direct bromination leads to a mixture of the 1,6, the 1,7 dibrominated PTCDA and the tribrominated regioisomers. Due to the insolubility of PTCDA and its derivatives in organic solvents, obtaining the regioisomerically pure dibrominated compounds is difficult.[156]

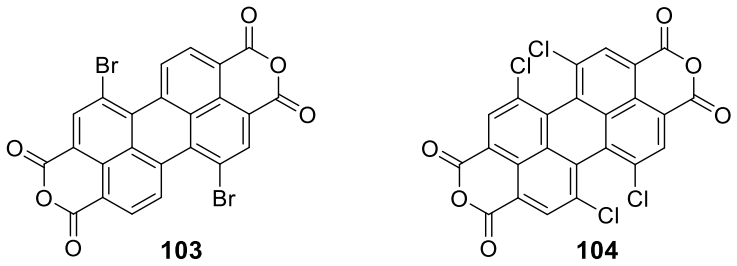

Figure 4.7: 1,7-dibromo and 1,6,7,12-tetrachloro perylene tetracarboxylic dianhydride **103** and **104**.

Recently, W.F. Jager and co-workers have developed a novel strategy towards regioisomerically pure **103**, using an early esterification of PTCDA as a key step (Scheme 4.7).[163] The intermediate **105**, which is now soluble in common organic solvents, is brominated in mild conditions to afford a mixture of the 1,6 and 1,7-dibromo-tetrabutylester perylene tetracarboxylic acid **106** and **107**. Their separation was performed by repetitive recrystallisations from DCM:ACN. **103** was obtained by acid catalysed cleavage of the esters and the subsequent regeneration of the anhydrides. One limitation of this approach is that the 1,6 regioisomer **107** could not be obtained isomerically pure.

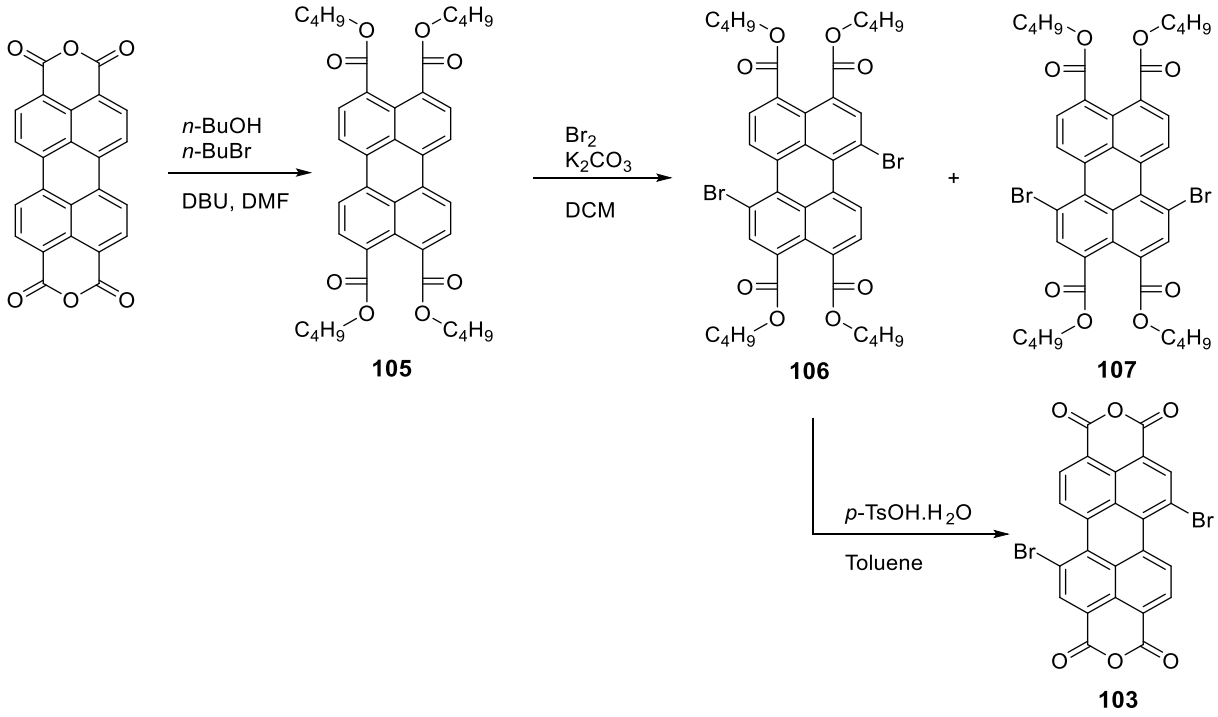

Scheme 4.7: Synthetic route towards regioisomerically pure **103**.

The nucleophilic substitution of the dibromo or tetrachloro derivative of PDI leads to a wide range of bay-substituted PDI, *via* a Suzuki, Sonogashira or Stille coupling and is limited to aryl, phenol, heteroaryl or alkynyl derivatives. However, the introduction of other nucleophiles (such as aliphatic alcohol) on the bay positions was showed to be difficult using this method.[157] To alleviate this synthetic issue, P. Hudhomme and co-workers published a synthetic access to of 1,7-dihydroxy perylene intermediates **108**, which can be subjected to a *Williamson* type ether synthesis (Scheme 4.8).[164] Although the mechanism was not described, it was claimed that the formation of the intermediate **108** is based on the oxidation of PDIs with manganese oxide in sulfuric acid, followed by the partial reduction in the presence of sodium bisulfite.

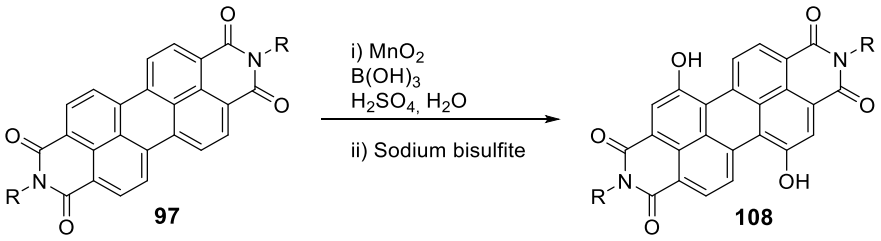

Scheme 4.8: Synthetic route towards 1,7-dihydroxy PDIs.

Recently, the synthesis of 2,5,8,11-substituted PDIs have been reported. This method, suitable for alkyl[165] or aryl[166] substitution, is based on a ruthenium-catalysed C-H activation and affords regioselective pure PDIs (Scheme 4.9).

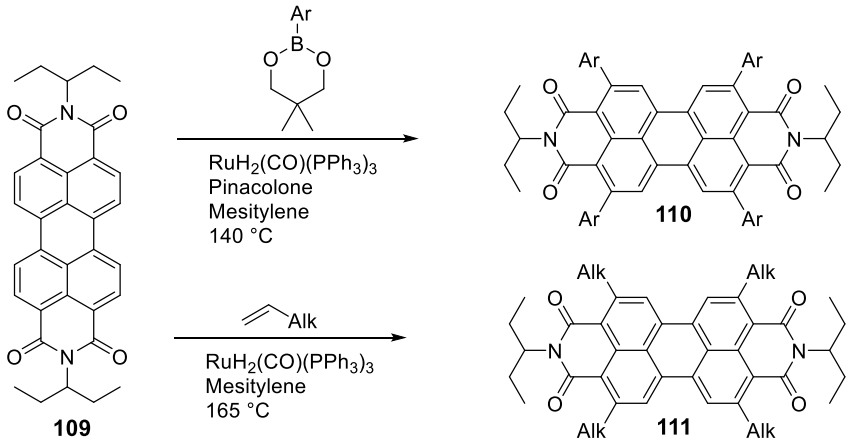

Scheme 4.9: Examples of *ortho*-substitution of **109**.[165,166]

In this thesis, the strategies described for the imidation and the substitution of the bay positions of PDIs will be used.

4.3.2 Properties of PDI

PDIs are considered as excellent organic dyes due to their high molar extinction coefficient, their large absorption spectra in the visible region and their high quantum yield. *N,N'*-dialkylated PDIs show characteristic absorption bands with a maximum absorption wavelength at *ca.* 526 nm, and is ascribed to a S_0-S_1 transition.[156] While a large palette of N,N'-disubstituted PDIs have been described in the literature, the influence of the substituent has little to no impact on their photophysical properties. Indeed, theoretical calculations showed that the nitrogen atoms are located on the nodal planes of both the HOMO and the LUMO. Changing the electronic effect of the substituent have therefore no influence on the HOMO and LUMO energies.[156] However, the optoelectronics can be tuned by introducing substituents on the bay or at the ortho position of the PDI core.

Due to their flat structure and the introduction of flexible surrounding chains, PDIs show liquid crystalline properties. The aggregation by π-π stacking of the aromatic core into columns allows PDIs to have high charge transport properties. Above average singlet exciton diffusion

has also been observed. As an example, an excellent exciton diffusion length of 96 nm was measured for the PDI derivative **112** (Figure 4.8).[167] PDIs have therefore been used in optoelectronics. Applications of PDIs include organic field effect transistors (OFETs), dye lasers[168,169], Organic Light Emitting Devices (OLEDs)[170], single-molecule sensing[171] or biology applications.[172]

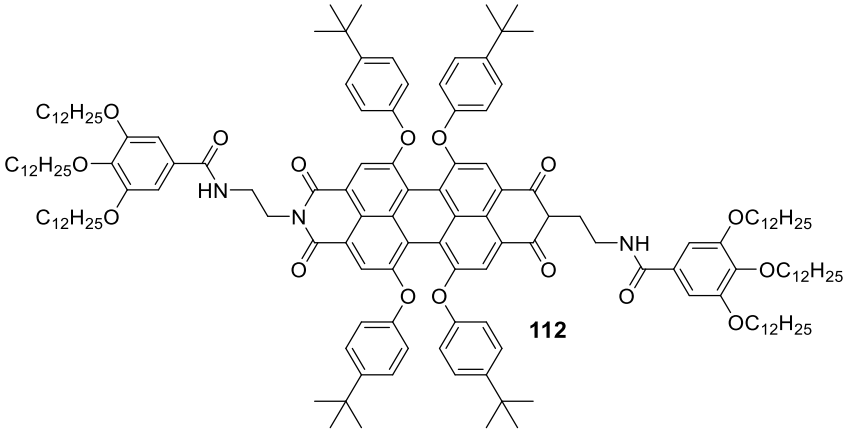

Figure 4.8: Chemical structure of **112**.

PDIs have also shown great promise in the area of organic solar cells. The first bilayer organic solar cell described by Tang was based on the PDI derivative **5** (see section 1.2.1). Due to the relatively high production cost of fullerenes, their low possibility of functionalisation and their limited absorption of the solar radiation, PDIs have been used as an interesting electron acceptor replacement.[11,12] Numerous examples of solar cells containing PDI derivatives have been published.[157,158,160,173]

4.4 Choice of the incompatible materials

As shown in the previous sections, HBCs and PDIs have been extensively studied as potential materials for optoelectronic applications. Organic solar cells based on these materials have been reported.[174] As published by J. D. MacKenzie and co-workers in 2001, the HBC derivative HBC-PhC12 and *N,N'*-bis(1-ethylpropyl)-3,4,9,10-perylene diimide PDI **113** have been used as

active components for solar cell applications and their photovoltaic properties (Figure 4.9). Using a 40:60 blend of HBC-PhC12:PDI, sandwiched between an aluminium and a indium tin oxide (ITO) electrode, a maximum power efficiency of 1.95% under a 490 nm illumination source was obtained. A morphological study of this blend was carried out using atomic force microscopy (AFM) and field-emission scanning electron microscopy (FESEM). It was claimed that the solubility difference between HBC-PhC12 and **113** induces a vertical macrophase separation of the two components during the thin film preparation onto a Si(100) wafer. Indeed, crystalline **113** was found at the surface, while HBC-PhC12 was located between **13** and the substrate. The blend therefore adopts a bilayer structure. Despite its acceptable PCE (1.95% at 490 nm), it was anticipated that this system could be optimized by modifying the morphology of the active layer.

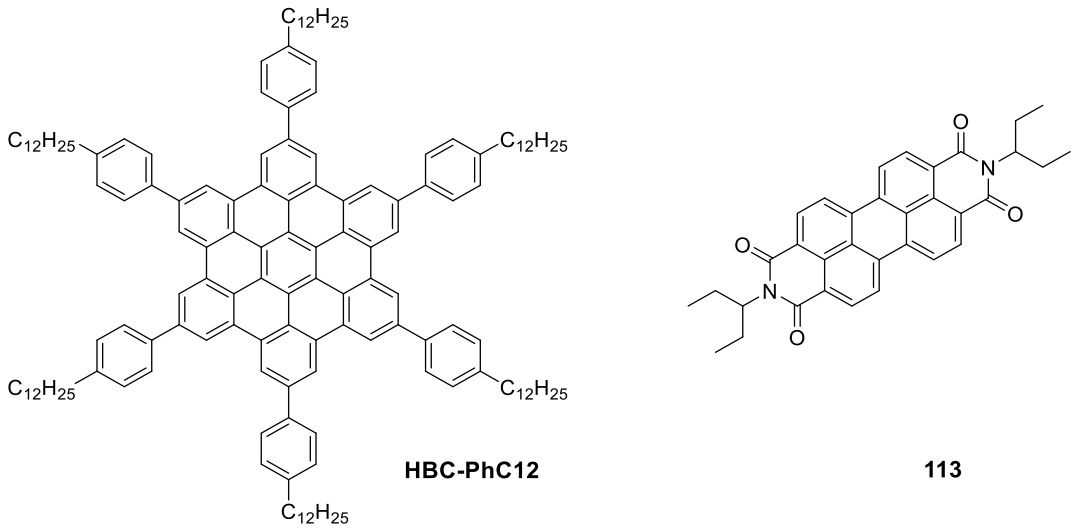

Figure 4.9: Structure of HBC-PhC12 and **113**.[174]

We therefore decided to base our morphology control of functional incompatible materials on these derivatives. As a way to introduce incompatibility between the HBC and the PDI derivative, the successful method of pendent-chain incompatibility used in the triphenylene work was adapted to the HBC:PDI binary mixture. The electron donor HBC-PhC12, containing

hydrophilic dodecyl chains was our first target. As a hydrophilic and electron acceptor PDI, we designed ethylene-glycol based PDIs substituted on either the imide or the bay position.

In this section, the synthesis and characterisation of HBC-PhC12 is described. Several designs of ethylene-glycol based PDIs, as well as will be targeted and their synthesis and characterisation are discussed.

4.4.1 Synthesis of HBC-PhC12

The target molecule HBC-PhC12 (Figure 4.10) was prepared following the literature procedure as shown in Scheme 4.10.[175]

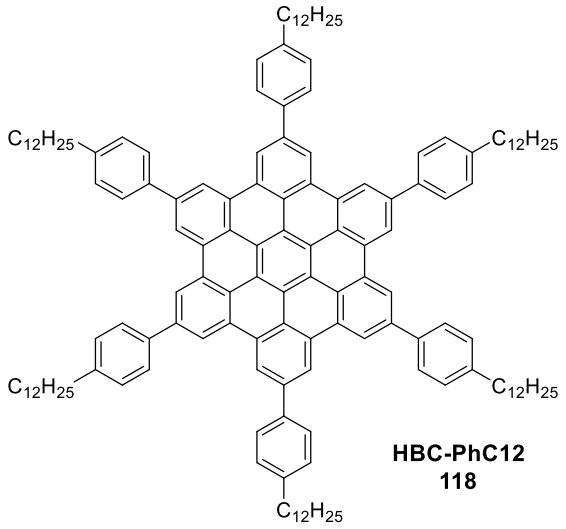

Figure 4.10: Structure of the target electron donor HBC-PhC12, **118**.

A *Kumada* coupling between the commercially available bis(4-bromophenyl)acetylene and the freshly synthesised 4-dodecylbenzene magnesium bromide **114**, using $PdCl_2$(dppf) as a catalyst, afforded the disubstituted acetylene derivative **115** in a 82% yield. **115** was then trimerised using dicobaltoctacarbonyl as the catalyst in dry dioxane and under argon and afforded the hexa-substituted benzene derivative **116** in moderate yield. It is worth noting

that extra care of the solvent dryness and the absence of air are crucial for the reaction to proceed.

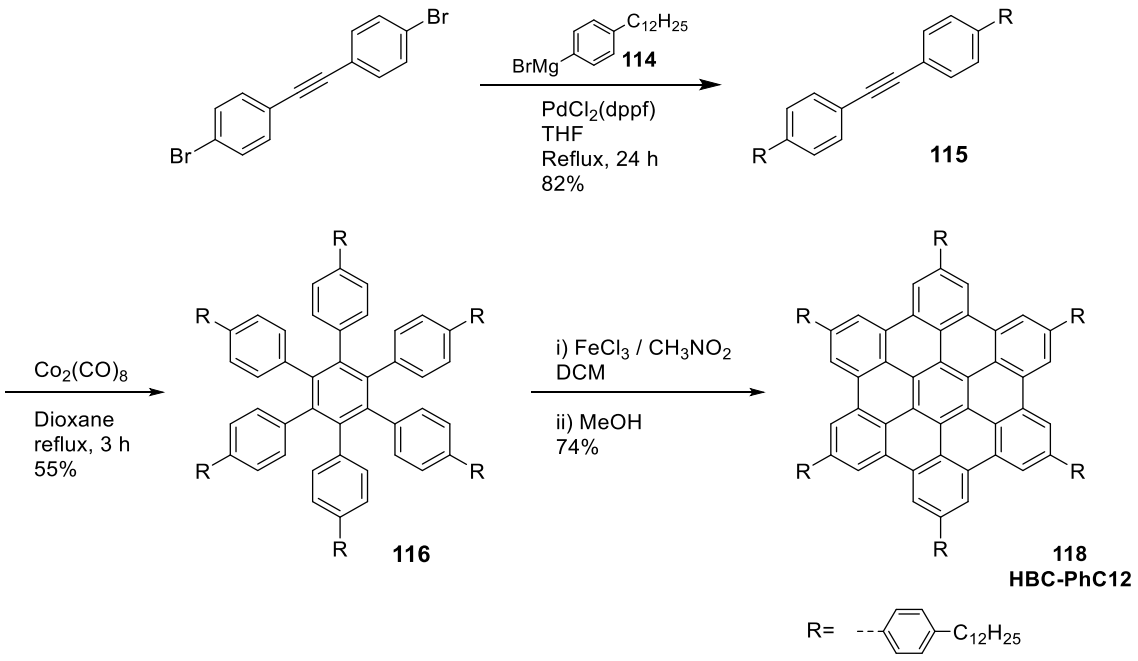

Scheme 4.10: Synthesis of HBC-Ph12, **118**.

The oxidative cyclodehydrogenation of **116** under *Scholl*'s conditions was investigated. Müllen, Spiess and co-workers suggested to dilute **116** in dichloromethane, and add a solution of iron(III) chloride in nitromethane, while the solution was bubbled with a constant stream of argon. However, neither the dilution, the temperature nor the equivalent of iron(III) chloride was mentioned. Test reactions were therefore carried out to find the optimal conditions for the reaction to proceed (Table 4.1) and were monitored by ^{1}H NMR (Figure 4.11).

Based on our previous work on the oxidative cyclodehydrogenation of 1,2-dialkoxybenzene to obtain triphenylene derivatives, we decided to react **116** with 3 equivalents of iron(III) chloride by C-C bond creation in a 0.1 M solution. A constant stream of argon was used during the entire reaction time as suggested by the literature. Indeed, it is used to remove the

hydrochloric acid produced during the reaction.[176] No conversion was observed when the gas flow was lacking. The same outcome was observed when no control of the temperature was done (Table 4.1, entry 1).

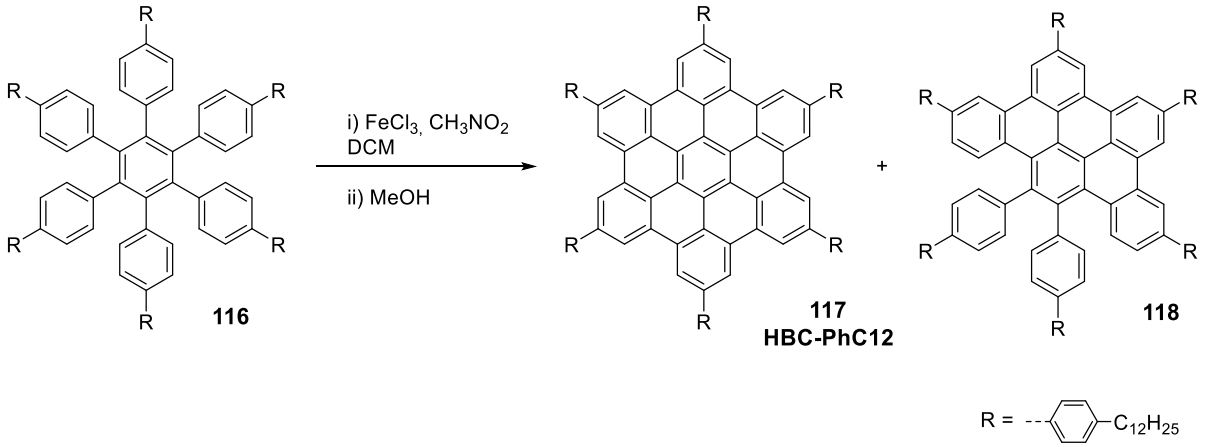

Scheme 4.11: Oxidative cyclodehydrogenation of **116** under *Scholl*'s conditions.

The number of equivalents of $FeCl_3$ was increased to 3.3 per C-C bond formed (Table 4.1, entry 2). ^{1}H NMR spectrum (Figure 4.11, 2) shows new peaks which do not fit to HBC-PhC12 but to a new product that corresponds to a semi-cyclized HBC-derivative **118** (Scheme 4.11), as previously described by J. S. Moore and co-workers on ethylene glycol based HBCs.[121] This result was also confirmed by LD+ mass spectrometry. Increasing the dilution leads to more half-cyclized HBC formation (Table 4.1, entry 3 and Figure 4.11, 3).

Those test reactions demonstrated the importance of controlling the temperature. Indeed, bubbling argon during the entire reaction time led to solvent evaporation as well as a decrease in the reaction mixture temperature. High dilution of the starting materials was required to avoid complete evaporation of the solvent. Furthermore, iron(III) chloride had to be used in a large excess to perform the complete cyclisation of the **116**.

The reaction using 7.5 equivalents per C-C bond creation, highly diluted (3 x 10^{-3} M), at a controlled temperature of 21 °C was therefore performed for 90 min (Table 4.1, entry 4). ^{1}H NMR of the crude shows very broad peaks. No starting materials were observed.

Entry	Eq. $FeCl_3$	Dilution (10^{-3} M)	T (°C)	T control[a]	Reaction time (min)	Result
1	18	100	rt	no	30	No conversion
2	20	40	21	yes	30	**118** (37%[b])
3	20	80	21	yes	30	**118** (76%[b])
4	45	3	21	yes	90	HBC-PhC12

Table 4.1: Study of the oxidative trimerisation of **045**. [a] The temperature control was achieved using a bain-marie. [b] The yields are determined by ^{1}H NMR.

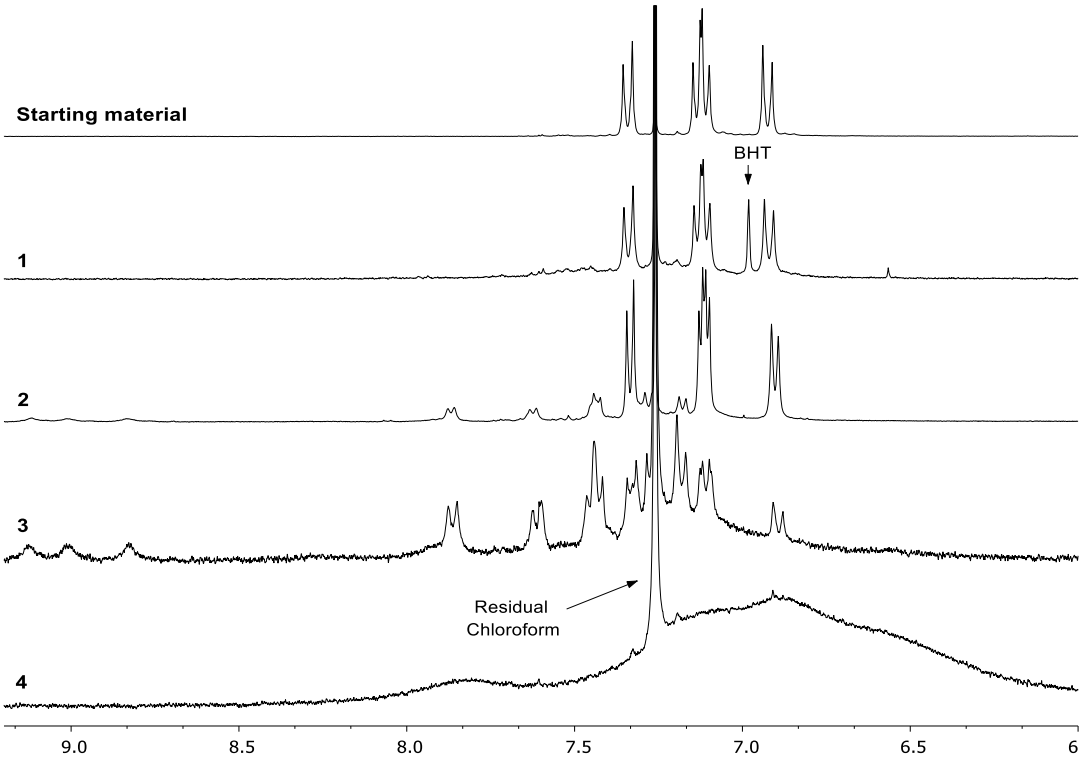

Figure 4.11: ^{1}H NMR ($CDCl_3$, rt) of the crude test reaction zoomed in the aromatic region (9-6 ppm).

After analysis by NMR in 1,4-dichlorobenzene-d4 at 85 °C, the shifts and the integration corresponds to the desire compound HBC-PhC12. The same procedure was carried out in larger scale and HBC-PhC12 was afforded in a 74% yield (Figure 4.12).

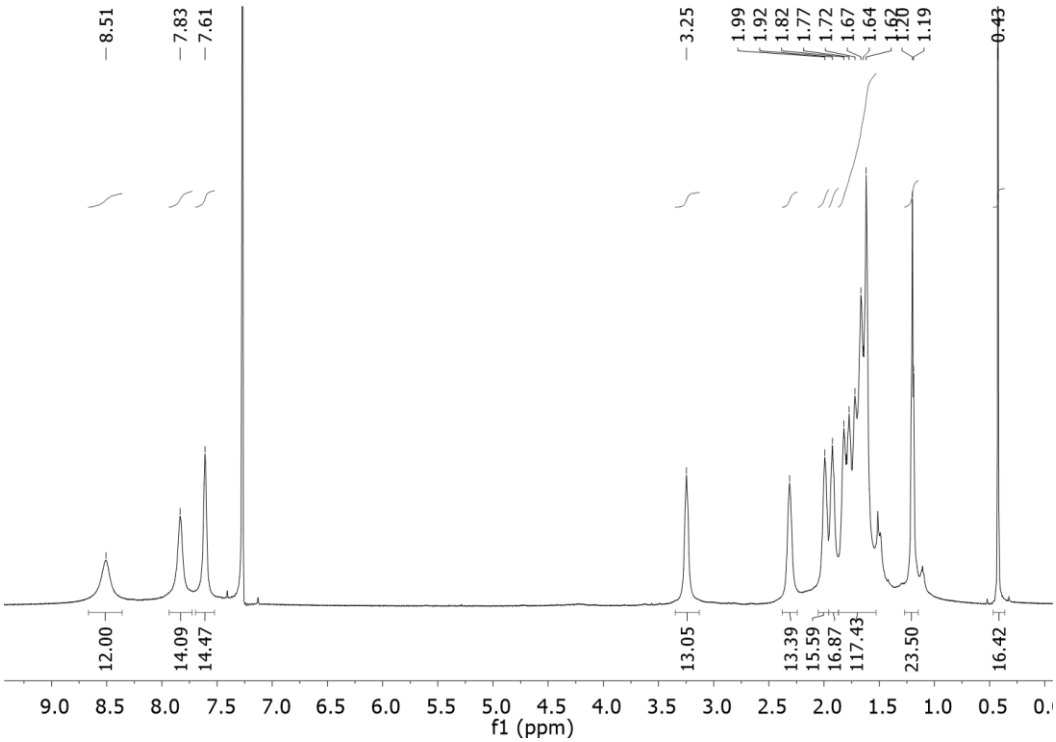

Figure 4.12: ^{1}H NMR spectra (*p*-$C_6D_4Cl_2$, 85 °C) of HBC-PhC12, **118**.

To conclude, the synthesis of HBC-PhC12 was carried out in 3 steps with an overall yield of 33%. The control of the temperature, the constant bubbling of argon, high dilution and the use of iron(III) chloride in large excess (7.5 eq. par C-C bond creation) are crucial in order to the oxidative cyclodehydrogenation to proceed and to avoid any residual half-cyclised HBC derivatives.

4.4.2 Properties of HBC-PhC12

The properties of HBC-PhC12 was investigated by absorption and emission spectroscopy in both solution and solid state. Its mesogenic properties were also determined by POM, XRD and AFM and discussed in this section.

The absorption of a solution of HBC-PhC12 in THF shows two main bands located at 380 nm and 415 nm (Figure 4.13, solid line). When excited at a wavelength of 380 nm, the maximum emission band is located at 515 nm, with a Stokes shift of 135 nm (Figure 4.13, dashed line).

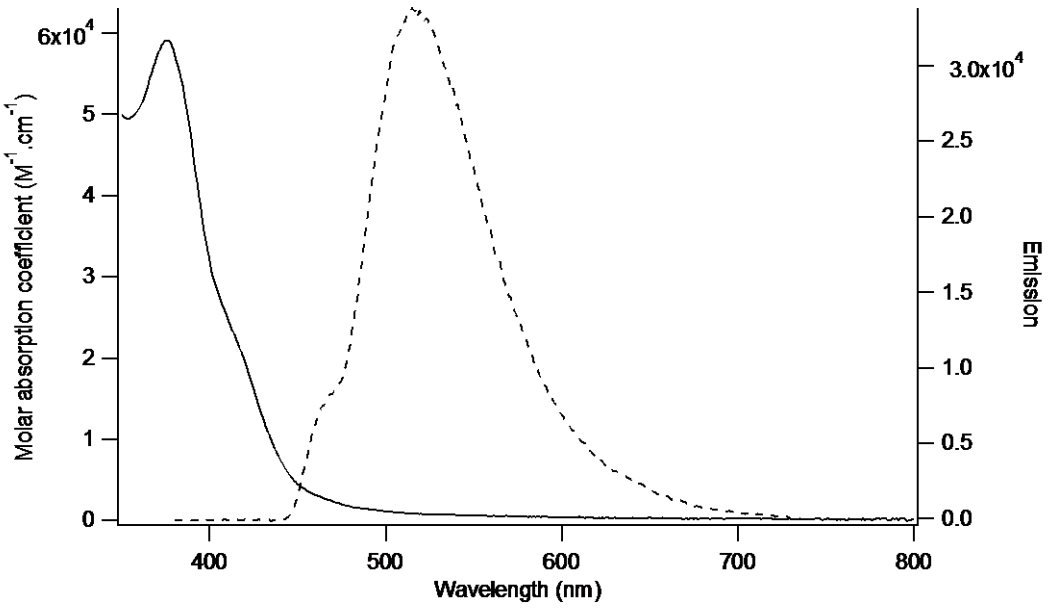

Figure 4.13: Absorption (solid line) and emission spectra (dashed line) of a 4 µM solution of HBC-PhC12 in THF. Excitation wavelength: 380 nm.

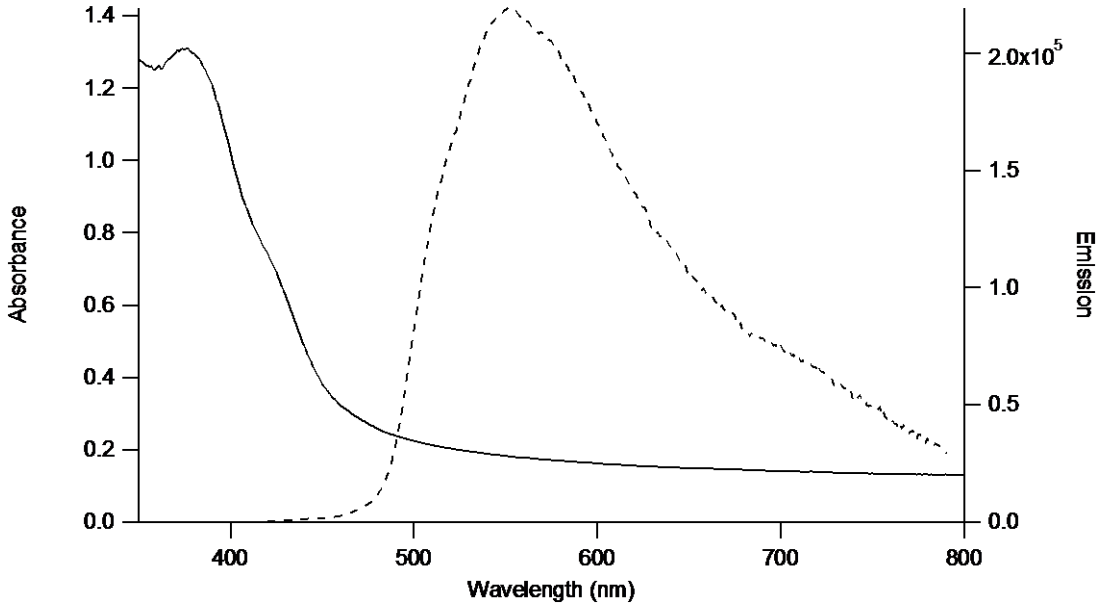

Figure 4.14: Absorption (solid line) and emission spectra (dashed line) of a thin film of HBC-PhC12 on a glass slide. Excitation wavelength: 405 nm.

Except for the presence of broader peaks, the absorption and emission profile of HBC-PhC12 in solid state does not differ from the one in THF (Figure 4.14).

The presented absorption and emission spectra are in accordance with those in the literature.[177,178]

The mesogenic properties of HBC-PhC12 have been investigated by polarized optical microscopy. As observed in Figure 4.15a, HBC-PhC12 does not show any birefringence. Attempted heating above the clearing point to reorganize the thin film was unsuccessful as decomposition occurs from 300 °C. Attempted thermal annealing below HBC-PhC12 clearing point (200 °C for 2 h) does not show any reorganisation of the film either (Figure 4.15b). In both pictures, numerous cracks are observed.

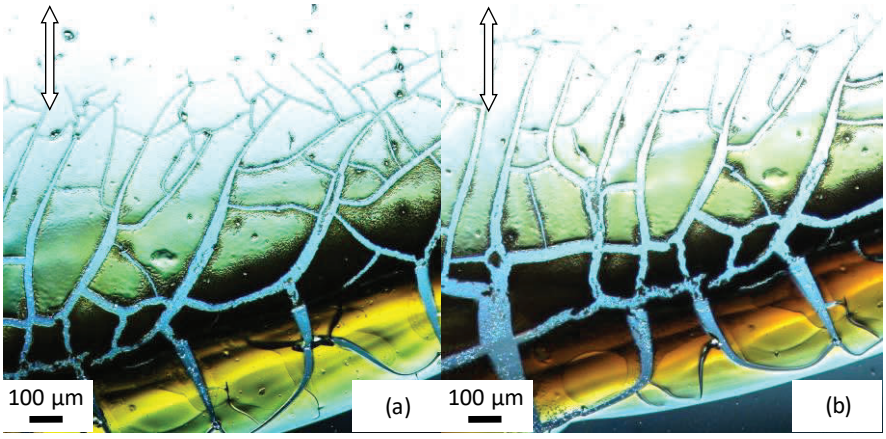

Figure 4.15: POM image of HBC-PhC12 from THF solution on regular glass: (a) as-casted, (b) after thermal annealing.

To force the reorganisation of HBC-PhC12 in solid state, another substrate was used. Glass can be coated by various silanes, and the interaction with the sample can be tuned. Aminopropyl silane (APS) was the coating used in this work. By covalently bonding to the glass, APS enhances the hydrophilicity of the glass due to the terminal amino groups at the end of the propyl chains (Figure 4.16).

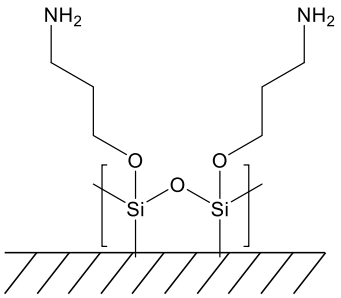

Figure 4.16: Structure of aminopropyl silane (APS) coated glass

Unfortunately, HBC-PhC12 deposited on APS-coated glass from drop-casting in THF did not show any birefringence either (Figure 4.17). A more even thin film was nevertheless obtained compared to regular glass. Attempted annealing below the clearing point of the compound (200 °C for 2 h) does not show any reorganization of the compound by POM (Figure 4.17b).

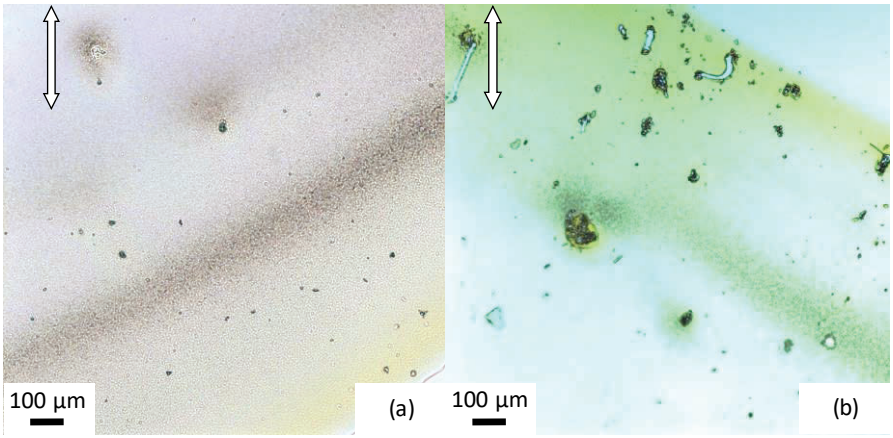

Figure 4.17: POM images of HBC-PhC12 from THF solution on APS-coated glass: (a) as-casted, (b) after thermal annealing. The pictures were taken at different regions.

To conclude the POM study, HBC-PhC12 does not show any birefringence on regular or APS-coated glass. Attempted annealing of the sample to reorganize the structure is not possible as the decomposition of the compound occurs before reaching its clearing point.

X-ray diffraction of HBC-PhC12 was therefore attempted to have a better understanding of the thin film structure. Unfortunately, no diffraction peak was observed using a copper or a cobalt source. This result is not in accordance with the literature, where an X-ray diffractogram has been obtained for this compound.[179]

By combining the POM and the XRD results, it can be therefore inferred that in our case, HBC-PhC12 is in amorphous form. Despite our efforts to change the organization by varying the type of substrate or by thermal annealing, no major reorganisation of the film has been observed. The high viscosity of HBC-PhC12 could explain this difficulty. A possible explanation for this counter intuitive result can be the presence of an impurity which prevents the crystallisation. It is also likely that the deposition method (drop-casting) and the solvent used (THF) could force HBC-PhC12 to adopt an amorphous structure. Unfortunately, no POM study of HBC-PhC12 was found in the literature to allow comparison with our results.

The organisation of HBC-PhC12 was therefore observed under atomic force microscopy (AFM) to obtain information on the structure at a micro/nano level. Due to the better uniformity of the film on APS-coated slides, the AFM study was solely investigated on this substrate. In as-casted HBC-PhC12 films, large columns are observed (Figure 4.18, left). Those columns, with a 10 to 20 nm height and 250 to 350 nm wide can be ascribed to large aggregates of HBC-PhC12 as the height and width is too large for a single column (Figure 4.19). The thermal annealing of the sample suppresses the formation of the column and a disorganized structure was observed (Figure 4.18, right).

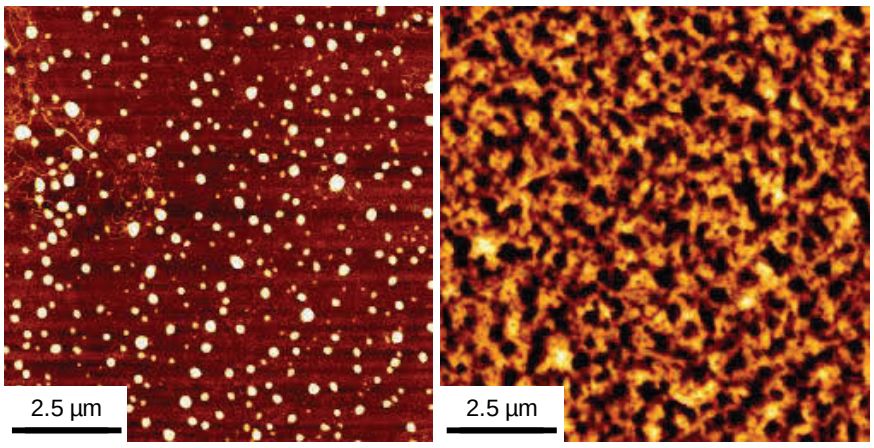

Figure 4.18: AFM of HBC-PhC12 on APS-coated glass: Left: as-casted, Right: after thermal annealing.

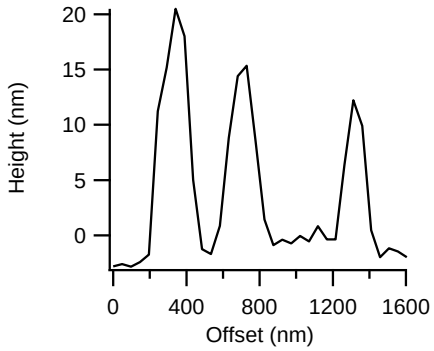

Figure 4.19: HBC-PhC12 as-casted thin film cross section on APS-coated glass.

To conclude, the synthesis of HBC-PhC12 was therefore achieved and efforts towards its characterization were attempted. However, the difficulty to handle HBC-PhC12 in thin film form prevents any definite conclusion about the organization by POM. POM and XRD studies of such thin films are pointing towards an amorphous film. Despite the definite presence of HBC-PhC12 by NMR and mass spectrometry, the presented results contradicts the studies in the literature of this material.[175,179]

4.4.3 Synthesis of ethylene glycol based perylene diimides

Based on our previous work on triphenylenes, we decided to design hydrophilic PDIs based on ethylene glycol pendant chains. In this section, the synthesis and characterisation of three different PDIs will be discussed. As a simple derivative, the substitution of the imide position with linear ethylene glycol-based chains will be described. The second strategy was to focus on substituting the bay position of the PDI core. Finally, branched chains were to be added at the imide position.

4.4.3.1 1st design: alkylation of the imide position with linear ethylene glycol based chains

As PDI derivatives bearing linear ethylene glycol-based chains at the imide positions, two PDIs **122a** and **122b** were designed (Figure 4.21).

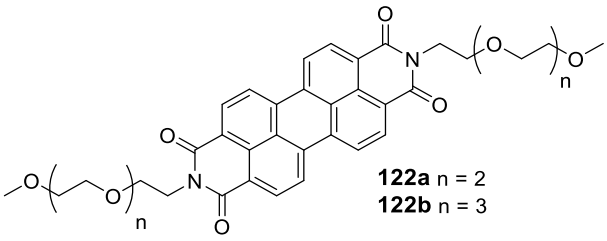

Figure 4.20: Chemical structures of **122a** and **122b**.

The synthesis of **122a** and **122b** was carried out *via* the substitution of the corresponding primary amines on perylene-3,4,9,10-tetracarboxylic dianhydride PTCDA (Scheme 4.12).

The linear primary amines were synthesised from the commercially available tri- or tetra- ethyleneglycol monomethyl ether (Figure 4.21). The terminal hydroxyl groups of the ethylene glycol monomethyl ether motifs were tosylated to generate a good leaving group for the nucleophilic substitution. The bromo compounds **119a** and **119b** were both obtained in quantitative yield. These halogenated chains were converted to the desired primary amine chains *via* a *Gabriel* reaction: a nucleophilic substitution using potassium phthalimide salt in DMF afforded the phthalimide intermediates **120a** and **120b** which, with subsequent hydrazinolysis led to the desired linear amines **121a** and **121b** in respectively a 59% and 67% overall yield.

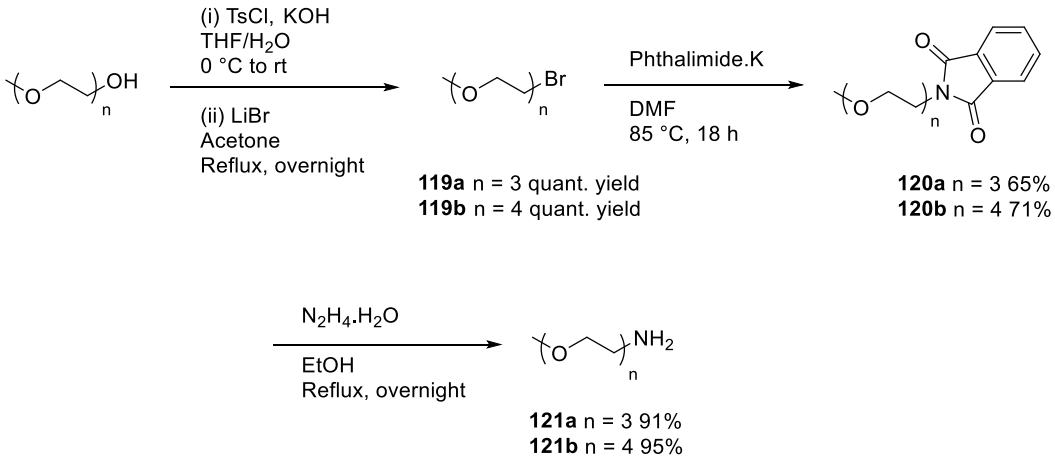

Figure 4.21: Synthesis of linear ethylene-glycol based primary amines **121a** and **121b**.

PTCDA was reacted with the synthesized primary amine (Scheme 4.12). The best conversion to *N*,*N*'-dialkylated perylene diimide was obtained with quinoline as solvent and a substoichoimetric amount of zinc acetate dihydrate at 180 °C for 6 h.[208] **122a** and **122b** were therefore obtained in respectively a 81% and 71% yield as dark red solid, characteristic of PDI derivatives.

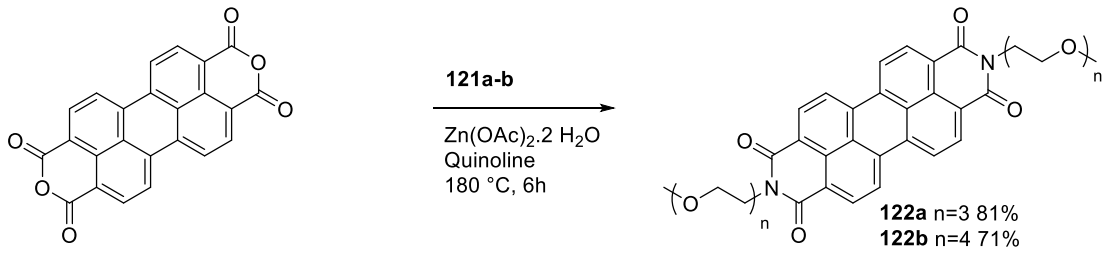

Scheme 4.12: 1st design PDI synthetic scheme.

Overall, the syntheses of the PDI derivatives **122a** and **122b** were carried out in 4 steps in a 48% yield in both cases. The properties of these derivatives were then investigated, as outlined below.

122a shows limited solubility in chloroform whereas **122b** is fully soluble. Their mesogenic properties were investigated by POM. The estimated clearing points of **122a** and **122b** are situated above 300 °C (320 °C for **122a** and 300 °C for **122b**). Due to the high viscosity of both components, the crystalline to liquid crystal transition could not be clearly observed on POM. DSC and X-ray diffraction were therefore required in order to obtain the full mesogenic properties of **122a** and **122b**. However, HBC-PhC12 decomposes in this temperature range. The morphology study of HBC-PhC12:**122a** and HBC-PhC12:**122b** is therefore challenging to investigate. Moreover, it was found that those derivatives are very viscous, even above their clearing points.

To conclude, two PDI derivatives **122a** and **122b** were synthesised by imidation of PTCDA. Those two liquid crystalline compounds show high clearing point temperatures, which can be a drawback for the morphological study of binary or ternary mixtures. To facilitate the morphology study, other PDI derivatives, with lower transition temperature were therefore designed.

4.4.3.2 2nd design: alkylation of the bay position

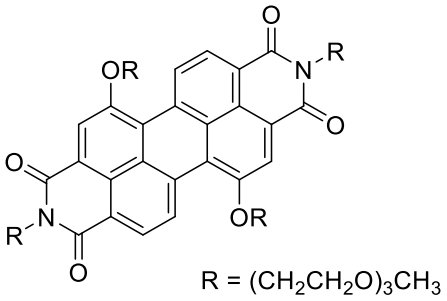

Figure 4.22: Structure of the target compound.

The synthesis of hydrophilic ethylene glycol-based perylene diimides, substituted at the 1,7-positions by linear chains, was investigated (Figure 4.22). Indeed, due to its steric hindrance, the introduction of substituents at the PDI bay position reduces the π-π stacking between the aromatic core, resulting in lower melting points and a better solubility in common organic solvents.

The synthesis of this second design of hydrophilic PDI is described in Scheme 4.13. Following the literature procedure, the regioisomerically pure 1,7-dibromo PTCDA **103** was used as an precursor of the desired targets (Scheme 4.13).[163] PTCDA was therefore esterified using 1-butanol and 1-bromobutane to obtain the perylene-3,4,9,10-tetrabutyl ester **105**. This intermediate was then brominated under mild conditions using bromine and potassium carbonate in dichloromethane. The resulting mixture of 1,6- and 1,7- dibrominated PDIs (respectively **107** and **106**) was separated by successive recrystallisations of the 1,7-isomer

from an ACN:DCM mixture. The conversion of the 1,7-dibrominated perylene tetraester **106** to the desired regioisomerically pure **103** was achieved by treatment with *p*-TsOH.H_2O in toluene. The overall yield was satisfactory (30%) and the reaction was easily scalable to obtain several grams of the intermediate **103**.

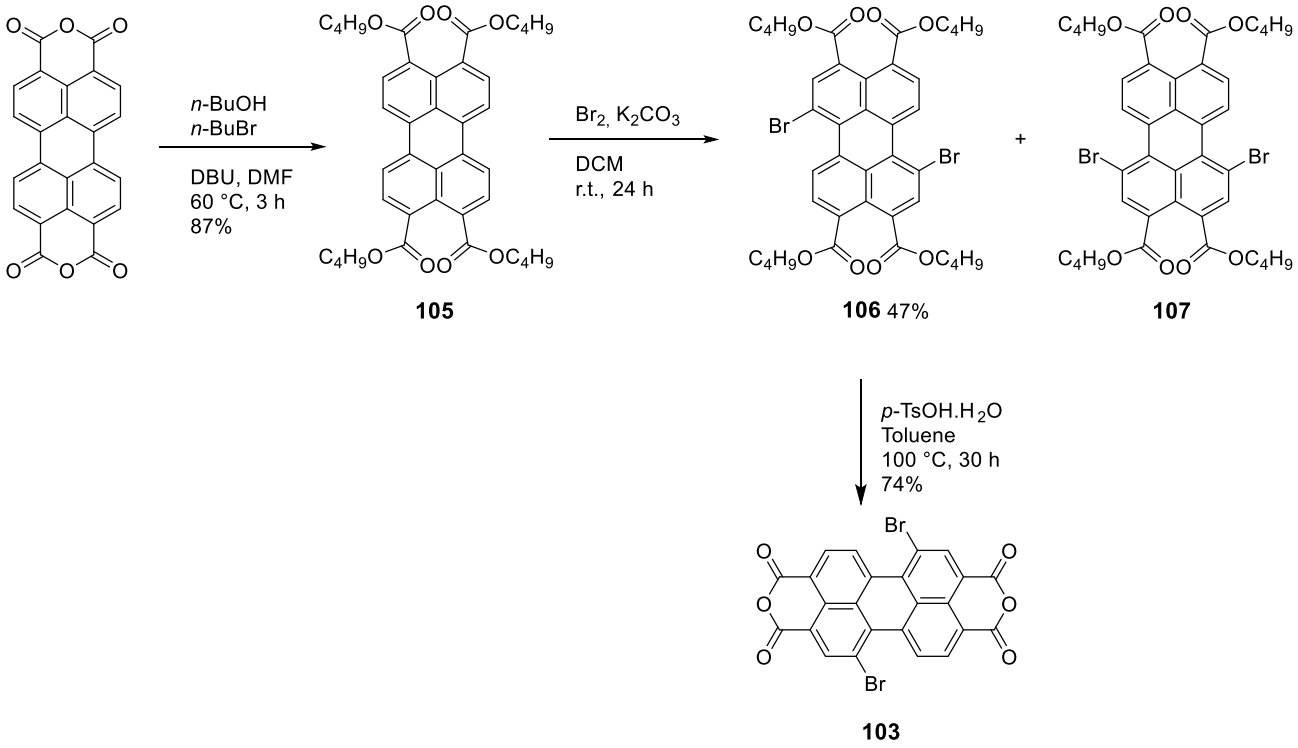

Scheme 4.13: Synthesis of 1,7-dibromo perylenetetracarboxylic acid **103**.

103 was then reacted with the linear amine **121a** to obtain the 1,7-dibrominated PDI **123** in a 51% yield (Scheme 4.14). The addition of ethylene glycol-based chains at the bay postion was carried out *via* a *Williamson* type reaction between the NaH-deprotonated triethylene glycol monomethyl ether and **123**. ^{1}H NMR of the crude reveals the presence of the free ethylene glycol monomethyl ether chains. After separation of the chains by column chromatography, the resulting dark red solid, present in low quantity was analysed by mass spectrometry (ES+ mode). Mass spectrometry (ES+) reveals the presence of the sodium adduct of the desired compound **124** (m/z = 1029.6 g.mol^{-1}) and the monoalkylated side product **125**

(m/z = 945.0 g.mol^{-1}) among other peaks that could not be attributed. No peak corresponding to the starting materials was found. Analytical HPLC of the fraction also shows a complex mixture, with no efficient separation. The alkylation on the 1,7 bay position of PDI for the 1,7-dibrominated PDI was reported as difficult[164] unlike the substitution of bromine to phenoxy or pyrrolidinyl groups.[180] P.Hudhomme and co-workers have inferred that the alkoxy chains could react with the imide positions.[164]

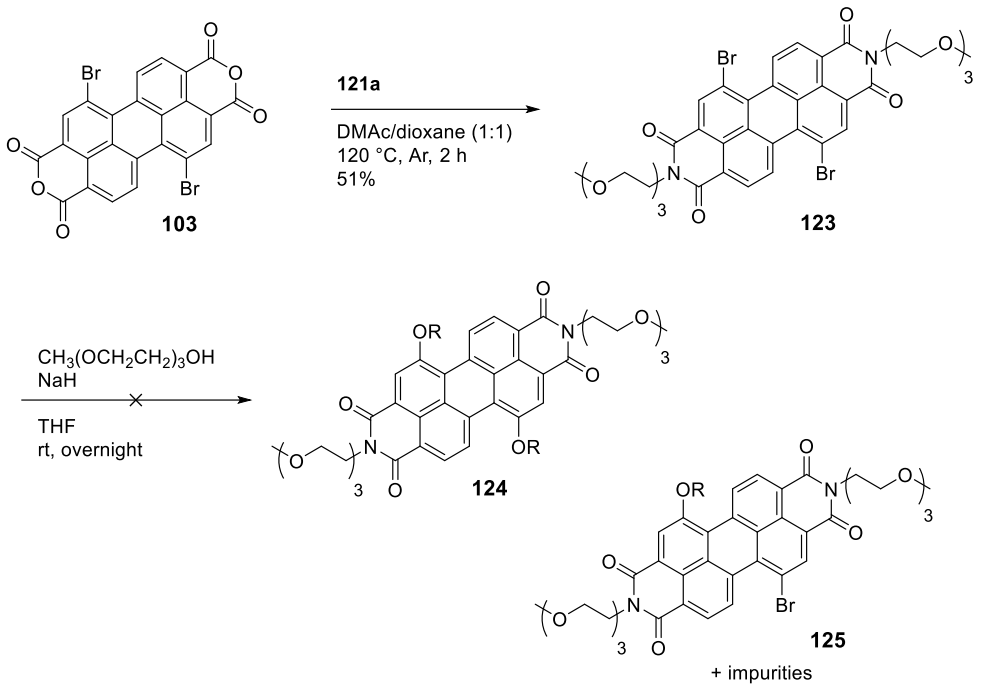

Scheme 4.14: Synthesis of 1,7-dialkoxy PDI from the corresponding 1,7-dibromo PDI.

Another synthetic route was therefore designed (Scheme 4.15). 1,7-Dihydroxyperylene diimides were successfully synthesised from perylene diimides *via* oxidation using manganese dioxide and boric acid in sulfuric acid:water followed by partial reduction with sodium bisulfide.[164,181] **122a** was therefore oxidised. After working-up, the resulting brown solid was found to be insoluble in common solvent and characterisation by ^{1}H NMR could not be carried out. The crude was therefore engaged in the next step without further purification. A *Williamson* type ether synthesis was performed using the brominated chain **119a** in DMF

(Scheme 4.15). Unfortunately, no traces of the product or the 1,7-hydroxy PDI was found in either ^{1}H NMR or mass spectrometry (ES +, LD+ or LD-).

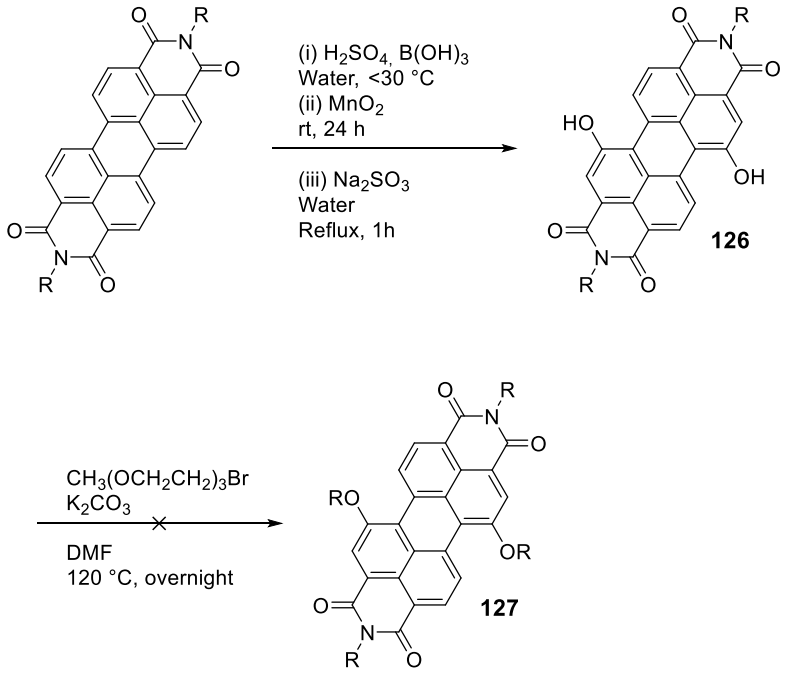

Scheme 4.15: Synthesis of **127** from the corresponding PDI **126**.

The synthesis of 1,7-disubstituted PDI with ethylene glycol based chains was therefore abandoned. As a new low-clearing point PDI, we decided to focus our research on the synthesis of PDI bearing branched ethylene glycol-based chains at the imide positions. The synthesis of this third design PDI will be discussed in the next section.

4.4.3.3 3rd design: alkylation of branched chains at the imide position

The synthesis of a PDI with branched ethylene-glycol based chains at the imide position was investigated. The compound, named BPDI thereafter and described in Figure 4.23 was designed. Due to the steric hindrance of the branched chains, we anticipated that the transition temperature would be lower than its analogues 1st design PDIs. This novel compound BPDI derives from similar PDIs found in the literature.[161,182]

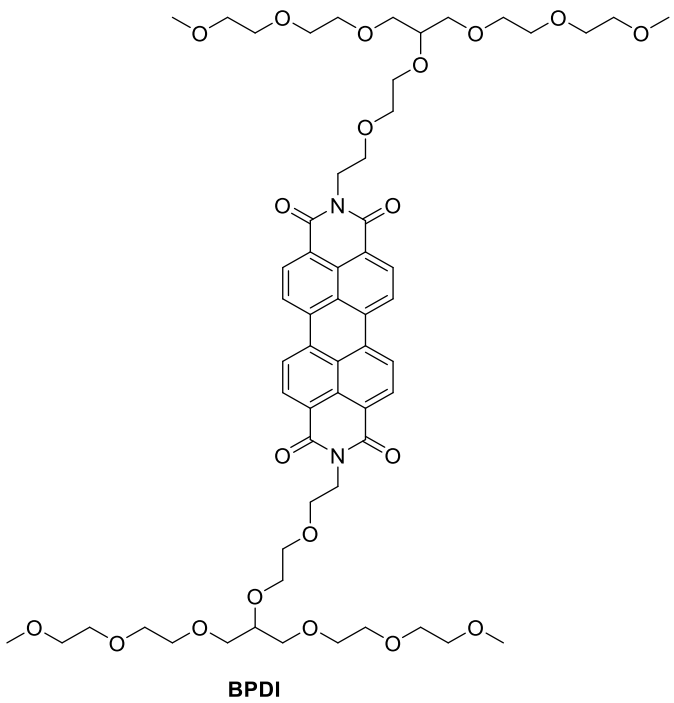

Figure 4.23: Structure of the target compound BPDI.

The synthesis of the primary amine branched chain is described in Scheme 4.16. The secondary alcohol building block **128** was prepared *via* a double nucleophilic substitution from the commercially available epichlorhydrin with the sodium salt of diethylene glycol monomethylether,[183] and was obtained in a multi gram scale in a 74% yield.

As described in the literature, the secondary alcohol **128** can be converted to its primary amine derivative using ammonia in combination with a ruthenium based catalyst[184] or *via* heterogenenous catalysis[185]. Secondary alcohols can also be converted to their corresponding primary amines *via* the formation of an azide followed by reductive hydrogenation.[186,187] To our knowledge, no conversion of secondary alcohol *via* a *Gabriel* synthesis was described in the literature. Considering the difficulty to handle gaseous ammonia and the potential explosive properties of azide derivatives, we decided to add an ethylene glycol-based spacer, the commercially available bis(2-bromoethyl)ether on the secondary alcohol before performing the *Gabriel* type reaction. Furthermore, the additional ethylene glycol spacer

would allow enhanced flexibility of the chains and therefore lower the transition temperature of the derivative. A *Williamson* type ether synthesis on **128** was therefore carried out by deprotonation of the alcohol with sodium hydride and then reacting it with bis(2-bromoethyl)ether, affording **129** in a satisfactory 51% yield (Scheme 4.16). The primary amine **131** was obtained *via* a *Gabriel* synthesis in a 56% yield. Overall the synthesis of the branched ethylene glycol-based chain **131** was performed in 4 steps with an overall yield of 21%.

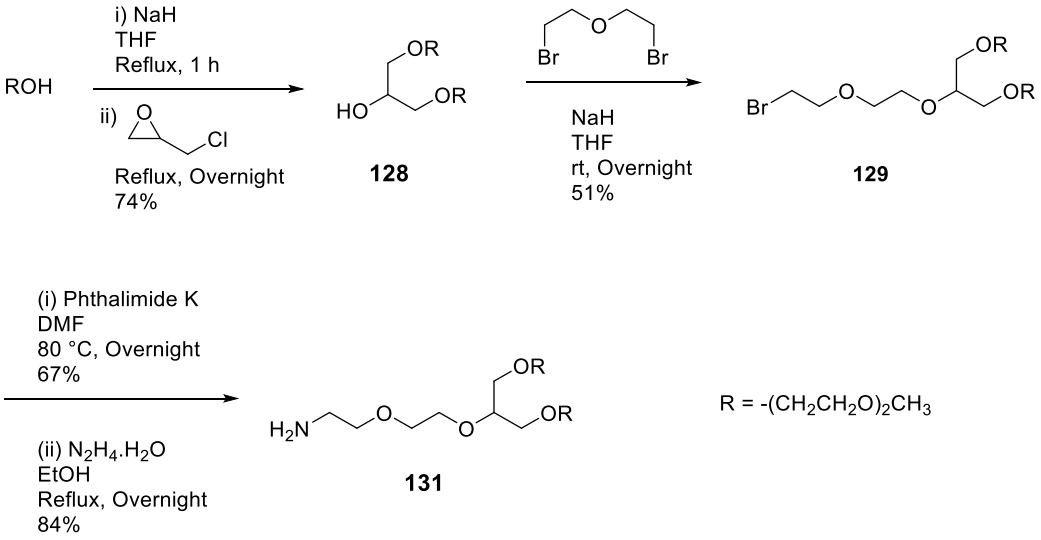

Scheme 4.16: Synthesis of the branched ethylene glycol based chain **131**.

The synthesis of the desired PDI derivative BPDI was carried out *via* the imidation of PTCDA with **131** (Scheme 4.17). Due to the high hydrophilicity of this PDI derivative, the purification by column chromatography on silica was precluded. BPDI, **132** was nevertheless successfully purified by preparative HPLC on a reverse phase C_{18} column.

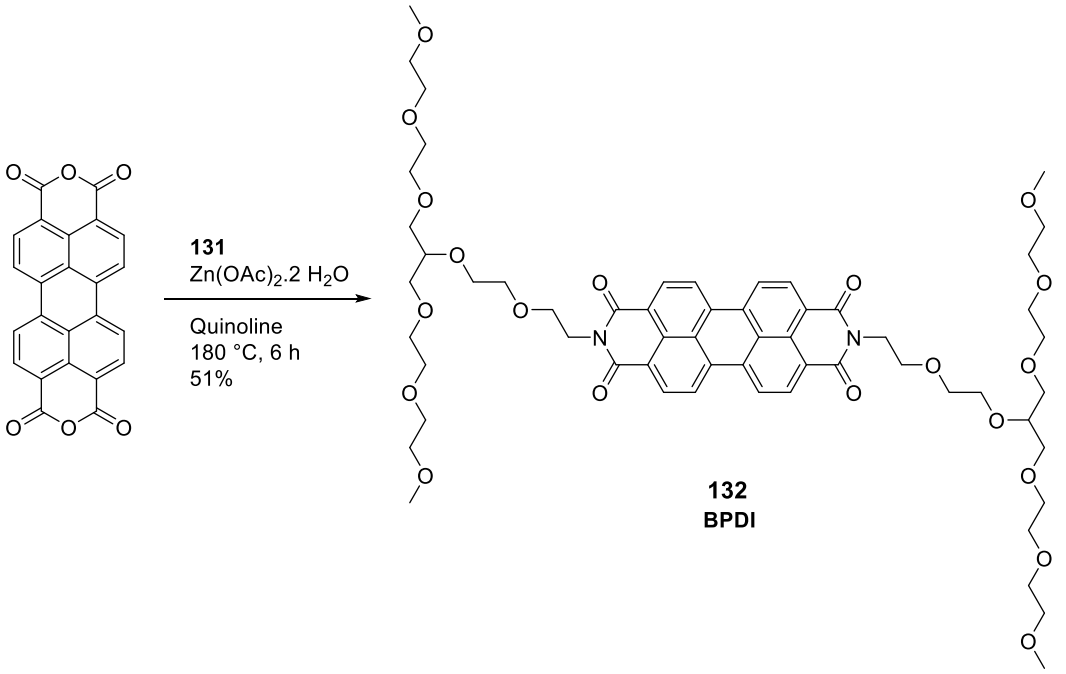

Scheme 4.17: Synthesis of BPDI, **132**.

Overall the synthesis of BPDI was carried out in 5 steps with an overall 10% yield.

4.4.3.4 Properties of BPDI

The properties of BPDI were investigated by absorption and emission spectroscopies in both solution in THF and solid state. Its mesogenic properties are also described in this section.

BPDI in solution shows three absorption bands, located at 454, 485 and 520 nm (Figure 4.24, solid line). At an excitation wavelength of 370 nm, the emission profile of BPDI shows again three bands at 530 nm, 569 nm, and 618 nm (Figure 4.24, dashed line). A small Stokes shift of 11 nm is observed and both the absorption and emission spectra are in accordance with the literature on similar compounds.[188]

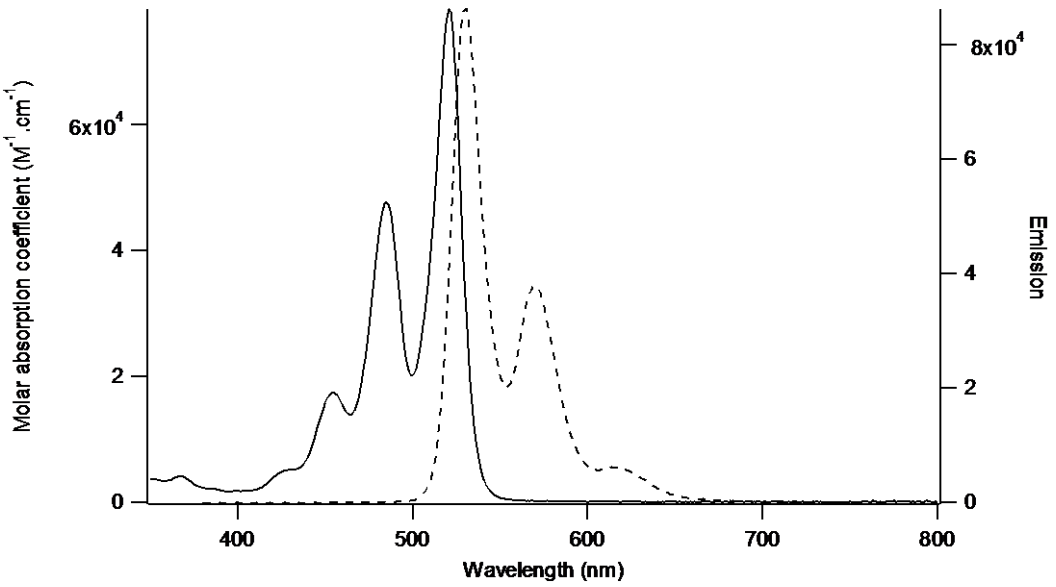

Figure 4.24: Absorption (solid line) and emission (dashed line) spectra of a 4 µM solution of BPDI in THF. Excitation wavelength: 370 nm.

Whilst the absorption and emission spectra of HBC-PhC12 in thin film show similar profiles compared to the ones in solution (see 4.4.2), the emission of BPDI in thin film is red-shifted by *ca.* 100 nm compared to its emission in solution (Figure 4.25). This behaviour was assigned to an excimer formation. Excimers of PDIs in thin films are common and have been described for example in PDI-based polymers.[189,190]

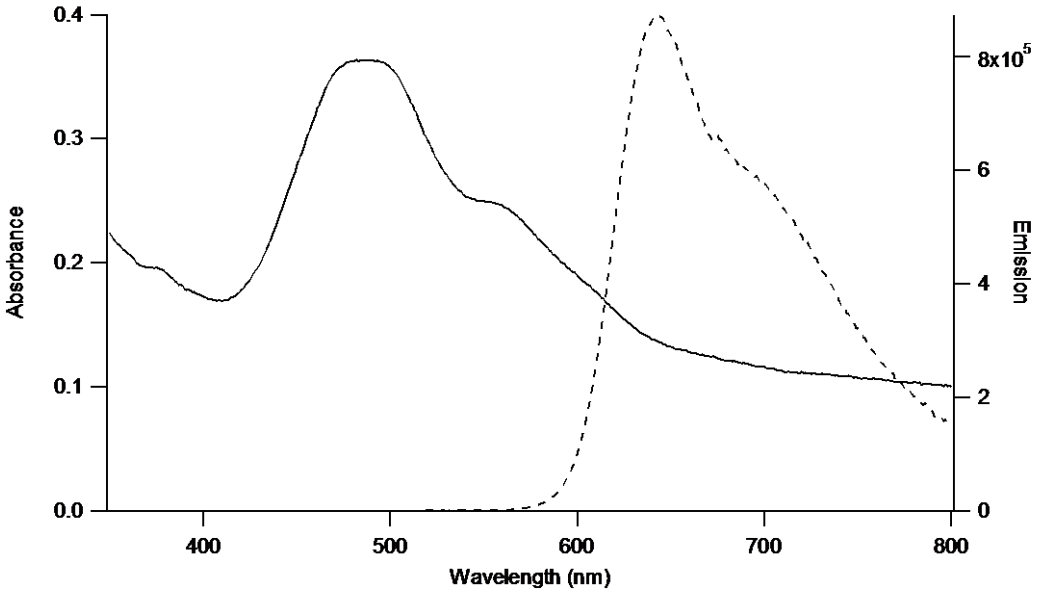

Figure 4.25: Absorption (solid line) and emission (dashed line) spectra of a thin film of BPDI on a glass slide. Excitation wavelength (488 nm).

The potential mesogenic properties of the novel BPDI have been studied by POM, DSC, X-ray diffraction and AFM.

In polarised optical microscopy on regular glass, BPDI tends to aggregate and does not spread on the slide (Figure 4.26). Homogenisation of the layer thickness was attempted by covering with a cover glass but remained unsuccessful even above the clearing point, probably due to the high viscosity of the compound. The POM shown in this section are therefore realized without cover slides. As for the POM study of HBC-PhC12 (see 4.4.2), the thin film of BPDI was also deposited on APS-coated glass (Figure 4.27).

At room temperature, BPDI is thought to be liquid crystalline, as shown in the POM study on both substrate (Figure 4.26 and Figure 4.27). Indeed, birefringence is observed and it can be spread upon shearing. It should be noted that the thin film is more even on APS-coated slides, which can be explained by the increased hydrophilicity of the substrate compared to regular glass slides.

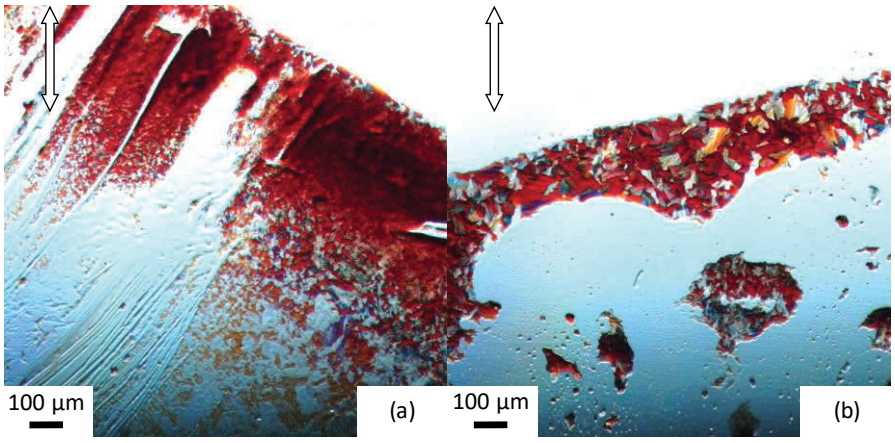

Figure 4.26: POM images on regular glass of BPDI at room temperature: (a) as-casted and (b) after thermal annealing. The pictures were taken at different regions.

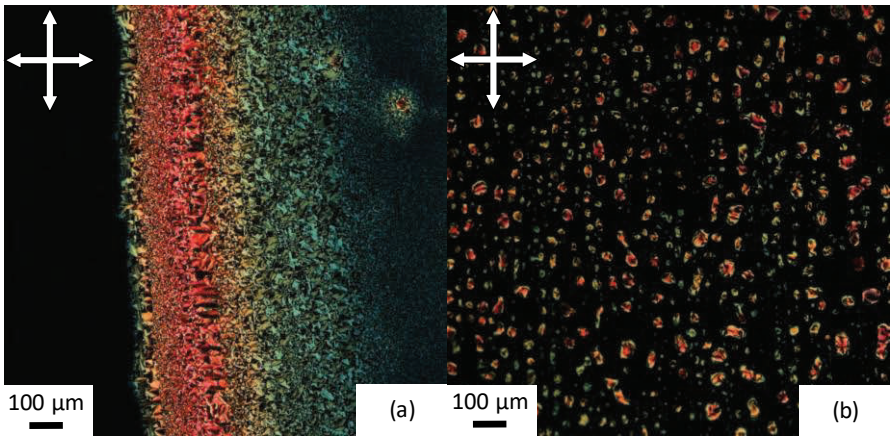

Figure 4.27: POM images on APS coated glass of BPDI at room temperature: (a) as-casted and (b) after thermal annealing. The pictures were taken at different regions.

The DSC of BPDI was also carried out. (Figure 4.28). Two main transitions can be observed: a very broad endothermic transition which occurs at *ca.* 40 °C and a small transition at *ca*. 120 °C. Is it worth noticing that the transitions were not seen under polarised microscopy. As the DSC experiment was performed under air, it is assumed that the unsatisfactory shape of the DSC curve and the interferences might be due to the absorption of water by the highly hydrophilic BPDI during the experiment.

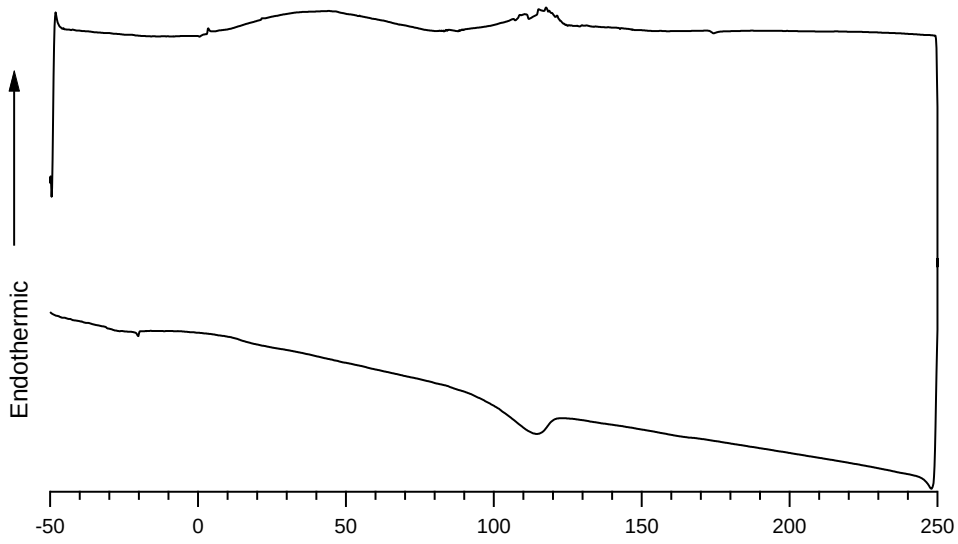

Figure 4.28: DSC curves of BPDI on fourth heating/cooling cycle. Temperature rate: 10 °C/min.

The resulting transition temperature could also be altered. DSC experiment under nitrogen atmosphere is needed to confirm the transition temperatures but was unfortunately not available.

The X-ray diffraction of BPDI show three main peaks, which follow a Q-ratio of 1:2:3, indicative of a lamellar structure with an interplane distance of 32.9 Å (Figure 4.29). This distance, compared to the maximum length of 46.8 Å of BPDI calculated by a MM2 model (Figure 4.30) is indicative of interpenetration of the chains.

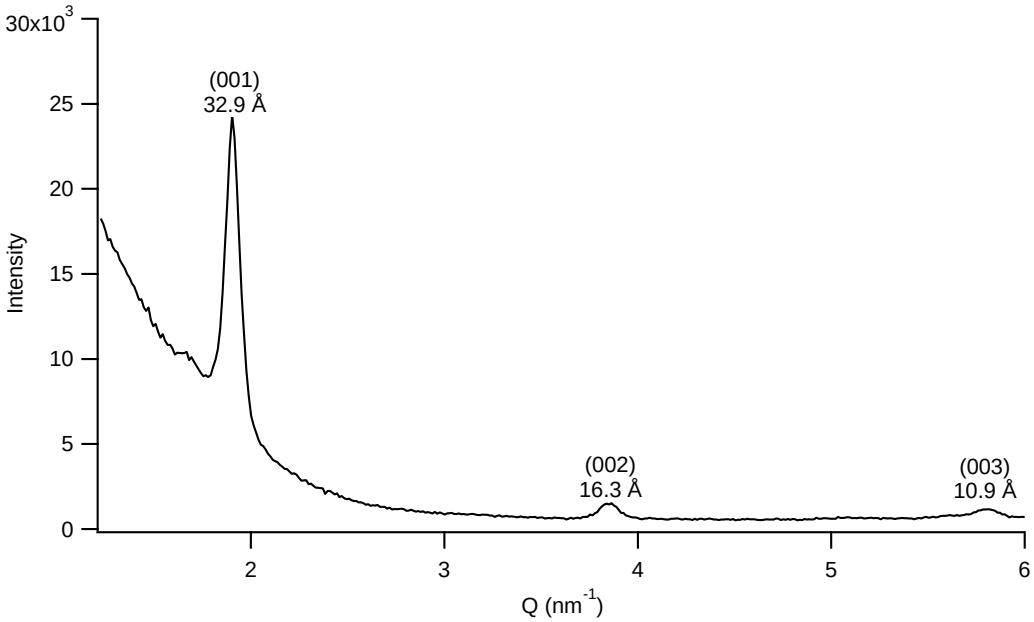

Figure 4.29: X-Ray diffraction pattern of as-casted BPDI at room temperature (cobalt source = 1.79026 Å).

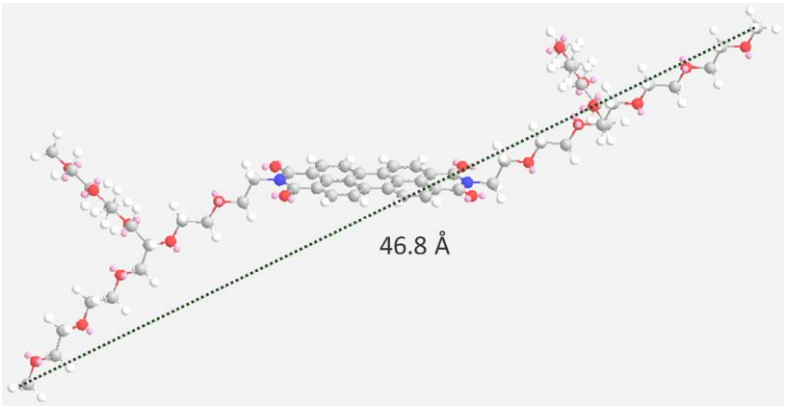

Figure 4.30: MM2 model of BPDI.

Atomic force microscopy was also investigated on as-casted and annealed BPDI thin film on APS-coated glass. The as-casted thin film AFM images showed clusters with a zigzag form. We believe that these clusters are due to interferences from the instrument.

After annealing, BPDI is aggregating and some crystals are observed in the AFM picture (Figure 4.31, right).

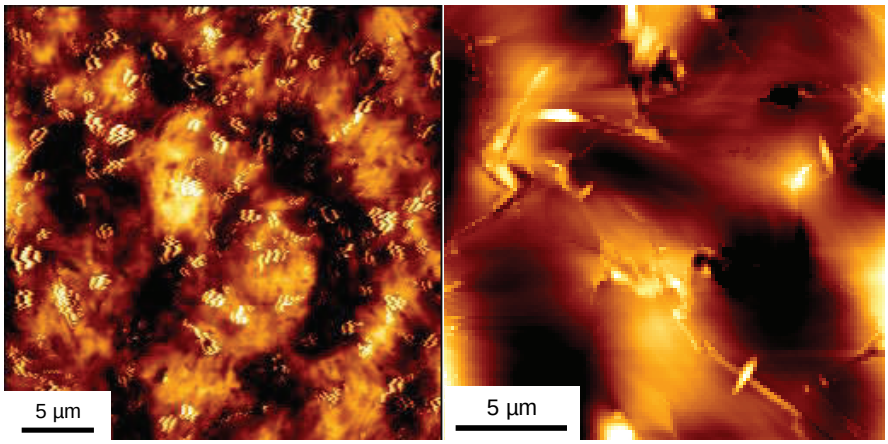

Figure 4.31: AFM pictures of BPDI drop-casted from a THF solution: Left: as-casted, Right: after annealing.

To conclude, BPDI is liquid crystalline at room temperature and shows a lamellar structure. However, the precise transition temperatures are unclear and DSC under protective atmosphere has to be carried out.

The synthesis of the two incompatible materials, the hydrophobic HBC-PhC12 and several hydrophilic PDIs were successfully carried out. BPDI was shown to have a lower clearing point and better handling than its homologue 1st design PDIs **059** and **073**. HBC-PhC12 and BPDI were therefore the chosen two pendant-chain incompatible materials for our morphology study.

4.5 Investigation of the compatibility between HBC-PhC12 and BPDI

The interaction between the two materials HBC-PhC12 and BPDI was studied, in solution and in a thin film. Their organisation in an equimolar blend as well as their photophysical properties are detailed in this section.

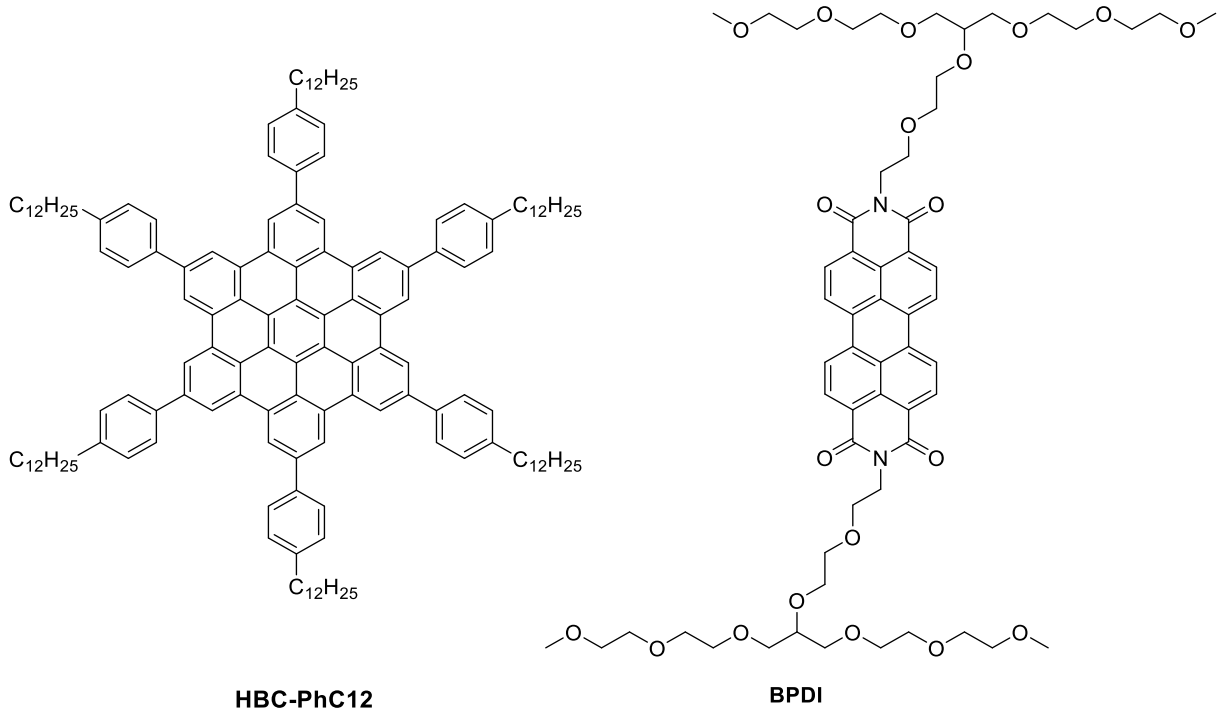

Figure 4.32: Structure of HBC-PhC12 and BPDI.

4.5.1 Polarised optical microscopy

The polarised optical microscopy study of an equimolar mixture of HBC-PhC12:BPDI drop-casted from THF on glass slide was carried out. Preliminary observation by naked eye shows a coffee-ring thin film, where the edge of the drop is bright red whereas the inner is slightly coloured (Figure 4.33).

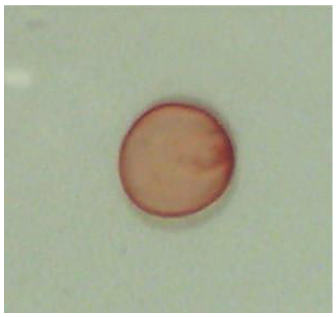

Figure 4.33: Image of an as-casted equimolar HBC-PhC12:BPDI thin film on regular glass.

On regular glass, POM images reveals that a non-even and heterogeneous thin film was obtained (Figure 4.34). Attempted thermal annealing of the thin film did not change the organisation at a microscopic level (Figure 4.35). This could be due to the high viscosity of the two materials and the inability to set the temperature above the clearing point of HBC-PhC12 before its decomposition point.

The POM study on heating stage shows no major reorganisation of the blend and no transition phase could be observed. We have therefore decided to focus our efforts on determining the organisation of the blend at room temperature before and after thermal annealing below the decomposition point of HBC-PhC12 (thermal annealing performed at 200 °C for 2 h). In this section, the presented POM images were taken at different region: the edge of the thin film, and the inner part of the drop.

Two main domains can nevertheless be differentiated: the edge of the drop is red, which can be indicative of a rich BPDI phase whereas the inner is more clear. The non-even thin film on regular glass preclude any further analysis of the blend. The high hydrophilicity of BPDI might lead to poor interactions between the glass and the compound. APS-coated glass was therefore used as a way to obtain thin films with an even thickness (Figure 4.36 and Figure 4.37).

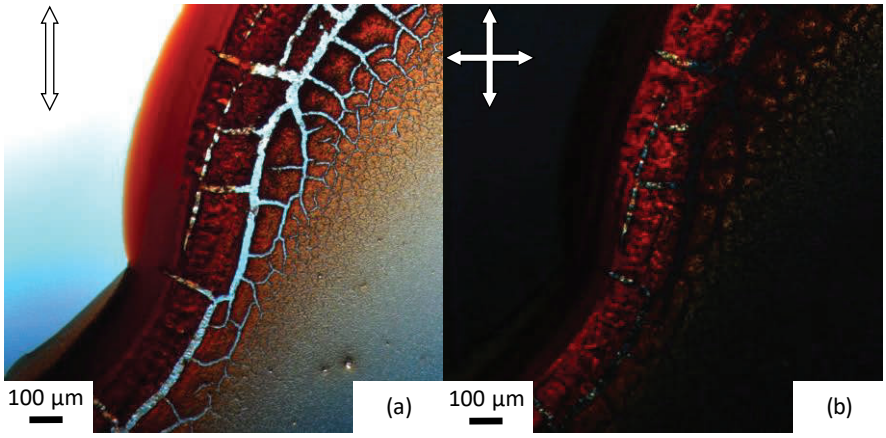

Figure 4.34: POM images of an as-casted equimolar HBC-PhC12:BPDI thin film on regular glass: (a) bright field and (b) dark field.

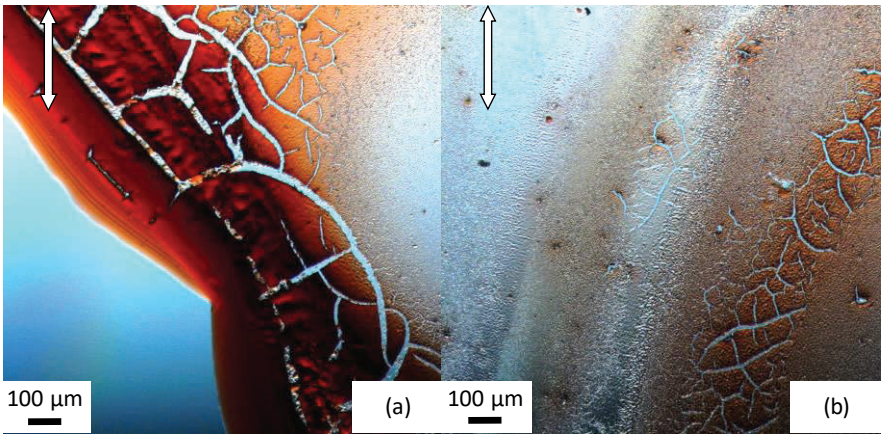

Figure 4.35: POM images of an equimolar HBC-PhC12:BPDI thin film on regular glass after thermal annealing: (a) edge and (b) inner film. The pictures were taken at different regions.

On APS-coated slides, a more even film was obtained (Figure 4.36). As for the drop-casting on regular glass, the thermal annealing does not induce a change in the morphology at a microscopic level (Figure 4.37). Again, two domains can be differentiated: a red domain mainly situated at the edge of the drop and a clearer domain in the inner part. The domains appear to be more define than on regular glass.

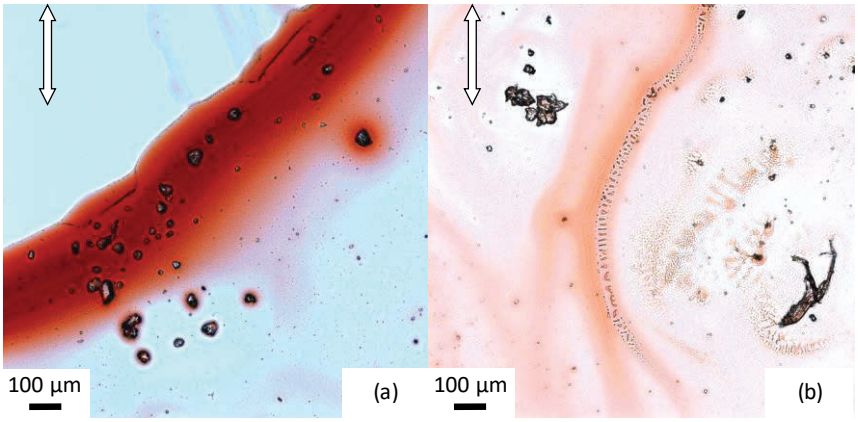

Figure 4.36: POM images of an as-casted equimolar HBC-PhC12:BPDI film on APS-coated slide: (a) edge and (b) inner part. The pictures were taken at different regions.

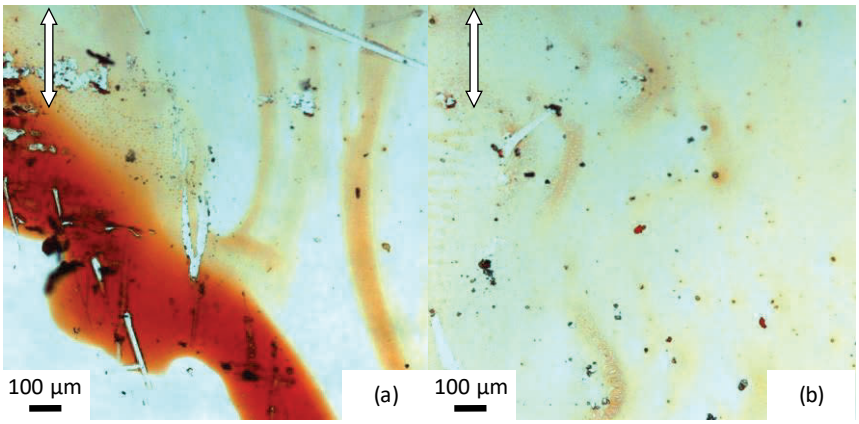

Figure 4.37: POM images of an equimolar HBC-PhC12:BPDI mixture drop-casted on APS-coated glass after annealing. (a) edge of the film and (b) inner part. The pictures were taken at different regions.

Solvent vapour annealing was also attempted to force the reorganization of the blend (Figure 4.38). The processing solvents were chosen according to their vapour pressure. The effects of THF (vapour pressure = 21.6 kPa at 25 °C), $CHCl_3$ (vapour pressure = 26.2 kPa at 25 °C) and DCM (vapour pressure = 58.2 kPa at 25 °C) were investigated on the equimolar thin film of HBC-PhC12:BPDI. After placing the as-casted film on a saturated atmosphere of THF, $CHCl_3$ or DCM, the macrophase separation between the two domains seems to be enhanced (Figure 4.38). While in THF and in $CHCl_3$ (Figure 4.38 a,b and c,d respectivelty), red clusters are observed in the inner part of the thin film, a slightly coloured domain surrounded by a red area was obtained after SVA in DCM (Figure 4.38 e). This could be explained by the higher

volatility of DCM, inducing enhanced solubilisation of the thin film and better reorganisation. However, no birefringence was observed at room temperature and no definite conclusion can be extracted on the composition of these domains.

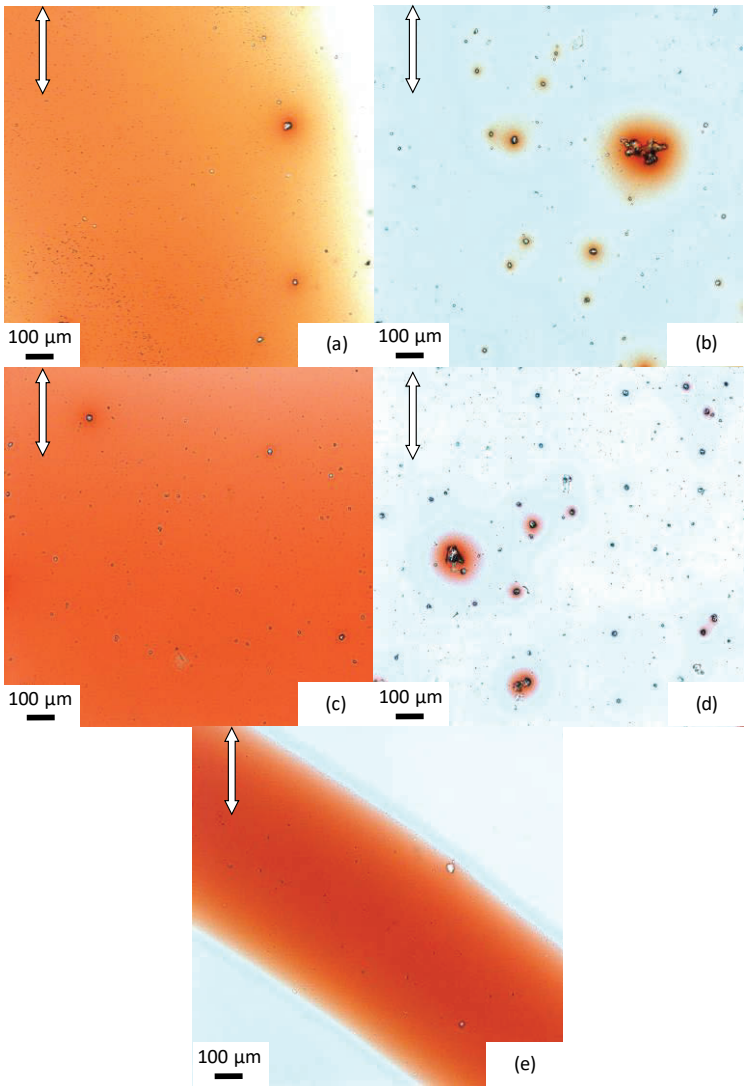

Figure 4.38: POM images of equimolar HBC-PhC12:BPDI mixtures after SVA. Top: using THF (a) outer ring, (b) inner ring. Middle: using $CHCl_3$ (c) outer ring, (d) inner ring. Bottom: (e) using DCM. The pictures were taken at different regions.

To conclude the compatibility study of an equimolar HBC-PhC12:BPDI thin film by POM, the hydrophobic HBC-PhC12 and the hydrophilic BPDI are not miscible. Two domains are distinguished, indicative of a macrophase separation between the two materials. Thermal annealing does not lead to any reorganisation of the blend. However, solvent vapour

annealing seems to be a suitable method, as reorganisation of the blend towards higher macrophase separation was discerned. However, no information on the compositions of the domains can be extracted and this hypothesis is solely based on the colour difference.

4.5.2 Photophysics

The photophysics of the equimolar HBC-PhC12:BPDI mixture was investigated both in a THF solution and in solid state. Due to their respective electron donor and acceptor properties, HBC-PhC12 and BPDI can be subjected to numerous energy and/or electron transfers.

The maximum absorption and emission wavelengths of the pure HBC-PhC12 (see 4.4.2) and BPDI (see 4.4.3.4) are summarized in Table 4.2 and will be used as a comparison with the binary mixture.

Compound	Solution in THF		Thin film	
	Abs max	Em max (λ_{ex}=370 nm)	Abs max	Em max (λ_{ex}=405 nm)
HBC	380	461	375	551
	415	515	424	694
BPDI	454	530	486	638
	485	569	556	679
	520	618	600	739

Table 4.2: Maximum absorption and emission wavelength of pure HBC-PhC12 and BPDI in THF solution and in thin film. The maxima were calculated by peak fitting using Gaussians.

In solution in THF, the absorption profile of this mixture is the sum of contribution from the two compounds without any interaction (Figure 4.39). Indeed, no additional peaks are observed pointing to the absence of charge transfer complexes, where an aggregate is composed of a donor:acceptor:donor stacking. As the concentration increases, the molar

extinction coefficient decreases, which is indicative of the independent aggregation of both HBC-PhC12 and BPDI in THF.

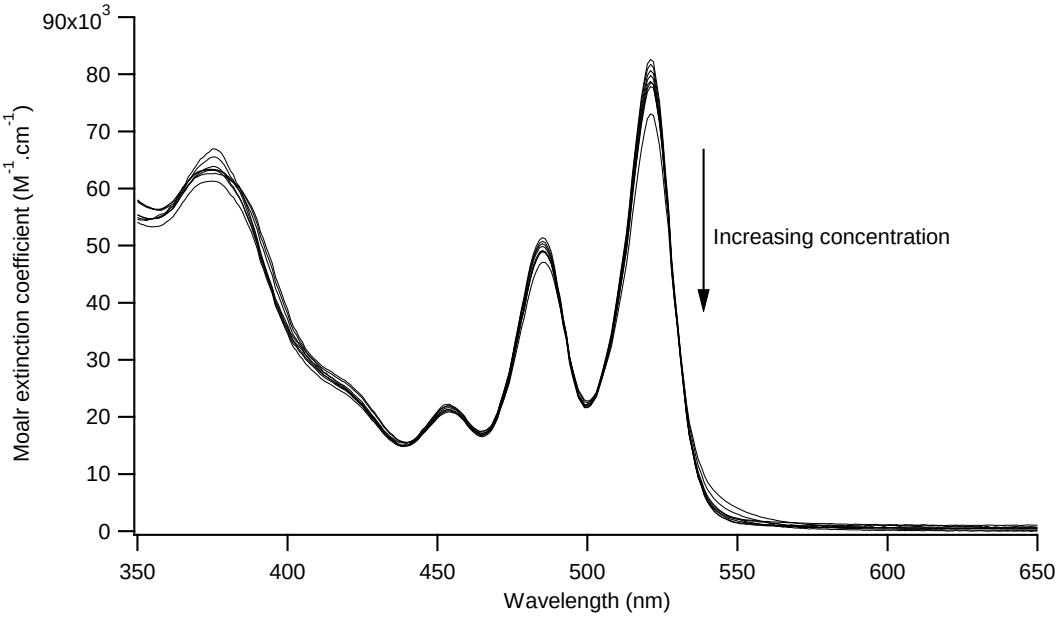

Figure 4.39: Molar extinction coefficient vs. wavelength at 375 nm for an equimolar HBC-PhC12:BPDI mixture (total concentration from 1.5 µM to 391 µM).

The emission profile, described in Figure 4.40 shows again the sum of contribution of the non-interacting compounds. As the total concentration increases, the donor emission (HBC-PhC12) is quenched, while the acceptor emission increases, which suggests a Förster resonance energy transfer (FRET) between the two components. Indeed, the large overlap between the emission profile of the pure HBC-PhC12 and the absorption of the pure BPDI favours this type of energy transfer.

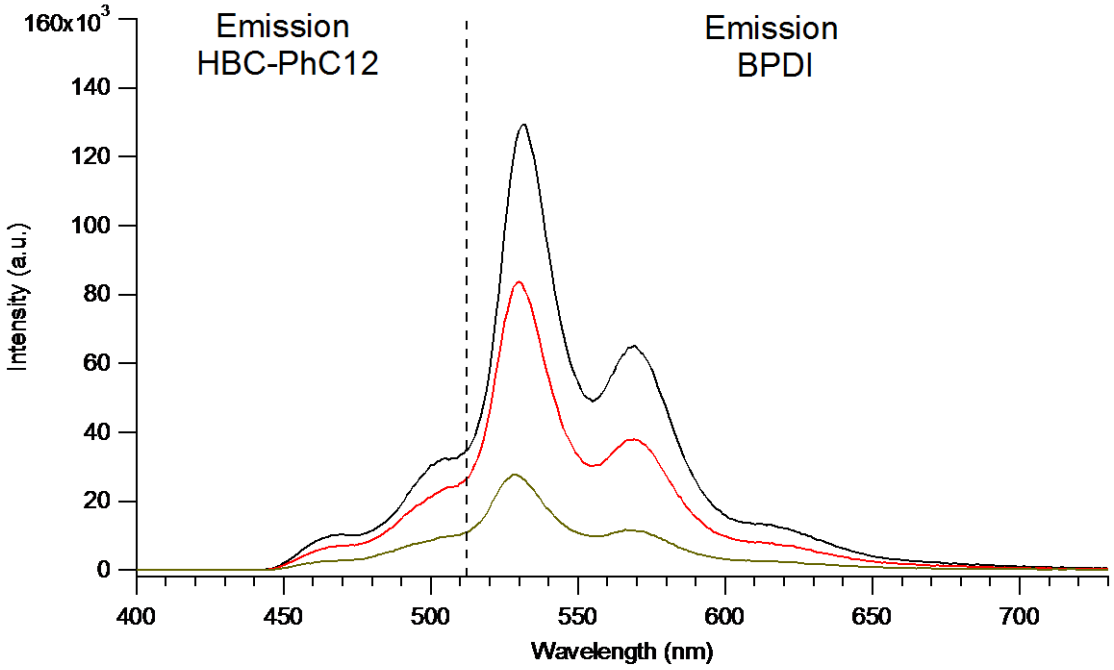

Figure 4.40: Emission spectra of an equimolar HBC-PhC12:BPDI mixture in THF. Total concentration: 12 µM (black curve), 6.2 µM (red curve) and 1.5 µM (green curve).

The solid state absorption and emission profiles are independent of the substrate used (regular glass or APS-coated glass) or the thermal treatment imposed. The absorption spectrum solely shows the sum of the HBC-PhC12 and BPDI profile with no additional bands up to 1100 nm (Figure 4.41).

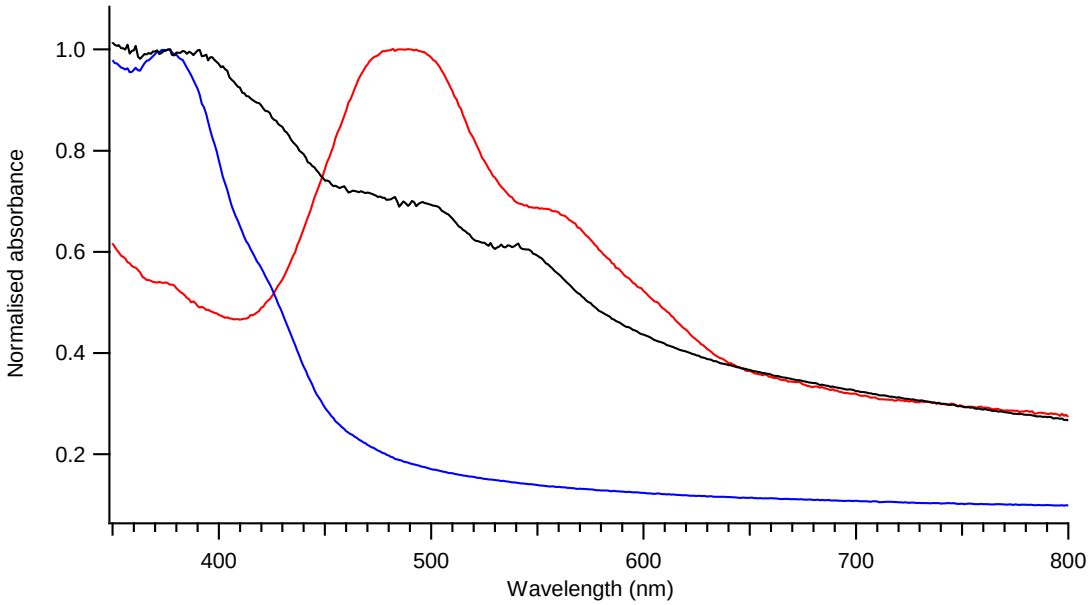

Figure 4.41: Normalized UV/Vis spectra of BPDI (red curve), HBC-PhC12 (blue curve) and an equimolar HBC-PhC12:BPDI blend (black curve) on a thin film on regular glass.

However, the emission spectrum changes dramatically (Figure 4.42). When excited at the wavelength of the donor HBC-PhC12 (405 nm), the emission does not show any contribution of the HBC-PhC12 emission and only a slight contribution of BPDI excimers. Instead, a large red-shifted band, with a maximum emission at 743 nm is observed. This shows that in a thin film form, HBC-PhC12 and BPDI are forming an exciplex. When excited at the wavelength of the acceptor BPDI (488 nm), the emission profile shows a large contribution of the BPDI excimer. The shoulder at 709 nm corresponds to a vibrational state.

Unfortunately, due to the non-even film thickness, the method of deposition and the setup of the instrument, no quantitative results could be extracted from the absorption/emission spectra.

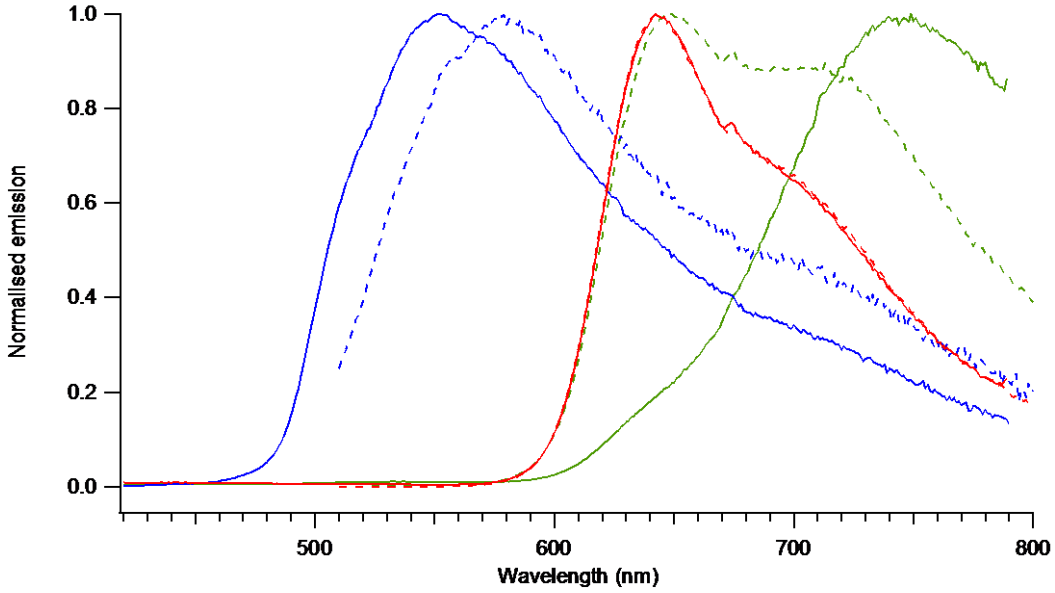

Figure 4.42: Normalized emission spectra of BPDI (red curves), HBC-PhC12 (blue curves) and an equimolar HBC-PhC12:BPDI blend (green curves) on a thin film. Excitation wavelength: 405 nm (solid line) and 488 nm (dashed line).

To conclude, it has been demonstrated that HBC-PhC12 and BPDI does no form charge transfer complexes in any of the studied solutions or thin films *i.e.* regular or APS-coated glass, with or without any thermal treatment. The incompatibility of the chains between the two

components counteracts the electrostatic interaction that can occur between an electron acceptor/donor to adopt the structure schematised in Figure 4.43. However, in a thin film, HBC-PhC12 and BPDI do form an exciplex, as demonstrated by the presence of a large and intense red-shifted emission band. Other photophysical phenomena such as electron transfer cannot be excluded and deeper and quantitative understanding of the exciton mechanism is needed to draw some definite conclusions on this blend. Indeed, this non-radiative process cannot be observed in photoluminescence study. However, quantitative study of the emission would allow us to determine if any decrease of the emission is observed compared to the pure materials and therefore conclude to quenching by electron transfer.

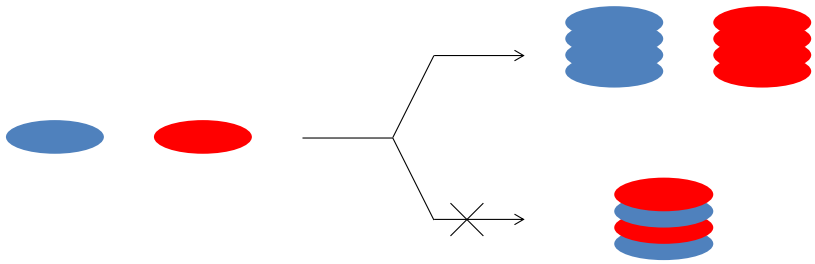

Figure 4.43: Schematic representation of the aggregation in a HBC-PhC12:BPDI equimolar blend.

The diffusion distance of an exciton in organic films are typically between 5 and 20 nm before it recombines.[16] The existence of an exciplex in the HBC-PhC12:BPDI thin film therefore suggests that the two components are in close contact.

By combining the results for the POM and the photophysics on film, it can be therefore concluded that the two domains observed in POM images are not composed of pure BPDI and HBC-PhC12. Instead, it is thought that the red domain is mainly composed of BPDI with a small fraction of HBC-PhC12. Likewise, the lightly coloured domain could be composed of mainly HBC-PhC12 with a small fraction of BPDI.

Efforts towards the validation of this hypothesis were investigated and presented in the next sections.

4.5.3 Other microscopy methods

4.5.3.1 Fluorescence microscopy

Fluorescence microscopy can be used to obtain optical image of a component by analysing their fluorescence emission. If two components, with characteristic emission profile are mixed together, it is therefore possible to obtain a distribution map of the two compounds into the blend. Due to the high fluorescence of both HBC-PhC12 and BPDI, fluorescence microscopy could be therefore an efficient method of analysing the morphology of blends. However, the formation of the exciplex preclude the use of this technique as a way to locate the two components in the thin film.

4.5.3.2 Raman microscopy

Raman microscopy of an equimolar HBC-PhC12:BPDI thin film was also attempted. Due to the difference in their chemical nature, we believe that the two materials can be differentiated by their Raman bands. HBC-PhC12 is composed of aliphatic C-H and aromatic C-C bonds while BPDI is composed of C=O and C-O-C bonds. Each of these bonds have characteristic strong or medium Raman frequencies, shown in Table 4.3, and can be used as a way to differentiate the two components.

Functional group	Raman frequencies (cm^{-1})	Functional group	Raman frequencies (cm^{-1})
v(C-H)	2800 – 3000 (s)	**v (C=O)**	1680 – 1820 (m)
v (C-C)	1580 – 1600 (s) 1000 (s)	**v(C-O-C) asymmetric**	1060-1150 (w)
		v(C-O-C)	800 – 970 (m)

Table 4.3: Raman frequencies range of the functional groups of interest.

When performing Raman microscopy with an excitation laser of 532 nm (green laser) or 633 nm (red laser), the high emission of both compounds interferes with the Raman spectrum. Attempted Raman microscopy using a 785 nm infrared laser on a different instrument leads to the decomposition of the compound, as observed with HBC-PhC12 optical image (Figure 4.44). We believe that Raman microscopy could still be a suitable method to analyse the morphology of this binary mixture. However, the available instrument setups and the difficulty to tune the laser power to avoid any decomposition of the compound preclude any observations of the morphology using the available instruments.

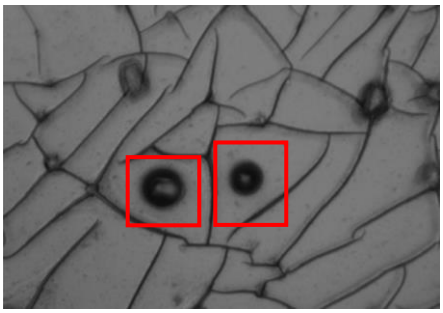

Figure 4.44: Optical image of HBC-PhC12 after Raman analysis. The dark spots highlighted in red show the decomposition of HBC-PhC12 after exposure to the laser beam.

4.5.3.3 Atomic force microscopy

Tapping-mode atomic force microscopy on equimolar HBC-PhC12:BPDI blends in thin film was also carried out. The results presented in this section focused on as-casted and thermally

annealed thin film deposited on APS-coated slides. Indeed, the more even thickness of the film allows easier interpretation of AFM images.

Whilst thermal annealing did not show any reorganization of the blend on POM, AFM pictures reveal reorganisation in a nanoscopic scale, as the textures differ between the as-casted (Figure 4.45) and the annealed samples (Figure 4.46). The textures observed in as-casted films are not conclusive on the composition of the two domains observed on POM. Nevertheless, two different textures can be discerned between the edge and the inner part of the thin film, indicating different compositions (Figure 4.45). However, after thermal annealing (Figure 4.46), the column like texture observed in the inner part of the drop-casted samples is similar to the pure HBC-PhC12 structure on APS-coated slide (Figure 4.18, section 4.4.2). The cross-section indicates nevertheless that the columns are wider (*ca.* 100 nm) and higher (400 to 500 nm) than the pure HBC-PhC12 thin film. The AFM is therefore in accordance with the previous hypothese made during the POM study: the inner of the sample seems to be mainly composed of HBC-PhC12. However, the texture observed on the edge of the annealed thin film could not be attributed (Figure 4.46, right).

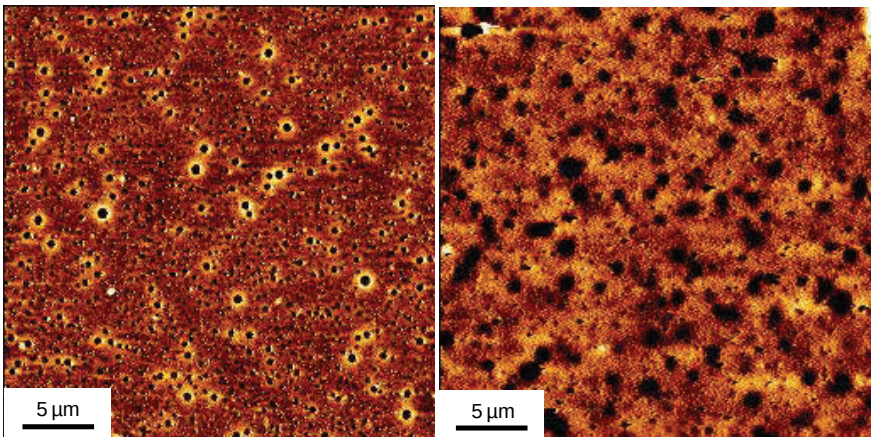

Figure 4.45: AFM images of an as-casted equimolar HBC-PhC12:BPDI mixture on APS-coated slide. Left: inner part and right: edge of the film.

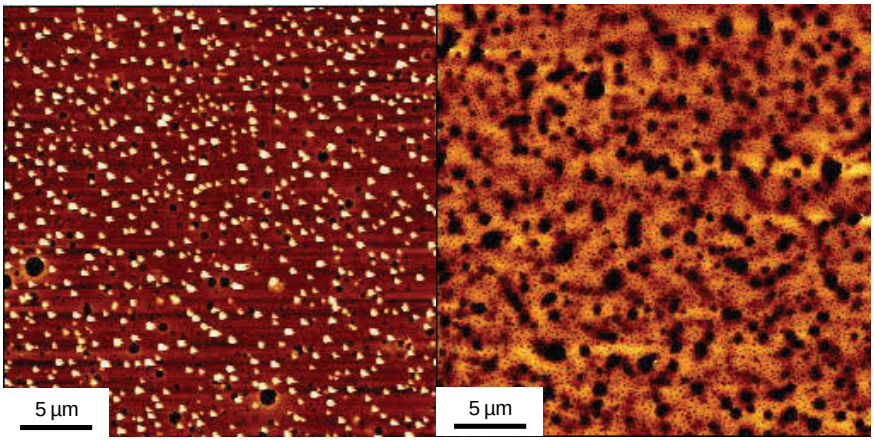

Figure 4.46: AFM images of an equimolar HBC-PhC12:BPDI mixture on APS-coated slide after thermal annealing. Left: inner part and right: edge of the film.

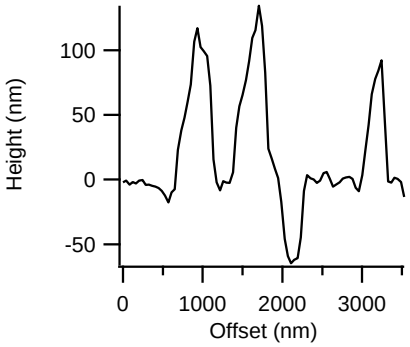

Figure 4.47: Cross section of the AFM image of an equimolar HBC-PhC12:BPDI mixture on APS-coated glass – Inner part.

To conclude, the precise morphology of a equimolar blend of HBC-PhC12:BPDI is unfortunately still unknown. However, from the various microscopy studies and the photophysics of both solution and thin film, several hypotheses could be raised. We believe that HBC-PhC12 and BPDI can be classified as “incompatible”. Indeed, the POM and AFM studies of the blend show a large macrophase separation, with two distinct domains. This hypothesis has been confirmed by absorption spectroscopy: the absence of additional red-shifted peaks in both solution and solid state preclude the presence of ground-state charge transfer complexes. However, from the exciplex emission, it can be inferred that the two domains are not composed of pure HBC-PhC12 and pure BPDI, but of a rich BPDI and

HBC-PhC12 phase with a small amount of respectively HBC-PhC12 and BPDI. The electrostatic acceptor/donor interaction is non-existent.

Further study needs to be investigated to understand the organisation of the blend. Varying the solvent for the drop-casting as well as deposition by spin-coating, can be used as an alternative to create thin film. Moreover, transient photoluminescence and absorption study would give us a better understanding of the exciplex formation mechanism. Quantitative emission study would indicate any emission quenching if occurring and therefore if an electron transfer takes place between HBC-PhC12 and BPDI. Solvent vapour annealing shows good promise as for the reorganisation of the blend into more thermodynamically favoured morphology.

However, the composition of the domains remains unclear. Further microscopy techniques could be an alternative strategy to obtain valuable information on the blend. Raman microscopy is still believed to be an interesting technique to obtain a distribution map of the component into the thin film, despite the disappointing preliminary results. Another microscopy method of interest could be electron microscopy. A distribution map can also be obtained based on their molecular weight. The so-called liquid extraction sample analysis (LESA) or MALDI-imaging have been successfully used to distinguish phospholipids or drugs in biological tissues.[191–193] This technique could be of great interest to obtain a distribution map of organic molecules such as the one described in this chapter.

In the next section, a suitable compatibiliser will be designed and synthesised. Its effect at different concentration on the HBC-PhC12:BPDI morphology will then be discussed.

Chapter five:

Compatibilisation of functional materials: morphology control of HBC-PhC12 and BPDI

5.1 Aims and objectives

As discussed in the previous chapter, two materials: the electron donor, the hydrophobic HBC-PhC12 and the electron acceptor, the hydrophilic BPDI were designed and synthesised. The morphology study of this equimolar binary proved that the two components are incompatible. This chapter focuses on the design of a tailor-made compatibiliser to suppress the incompatibility between HBC-PhC12 and BPDI. The synthesis of this third component will be described and preliminary results of its effect on the binary HBC-PhC12:BPDI mixture will be discussed.

5.2 Synthesis of the HBC-PhC12:BPDI compatibiliser

As a way to control the morphology of a binary mixture of HBC-PhC12 and BPDI, the compatibiliser HBC-BPDI was designed (Figure 5.1). This novel compound is composed of a HBC moiety covalently linked to two PDI moieties *via* an ethylene glycol-based spacer.

A few dyads based on linked HBC and PDI derivatives have already published by K. Müllen and co-workers.[194–197] HBC-BPDI differs from previously described dyads due to its amphiphilicity: the HBC moiety bears hydrophobic dodecyl chains while the PDI moiety carries hydrophilic ethylene glycol-based chains. Moreover, the two parts of HBC-BPDI are linked *via* a flexible ethylene glycol spacer whilst examples of dyads in the literature are composed of an alkyne-based linker.

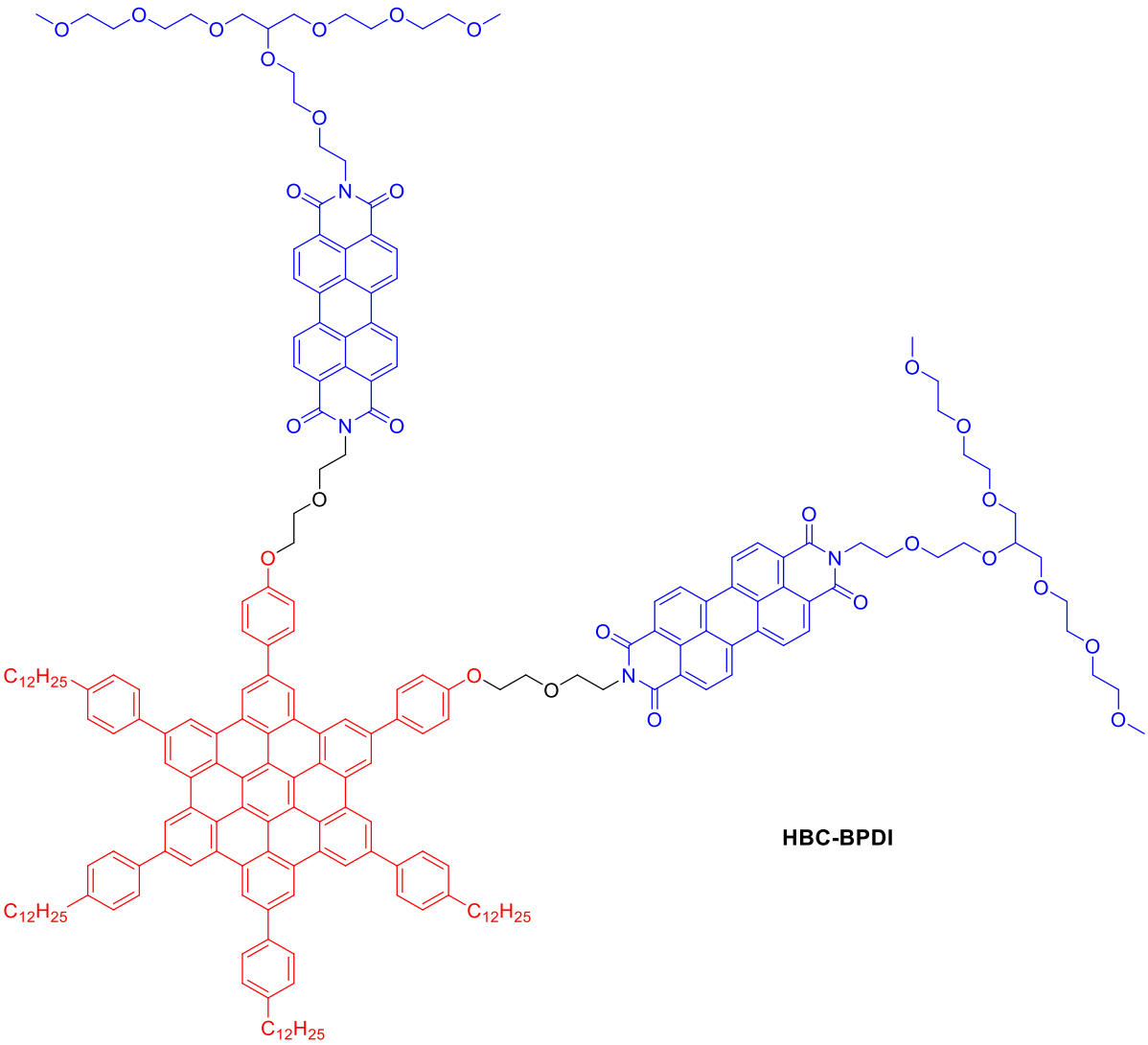

Figure 5.1: Structure of the target compatibiliser HBC-BPDI.

The synthesis of this functional and amphiphilic dyad, presented in Scheme 5.1, is derived from the convergent synthesis between an asymmetrical HBC **153** and PDI **135** moiety, respectively bearing hydrophobic dodecyl and hydrophilic ethylene glycol-based chains. The HBC moiety is prepared from the cyclopentadienone derivative **92** and the acetylene derivative **145** following the literature procedure for the synthesis of C_2 symmetric HBC (described in section 4.2.1). The PDI moiety is obtained from the commercially available PTCDA.

In this section, the synthesis of the two parts of HBC-BPDI and their coupling will be described.

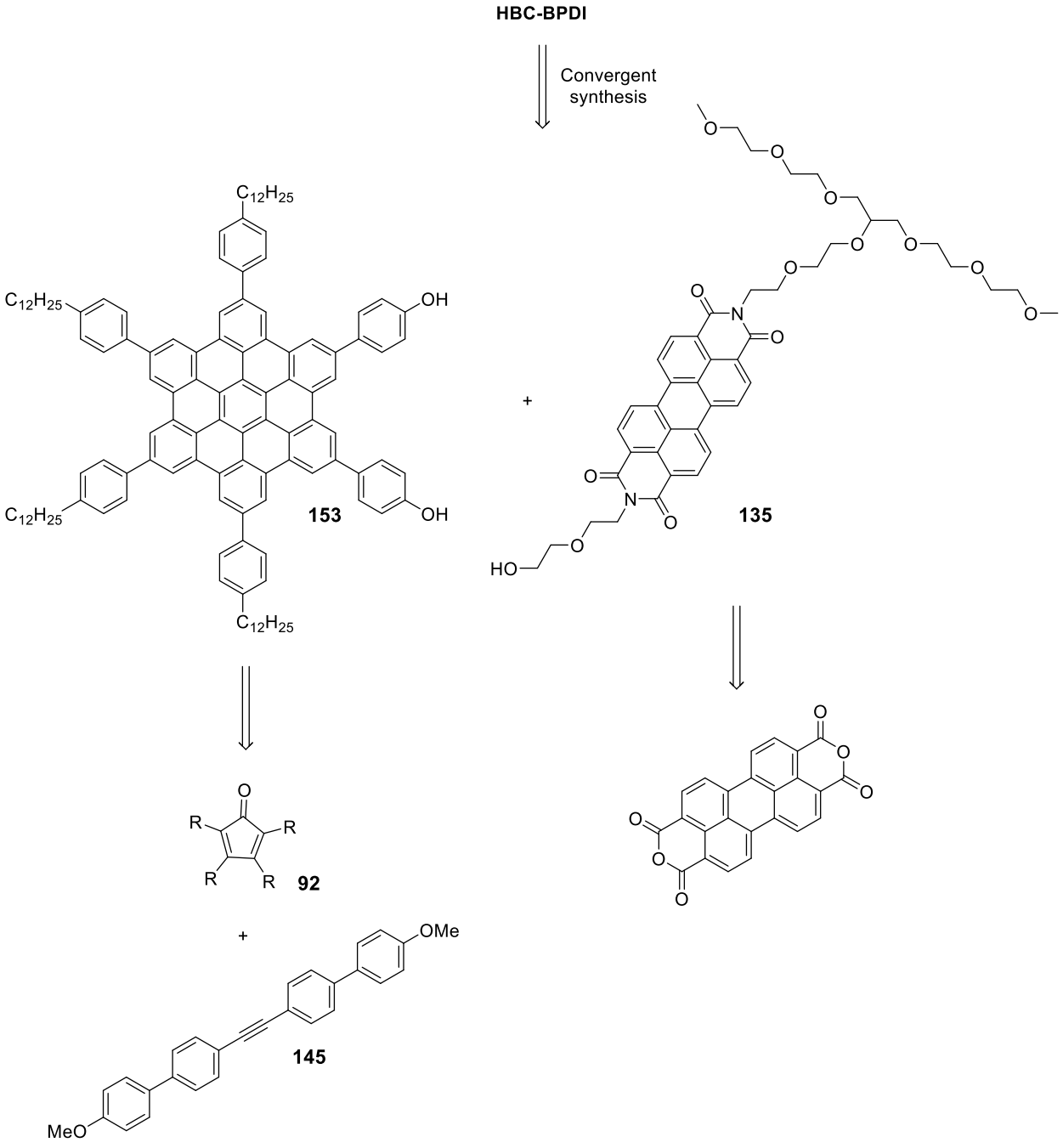

Scheme 5.1: Retrosynthesis of HBC-BPDI.

5.2.1 Synthesis of the PDI-based hydrophilic moiety

The synthesis of the PDI moiety **135** was carried out from PTCDA following a literature procedure and is described in Scheme 5.2.[161,198] **135** is asymmetric and contains a branched ethylene glycol-based chain on one imide position, whereas the other is substituted by a linear

ethylene glycol-based chain. The free hydroxy group was to be used as a linking group for the coupling with the HBC moiety of HBC-BPDI.

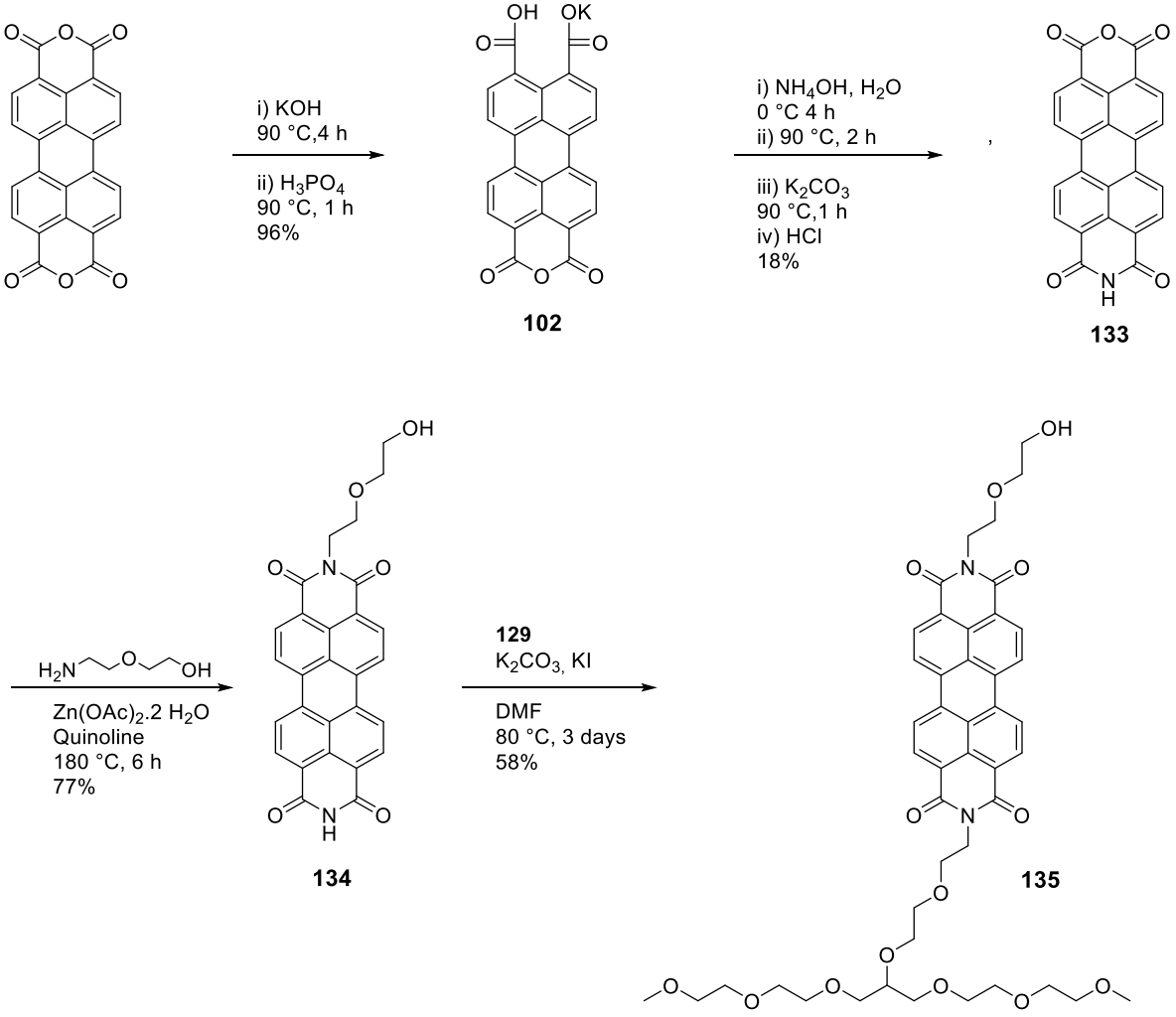

Scheme 5.2: Synthesis of the PDI moiety.

Firstly, PTCDA was partially hydrolysed affording the monoanhydride monopotassium carboxylate salt **102**. **102** was then reacted with an aqueous solution of ammonium hydroxide to obtain the intermediate **133** in an overall yield of 17%. The low yield can be explained by the repetitive precipitations required to obtain a pure product. Moreover, all the steps are statistical reactions and result in poor control of the substitutions. The imidation of the free anhydride position using 2-(2-aminoethoxy)ethanol on **133** was followed by the subsequent

addition of the bromo-substituted branched chain **129** to afford the desired compound **135** in 4 steps with a low 7% overall yield.

5.2.2 Synthesis of the HBC-based hydrophobic moiety

In this section, the synthesis of the hydrophobic HBC moiety will be discussed. As described in the introduction of HBC derivative synthesis (See 4.2.1), the unsymmetrical hexasubstituted benzene precursor can be obtained *via* a Diels-Alder [4+2] cycloaddition between a tetrasubstituted cyclopentadienone and an acetylene derivative. After describing two synthetic routes towards the desired HBC moiety, *via* early and late functionalisation, the synthesis of the acetylene derivative and the coupling between the two building blocks will be presented.

5.2.2.1 Synthesis *via* early functionalisation

The synthesis of the HBC moiety *via* early functionalisation is depicted in Scheme 5.3. The phenol groups of **153** were methyl-protected to avoid any undesired side-reactions. The building block **152** can be derived from a *Scholl* type reaction of the hexasubstituted benzene **150** which can be obtained *via* a [4+2] cycloaddition between the tetrasubstituted cyclopentadienone **141** and the acetylene derivative **145**. **141** can be obtained *via* the double aldol condensation of **140** and **136a**. The synthetic routes were designed following previous literature on similar substrates.[142]

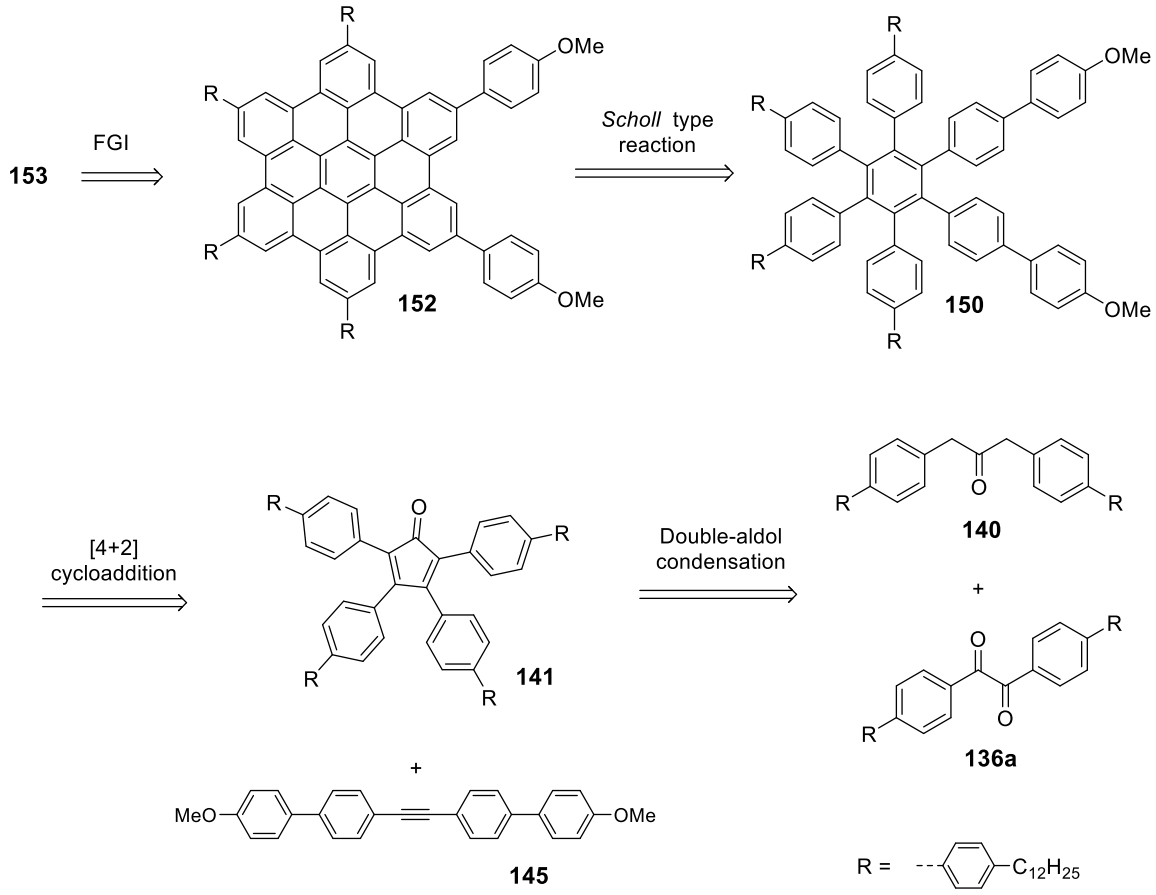

Scheme 5.3: Retrosynthetic scheme – coronene moiety *via* early functionalization.

This section is focussed on the preparation of the building block **141**.

The synthesis of the 1,2-diketone **136a** was carried out in one step *via* the I_2 mediated oxidation of **115** in DMSO in a 77% yield (Scheme 5.4).

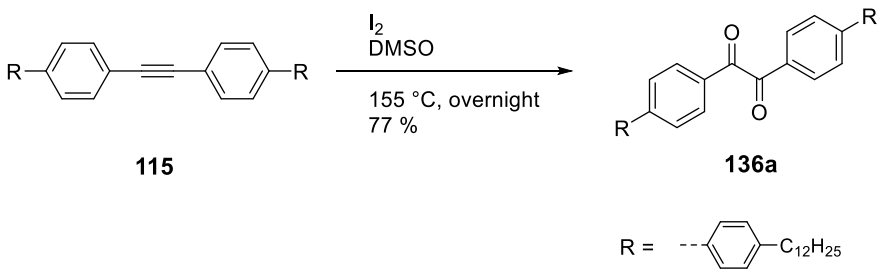

Scheme 5.4: Synthesis of diketone **136a**.

The 1,3-disusbtitutedpropan-2-one **140** was synthesised using 4-bromophenylacetic acid as the starting material (Scheme 5.5). The condensation of 4-bromophenylacetic acid using DCC

and DMAP as reagents afforded the 1,3-di(4-bromophenyl)propan-2-one building block **137**. The substitution of the bromo- to the *p*-dodecylphenyl *via* a *Kumada* coupling required protecting the ketone. The ketone was therefore converted to acetal **138** with ethylene glycol using a Dean-Stark apparatus. It is worth noting that toluene, the solvent of choice for the protection of ketones, does not show any conversion and benzene was used instead. A Kumada coupling between **138** and the freshly prepared 4-dodecylbenzenemagnesium bromide **114** followed by cleavage of the acetal in sulfuric acid afforded the desired 1,3-di(4-dodecylbiphen-4'-yl)propan-2-one **140**. The synthesis of **140** was carried out in 4 steps in an overall yield of 24%.

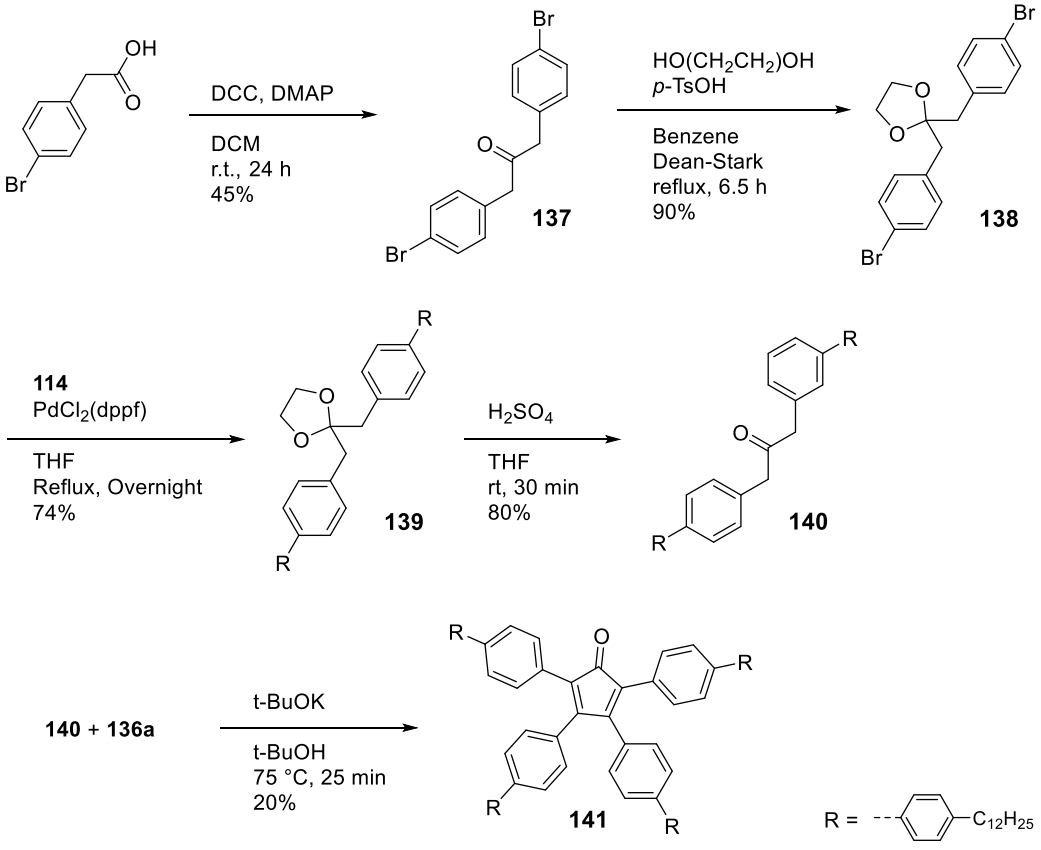

Scheme 5.5: Synthesis of the cyclopentadienone precursor **141**.

The preparation of the tetrasubstituted cyclopentadienone **141** was carried out *via* a double-aldol condensation between **140** and **136a**. Using the most described reagent for this

reaction, *i.e.* a substoechiometric amount of potassium hydroxide in ethanol, no conversion of the starting materials was observed (Table 5.1, entry 1). The attempted conversion by microwave irradiation, using sodium hydroxide and ethanol was also unsuccessful, even at a high temperature (Table 5.1, entry 2).[199]

Another procedure described by K. Müllen and co-workers used TBAOH in *t*-BuOH or dioxane and attempted on our system (Table 5.1,entry 3 and 4).[200,201] Even if conversion of the starting material was observed, the resulting ^{1}H NMR of the crude shows a very complicated aromatic region and attempted purification by column chromatography was unsuccessful.

It was therefore decided to use a stronger base. *t*-BuOK in *t*-BuOH was chosen (Table 5.1, entry 5). The reaction mixture quickly turned to dark red. After purification by column chromatography, the desired cyclopentadienone **141** was afforded in a low 20 % yield. On adding two equivalents of the base (Table 5.1, entry 6), the solution again turned to dark red but surprisingly gradually returned to its original colour. After checking the crude ^{1}H NMR, it was shown that the starting materials had been recovered.

Unfortunately, the best method found, using one equivalent on potassium *tert*-butoxide in *tert*-butanol afforded the desired product **141** in only a 20% yield. The low yield could be explained by the stabilisation of the negative charge after the deprotonation of the hydrogen at the propan-2-one α position. Indeed, the charge is highly delocalised by resonance on the biphenyl ring.

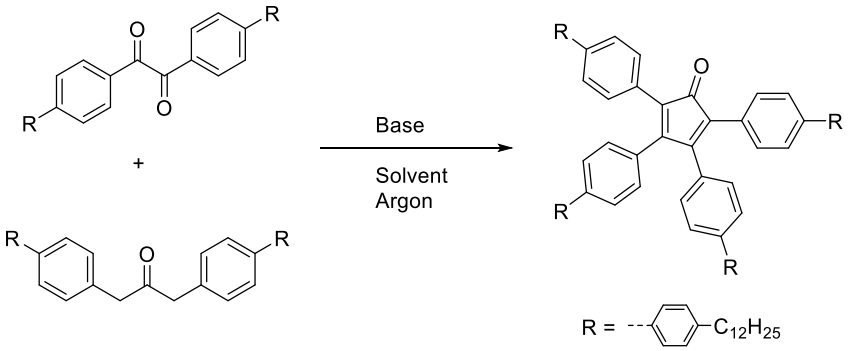

Entry	Base	Solvent	Reaction conditions	% conversion
1	KOH	EtOH	20.5 h	0
2	NaOH	EtOH	30 min (MW – 150 °C)	0
3	TBAOH – 1 M in MeOH	t-BuOH	1 h	-
4	TBAOH.30 H_2O	1,4-dioxane	1 h	-
5	t-BuOK (1 equiv)	t-BuOH	25 min	20%
6	t-BuOK (2 equiv)	t-BuOH	15 min	0

Table 5.1: Investigation on the double-aldol condensation between **140** and **136a**.

To conclude, the synthesis of **141** *via* early functionalisation was carried out in 5 steps with an overall yield of 5%. The synthetic route was not satisfactory and another procedure based on late functionalisation was attempted.

5.2.2.2 Synthesis *via* late functionalisation

The synthesis of the HBC moiety was carried out *via* late functionalisation (Scheme 5.6). Unlike the previous strategy, the bromine groups were to be kept until the synthesis of **149**. The desired HBC moiety **150** is obtained *via* a *Kumada* coupling followed by a *Scholl* type reaction. The synthesis of the precursor **149** is the result of a Diels-Alder [4+2] cycloaddition between the cyclopentadienone **142** and the acetylene derivative **145**. The new cyclopentadienone **142** was to be synthesized *via* the double-aldol condensation between **137** and **136b**.

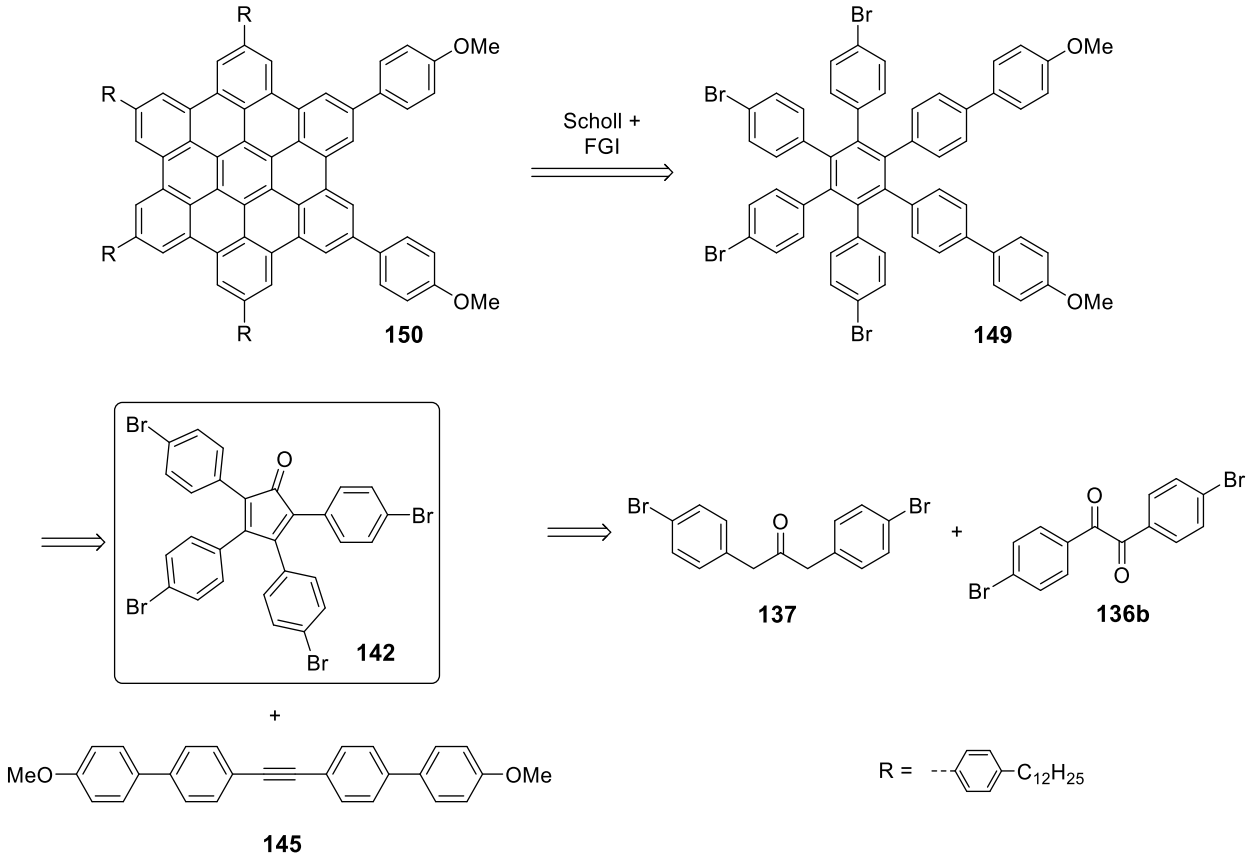

Scheme 5.6: Retrosynthetic scheme - synthesis of the coronene moiety *via* late functionalisation.

This new synthetic route offered better versatility, as the chains were added at a later stage of the synthesis. Furthermore, fewer steps are required compared to the early functionalisation and alleviated some of the synthetic issues encountered in the previous strategy.

The synthesis of the new cyclopentadienone derivative **142** is presented in Scheme 5.7. The di(4-bromophenyl)diketone **136b** was synthesised *via* a I_2 mediated oxidation of di(4-bromophenylacetylene) in DMSO and afforded the desired compound **136b** in a 65% yield. The double-aldol condensation between **136b** and **137** was successful and afforded **142** in a satisfactory 62% yield using KOH as a base.

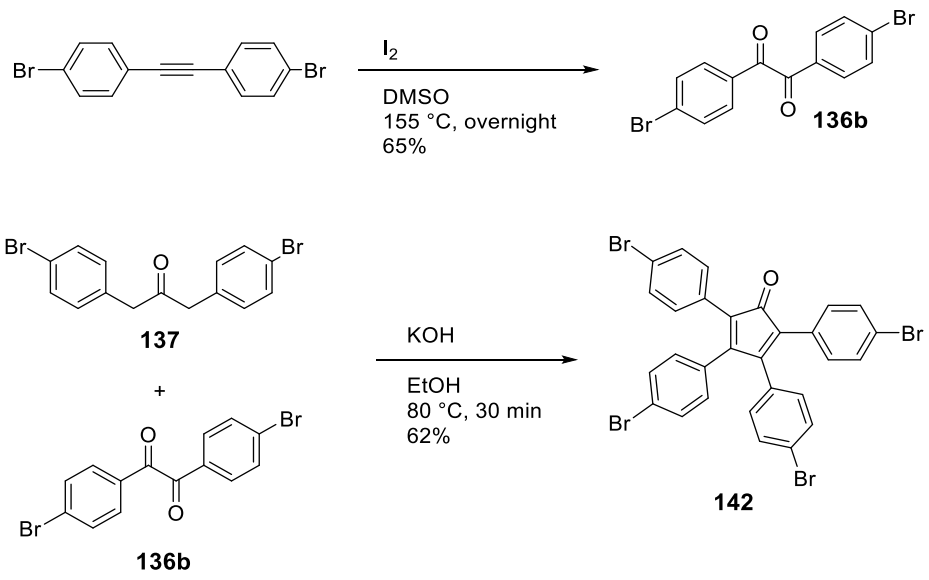

Scheme 5.7: Synthesis of cyclopentadienone **142**.

The synthesis of the cyclopentadienone **142** was therefore achieved in three steps with an overall 40% yield. This method is more advantageous compared to the early functionalisation described in the previous section. The synthesis of the desired HBC moiety was therefore continued.

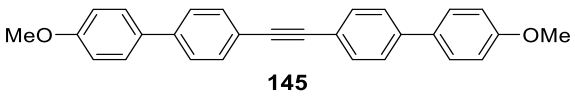

Figure 5.2: Structure of the target compound **145**.

The synthesis of the symmetrical di(biphenyl)acetylene building block **145** (Figure 5.2) was carried out.The substitution of an acetylene derivative is usually performed *via* a *Sonogashira* cross-coupling. This C-C bond creation, using a palladium catalyst and a copper co-catalyst was shown to be suitable for the preparation of aryl or heteoaryl substituted symmetrical or unsymmetrical acetylenes.[202] As an example, R.G. Brisbois, P. A. Grieco and co-workers have developed a one-pot synthesis of symmetrical and unsymmetrical derivatives from the commercially available trimethylsilyl monoprotected terminal alkyne, using a palladium(0) source, copper iodide and an amidine base (DBU) in benzene:water solvent mixture.[203] This

method relies on *in situ* desilylation and is suitable for a large variety of aryl substituent and produces excellent yields. However, no biaryl moieties were substituted in this paper. This strategy was nevertheless used to couple the 4-bromo-4'-hexyloxybiphenyl **143**, already synthesized in the Baranoff group, to the commercially available trimethylsilylacetylene (Scheme 5.8) based on the literature procedure. [202] After several attempts, no conversion of the starting material was observed.

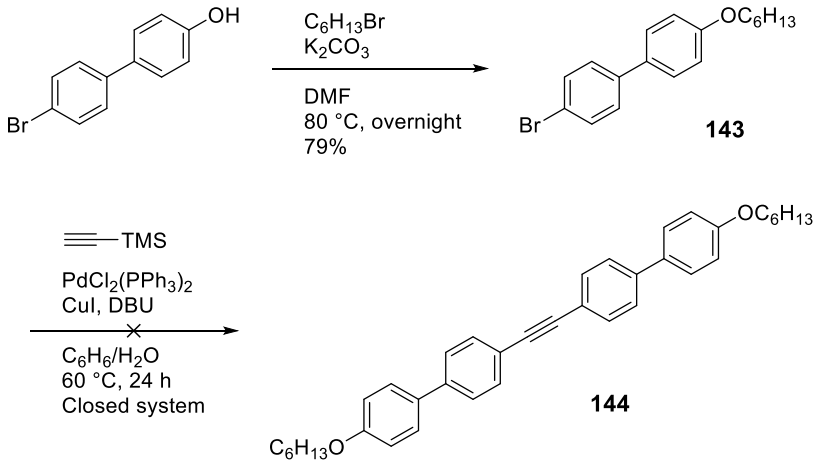

Scheme 5.8: Attempted test synthesis of symmetrical acetylene derivative *via* a Sonogashira coupling.

As an alternative route, a Kumada coupling between the 4,4'-bromotolane and the freshly prepared 4-methoxyphenylmagnesium bromide **114b** was carried out (Scheme 5.9). The desired di-substituted acetylene derivative **145** was obtained in an excellent yield (80%).

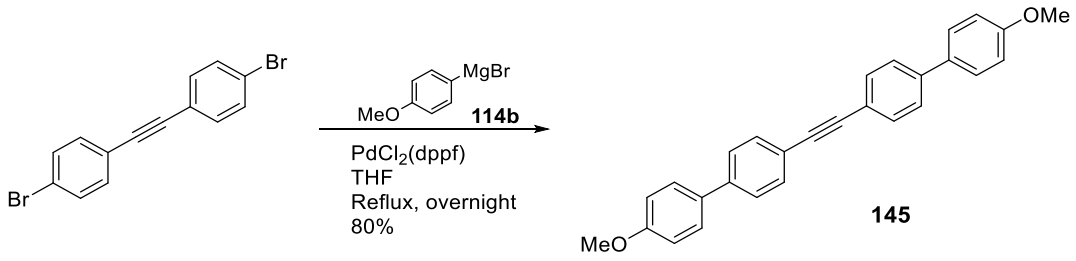

Scheme 5.9: Synthesis of a symmetrical acetylene derivative **145** *via* a Kumada coupling.

The [4+2] cycloaddition between cyclopentadienones and acetylene derivatives forms a bridged carbonyl compound **146** and requires a high temperature and therefore a high boiling point solvent to allow the release of carbon monoxide and the subsequent rearomatisation of the cyclic moiety (Scheme 5.10).[204]

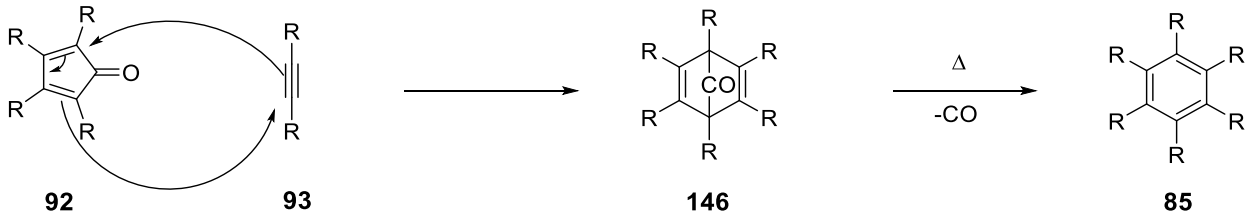

Scheme 5.10: [4+2] cycloaddition mechanism between cyclopentadienones and acetylene derivatives.

Based on the work of A. Takuzo and co-workers, diphenyl ether (b.p.= 258 °C) was used as the solvent.[205] A protective atmosphere is crucial for the reaction to proceed. Indeed, performing the reaction under air leads to the degradation of the cyclopentadienone due to the formation of its oxidation products, as described by T. Thiemann and co-workers.[206] The [4+2] cycloaddition between **142** and **145** without a protective atmosphere (Scheme 5.11) leads to the diketone and the lactone side-products, respectively **147** ($[M+H]^+$ = 700.8 g/mol) and **148** ($[M+H]^+$ = 7112.8 g/mol) , as observed by mass spectrometry (MS AP+) (Scheme 5.11). **149** was nevertheless observed in trace amounts.

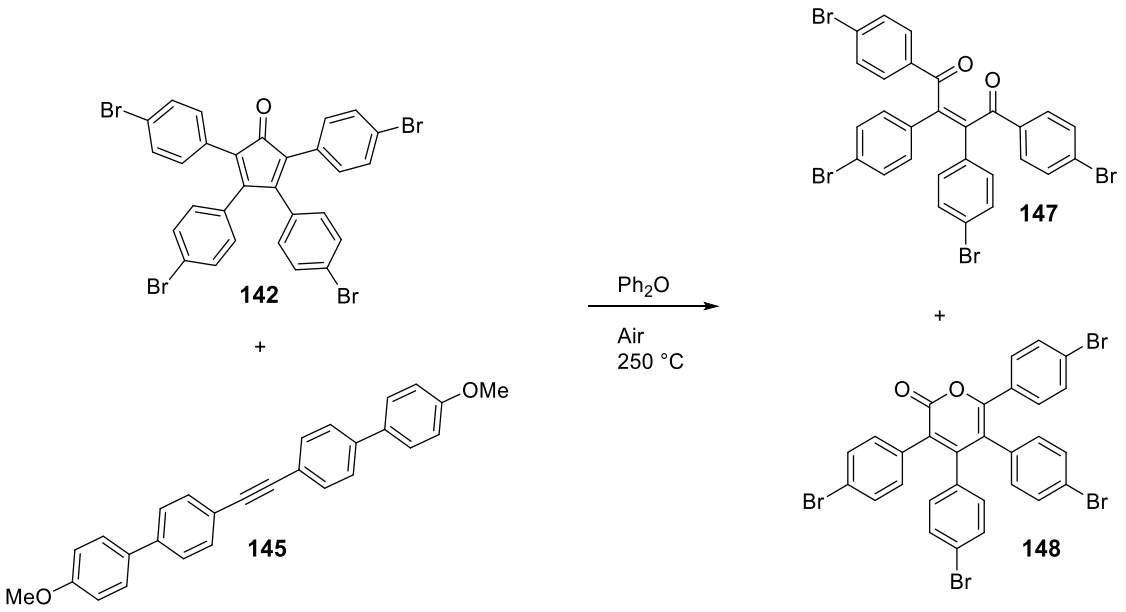

Scheme 5.11: Air-promoted oxidation of the cyclopentadienone **142**.

However, under an argon atmosphere, **149** was obtained as the main product in a 71% yield and no oxidation products were found (Scheme 5.12).

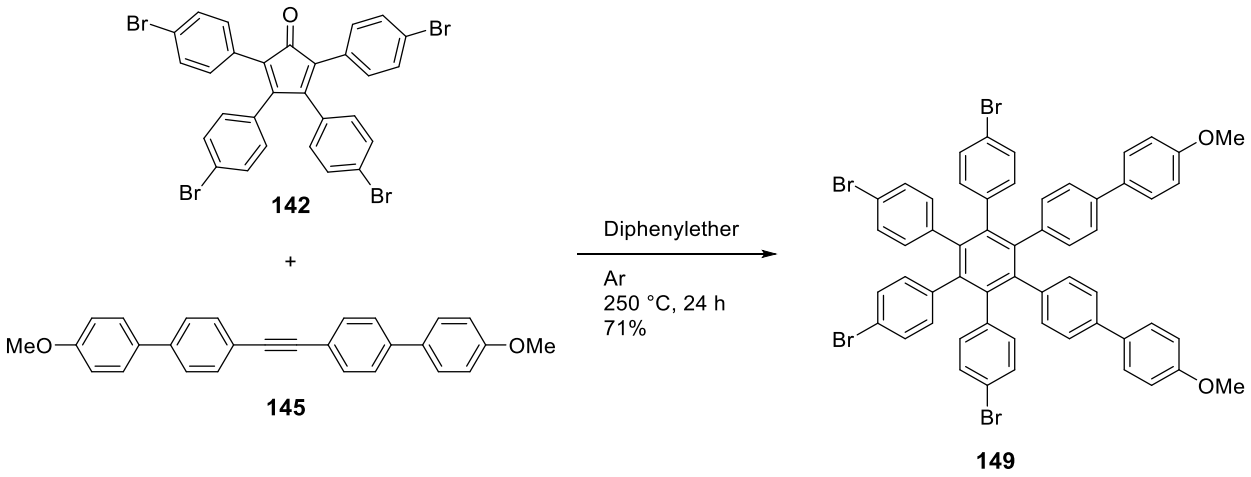

Scheme 5.12: [4+2] cycloaddition between **142** and **145**.

The functionalisation of **149** with dodecyl benzene substituents was performed *via* a *Kumada* reaction using *trans*-$PdCl_2(PPh_3)_2$ as the catalyst (Scheme 5.13). The desired derivative **150** was obtained in a 71% yield. The purification of **150** was found to be tedious, due to the incomplete substitution of the bromines. Despite several successive purifications by column

chromatography and the use of **114b** in large excess (10 eq.), traces of the side product **151** were found by mass spectrometry (LD+, retinoic acid).

The oxidative cyclodehydrogenation of **150** using *Scholl's* conditions afforded the desired HBC derivative **152** in an excellent yield. Due to the high aggregation of HBC in solution and its poor solubility in common solvents, the characterisation by ambient temperature NMRs was precluded. **152** was nevertheless characterised by mass spectrometry (LD+, retinoic acid).

The cleavage of the methyl groups was carried out using BBr_3, affording the building block **153** in a quantitative yield.

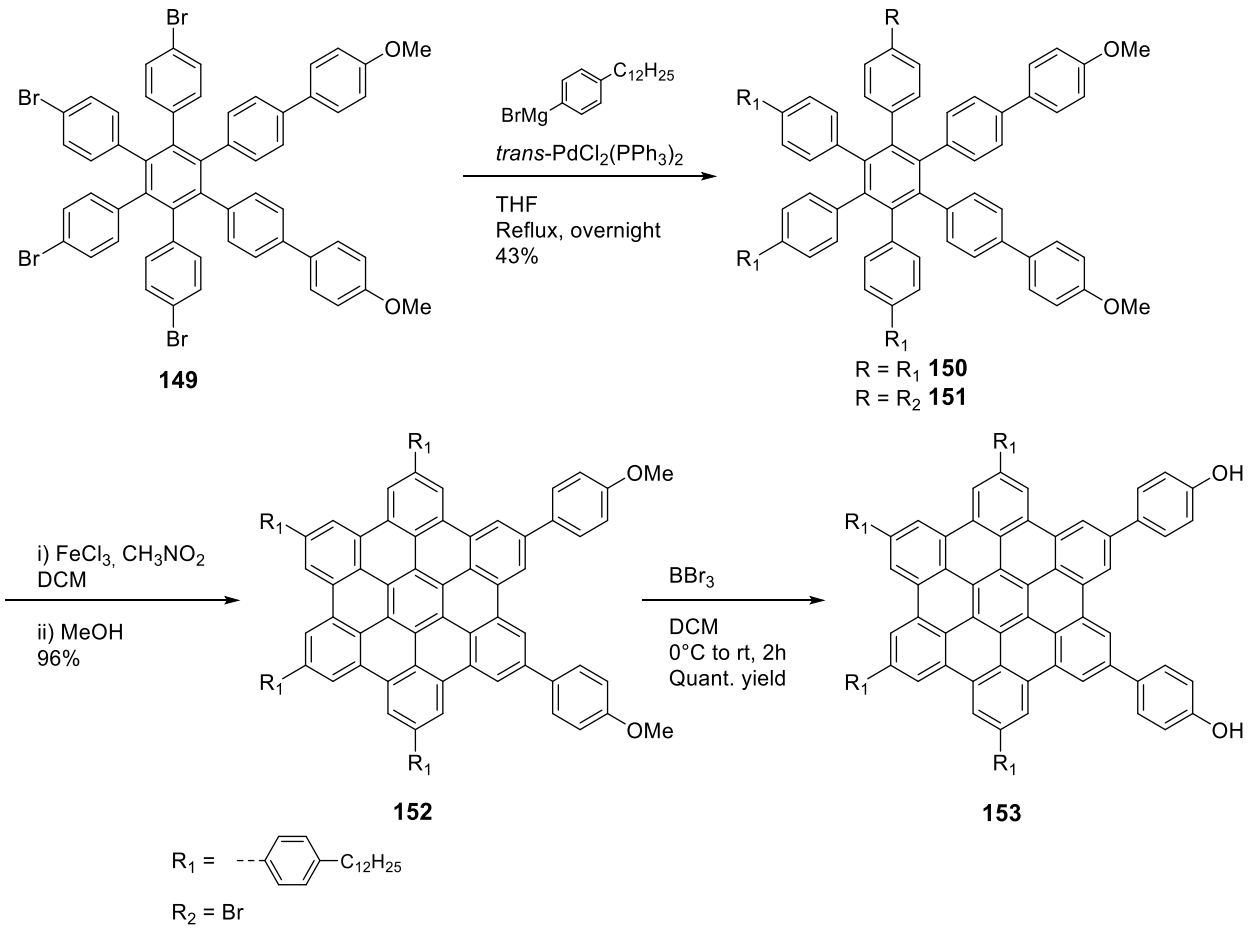

Scheme 5.13: Synthesis of the HBC moiety **153**.

To conclude, the synthesis of the HBC moiety **153** was carried out *via* late functionalisation in 8 steps with an overall yield of 12% from the commercially available 4-bromophenyl acetic acid. However, due to their large aromatic system and therefore their high aggregation by π-π stacking, the common available purification techniques could not be applied to the HBC derivatives. Moreover, high temperature NMR, unavailable at the time of the synthesis is required to obtain the full characterisation. Despite these characterisation issues, it was proved that the impurity **151** and its subsequent derivatives is coexisting with the desired product. The preparation of the compatibiliser HBC-BPDI **155** was nevertheless pursued.

5.2.3 Coupling of the two moieties

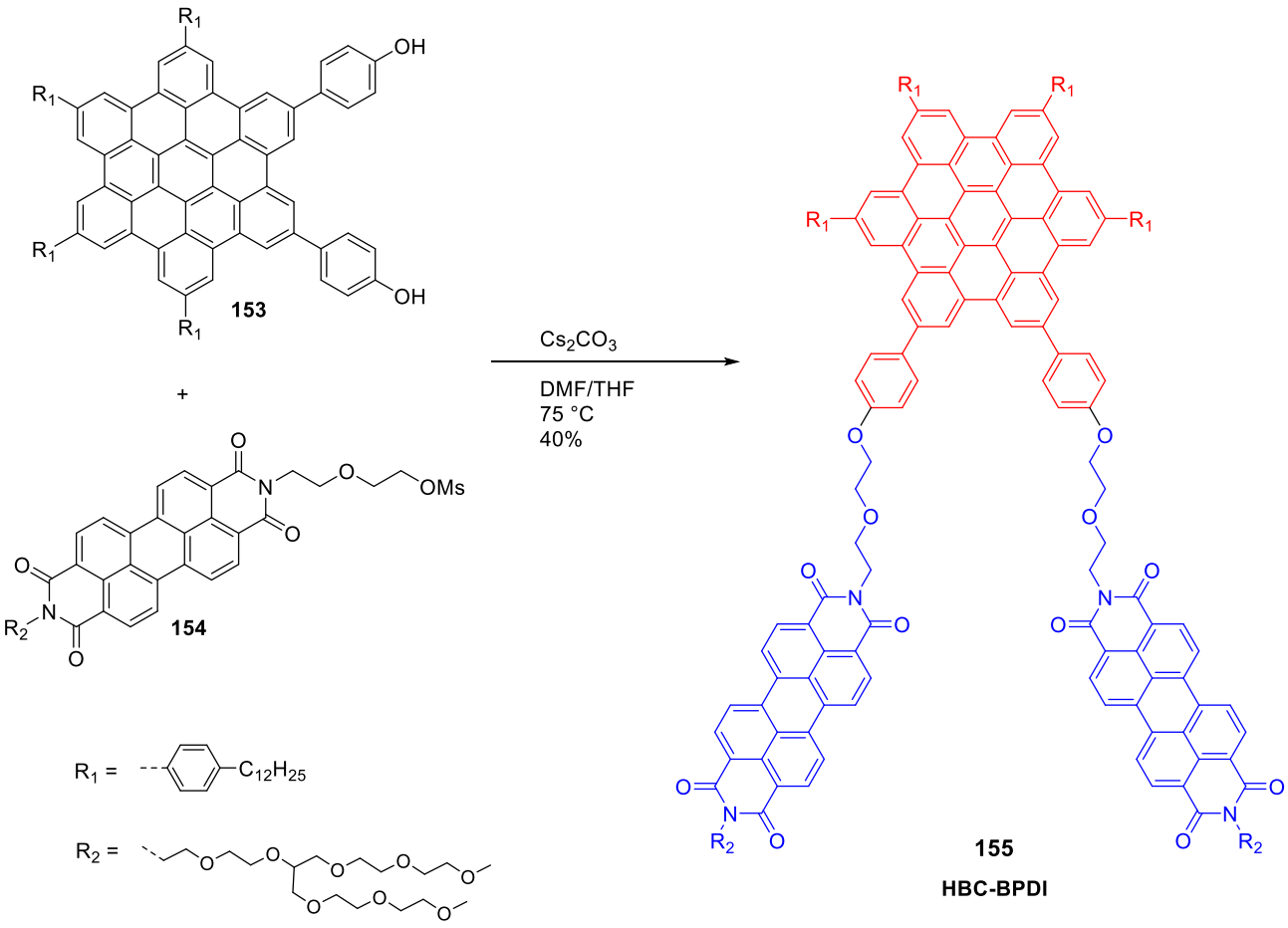

Scheme 5.14: Synthesis of HBC-BPDI.

The coupling between the hydrophobic HBC and the hydrophilic PDI moieties was carried out *via* a *Williamson* type ether synthesis between **153** and the mesyl-activated **154** (Scheme 5.14). THF was added as a co-solvent due to the poor solubility of **153** in DMF, even at high temperatures. To avoid any further solubility issues, cesium carbonate was used instead of potassium carbonate, as Cs_2CO_3 is soluble in organic solvents. Monitoring of the reaction by mass spectrometry was carried out. After refluxing under argon for 2.5 days at 75 °C, the MALDI spectra (Figure 5.3a) revealed the presence of compounds with a molecular weight of 945.2 and 1684.2 $g.mol^{-1}$ corresponding to the starting materials (TOF LD+, dithranol [**154**+Na]$^+$=945.2, [**153**+H]$^+$=1684.2) The temperature was therefore increased to 90 °C and the reaction refluxed for a further 24 h. After working-up, the resulting dark-red powder was analysed by mass spectrometry. The MALDI TOF spectra of the crude (Figure 5.3b) showed a new peak at 3358.4 $g.mol^{-1}$ which corresponded to the sodium adduct of the desired product HBC-BPDI. Impurities were however observed. Indeed, a mass of 3114.2 $g.mol^{-1}$ was ascribed to the sodium adduct of the impurity **156** (Figure 5.4). This impurity was derived from **151**. We believe that the bromo group was cleaved and replaced by a hydrogen atom during the analysis. The others impurities at 1990.4, 1738.3, and 1606.3 $g.mol^{-1}$ could not be attributed.

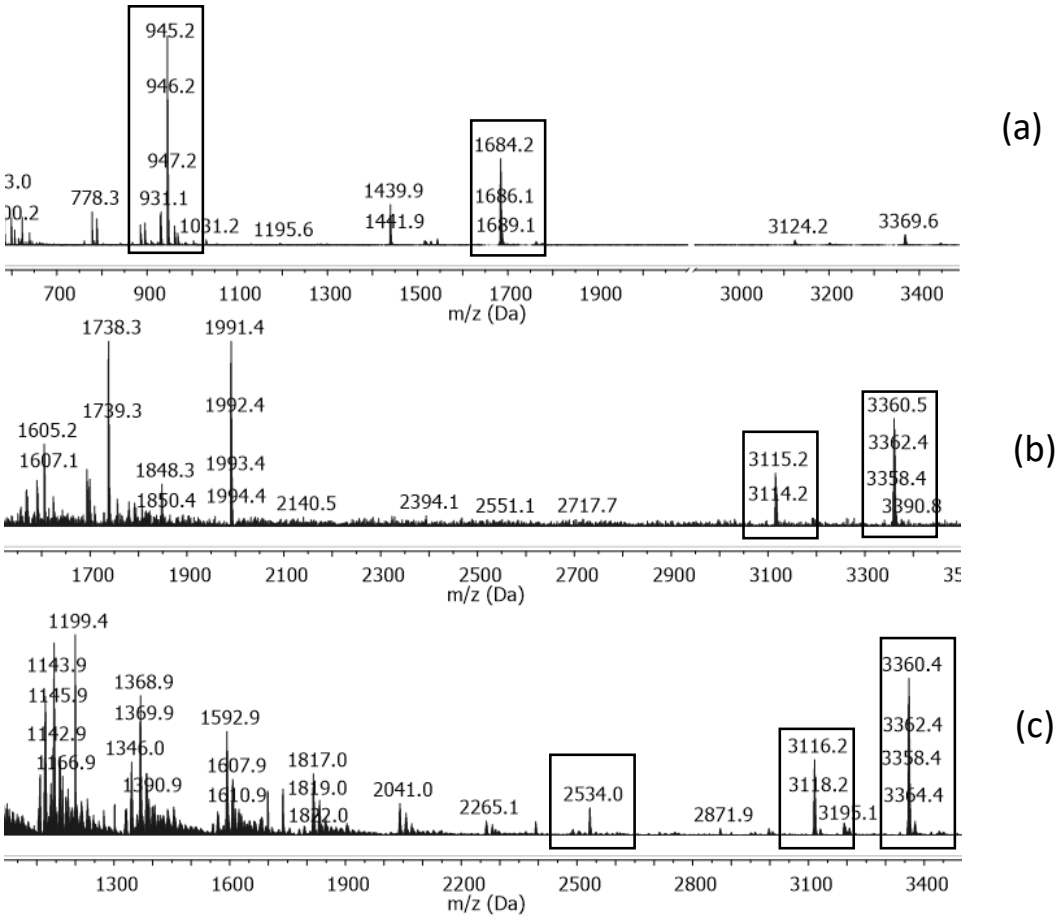

Figure 5.3: MALDI chromatograms (matrix: dithranol) of the coupling reaction between **153** and **154**. (a) Crude reaction after 2.5 d at 75 °C. (b) Crude reaction after further 24 h at 90 °C. (C) purified fraction by Sephadex LH-20 and subsequent recrystallisation in ACN.

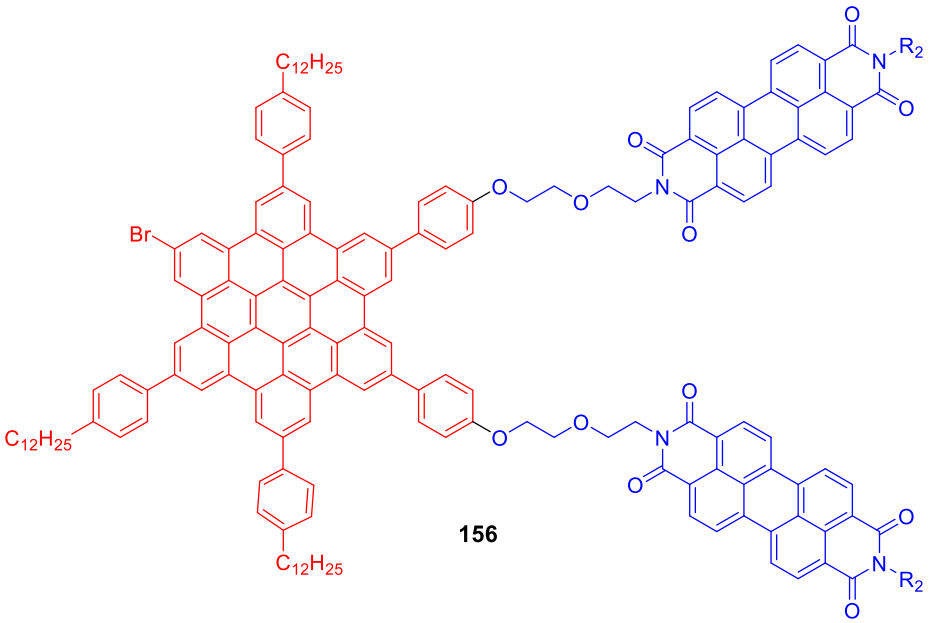

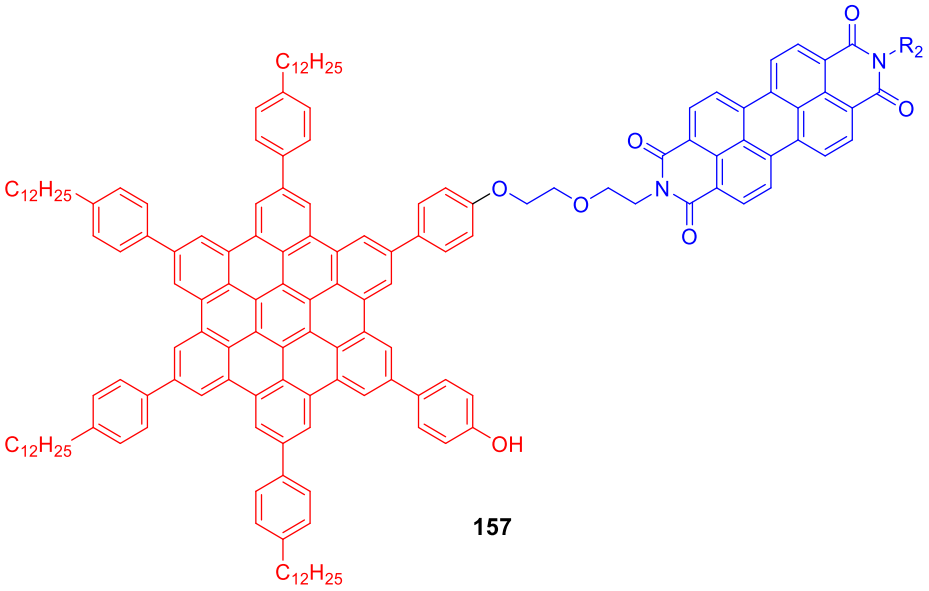

Figure 5.4: Impurities **156** and **157** observed in MALDI spectroscopy.

Attempted purification by column chromatography using silica or alumina did not show any separation, due to the amphiphilic character and the strong aggregation of HBC-BPDI. Purification by reverse phase size exclusion chromatography, using Sephadex LH-20 as the stationary phase allowed for some limited separation. Attempted purification by preparative HPLC, using various solvent systems, such as THF:H_2O or ACN:H_2O were unfortunately unsuccessful as no efficient separation was achieved. It was found that the best method of

purification was slow recrystallisation in acetonitrile from a THF solution of the crude. However, the product was still contaminated by **156** and a small fraction of the monoalkylated **157** ($[M+Na]^+$= 2534.0 $g.mol^{-1}$) was shown (Figure 5.3c and Figure 5.4). It is worth noting that new peaks were observed compared to the crude reaction, which could be explained by the contamination of the mass spectrometry instrument. Moreover, it is likely that the impurities are due to the degradation of the compound during the MALDI. MSMS spectrometry has to be investigated to reject his hypothesis.

Due to the high π-π stacking of the aromatic cores, the characterisation of HBC-BPDI by NMR is precluded, even at high temperature in 1,4-dichlorobenzene-d4, the solvent of choice for HBC derivatives (Figure 5.5). It is nevertheless possible to qualitatively assign the 8.5-7.5 ppm, the 3.7-2.7 ppm and the 2.5-0.5 ppm region to respectively the aromatic, the ethylene-glycol and the alkyl region. It is possible that solid-state cross polarization magic angle spinning (CPMAS) could be used as an alternative NMR method to analyse the compound.

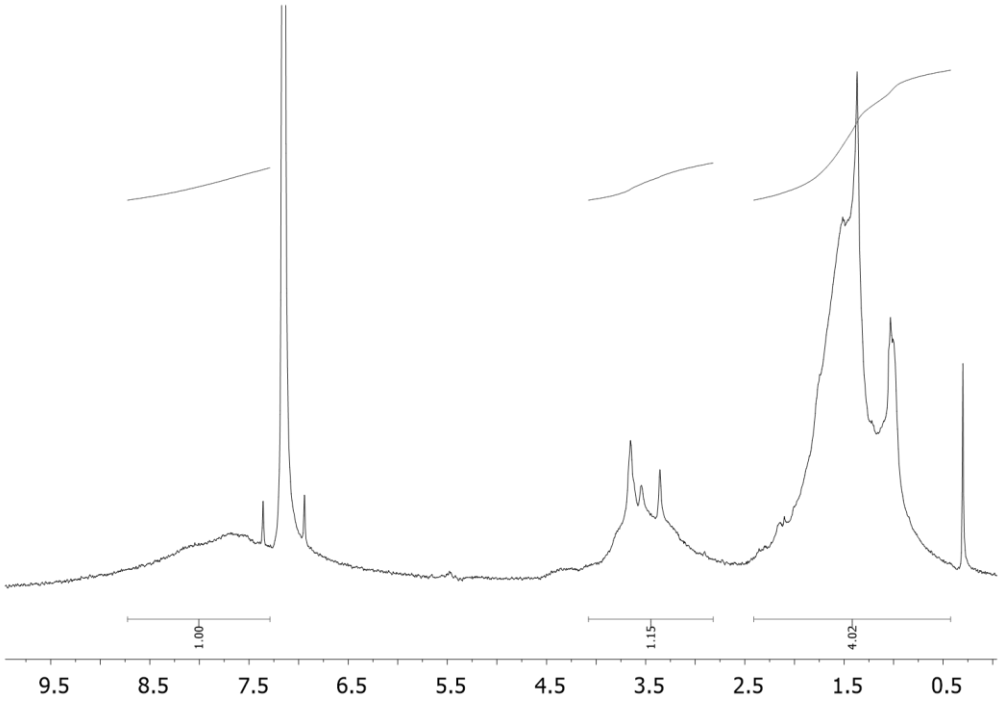

Figure 5.5: ^1H NMR (*p*-$C_6D_4Cl_2$, 85 °C) of HBC-BPDI.

To conclude, the synthesis of the compatibiliser **HBC-BPDI** was successfully carried out using a convergent synthesis to couple a hydrophobic HBC and a hydrophilic PDI moiety. Overall this synthetic route was achieved in 14 steps with an overall yield of 5% from 4-bromophenyl acetic acid. However, given the high molecular weight of this compatibiliser and its strong aggregation due to π-π stacking, the full characterisation by NMR was unsuccessful, even at high temperature. Nevertheless, mass spectrometry indicated the presence of the desired product. Despite efforts to purify HBC-BPDI, traces of impurities remained. The purity of HBC-BPDI could unfortunately not be quantified. Further investigation on the determination of the impurities in the MALDI spectrum as well as finding an efficient purification is needed to obtain pure HBC-BPDI. However, it was decided to pursue this project on this HBC-BPDI batch.

5.2.4 Properties of HBC-BPDI

Preliminary results on the potential mesogenic properties of HBC-BPDI and its photophysics were carried out and are described in this section.

5.2.4.1 Mesogenic properties of HBC-BPDI

HBC-BPDI was firstly characterised by POM. A thin film of the compatibiliser was created by drop-casting from a THF solution on regular glass and APS-coated glass. On regular glass, as-casted HBC-BPDI shows a very brittle dark red texture (Figure 5.6a). Homogenization by heating the sample above its clearing point was attempted. However, no change was observed up to 350 °C. It can therefore be inferred that despite its flexible surrounding chains, HBC-BPDI has a high clearing point (> 350 °C).

On APS-coated slides, a more uniform thin film of HBC-BPDI was observed (Figure 5.6b). However, the thin film is still composed of numerous cracks. It is worth noticing that no birefringence was observed on any analysed samples.

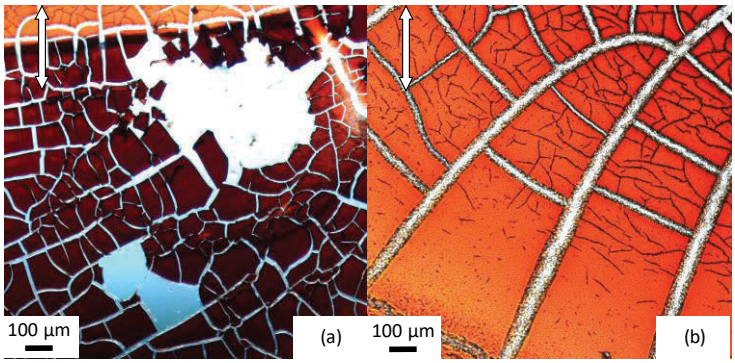

Figure 5.6: POM images of an as-casted HBC-BDPI thin film on: (a) regular glass and (b) APS-coated glass.

Attempted reorganization of the thin film was carried out by solvent vapour annealing using DCM (Figure 5.7). An even film thickness was obtained. However, the thin film is still non birefringent.

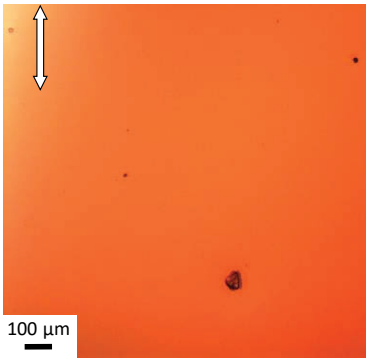

Figure 5.7: POM image of an HBC-BPDI thin film after SVA in DCM.

The POM study of HBC-BPDI on several substrate and using different reorganisation techniques results in non-birefringent thin films. Detailed analysis of those films by POM is therefore precluded and further investigation is required.

X-ray diffractometry of HBC-BPDI was also carried out. Unfortunately, as for HBC-PhC12 (see section 4.4.2), no X-ray diffraction pattern could be obtained using a copper or a cobalt source.

By combining the observation of the POM and the XRD, it can be therefore inferred that this dyad is in an amorphous form.

To conclude, based on the presented results, no definitive conclusion can be drawn on the mesogenic properties of HBC-BPDI. Complementary investigation by changing the drop-casting solvent, the substrate or the method of deposition would be an interesting strategy to follow. Based on similar HBC-PDI dyads, other deposition methods such as solvent vapour diffusion or using different substrates could be an alternative.[195] Moreover, DSC of HBC-BPDI would allow the determination of its transition temperatures.

5.2.4.2 Photophysics

The photophysics of HBC-BPDI was investigated in both solution in THF and in solid state.

The absorption profile of HBC-BPDI in THF is the sum of contribution from the HBC moiety, with characteristic absorption bands located at 376 nm and 414 nm, and from the PDI moiety, at 449 nm, 486 nm and 522 nm (Figure 5.8). It is worth noticing that the absorption wavelengths are the same as the equimolar HBC-PhC12:BPDI mixture studied in section 4.5.2. However, while the molar absorption coefficient value of HBC-PhC12 in the binary blend is between 60 000 and 70 000 $M^{-1}.cm^{-1}$, the intensity of the HBC moiety of HBC-BPDI is two times higher for the same range of concentration. The molar absorption coefficient is nevertheless in accordance with similar HBC derivative bearing ethylene glycol based chains.[207]

The molar extinction coefficient decreases as the concentration increases, indicative of the formation of aggregates in THF.

Compared to the binary mixture of HBC-PhC12 and BPDI, an additional shoulder located at 541 nm is observed. This new absorption band was attributed to a ground state charge transfer complex between the HBC and the PDI moiety. Nevertheless, due to the low intensity of this absorption band, the charge transfer is limited. Additional studies, such as the UV-Visible spectroscopy at lower and higher concentration, is needed to confirm this hypothesis. Indeed, at high dilution, HBC-BPDI exists as a monomer and the additional charge transfer complex band should not be observed. On the contrary at high concentration, the intensity of the band should increase. It should be noted that a similar behaviour has been reported in the literature on the mixing of **158** and **159** (Figure 5.9). The additional absorption band was also ascribed to a ground state charge transfer complex in that binary blend.[208]

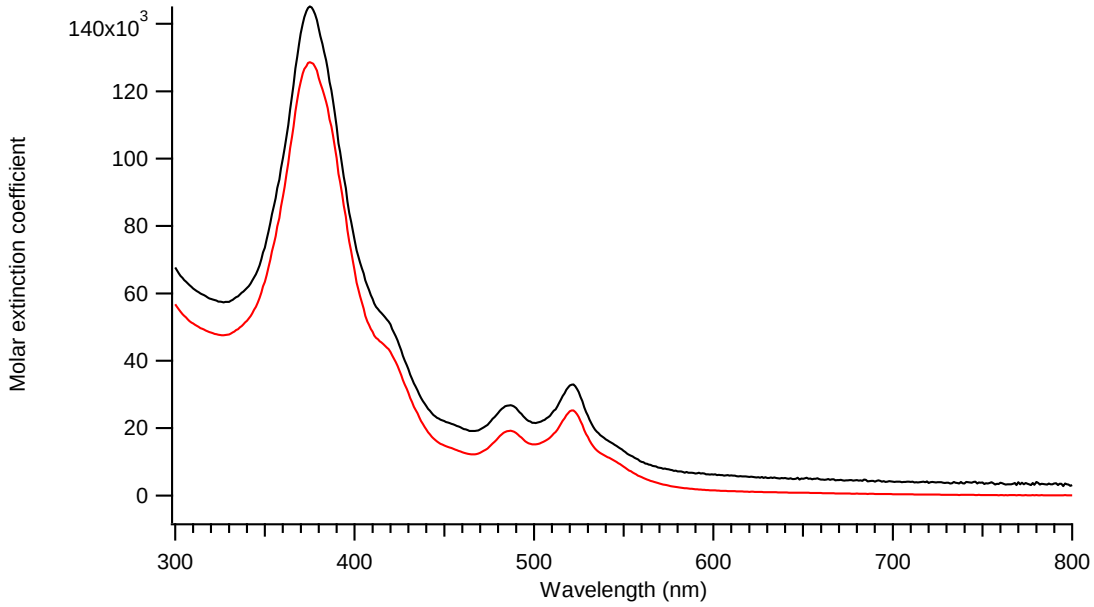

Figure 5.8: Absorption spectra of HBC-BPDI in THF solution at: 13.8 µM (red curve) and 1.5 µM (black curve).

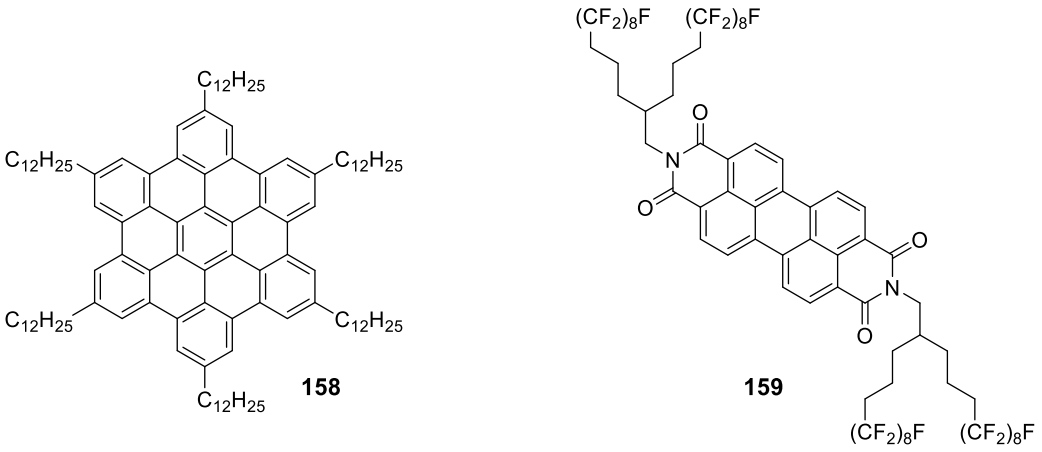

Figure 5.9: Chemical structure of **117** and **158**.[208]

As seen by naked eye, the emission of HBC-BPDI under long wave UV light is quenched compared to the emission of the pure HBC-PhC12 or BPDI. This observation is pointing towards a strong non-radiative process between the two moieties and is likely to be an electron transfer.

The emission profile of HBC-BPDI in THF was also taken. The spectrum is again the sum of contribution from both the HBC (456 nm, 487 nm and 505 nm) and of the PDI (530 nm, 565 nm, and a shoulder at *ca.* 600 nm) moiety (Figure 5.10). No additional red-shifted peaks were found, excluding the formation of exciplexes. When excited at the excitation wavelength of the HBC moiety (λ_{exc} = 405 nm), the main emission is from the PDI moiety, indicating a strong Förster energy resonance transfer.

By comparing HBC-BPDI emission profile with the emission profile of the equimolar HBC-PhC12:BPDI blend at similar concentration (4.5.2, Figure 4.40), the emission intensity of the compatibiliser is lower. This could be explained by non-radiative emission *via* an intramolecular electron transfer between the two moieties.

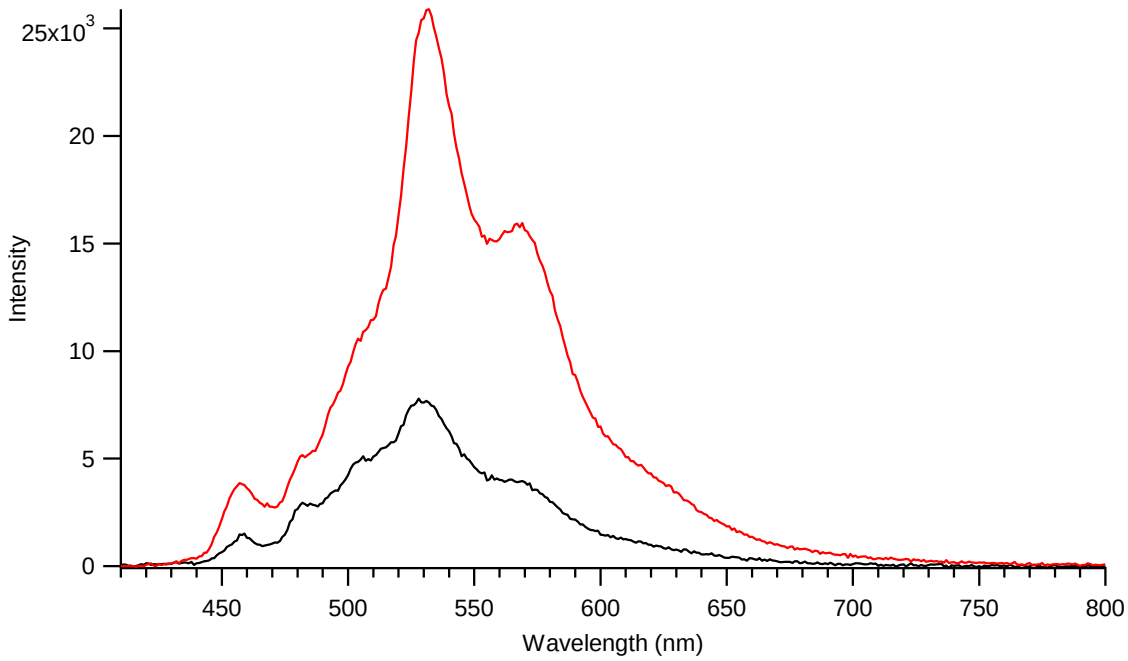

Figure 5.10: Emission spectra of HBC-BPDI in THF solution at: 13.8 µM (red curve) and 1.5 µM (black curve). Excitation wavelength: 405 nm.

On solid state on regular glass, the absorption profile of HBC-BPDI shows broad transitions (Figure 5.11). Nevertheless, the absorption maxima wavelengths do not change compared to in solution in THF (Figure 5.8). Due to the broadness of the absorption bands, no definite conclusion about an additional charge transfer complex band can be drawn.

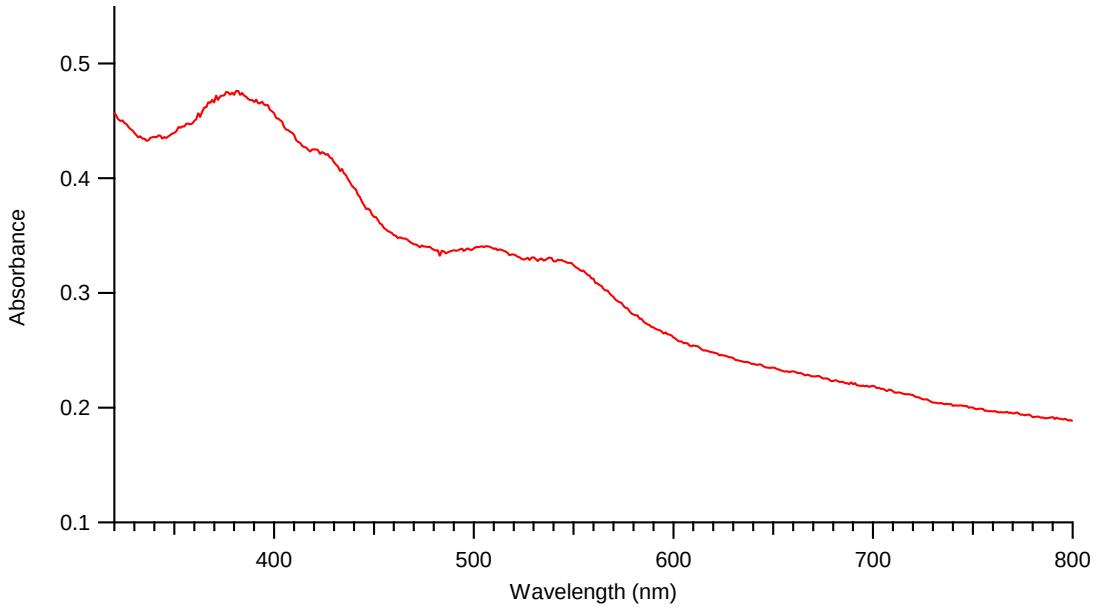

Figure 5.11: Absorption spectra of an as-casted HBC-BPDI thin film on regular glass.

The solid state emission profile does not show any contribution of the HBC nor the PDI moiety (Figure 5.12). Instead, a large red-shifted band, with a maximum wavelength of 774 nm is observed, indicative of an exciplex state. Excitation at the wavelength of either the HBC or the PDI moiety does not change significantly the emission profile of HBC-BPDI.

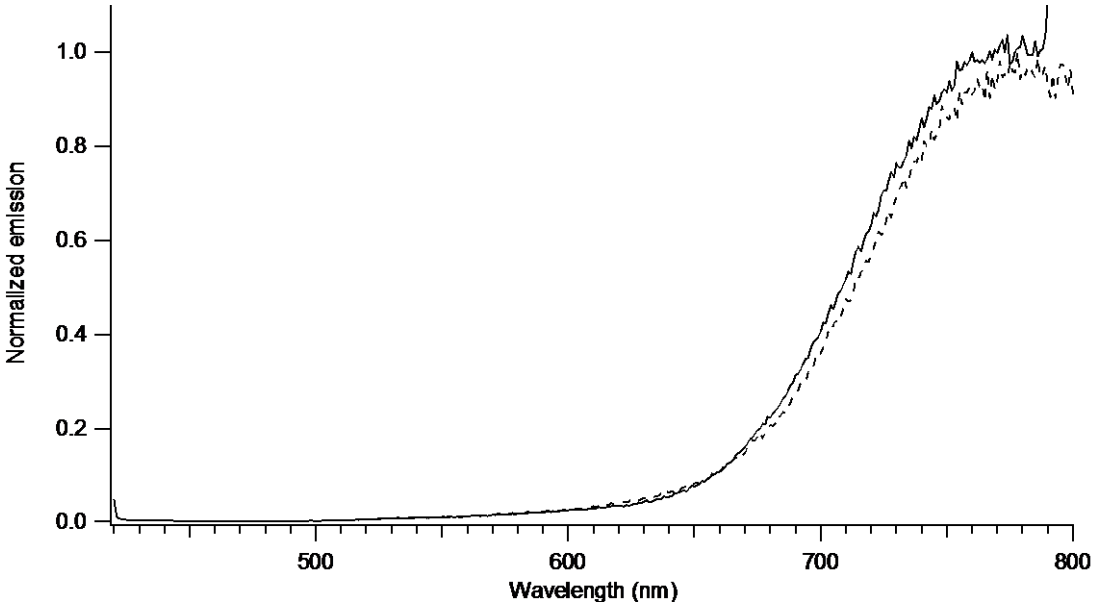

Figure 5.12: Normalised emission spectra of HBC-BPDI thin film on regular glass. Excitation wavelength: 405 nm (solid line) and 488 nm (dashed line).

To conclude, we believe that the favoured ground state charge transfer that is usually occurring between an electron acceptor and donor moiety is greatly reduced by the immiscibility of the chains of the two different moiety of HBC-BPDI. Indeed, the charge transfer band intensity is minor compared to the absorption of the two different moieties. The emission profile in solution shows a high Förster resonance transfer energy between the HBC and the PDI moiety, which is expected for a covalently linked donor/acceptor component.

The quenching of the emission in solution in indicative of electron transfer between the two electron acceptor and donor moiety. It is therefore inferred that electron transfer is also

occurring in solid state, even though the exciplex is coexisting. However, additional investigation is needed to quantify these qualitative results.

5.3 Compatibilisation of HBC-PhC12 and BPDI: use of HBC-BPDI

As discussed in the previous chapter, an equimolar mixture of the electron donor and hydrophobic HBC-PhC12 and the electron acceptor and hydrophilic BPDI results in macrophase separation. The effect of the compatibiliser HBC-BPDI was investigated by POM and photophysics in solid state and the preliminary results are discussed in this section.

5.3.1 POM

The POM study of a ternary blend composed of an equimolar mixture of HBC-PhC12 and BPDI with different concentrations of the compatibiliser HBC-BPDI (10mol% and 50mol%) was carried out. The results were compared to the equimolar and undoped HBC-PhC12:BPDI binary mixture (see section 4.5).

Upon addition of 10 mol% HBC-BPDI into the equimolar blend of HBC-PhC12:BPDI, the as-casted thin film obtained on regular or APS-coated slide is very heterogeneous and preclude the detailed analysis of the blend (Figure 5.13). However, the texture of the thin film is different from the undoped HBC-PhC12:BPDI blend (Figure 4.34 and Figure 4.35), indicating an effect of HBC-BPDI on the morphology of the thin film. Upon addition of 50 mol% HBC-BPDI into the equimolar mixture of the incompatibles, the as-casted POM on regular or APS-coated glass shows a similar texture as the samples doped with 10 mol% HBC-BPDI (Figure 5.14).

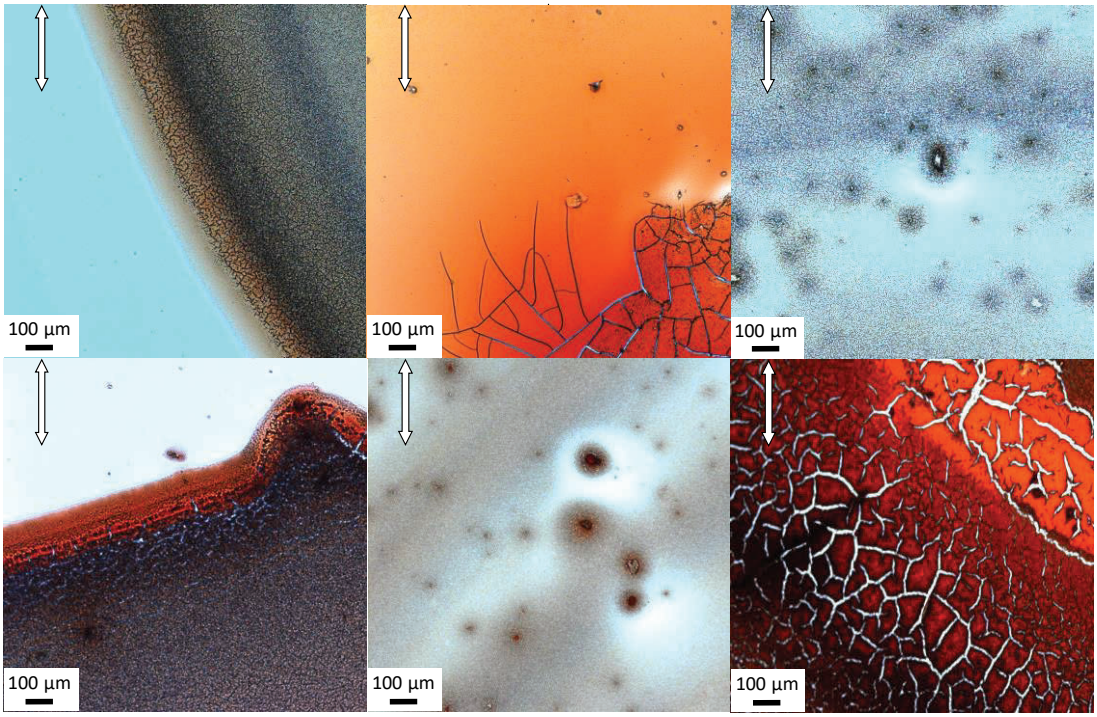

Figure 5.13: POM images at room temperature of an HBC-PhC12:BPDI equimolar mixture with 10mol% HBC-BPDI: Top: as-casted on regular glass. Bottom: as-casted on APS-coated glass. The pictures were taken at different regions.

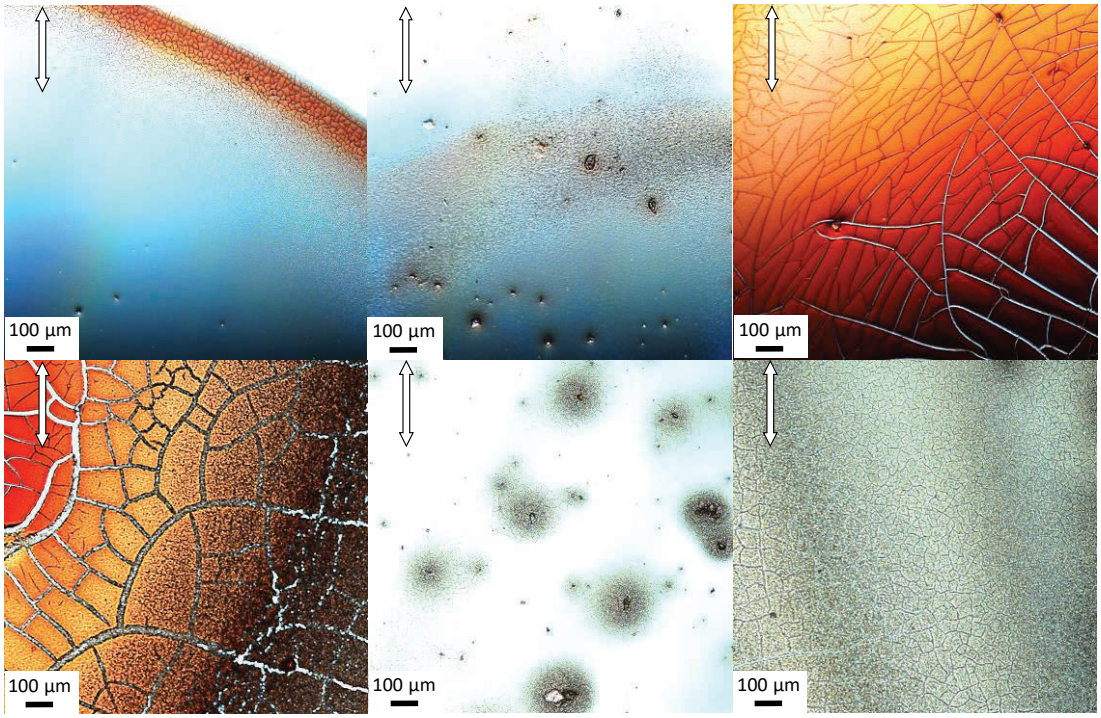

Figure 5.14: POM images at room temperature of an HBC-PhC12:BPDI equimolar mixture with 50mol% HBC-BPDI: Top: as-casted on regular glass. Bottom: as-casted on APS-coated glass. The pictures were taken at different regions.

Due to the successful strategy to reorganise the film using solvent vapour annealing on the equimolar undoped mixture (see section 4.5.1), the equimolar HBC-PhC12:BPDI blends containing 10mol% and 50mol% HBC-BPDI were placed into a saturated atmosphere of THF and $CHCl_3$.

The SVA of an equimolar blend of HBC-PhC12:BPDI containing 10mol% HBC-BPDI showed similar textures compared to the undoped blend: the edge of the drop casted film is red whilst the inner part of the drop is mostly clear (Figure 5.15). This seems to indicate that no significant compatibilisation of the binary blend of the incompatibles materials is observed.

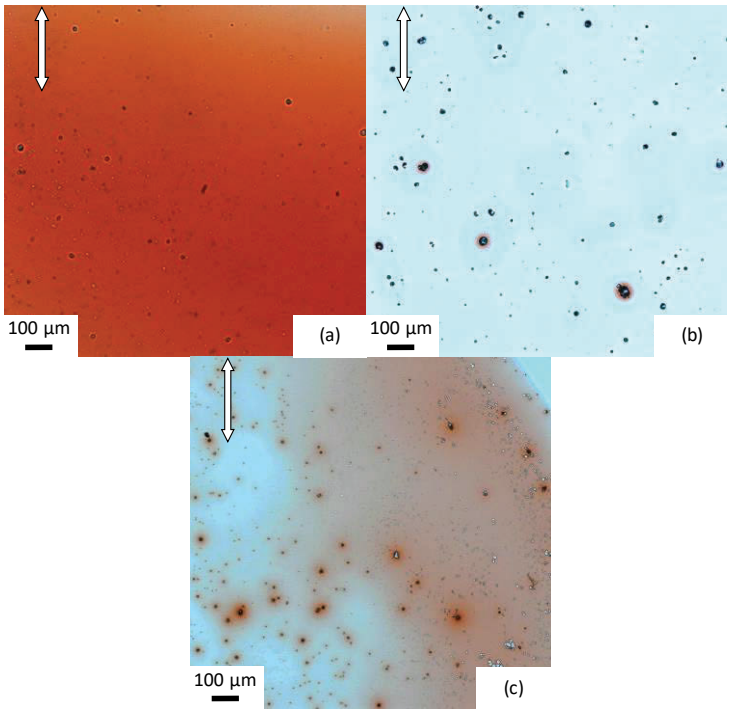

Figure 5.15: POM image at room temperature of an HBC-PhC12:BPDI equimolar mixture with 10mol% HBC-BPDI after SVA from: (a) and (b) THF; (c) $CHCl_3$. The pictures were taken at different regions.

However, upon addition of 50mol% of HBC-BPDI into the equimolar mixture of HBC-PhC12:BPDI, the texture differed greatly from the undoped or the dopped blend with 10mol% HBC-BPDI. However, no clear domains were observed. No detailed information about the composition of the domains can be extracted.

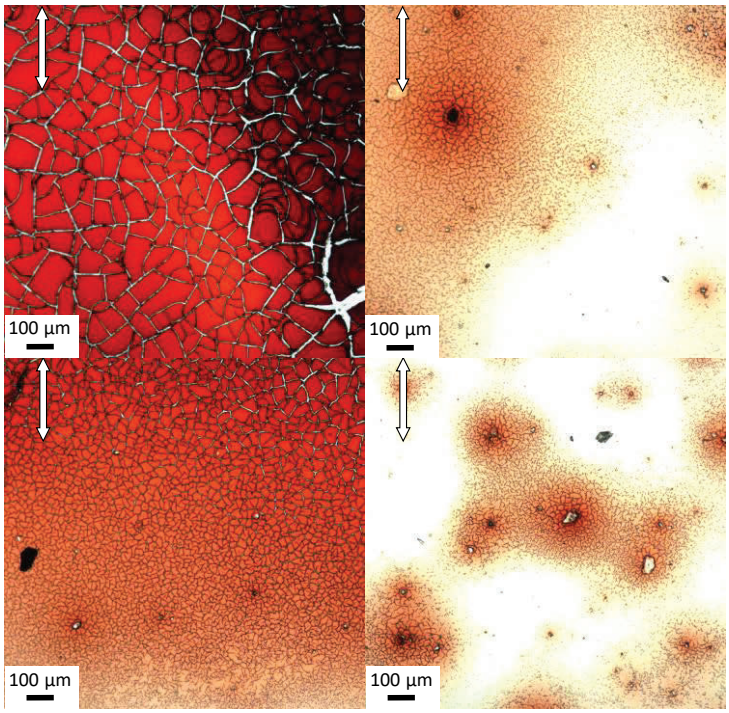

Figure 5.16: POM image at room temperature of an HBC-PhC12:BPDI equimolar mixture with 50mol% HBC-BPDI after SVA from: Top: THF. Bottom: $CHCl_3$. The pictures were taken at different regions.

To conclude, it can be inferred that the compatibiliser HBC-BPDI influences the organization of an equimolar mixture of the two incompatible materials HBC-PhC12 and BPDI. Indeed, the POM study shows that at a 50mol% doping of HBC-BPDI into the equimolar HBC-PhC12:BPDI blend, solvent vapour annealing the texture greatly differs from the undoped blend. However, no information on the composition or how the thin film is organised could be extracted from these preliminary results. Further investigation is therefore required.

5.3.2 Photophysics

The photophysics of an equimolar HBC-PHC12:BPDI blend containing 10mol% and 50mol% HBC-BPDI were also studied and the results were compared to the undoped blend.

Whilst the absorption spectrum of the thin film containing 10mol% HBC-BPDI does not differ from the undoped thin film, the absorption spectrum of the thin film containing 50mol% shows an intense absorption band at the absorption wavelength of the HBC core (Figure 5.17).

The high intensity of this band compared to the absorption of PDIs can be explained by the high molar extinction coefficient at 380 nm of the compatibiliser HBC-BPDI.

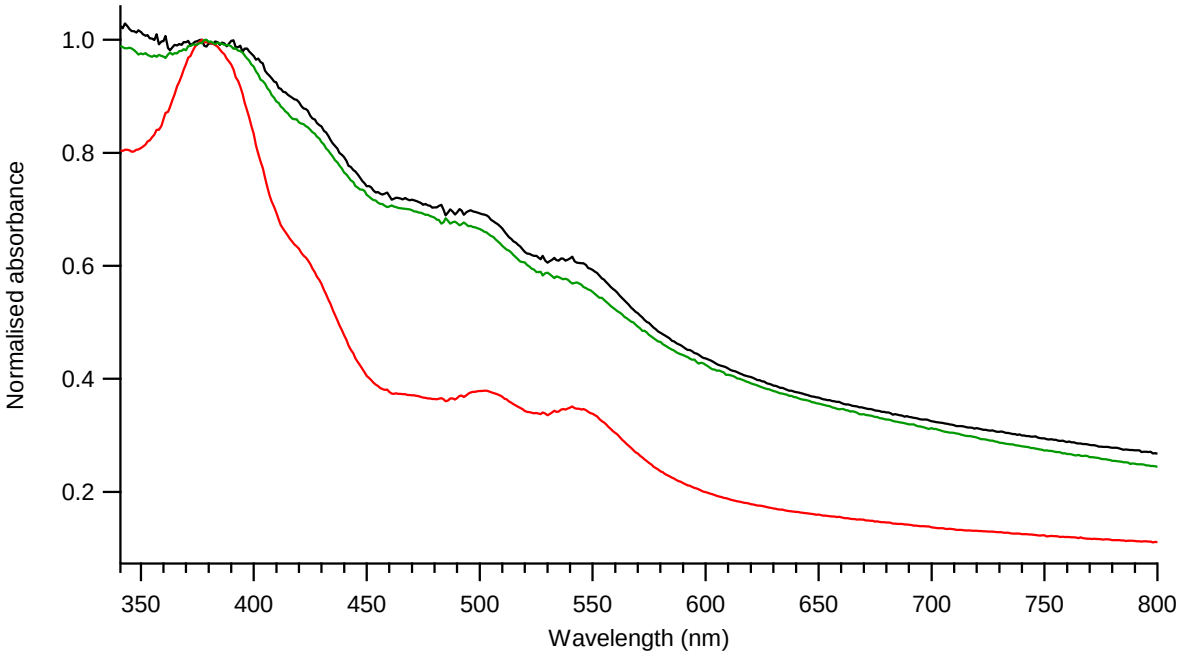

Figure 5.17: Normalised absorption spectra on solid state of an equimolar HBC-PhC12:BPDI blend with: 0mol% HBC-BPDI (black line); 10mol% HBC-BPDI (green line); 50mol% HBC-BPDI (red line). The sample was drop-casted on regular glass.

The emission properties on solid state were also investigated when the thin film was created on regular glass (Figure 5.18). The emissive properties of a thin film containing 10mol% HBC-BPDI are similar than the undoped mixture. The additional band located at 525 nm when the thin film is excited at the wavelength of the HBC moiety is ascribed to the emission of HBC-PhC12.

At 50mol%, the formation of the exciplex is still predominant. However, when excited at the excitation wavelength of the BPDI moiety (488 nm), the exciplex emission band still remains, unlike the undoped or the 10mol% HBC-BPDI thin films. This transition can be explained by the emission of the compatibiliser.

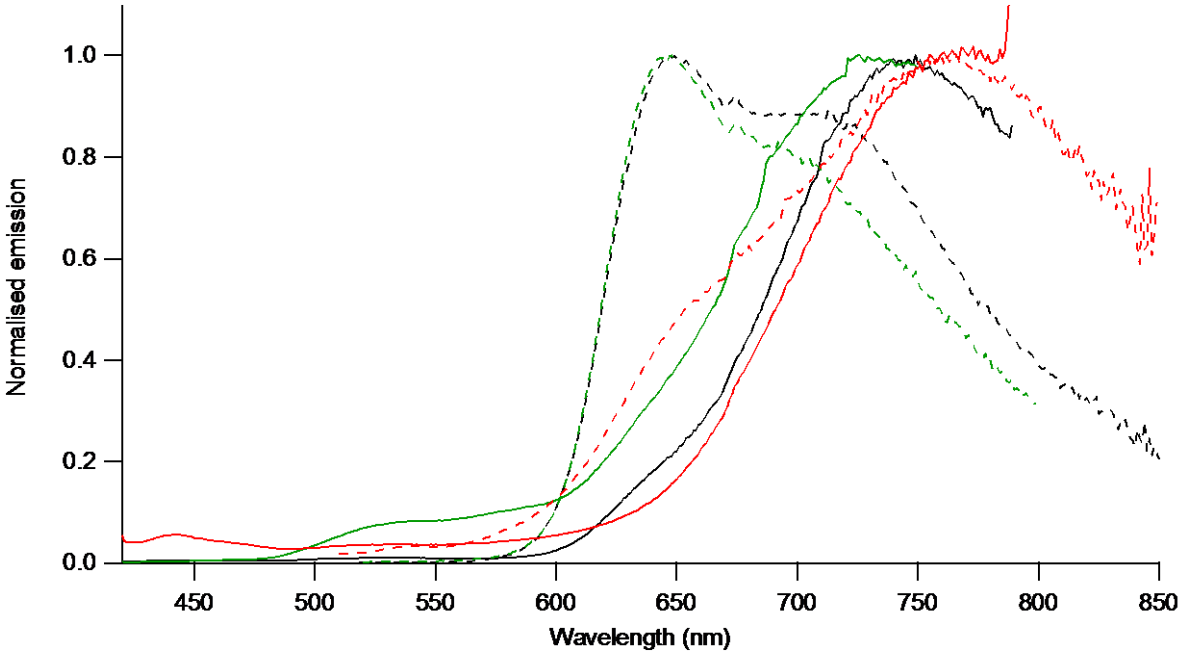

Figure 5.18: Normalised emission spectra of an equimolar HBC-PhC12:BPDI thin film on regular glass with: 0mol% HBC-BPDI (black line); 10mol% HBC-BPDI (green line); 50mol% HBC-BPDI (red line). Excitation wavelength: 405 nm (solid line) and 488 nm (dashed line).

Is it worth noting that the absorption and the emission spectra does not differ when the thin film is created on APS-coated glass.

To conclude, preliminary results on the photophysical properties of a ternary blend of HBC-PhC12:BPDI:HBC-BPDI at different ratio of HBC-BPDI shows an effect of the compatibiliser. However, due to the instrument setup, no definite correlation between these observations and the organisation of the compounds into the blend can be made. The preliminary results presented in this section requires further investigation. As for the undoped blend presented in section 4.5.2, it would be interesting to obtain quantitative results of the emission and to compared the intensities between the different composition of the thin film. Moreover, transient absorption and emission spectroscopies would allow a better understanding of the exciplex formation.

5.4 Summary

As a compatibilising agent to supress the macrophase separation between HBC-PhC12 and BPDI, a tailor-made compatibiliser, HBC-BPDI was design. This amphiphilic donor/acceptor dyad was successfully synthesised. However, given its molecular weight, its complexity and its strong aggregation in organic solvents, the common purification procedures (column chromatography, preparative HPLC) were unsuccessful. Moreover, the full analysis by NMR was unsatisfactory due to the high aggregation. The crude product was nevertheless partly purified by recrystallisation but impurities remained.

Preliminary results on the mesogenic properties of HBC-BPDI by POM were unsatisfactory. Further investigation using different deposition techniques, substrates or solvents could be an interesting strategy to obtain further information on its thin film structure. Moreover, X-ray analysis and DSC could provide valuable data.

The study on the effect of HBC-BPDI on an equimolar HBC-PhC12:BPDI was also carried out. On adding 10mol% of the compatibiliser into the binary blend, POM reveals that no to little effect on the morphology is observed. On adding 50mol%, an unambiguous texture change was observed. These preliminary results need nevertheless further investigation.

As for the equimolar mixture of HBC-PhC12:BPDI described in the previous chapter, it is believed that the use of other microscopy techniques, unavailable at the time of this thesis, could give valuable information on the organisation of the blends. Raman microscopy or electron microscopy equipped with an energy dispersive X-ray spectroscopy detector could be used to obtain a distribution map of the different components, based on their structure and their elemental composition. Based on their molecular weight LESA or MALDI-imaging could also be investigated.

Chapter six:

Conclusions and further work

6 Conclusions and future work

The aim of this project was to explore an efficient strategy to control the morphology of incompatible components based on adding a third component into the binary blend. The third component, called compatibiliser, aims at suppressing the thermodynamically favoured macrophase separation to obtain a reproducible micro-phase segregation of the two components.

A model study based on triphenylene derivative was first investigated. The well-known hydrophobic TP6 and hydrophilic TP6EOnM (n = 2, 3, 4) were prepared. While TP6 is a thermotropic liquid crystal, TP6EOnM showed chromonic properties and their self-association in water was studied. Valuable information on the bond energy between two triphenylene in the aggregate were obtained based on the theory of aggregation, using an isodesmic type aggregation. Is was experimentally shown that the energy bond is decreasing as the length of the surrounding chains is increasing, and led to smaller aggregates with higher molar extinction coefficients for a given concentration.

TP6 and TP6EO2M were proved to be incompatible, by macrophase separating when blended in an equimolar ratio. This system was therefore ideal for the study of adding a third compatibilising agent into the blend. The use of a purely structural additive, C6E3M was proved to suppress the macrophase separation and induces a micro segregation of TP6 and TP6EO2M when incorporated. In addition, TP6-Gall, a novel amphiphilic dyad composed on a hydrophobic triphenylene and a hydrophilic gallate moieties was successfully prepared. Using TP6-Gall into the incompatible blend of TP6 and TP6EO2M led to the suppression of the macrophase separation towards micro segregation. Importantly, this new organisation of TP6

and TP6EO2M is stable upon several heating/cooling cycle, proving its thermodynamically stability, even in the isotropic phase.

Our efforts were then focused on incompatible functional materials, used in various optoelectronic applications, including organic solar cells. The hydrophobic and electron donor HBC-PhC12 and the hydrophilic electron acceptor BPDI were the chosen materials, due to their liquid crystalline properties and previous use as active components for solar cells. It was shown that HBC-PhC12 and BPDI, despite their coulombically favoured attraction, macrophase separate, due to the incompatibility of their surrounding chains.

A tailor-made compatibiliser for the HBC-PhC12:BPDI system was designed. HBC-BPDI, an amphiphilic functional dyad, composed of one HBC and two PDI moiety, was successfully prepared. Preliminary results on the effect of HBC-BPDI on the morphology of the incompatible HBC-PhC12 and BPDI indicate a positive effect by modifying the organisation of the blend. However, no definite conclusion on the reasons underpinning this effect could be made and further, more specialised and sophisticated studies are necessary. For example, it would be of great interest to have a deeper understanding of the effect of HBC-BPDI into the HBC-PhC12:BPDI blend. The use of other deposition method for the preparation of the thin film could be an alternative to alleviate the characterization issues observed in this project. Furthermore, other characterization methods, such as Raman or electron microscopy, as well as LESA or MALDI-imaging could be used.

Due to their electron donor and acceptor properties and their great promises in optolectronic devices, solar cell testing of HBC-PhC12 and BPDI blends without and with the dyad HBC-BPDI would be an interesting way to investigate the effect of the compatibiliser on the solar cell efficiency.

In conclusion, we have shown that the use of a small molecule compatibiliser is a promising strategy to control the morphology of blends.

Chapter seven:

Experimental part

7.1 General experimental

Dichloromethane, hexane, ethanol, methanol, *N,N*-dimethylformamide, tetrahydrofuran, acetic acid, and sulphuric acid were purchased from Fisher. Acetone and ethyl acetate were purchased from VWR. Diethyl ether was purchased from Sigma Aldrich. Hydrobromic acid was purchased from Alfa Aesar. All solvents were used without further purification except for ethyl acetate which was distilled *in vacuo*. Column chromatography was carried out on silica gel 60 [Alfa Aesar, 0.040-0.063 mm] or on activated neutral alumina [Sigma-Aldrich, 58 Å pore size].

Reaction progresses were followed with TLC plate on aluminium support (Alumina : Fluka; Silica : Alugram® SIL G/UV_{254}).

THF, toluene and DCM were dried by a solvent purification system (Pure Solv-MD Solvent instrument from Innovative Technology). Dioxane was dried by over 3 Å molecular sieve. Dry acetone was obtained by distillation over CaH_2.

The thin films were prepared by dropcasting a solution of the sample in either DCM (for triphenylene derivatives) or THF (for HBC and PDI derivatives). The films were dried at ambient conditions.

APS-coated slides were prepared according to the literature procedure[209]: the glass slides were washed with successively, detergent, tap water and distilled water. The slides were then soaked into an acetone bath (x2) and dipped into a 2% dry acetone solution of (3-aminopropyl)triethoxysilane for 2 min. The coated slides were dipped into two distilled water baths, and dried in the oven (T = 42 °C) overnight.

Thermal annealing was performed as follows: the thin film was placed at 200 °C for 2h. Solvent vapour annealing was carried out by placing the thin film into a saturated atmosphere of the solvent of choice for 17 h.

Room temperature NMR spectra were recorded on a Brucker Avance III 300 (^{1}H 300 MHz, ^{13}C 101 MHz) instrument and are reported relative to the residual deuterated solvent as the internal standard ($CDCl_3$: $\delta[^{1}H]$ = 7.26 ppm; $\delta[^{13}C]$ = 77.16 ppm; DMSO-d6: $\delta[^{1}H]$ = 2.50 ppm; $\delta[^{13}C]$ = 39.52 ppm; *p*-$C_6D_4Cl_2$: $\delta[^{1}H]$ = 7.27 ppm; $\delta[^{13}C]$ = 132.50, 129.80 ppm). High temperature NMR spectra were recorded on a JEOL ECA-600 instrument (^{1}H 600 MHz, ^{13}C 151 MHz) or a Bruker Advance III 400 (^{1}H 400 MHz). Coupling constants are expressed in Hz.

High resolution mass spectra were determined from Micromass ZABspec mass spectrometer in TOF MS ES+ or TOF MS AP+ mode and are reported as (m/z (%)). MALDI mass spectra were recorded on a Waters Micromass Mx instrument with a time of flight detection mode.

IR spectra were recorded on Perkin Elmer Sprectrum100 FT-IR spectrometer. Melting points were taken on a Stuart Scientific melting point SMP1 device.

Analytical chromatograms were recorded on a Shimatdzu LC-20AD/T device, using a Phenomenex Kinetex 5 µ, C18, 100 Å column at a constant temperature of 35 °C. All samples were filtered through a 0.45 µm syringe filter before injection and solvent were degassed with helium. Purification by preparative HPLC were done using a Phenomenex Kinetex 5 µ, C18, 100 Å, AXIA packed preparative column equipped with a SecurityGuard PREP Cartridge Core-Shell C18 at room temperature. Data were collected and processed using the Dionex Chromeleon 6.11 software package.

UV-visible spectra were recorded using a Cary 50 Spectrophotometer at a temperature of 20°C ± 1°C.

Solid state emission spectra were recorded on an Edinburgh FLSP920 Time resolved spectrometer instrument while emission spectra in solution were recorded on a Shimatzu RF5301-PC spectrofluoreometer.

An Olympus C-CMAD-2 device using a JVC TK-C1380 camera was used to perform temperature dependent polarized optical microscopy. Heating was controlled using a Linkam Scientific LTS 350 apparatus. Room temperature polarised optical microscopy were done ona Zeiss Axio Imager.A1M microscope equipped with a Axio Cam MRc camera.

DSC curves were recorded on a Perkin Elmer DSC 7 device (for ambient to high temperature) or on a Mettler Toledo DSC 1 STAR^{e} System (for sub-ambient to high temperature). All DSC results shown are taken during a second heating-cooling cycle. Transition temperatures are taken at the maximum transition peak.

X-Ray diffraction measurements were recorded using a Macor cup on an Anton Paar PANalytical empyrean X-ray diffractometer equipped with a CuKα X-ray source (λ = 1.540598 Å) or on a Bruker D2 PHASER X-ray diffractometer equipped with a CoKα source (λ = 1.79026 Å).

The topography images were recorded on a JPK NanoWizard atomic force microscope in tapping mode with a Veeco FESP AFM probe at room temperature.

Raman spectra were recorded on either a Renishaw in*Via* raman microscope equipped with a green (λ = 532 nm) or red laser (λ = 633 nm) source or on a Witec Alpha 300R Raman microscope equipped with an infrared laser (λ = 785 nm).

7.2 Experimental procedures and analytical data for chapter two

1,2 -Dihexyloxybenzene (44)

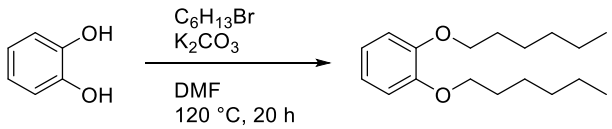

44

A known compound prepared according to modified literature procedures. [92,101] To a solution of K_2CO_3 (5.02 g, 36.4 mmol) and catechol (2.00 g, 18.2 mmol) in DMF (1 mL), was added dropwise 1-bromohexane (7.7 mL, 54.5 mmol). The mixture was stirred at 120 °C for 20 h. The solvent was evaporated *in vacuo* and the resulting solid was filtered through a pad of silica (eluent: EtOAc). Purification by column chromatography (SiO_2, hexane:EtOAc = 20:1) afforded **44** as a colourless oil (3.69 g, 77%).

^{1}H NMR (300 MHz, $CDCl_3$) δ 6.89 (s, 4H, CH_{Ar}), 3.99 (t, J = 6.7 Hz, 4H, OCH_2), 1.88-1.72 (m, 4H, CH_2), 1.52-1.23 (m, 12H, CH_2), 0.90 (t, J = 7.0 Hz, 6H, CH_3).

^{13}C NMR (101 MHz, $CDCl_3$) δ 149.4 (2 x C_{Ar}), 121.2 (2 x CH_{Ar}), 114.3 (2 x CH_{Ar}), 69.5 (2 x OCH_2), 31.8 (2 x CH_2), 29.5 (2 x CH_2), 25.9 (2 x CH_2), 22.8 (2 x CH_2), 14.2 (2 x CH_3).

HRMS (TOF ES+): m/z $[M+H]^+$= 279.2250 (Calculated: 279.2246).

IR ν_{max}(film)/cm^{-1}: 2954 (m), 2927 (m), 2859 (m), 1502 (s), 1252 (s), 739 (m).

2,3,6,7,10,11-Hexahexyloxytriphenylene (45 - TP6)

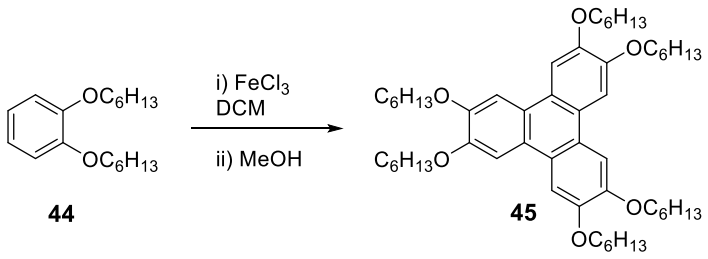

44 45

A known compound prepared according to the literature procedure.[92] To a vigorously stirred solution of $FeCl_3$ (3.5 g, 21.57 mmol) in CH_2Cl_2 (26 mL) was added sulphuric acid (2 drops) and 1,2-dihexyloxybenzene **44** (2.00 g, 7.19 mmol). The dark blue solution was stirred at room temperature for 1 h. The reaction mixture was then cooled down to 0 °C and methanol (90 mL) was slowly added until a precipitate was formed. After 2 h at 0 °C, the green solution was filtered and the precipitate was washed with cold methanol. The gray solid was dissolved in CH_2Cl_2 and purified through a pad of silica (eluent: DCM). The resulting filtrate was concentrated *in vacuo* and purified by column chromatography (SiO_2, hexane:DCM = 1:1) to afford **45** as white crystals (1.220 g, 61%).

^{1}H NMR (300 MHz, $CDCl_3$) δ 7.83 (s, 6H, CH_{Ar}), 4.23 (t, J = 6.6 Hz, 12H, OCH_2), 2.04-1.80 (m, 12H, CH_2), 1.66-1.51 (m, 12H, CH_2), 1.49-1.30 (m, 24H, CH_2), 0.93 (t, J = 7.0 Hz, 18H, CH_3).

^{13}C NMR (101 MHz, $CDCl_3$) δ 149.1 (6 x C_{Ar}), 123.8 (6 x C_{Ar}), 107.6 (6 x CH_{Ar}), 69.9 (6 x OCH_2), 31.8 (6 x CH_2), 29.6 (6 x CH_2), 26.0 (6 x CH_2), 22.8 (6 x CH_2), 14.2 (6 x CH_3).

HRMS (TOF ES+): m/z$[M+H]^+$= 828.6, m/z$[M+Na]^+$= 851.6169 (Calculated: 851.6166), m/z$[M+K]^+$= 867.6.

IR ν_{max}(film)/cm^{-1}: 2923 (m), 2855 (m), 1617 (w), 1516 (m), 1436 (m), 1257 (s), 1170 (s), 837 (m).

2,3,6,7,10,11-Hexamethoxytriphenylene (46)

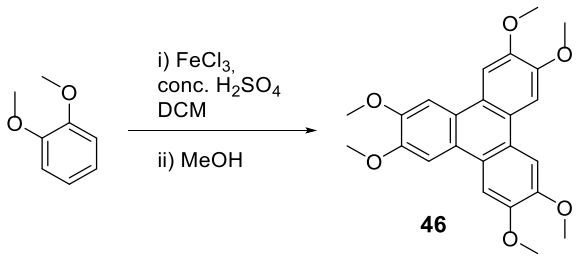

A known compound prepared according to the literature procedure.[92] To a suspension of $FeCl_3$ (36.96 g, 227.85 mmol) and conc. H_2SO_4 (0.5 mL) in CH_2Cl_2 (200 mL) was added dropwise a solution of veratrole (9.4 mL, 73.5 mmol) in CH_2Cl_2 (100 mL). The black mixture was stirred at room temperature for 3 h. The solution was then cooled down to 0 °C and methanol (300 mL) was slowly added. The mixture was further stirred for 0.5 h. The precipitate was filtered, washed with methanol, and dried *in vacuo*. **46** was obtained as a gray solid (7.75 g, 78%) and was used in the next step without further purification.

^{1}H NMR (300 MHz, $CDCl_3$) δ 7.78 (s, 6H, CH_{Ar}), 4.13 (s, 18H, OCH_3).

^{13}C NMR (101 MHz, $CDCl_3$) δ 149.0 (6 x C_{Ar}), 123.4 (6 x C_{Ar}), 104.6 (6 x CH_{Ar}), 56.3 (6 x OCH_3).

HRMS (TOF ES+): m/z$[M+Na]^+$= 431.1741 (Calculated: 431.1471).

m.p.: 312 -316 °C.

IR ν_{max}(film)/cm^{-1}: 1621 (m), 1518 (m),1459 (m), 1261 (m), 1046 (m), 830 (m), 776 (m).

2,3,6,7,10,11-Hexahydroxytriphenylene (47)

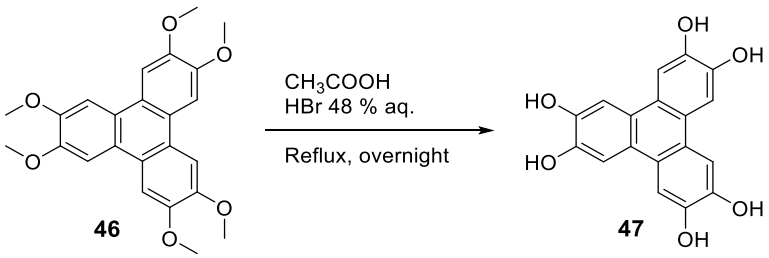

A known compound prepared according to the literature procedure.[210] A solution of **46** (3.00 g, 7.2 mmol) in a mixture of glacial CH_3COOH (100 mL) and 48 wt% aqueous HBr (100 mL) was bubbled with argon for 0.5 h. The grey suspension was stirred at reflux under argon for 12 h. The reaction mixture was then filtered, washed with cold water. The resulting gray solid was recrystallised from a hot CH_3COOH:H_2O solution (3:2, 200 mL) by treating with activated carbon. **47** was afforded as grey crystals (1.12 g, 48%), which were stored under argon.

^{1}H NMR (300 MHz, DMSO-d6) δ 9.31 (s, 6H, OH), 7.59 (s, 6H, CH_{Ar}).

^{13}C NMR (101 MHz, DMSO-d6) δ 145.2 (6 x C_{Ar}), 121.8 (6 x C_{Ar}), 107.7 (6 x CH_{Ar}).

HRMS (TOF ES+): m/z$[M+Na]^+$= 347.0546 (Calculated: 347.0532).

IR ν_{max}(film)/cm^{-1}: 3389 (br), 3273 (br), 1703 (m), 1531 (m), 1447 (m), 1388 (m), 1248 (m), 1138 (m), 997 (m), 791 (m).

Mesylation of ethylene-glycol based aliphatic chains-general procedure

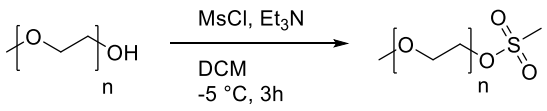

To a solution of the oligoethylene glycol monomethyl ether (1 eq.) and triethylamine in CH_2Cl_2 at -5 °C was added dropwise a solution of mesyl chloride (2.5 eq.) in CH_2Cl_2. After 3h stirring,

the orange solution was washed with water, brine, and dried over $MgSO_4$. The solvent was evaporated *in vacuo*. The resulting orange oil was used in the next step with no further purification.

2,5-Dioxahept-7-yl methanesulfonate (48a)

48a

To a solution of diethylene glycol monomethyl ether (3.1 mL, 25.8 mmol) and triethylamine (15 mL) in DCM (40 mL), a solution of mesyl chloride (5 mL, 64.7 mmol) in DCM (30 mL) was slowly added. **48a** was obtained in a quantitative yield.

^{1}H NMR (300 MHz, $CDCl_3$) δ 4.38-4.32 (m, 2H, OCH_2), 3.78-3.69 (m, 2H, OCH_2), 3.67-3.60 (m, 2H, OCH_2), 3.54-3.47 (m, 2H, OCH_2), 3.34 (s, 3H, OCH_3), 3.04 (s, 3H, $CH_{3\text{-mesyl}}$).

2,5,8-Trioxadec-10-yl methanesulfonate (48b)

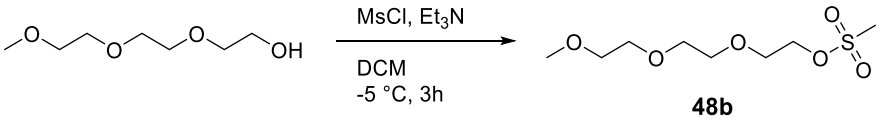

48b

To a solution of triethylene glycol monomethyl ether (2.65 mL, 16.38 mmol) and triethylamine (10 mL) in CH_2Cl_2 (25 mL), a solution of mesyl chloride (3.2 mL) in CH_2Cl_2 (20 mL) was added. **48b** was obtained in a quantitative yield.

^{1}H NMR (300 MHz, $CDCl_3$) δ 4.41-4.36 (m, 2H, OCH_2), 3.80-3.74 (m, 2H, OCH_2), 3.71-3.59 (m, 6H, OCH_2), 3.58-3.51 (m, 2H, OCH_2), 3.38 (s, 3H, OCH_3), 3.08 (s, 3H, $CH_{3\text{-mesyl}}$).

2,5,8,11-Tetraoxatridec-13-yl methanesulfonate (48c)

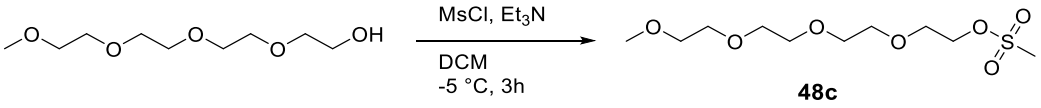

To a solution of tetraethylene glycol monomethyl ether (3.57 mL, 16.92 mmol) and triethylamine (8.7 mL) in CH_2Cl_2 (25 mL), a solution of mesyl chloride (3.2 mL) in CH_2Cl_2 (20 mL) was added. **48c** was obtained in a quantitative yield.

^{1}H NMR (400 MHz, $CDCl_3$) δ 4.40-4.36 (m, 2H, OCH_2), 3.79-3.74 (m, 2H, OCH_2), 3.67-3.63 (m, 10H, OCH_2), 3.57-3.53 (m, 2H, OCH_2), 3.38 (s, 3H, OCH_3), 3.08 (s, 3H, $CH_{3\text{-mesyl}}$).

Alkylation of 47-general procedure

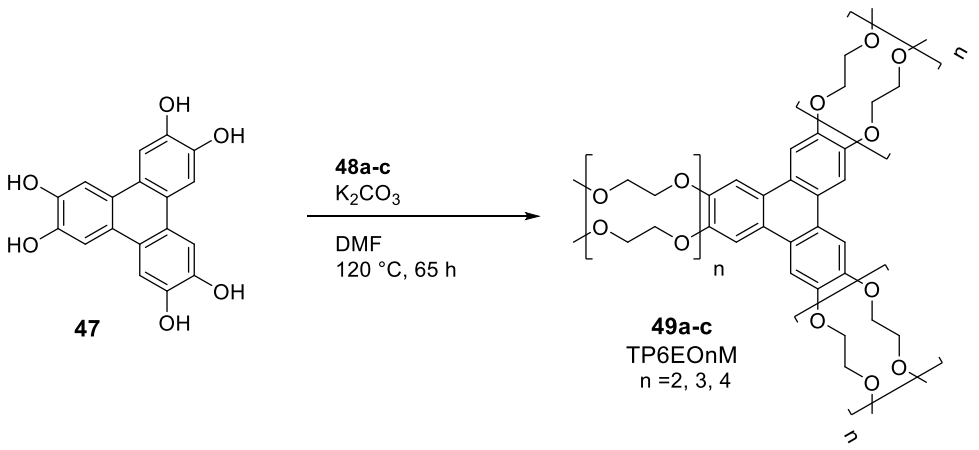

A solution of **47** (1 eq.), K_2CO_3 (15 eq.) and the corresponding mesylated oligoethylene glycol monomethyl ether **49a-c** (12 eq.) in dry DMF was stirred at 120 °C for 65 h under argon. The reaction mixture was evaporated *in vacuo*. Filtration through a pad of silica (eluent: DCM:MeOH = 98:2) followed by evaporation of the solvent afforded a brown oil which was purified by column chromatography and preparative HPLC.

2,3,6,7,10,11-Hexa(1,4,7-trioxaoctyl)triphenylene - TP6EO2M (49a)

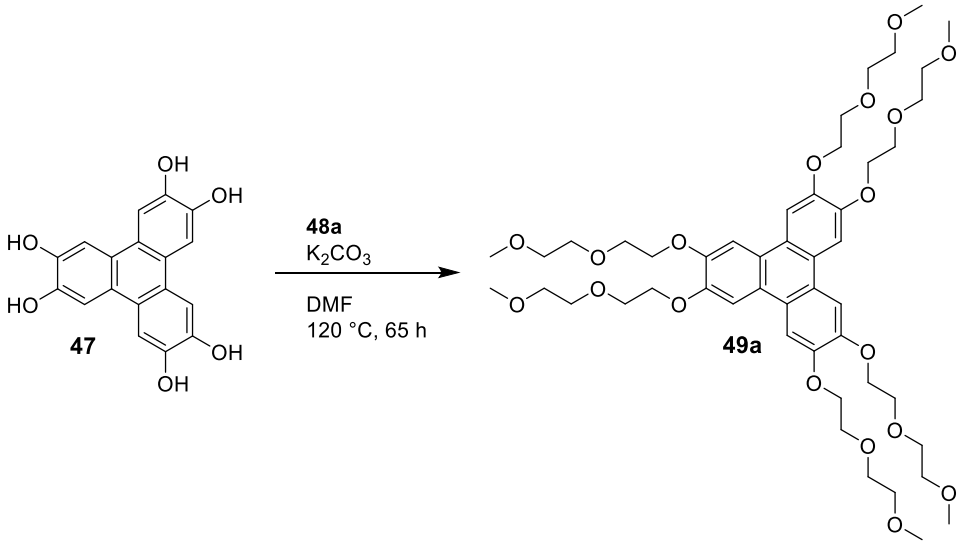

From **47** (700 mg, 2.15 mmol), K_2CO_3 (4.46 g, 32.25 mmol) and freshly prepared **48a** (25.8 mmol) in degassed DMF (100 mL). Purification by column chromatography (SiO_2, neat $CHCl_3$ to $CHCl_3$:MeOH = 95:5) afforded a light brown crystalline solid (604 mg, 30%) which was further purified by preparative HPLC using an isocratic mixture of water and acetonitrile (40vol%) as the eluent system, affording HPLC pure **49a** as a white crystalline solid.

^{1}H NMR (300 MHz, $CDCl_3$) δ 7.87 (s, 6H, CH_{Ar}), 4.41 (t, *J* = 5.1 Hz, 12H, OCH_2), 4.00 (t, *J* = 5.0 Hz, 12H, OCH_2), 3.84-3.76 (m, 12H, OCH_2), 3.65-3.56 (m, 12H, OCH_2), 3.40 (s, 18H, OCH_3).

^{13}C NMR (101 MHz, $CDCl_3$) δ 148.9 (6 x C_{Ar}), 124.1 (6 x C_{Ar}), 108.2 (6 x CH_{Ar}), 72.2 (6 x OCH_2), 71.0 (6 x OCH_2), 70.1 (6 x OCH_2), 69.4 (6 x OCH_2), 59.2 (6 x OCH_3).

HRMS (TOF ES+): m/z $[M+H]^+$= 937.4846 (Calculated: 937.4797). $[M+Na]^+$= 959.4614, $[M+Na]^{2+}$= 491.2.

IR ν_{max}(film)/cm^{-1}: 2926 (m), 2874 (br), 2826 (m), 1618 (w), 1519 (s), 1436 (s), 1262 (s), 1104 (br), 1061 (m), 838 (m).

Analytical HPLC (H_2O:MeOH gradient 0-70% MeOH over 40 min, plateau for 10 min, gradient 70-100% MeOH in 10 min); retention time: 47.9 min

2,3,6,7,10,11-hexa-(1,4,7,10-tetraoxaundecyl)triphenylene - TP6EO3M (49b)

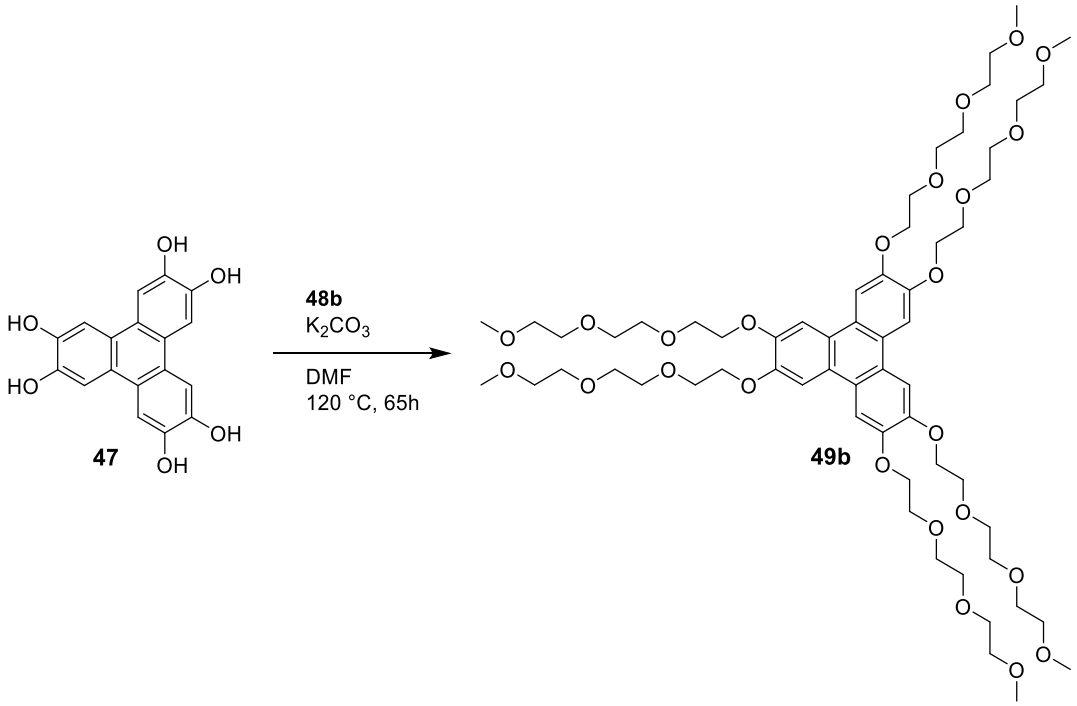

From **47** (457 mg, 1.41 mmol), K_2CO_3 (2.83 g, 20.48 mmol) and freshly prepared **48b** (16.9 mmol) in degassed DMF (65 mL). Purification by column chromatography (SiO_2, ACN:DCM = 9:1 to ACN:MeOH = 98:2) afforded a light brown liquid (593 mg, 35%) which was further purified by preparative HPLC using an isocratic mixture of water and acetonitrile (40 vol%) as the eluent system, affording HPLC pure **49b** as a colourless liquid.

^{1}H NMR (400 MHz, $CDCl_3$) δ 7.85 (s, 6H, CH_{Ar}), 4.38 (t, *J* = 5.0 Hz, 12H, OCH_2), 3.98 (t, *J* = 5.0 Hz, 12H, OCH_2), 3.86-3.75 (m, 12H, OCH_2), 3.73-3.67 (m, 12H, OCH_2), 3.66-3.60 (m, 12H, OCH_2), 3.56-3.48 (m, 12H, OCH_2), 3.34 (s, 18H, OCH_3).

^{13}C NMR (101 MHz, $CDCl_3$) δ 148.8 (6 x C_{Ar}), 124.0 (6 x C_{Ar}), 108.1 (6 x CH_{Ar}), 72.0 (6 x OCH_2), 71.0 (6 x OCH_2), 70.8 (6 x OCH_2), 70.6 (6 x OCH_2), 70.0 (6 x OCH_2), 69.3 (6 x OCH_2), 59.1 (6 x OCH_3).

HRMS (TOF ES+): m/z $[M+H]^+$= 1200.6288 (Calculated : 1200.6292).

IR ν_{max}(neat)/cm^{-1}: 2872 (br), 1615 (w), 1510 (S), 1433 (s), 1262 (s), 1099 (br), 1059 (m), 848 (m).

Analytical HPLC (H_2O:MeOH gradient 0-70% MeOH over 40 min, plateau for 10 min, gradient 70-100% MeOH in 10 min); retention time: 46.9 min.

2,3,6,7,10,11-hexa-(1,4,7,10,13-pentaoxatetradecyl)triphenylene - TP6EO4M (49c)

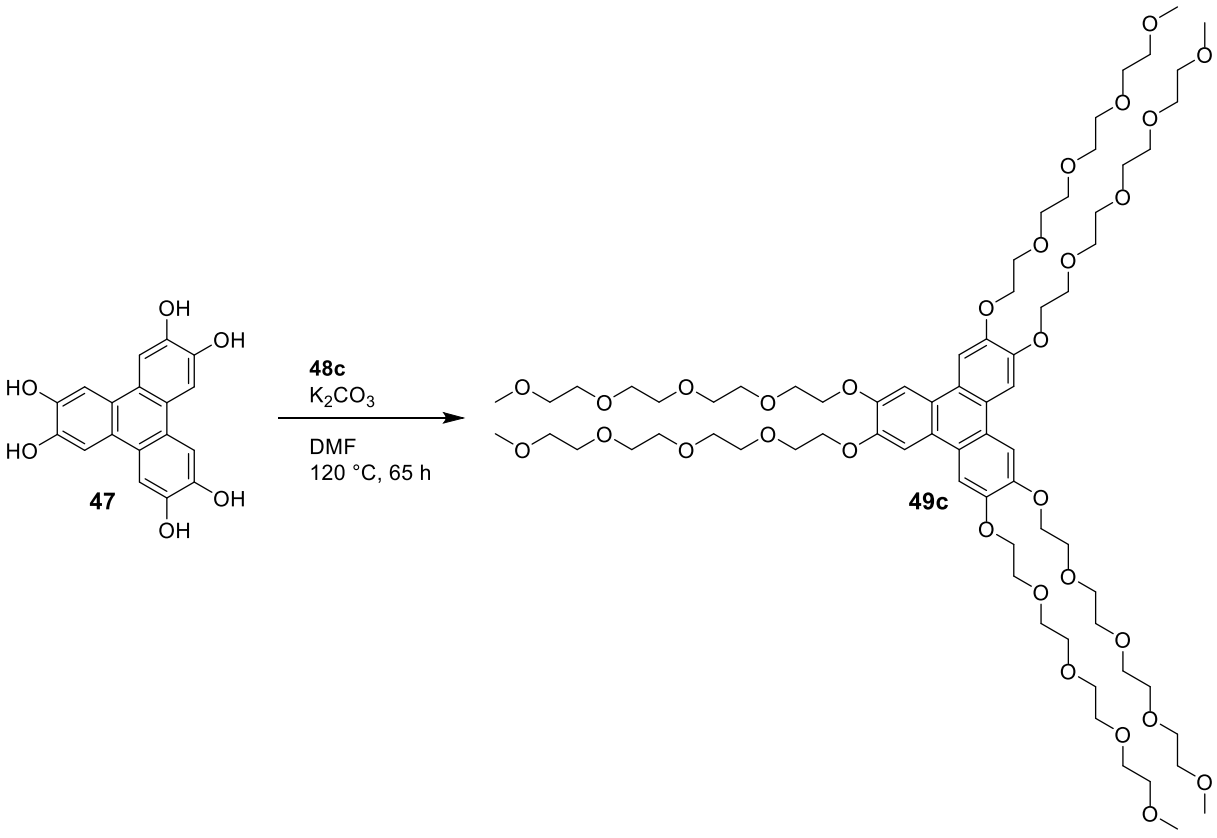

From **47** (457 mg, 1.41 mmol), K_2CO_3 (2.91 g, 21.08 mmol) and freshly prepared **48c** (16.9 mmol) in degassed DMF (65 mL). Purification by column chromatography (SiO_2, neat

ACN to ACN:MeOH = 98:2) afforded a light brown oil (604 mg, 30%) which was further purified by preparative HPLC using an isocratic mixture water and acetonitrile (45vol%) as the eluent system, affording HPLC pure **49c** as a colourless liquid.

^{1}H NMR (400 MHz, $CDCl_3$) δ 7.86 (s, 6H, CH_{Ar}), 4.39 (t, *J* = 5.0 Hz, 12H, OCH_2), 3.99 (t, *J* = 5.0 Hz, 12H, OCH_2), 3.84-3.76 (m, 12H, OCH_2), 3.74-3.58 (m, 48H, OCH_2), 3.56-3.48 (m, 12H, OCH_2), 3.35 (s, 18H, OCH_3).

^{13}C NMR (101 MHz, $CDCl_3$) δ 148.8 (6 x C_{Ar}), 124.0 (6 x C_{Ar}), 108.1 (6 x CH_{Ar}), 72.0 (6 x OCH_2), 71.0 (6 x OCH_2), 70.8 (6 x OCH_2), 70.7 (12 x OCH_2), 70.6 (6 x OCH_2), 70.0 (6 x OCH_2), 69.3 (6 x OCH_2), 59.1 (6 x OCH_3).

MS (TOF ES+): m/z$[M+Na]^+$= 1487.8.

Analytical HPLC (H_2O:MeOH gradient 0-100% MeOH over 40 min); retention time : 34.0 min.

7.3 Experimental procedures and analytical data for chapter three

2,5,8,11-Tetraoxaheptadecane - C6E3M (52)

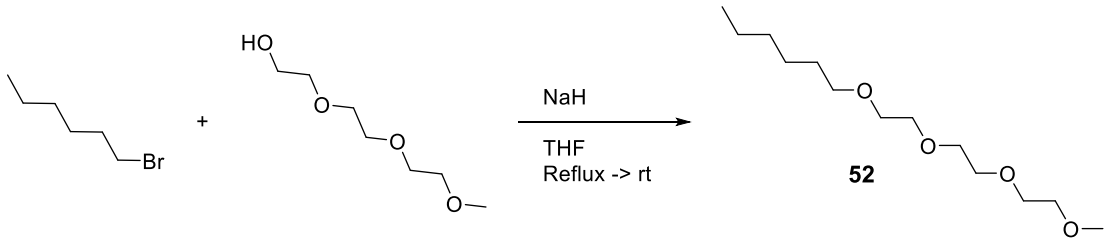

A known compound prepared according to the literature procedure.[117] A solution of sodium hydride (60% in mineral oil, 4.83 g, 121 mmol) in dry THF (100 mL) was stirred at reflux under argon. Triethylene glycol monomethyl ether (9.92 g, 60.4 mmol) was then added slowly and the reaction mixture was further stirred at reflux for 1h under argon. After cooling down to room temperature, 1-bromohexane (12.8 mL, 91 mmol) was added dropwise and stirred at

room temperature overnight under argon. Isopropanol (50 mL) was then added to quenched the residual sodium hydride. Filtration over a pad of Celite (eluent: DCM) followed by evaporation of the solvent *in vacuo* afforded a brown oil which was purified by column chromatography (SiO_2, DCM) to afford **52** as a light yellow oil in a 74% yield (11.920 g).

^{1}H NMR (400 MHz, $CDCl_3$) δ 3.70-3.62 (m, 8H, OCH_2), 3.60-3.53 (m, 4H, OCH_2), 3.44 (t, *J* = 6.8 Hz, 2H, OCH_2), 3.38 (s, 3H, OCH_3), 1.65-1.46 (m, 2H, CH_2), 1.39-1.13 (m, 6H, CH_2), 0.91-0.85 (t, J = 6.9 Hz, 3H, CH_3).

^{13}C NMR (101 MHz, $CDCl_3$) δ 72.0 (OCH_2), 71.6 (OCH_2), 70.6 (3 x OCH_2), 70.5 (OCH_2), 70.1 (OCH_2), 59.1 (OCH_3), 31.7 (CH_2), 29.6 (CH_2), 25.8 (CH_2), 22.6 (CH_2), 14.1 (CH_3).

HRMS (TOF ES+): m/z[M+Na]$^+$= 271.1884 (Calculated: 271.1885).

IR ν_{max}(film)/cm^{-1}: 2926 (m), 2859 (m), 1457 (m), 1351 (w), 1107 (s), 750 (m).

3,3',4,4'-Tetramethoxybiphenyl (57)

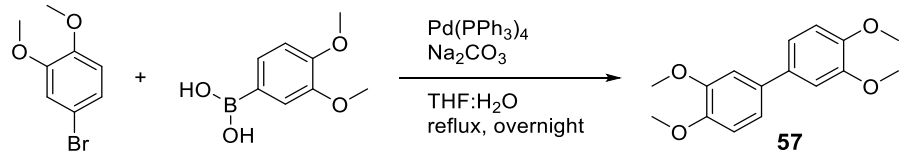

A known compound prepared according to a modified literature procedure.[211] $Pd(PPh_3)_4$ (428 mg, 0.37 mmol, 1 mol%) was dissolved in a mixture of degassed THF (200 mL) and water (90 mL) and the solution was bubbled with argon for 10 min. 4-Bromo-1,2-dimethoxybenzene (8.00 g, 37.04 mmol) and 3,4-dimethoxybenzeneboronic acid (8.09 g, 44.45 mmol) were added and the reaction mixture was stirred at reflux overnight under argon. The solvent was evaporated *in vacuo*, and the crude was recrystallised from MeOH, affording **57** as a light brown solid (8.13 g, 80%)

^{1}H NMR (400 MHz, $CDCl_3$) δ 7.10 (dd, *J* = 8.2, 2.1 Hz, 2H, CH_{Ar}), 7.06 (d, *J* = 2.1 Hz, 2H, CH_{Ar}), 6.93 (d, *J* = 8.3 Hz, 2H, CH_{Ar}), 3.95 (s, 6H, OCH_3), 3.92 (s, 6H, OCH_3).

^{13}C NMR (101 MHz, $CDCl_3$) δ 149.3 (2 x C_{Ar}), 148.5 (2 x C_{Ar}), 134.4 (2 x C_{Ar}), 119.3 (2 x CH_{Ar}), 111.7 (2 x CH_{Ar}), 110.6 (2 x CH_{Ar}), 56.2 (4 x OCH_3).

HRMS (TOF ES+): m/z$[M+H]^+$= 275.1191 (Calculated: 275.1283), m/z$[M+Na]^+$= 297.1, $[2M+Na]^+$= 571.3.

IR ν_{max}(film)/cm^{-1}: 2993 (w), 2932 (br), 2908 (w), 2835 (w), 1602 (w), 1574 (w), 1500 (m), 1441 (m), 1138 (s), 1021 (s), 809 9 (m).

3,3',4,4'-Tetrahydroxybiphenyl (58)

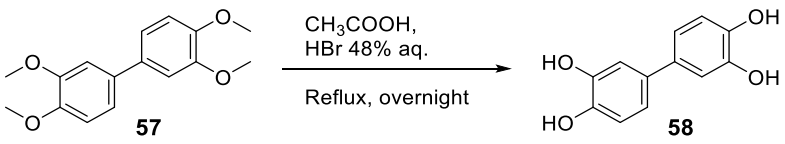

A known compound prepared according to a modified literature procedure.[210] A solution of **57** (4,00 g, 14.58 mmol) in a previously degassed mixture of 48wt% aq. hydrobromic acid (120 mL) and glacial acetic acid (120 mL) was stirred overnight at reflux under argon. The reaction mixture was cooled down to room temperature and extracted with diethyl ether (x5). The combined etherated phases were washed with a saturated solution of $NaHCO_3$, brine, dried over $MgSO_4$ and the solvent was evaporated *in vacuo*. **58** was obtained as a gray powder (3.14 g, 99%) and was used in the next step with no further purification.

^{1}H NMR (400 MHz, DMSO-d_6) δ 8.87 (s, 4H, OH), 6.88 (d, *J* = 1.6 Hz, 2H, CH_{Ar}), 6.80-6.71 (m, 4H, CH_{Ar}).

^{13}C NMR (101 MHz, DMSO-d_6) δ 145.8 (2 x C_{Ar}), 144.7 (2 x C_{Ar}), 132.5 (2 x C_{Ar}), 117.3 (2 x CH_{Ar}), 116.4 (2 x CH_{Ar}), 113.9 (2 x CH_{Ar}).

HRMS (TOF ES+): m/z$[M+H]^+$= 219.0651 (Calculated: 219.0657), m/z$[M+Na]^+$= 241.0.

IR ν_{max}(film)/cm^{-1}: 3404 (br), 1608 (m), 1514 (m), 1112 (m), 850 (n), 804 (m).

3,3',4,4'-Tetrahexyloxybiphenyl (59a)

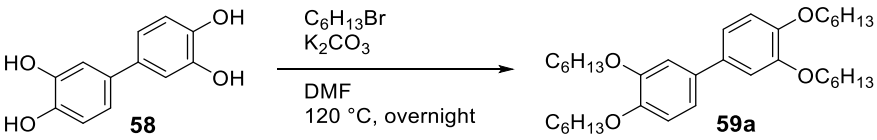

A known compound prepared according to a modified literature procedure.[212] A solution of **58** (3.14 g, 14.39 mmol), potassium carbonate (23.8 g, 172.7 mmol) and 1-bromohexane (16.2 mL, 115.1 mmol) in DMF (8 mL) was stirred overnight at 120 °C. The reaction mixture was cooled down to room temperature, the solvent was evaporated *in vacuo* and the resulting solid was filtered through a pad of silica (eluent: EtOAc). The solvent was evaporated and the product was recrystallised from acetonitrile to afford **59a** as a light brown solid (4.71 g, 59%).

^{1}H NMR (400 MHz, $CDCl_3$) δ 7.10-7.03 (m, 4H, CH_{Ar}), 6.92 (d, *J* = 8.0 Hz, 2H, CH_{Ar}), 4.04 (m, 8H, OCH_2), 1.91-1.77 (m, 8H, CH_2), 1.54-1.43 (m, 8H, CH_2), 1.42-1.28 (m, 16H, CH_2), 0.99-0.84 (m, 12H, CH_3).

^{13}C NMR (101 MHz, $CDCl_3$) δ 149.5 (2 x C_{Ar}), 148.7 (2 x C_{Ar}), 134.5 (2 x C_{Ar}), 119.5 (2 x CH_{Ar}), 114.4 (2 x CH_{Ar}), 113.4 (2 x CH_{Ar}), 69.7 (2 x OCH_2), 69.6 (2 x OCH_2), 31.8 (4 x CH_2), 29.5 (2 x CH_2), 29.5 (2 x CH_2), 25.9 (4 x CH_2), 22.8 (4 x CH_2), 14.2 (4 x CH_3).

HRMS (TOF ES+): m/z $[M+H]^+$= 555.4443 (calculated: 555.44083), $[2M+Na]^+$= 1131.8901.

IR ν_{max}(film)/cm^{-1}: 2952 (m), 2932 (m), 2872 (m), 2859 (m), 1577 (w), 1601 (w), 1509 (s), 1468 (s), 1229 (s), 1142 (s), 793 (s).

3,3',4,4'-Tetrakis(2,5-dioxahept-7-oxy)-biphenyl (59b)

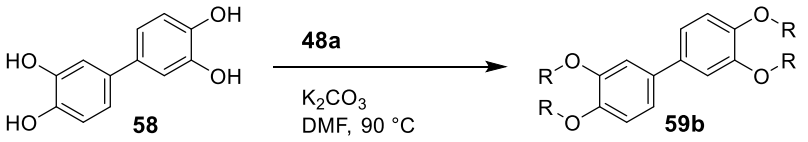

R = $-(CH_2CH_2O)_2CH_3$

A novel compound. A solution of **58** (324 mg, 1.47 mmol), potassium carbonate (813 mg, 5.88 mmol) and **48a** (12 mmol) in DMF (5 mL) was stirred at 90 °C over the weekend. Water was added, and the reaction mixture was extracted with DCM (x3). The combined organic phases were washed with brine, dried over $MgSO_4$ and the solvent was evaporated *in vacuo*. The brown oil was purified by column chromatography (SiO_2, $CHCl_3$:ACN = 9:1) to afford **59b** as a brown oil (145.6 mg, 16%).

^{1}H NMR (400 MHz, $CDCl_3$) δ 7.10 (d, *J* = 2.0 Hz, 2H, CH_{Ar}), 7.07 (dd, *J* = 8.3, 2.1 Hz, 2H, CH_{Ar}), 6.95 (d, *J* = 8.3 Hz, 2H, CH_{Ar}), 4.29-4.16 (m, 8H, OCH_2), 3.93-3.85 (m, *J* = 8.7, 4.3 Hz, 8H, OCH_2), 3.79-3.71 (m, *J* = 5.6, 3.7 Hz, 8H, OCH_2), 3.62-3.53 (m, 8H, OCH_2), 3.40 (s, 6H, OCH_3), 3.38 (s, 6H, OCH_3).

^{13}C NMR (101 MHz, $CDCl_3$) δ 149.2 (2 x C_{Ar}), 148.4 (2 x C_{Ar}), 134.8 (2 x C_{Ar}), 120.1 (2 x CH_{Ar}), 115.2 (2 x CH_{Ar}), 114.0 (2 x CH_{Ar}), 72.2 (4 x OCH_2), 70.9 (4 x OCH_2), 70.0 (2 x OCH_2), 69.9 (2 x OCH_2), 69.3 (2 x OCH_2), 69.2 (2 x OCH_2), 59.2 (4 x OCH_3).

MS (MS ES+): m/z$[M+Na]^+$= 649.3; $[M+Na]^{2+}$= 336.2.

Synthesis of 1-alkoxyphenol - general procedure

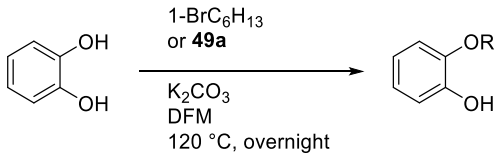

A solution of catechol (1 eq.), K_2CO_3 (1 eq.) and the corresponding 1-bromohexane or **49a** was heated at 90 °C for 24 h under argon. The solvent was removed *in vacuo* and the resulting dough was filtered through a pad of Celite (eluent: DCM). The filtrate was concentrated *in vacuo* and purified by column chromatography.

2-Hexyloxyphenol (60a)

A known compound prepared according to a modified literature procedure.[213] From catechol (5.670 g, 51.5 mmol), K_2CO_3 (14.21 g, 103 mmol) and 1-bromohexane (7.3 mL, 51.5 mmol) in DMF (27 mL). The reaction mixture was stirred overnight at 120 °C. The solvent was evaporated *in vacuo* and the resulting solid was filtered through a pad of silica (eluent: EtOAc). Purification by chromatography (SiO_2, hexane:EtOAc = 20:1) afforded **60a** as a colourless oil (4.652 g, 47%).

^{1}H NMR (400 MHz, $CDCl_3$) δ 6.95-6.90 (m, 1H, CH_{Ar}), 6.88-6.79 (m, 3H, CH_{Ar}), 5.64 (s, 1H, OH), 4.04 (t, *J* = 6.6 Hz, 2H, OCH_2), 1.87-1.76 (m, 2H, CH_2), 1.53-1.29 (m, 6H, CH_2), 0.91 (t, *J* = 7.1 Hz, 3H, CH_3).

^{13}C NMR (101 MHz, $CDCl_3$) δ 146.1 (C_{Ar}), 146.0 (C_{Ar}), 121.4 (CH_{Ar}), 120.2 (CH_{Ar}), 114.6 (CH_{Ar}), 111.8 (CH_{Ar}), 69.1 (OCH_2), 31.7 (CH_2), 29.4 (CH_2), 25.9 (CH_2), 22.7 (CH_2), 14.2 (CH_3).

HRMS (TOF ES+): m/z $[M+H]^+$= 195.1386 (Calculated: 195.1385).

2-(1,4,7-trioxaoctyl)phenol (60b)

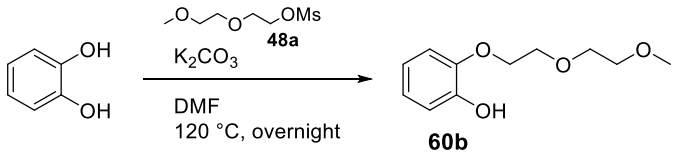

From catechol (3.33 g, 33 mmol), K_2CO_3 (4.55 g, 33 mmol) and **48a** (33 mmol) in DMF (25 mL). Purification by column chromatography (SiO_2, $CHCl_3$:ACN = 8:2) afforded **60b** as a brown oil (621 mg, 8%).

^{1}H NMR (400 MHz, $CDCl_3$) δ 6.97-6.77 (m, 4H), 4.22-4.15 (m, 2H), 3.84-3.79 (m, 2H), 3.76-3.70 (m, 2H), 3.63-3.58 (m, 2H), 3.41 (s, 3H).

^{13}C NMR (101 MHz, $CDCl_3$) δ 147.6 (C_{Ar}), 146.0 (C_{Ar}), 123.2 (CH_{Ar}), 120.1 (CH_{Ar}), 115.8 (CH_{Ar}), 115.7 (CH_{Ar}), 72.0 (OCH_2), 70.7 (OCH_2), 70.3 (OCH_2), 69.7 (OCH_2), 59.2 (OCH_3).

Synthesis of 1-alkoxy-2-isopropoxybenzene - general procedure

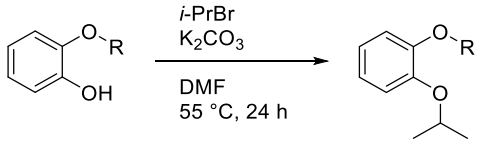

R = $-C_6H_{13}$ or $-(CH_2CH_2O)_2CH_3$

The purified 1-alkylated-2-hydroxybenzene (1 eq.) was reacted with 2-bromopropane (3 eq.) and K_2CO_3 (1 eq.) in DMF at 55 °C for 24 h. Water was added and the reaction mixture was extracted with ethyl acetate (x3). The combined organic phases were washed with water (x2), brine, dried over $MgSO_4$ and the solvent was evaporated *in vacuo*. The crude was purified by column chromatography.

1-Hexyloxy-2-isopropoxybenzene (61a)

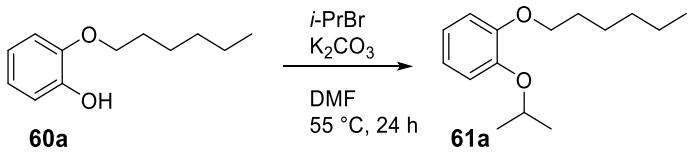

A novel compound. A solution of K_2CO_3 (1.07 g, 7.7 mmol), **60a** (1.5 g, 7.7 mmol), and 2-bromopropane (2.16 mL, 23.2 mmol) in DMF (5.8 mL) was stirred at 55 °C and the reaction was monitored by TLC. After 44 h stirring, 2-bromopropane (0.72 mL, 7.7 mmol) was added and further reacted for 22 h. Water was added and the reaction mixture was extracted with EtOAc (x3). The combined organic phases were washed with brine, dried over $MgSO_4$ and the solvent was evaporated *in vacuo*. Purification by column chromatography (SiO_2, hexane:EtOAc = 20:1) afforded **61a** as a colourless oil (1.240 g, 68%).

^{1}H NMR (400 MHz, $CDCl_3$) δ 6.96-6.83 (m, 4H, CH_{Ar}), 4.46 (hept, *J* = 6.1 Hz, 1H, OC**H**$(CH_3)_2$), 3.98 (t, *J* = 6.6 Hz, 2H, OCH_2), 1.81 (m, 2H, CH_2), 1.58-1.30 (m, 12H, CH_2), 0.91 (t, *J* = 7.1 Hz, 3H, CH_3).

^{13}C NMR (101 MHz, $CDCl_3$) δ 150.9 (C_{Ar}), 148.0 (C_{Ar}), 122.2 (CH_{Ar}), 121.0 (CH_{Ar}), 118.7 (CH_{Ar}), 114.5 (CH_{Ar}), 72.6 (OC**H**$(CH_3)_2$), 69.3 (OCH_2), 31.7 (CH_2), 29.5 (CH_2), 25.9 (CH_2), 22.8 (CH_2), 22.4 (2 x OCH(**C**$H_3)_2$), 14.2 (CH_3).

HRMS(TOF ES+): $[M+H]^+$= 236.1778 (Calculated: 236.1776).

IR ν_{max}(film)/cm^{-1}: 2958 (w), 2930 (br), 2863 (br), 1592 (w), 1497 (m), 1252 (m), 741 (m).

1-(2,5-dioxahept-7-oxy)-2-isopropoxybenzene (61b) - from 60b

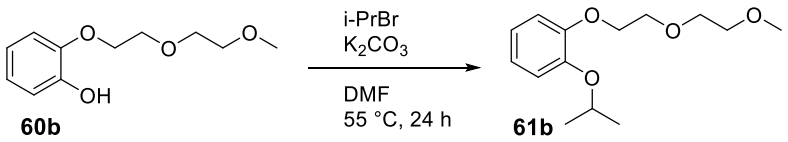

From **60b** (621 mg, 2.93 mmol), K_2CO_3 (405 mg, 2.93 mmol) and 2-bromopropane (1.07 g, 8.78 mmol) in DMF (2 mL). Purification by column chromatography (SiO_2, $CHCl_3$:ACN = 9:1) afforded **61b** as a brown oil (328 mg, 45%).

^{1}H NMR (400 MHz, $CDCl_3$) δ 6.96-6.85 (m, 4H, CH_{Ar}), 4.48 (hept, *J* = 6.1 Hz, 1H, OC**H**$(CH_3)_2$), 4.19-4.13 (m, 2H, OCH_2), 3.91-3.84 (m, 2H, OCH_2), 3.79-3.71 (m, 2H, OCH_2), 3.61-3.52 (m, 2H, OCH_2), 3.39 (s, 3H, OCH_3), 1.33 (s, 3H, OCH(C**H**$_3)_2$), 1.32 (s, 3H, OCH(C**H**$_3)_2$).

^{13}C NMR (101 MHz, $CDCl_3$) δ 150.3 (C_{Ar}), 148.2 (C_{Ar}), 121.9 (CH_{Ar}), 121.7 (CH_{Ar}), 118.1 (CH_{Ar}), 115.3 (CH_{Ar}), 72.2 (O**C**H$(CH_3)_2$), 72.1 (OCH_2), 70.9 (OCH_2), 69.9 (OCH_2), 69.0 (OCH_2), 59.2 (OCH_3), 22.4 (2 x OCH(**C**H$_3)_2$).

HRMS (MS ES+): m/z$[M+Na]^+$= 277.1411 (Calculated: 277.1416).

IR ν_{max}(film)/cm^{-1}: 2975 (w), 2927 (w), 2821 (w), 1592 (w), 1497 (m), 1253 (m), 11106 (m), 742 (m).

1-(2,5-dioxahept-7-oxy)-2-isopropoxybenzene (61b) - One pot synthesis

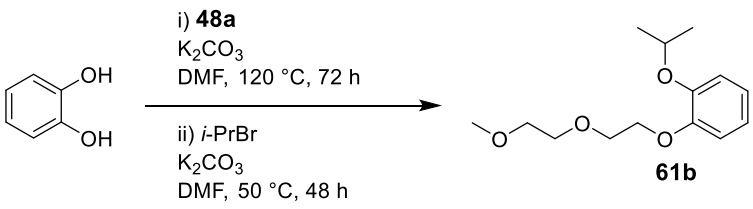

A novel compound. A solution of catechol (2.163 g, 19.66 mmol), potassium carbonate (2.717 g, 19.66 mmol) and **48a** (24 mmol) in DMF (5 mL) was stirred at reflux for 3 days. The

reaction mixture was cooled down to room temperature and filtered through a pad of silica (eluent: EtOAc). The solvent was evaporated *in vacuo* and the crude was further reacted with 2-bromopropane (7.3 mL, 78.64 mmol) in DMF (1 mL) at 50 °C for 2 days. Filtration of the reaction mixture through a pad of silica (eluent: EtOAc) followed by purification by column chromatography (SiO_2, $CHCl_3$:ACN = 9:1) afforded **61b** as a brown oil (1.1088 g, 22%).

2-Hydroxy-3,6,7,10,11-pentahexyloxytriphenylene (62) - biphenyl-phenyl coupling

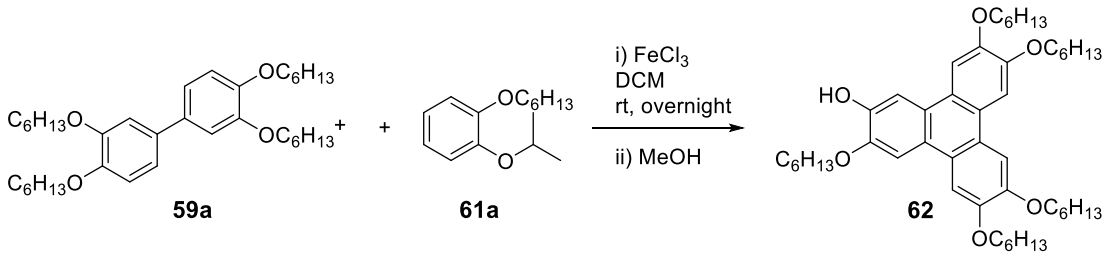

A known compound prepared according to a modified literature procedure.[214] To a solution of **61a** (670 mg, 2.84 mmol) and **59a** (943 mg, 1.70 mmol) in DCM (6 mL), $FeCl_3$ (1.38 g, 8.50 mmol) was slowly added. The dark blue solution was stirred overnight at room temperature. The mixture was then poured into cold methanol (40 mL) and stirred for 0.5 h. The solution was filtered and the gray precipitate was washed with cold methanol. Purification by column chromatography (SiO_2, petroleum ether:DCM = 7:3 to 4:6), followed by recrystallisation from ethanol afforded **62** as white crystals (360.8 mg, 48%).

^{1}H NMR (400 MHz, $CDCl_3$) δ 7.96 (s, 1H, CH_{Ar}), 7.86-7.80 (m, 4H, CH_{Ar}), 7.77 (s, 1H, CH_{Ar}), 5.91 (s, 1H, OH), 4.29 (t, *J* = 6.4 Hz, 2H, OCH_2), 4.26-4.17 (m, 8H, OCH_2), 2.03-1.87 (m, 10H, CH_2), 1.57 (m, 10H, CH_2), 1.49-1.29 (m, 20H, CH_2), 1.01-0.83 (m, 15H, CH_3).

^{13}C NMR (101 MHz, $CDCl_3$) δ 149.3 (C_{Ar}), 149.2 (C_{Ar}), 149.0 (C_{Ar}), 148.9 (C_{Ar}), 146.0 (C_{Ar}), 145.4 (C_{Ar}), 124.1 (C_{Ar}), 123.8 (C_{Ar}), 123.8 (C_{Ar}), 123.7 (C_{Ar}), 123.4 (C_{Ar}), 123.1 (C_{Ar}), 107.9 (CH_{Ar}), 107.7 (CH_{Ar}), 107.5 (CH_{Ar}), 106.7 (CH_{Ar}), 104.5 (CH_{Ar}), 70.1 (OCH_2), 70.0 (OCH_2), 69.8 (OCH_2), 69.3

(OCH_2), 31.8 (CH_2), 31.8 (CH_2), 31.8 (CH_2), 29.6 (CH_2), 29.6 (CH_2), 29.5 (CH_2), 29.4 (CH_2), 26.0 (CH_2), 26.0 (CH_2), 22.8 (CH_2), 14.20 (5 CH_3). The carbons could not be attributed due to overlapping peaks.

HRMS (TOF ES+): m/z $[M+H]^+$= 745.5410 (Calculated: 745.5407), $[M+Na]^+$= 767.7.

IR ν_{max}(film)/cm^{-1}: 3551 (w), 2951 (m), 2924 (m), 2856 (m), 1617 (m), 1514 (m), 1436 (s), 1257 (s), 835 (m).

1,2-di(2,5-dioxahept-7-oxy)benzene (67)

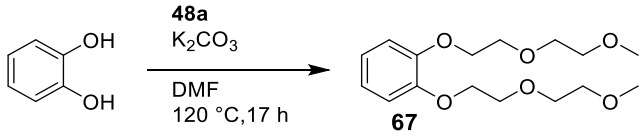

67

A solution of catechol (1.750 g, 15.90 mmol), K_2CO_3 (8.790 g, 63.60 mmol) and **48a** (95.4 mmol) in DMF (90 mL) was stirred at 120 °C for 17 h. The solvent was evaporated *in vacuo* and the resulting dark brown oil was filtered through a pad of silica (eluent = DCM:MeOH). The filtrate was concentrated *in vacuo* and purified by column chromatography (SiO_2 conditioned with Et_3N, $CHCl_3$:ACN = 6:4). **67** was afforded as a light brown oil (667 mg, 13 %).

^{1}H NMR (400 MHz, $CDCl_3$) δ 6.94-6.88 (m, 4H, CH_{Ar}), 4.20-4.15 (m, 4H, OCH_2), 3.89-3.85 (m, 4H, OCH_2), 3.76-3.71 (m, 4H, OCH_2), 3.60-3.54 (m, 4H, OCH_2), 3.39 (s, 6H, OCH_3).

^{13}C NMR (101 MHz, $CDCl_3$) δ 149.2 (2 x C_{Ar}), 121.8 (2 x CH_{Ar}), 115.1 (2 x CH_{Ar}), 72.2 (2 x OCH_2), 70.9 (2 x OCH_2), 70.0 (2 x OCH_2), 69.0 (2 x OCH_2), 59.2 (2 x OCH_3).

HRMS (TOF ES+): m/z $[M+Na]^+$= 337.1639 (Calculated : 337.1627).

IR ν_{max}(film)/cm^{-1}: 2875 (br), 1501 (m), 1254 (m), 1105 (s), 743 (m).

2,5-Dioxahept-7-yl-4-methylbenzenesulfonate (68)

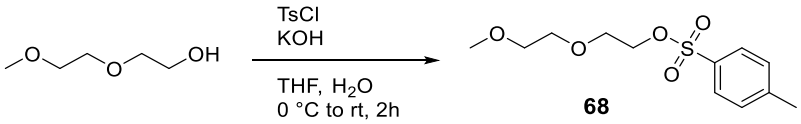

To a solution of diethylene glycol monomethyl ether (11.61 g, 96.6 mmol) in THF (40 mL) at 0 °C was added a solution of potassium hydroxide (9.660 g, 214.5 mmol) in water (40 mL). A solution of tosyl chloride (27.63 g, 144.9 mmol) in THF (40 mL) was then added dropwise and stirred for 1 h at 0 °C. The reaction mixture was brought back to room temperature and further stirred for 1 h. Diethyl ether was added and the solution was washed with a 1 M aq. solution of potassium hydroxide, water and brine, dried over $MgSO_4$ and the solvent was evaporated *in vacuo*. The resulting oil was used in the next step with no further purification.

Ethyl 3,4,5-trisubstituted benzoate - general procedure

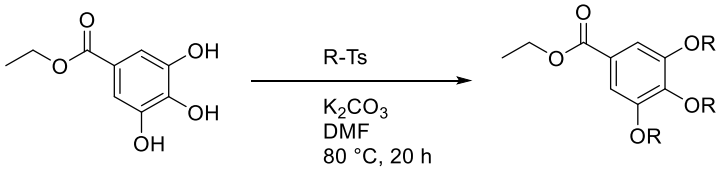

Known compounds prepared according to the literature procedure.[133] A solution of ethyl gallate (1 eq.), K_2CO_3 (10 eq.) and the corresponding 1-tosyl (4.5 eq) or 1-bromo (6 eq.) derivative in degassed DMF was stirred at 80 °C for 20 h under argon. The solvent was then removed *in vacuo* and the crude filtered through a pad of Celite. DCM was added and the organic phase was washed with a 1 M solution of HCl, brine and dried over $MgSO_4$. The solvent was evaporated *in vacuo* and the resulting yellow oil was purified by column chromatography.

Ethyl 3,4,5-tris(1,4,7-trioxaoctyl) benzoate (69a)

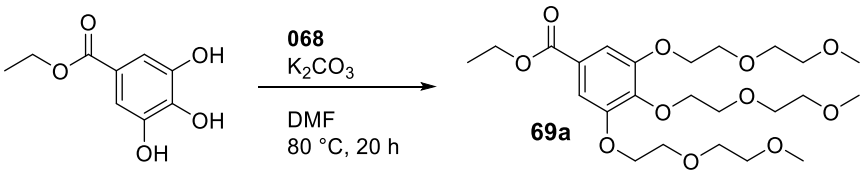

A known compound prepared according to the literature procedure.[133] From ethyl gallate (293 mg, 1.61 mmol), K_2CO_3 (2.23 g, 16.1 mmol) and the freshly prepared **68** (7.25 mmol) in degassed DMF (10 mL). The resulting yellow oil was purified by column chromatography (SiO_2, DCM:MeOH = 97:3) to afford **69a** as a colourless viscous oil (486 mg, 49%).

^{1}H NMR (400 MHz, $CDCl_3$) δ 7.28 (s, 2H, CH_{Ar}), 4.33 (q, J = 7.1 Hz, 2H, $COOCH_2$), 4.26-4.17 (m, 6H, CH_2), 3.89-3.84 (m, 4H, CH_2), 3.82-3.78 (m, 2H, CH_2), 3.74-3.68 (m, 6H, CH_2), 3.58-3.50 (m, 6H, CH_2), 3.37 (s, 6H, CH_2), 3.36 (s, 3H, CH_3), 1.36 (t, J = 7.1 Hz, 3H, $COOCH_2C\mathbf{H_3}$).

^{13}C NMR (101 MHz, $CDCl_3$) δ 166.2 (C=O), 152.4 (2 x C_{Ar}), 142.6 (C_{Ar}), 125.5 (C_{Ar}) 109.1 (2 x CH_{Ar}), 72.6 (OCH_2), 72.2 (OCH_2), 72.1 (2 x OCH_2), 70.9 (2 x OCH_2), 70.7 (OCH_2), 70.6 (OCH_2), 69.8 (2 x OCH_2), 69.0 (2 x OCH_2), 61.1 ($COOCH_2$), 59.2 (2 x CH_3), 59.1 (CH_3), 14.5 ($COOCH_2\mathbf{C}H_3$).

HRMS (TOF ES+): m/z $[M+Na]^+$= 527.2479 (Calculated: 527.2468), $[M+K]^+$=543.5.

IR ν_{max}(film)/cm^{-1}: 3429 (br), 2875 (br,w), 1714 (w), 1666 (w), 1100 (br, s).

Ethyl 3,4,5 tris(hexahexyloxy)benzoate (69b)

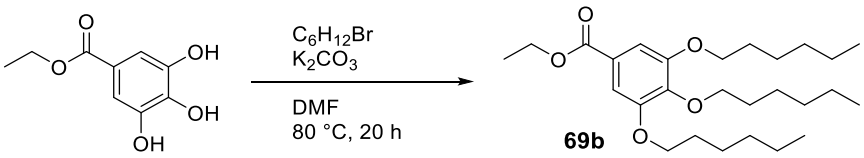

A known compound prepared according to the literature procedure.[133] From ethyl gallate (607 mg, 3.33 mmol), K_2CO_3 (2.76 g, 20 mmol) and 1-bromohexane (2.8 mL, 20 mmol) in

degassed DMF (20 mL). The resulting yellow waxy solid was purified by column chromatography (SiO_2, hexane:EtOAc= 95:5) to afford **69b** as a light yellow oil (1.2065 g, 80%).

^{1}H NMR (400 MHz, $CDCl_3$) δ 7.25 (s, 2H, CH_{Ar}), 4.35 (q, *J* = 7.1 Hz, 2H, $COOCH_2$), 4.01 (t, *J* = 6.5 Hz, 6H, OCH_2), 1.87-1.68 (m, 6H, CH_2), 1.53-1.42 (m, 6H, CH_2), 1.43-1.27 (m, 15H, $COOCH_2CH_3$ + CH_2), 0.99-0.85 (m, 9H, CH_3).

^{13}C NMR (101 MHz, $CDCl_3$) δ 166.6 (C=O), 152.9 (2 x C_{Ar}), 142.5 (C_{Ar}), 125.2 (C_{Ar}), 108.1 (2 x CH_{Ar}), 73.6 (OCH_2), 69.3 (2 x OCH_2), 61.1 ($COO\mathbf{C}H_2CH_3$), 31.9 (CH_2), 31.7 (2 x CH_2), 30.4 (CH_2), 29.4 (2 x CH_2), 25.9 (2 x CH_2), 25.9 (CH_2), 22.8 (CH_2), 22.8 (2 x CH_2), 14.6 ($COOCH_2\mathbf{C}H_3$), 14.2 (CH_3), 14.2 (2 x CH_3).

HRMS (TOF ES+): m/z $[M+H]^+$= 451.3418 (Calculated: 451.3423).

IR ν_{max}(film)/cm^{-1}: 2954 (m), 2930 (m), 2860 (m), 1717 (s), 1586 (m), 1500 (m), 1466 (m), 1429 (s), 1331 (s), 1213 (s), 1108 (s), 1032 (m), 765 (m).

3,4,5-Tris(1,4,7-trioxaoctyl) benzoic acid (70a)

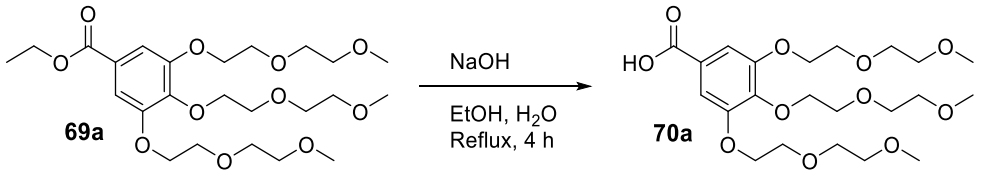

A known compound prepared according to the literature procedure.[133] To a solution of **69a** (486.9 mg, 0.78 mmol) in ethanol (6 mL) was added a solution of NaOH (53 mg, 1.325 mmol) in water (0.4 mL). The reaction mixture was stirred at reflux for 4 h. A 1 M aq. HCl solution was added and the reaction mixture was extracted with DCM (x3). The combined organic phases were washed with brine and dried over $MgSO_4$. Evaporation of the solvent *in vacuo* afforded **70a** as a light yellow oil (370 mg, quantitative yield).

^{1}H NMR (400 MHz, $CDCl_3$) δ 7.34 (s, 2H, CH_{Ar}), 4.26 (m, 2H, OCH_2), 4.23-4.17 (m, 4H, OCH_2), 3.90-3.85 (m, 4H, CH_2), 3.82 (m, 2H, CH_2), 3.75-3.68 (m, 6H, CH_2), 3.59-3.51 (m, 6H, CH_2), 3.38 (s, 6H, OCH_3), 3.37 (s, 3H, OCH_3).

^{13}C NMR (101 MHz, $CDCl_3$) δ 170.4 (C=O), 152.4 (2 x C_{Ar}), 143.3 (C_{Ar}), 124.3 (C_{Ar}), 109.6 (2 x CH_{Ar}), 72.7 (OCH_2), 72.2 (OCH_2), 72.1 (2 x OCH_2), 70.9 (2 x OCH_2), 70.7 (OCH_2), 70.6 (OCH_2), 69.8 (2 x OCH_2), 69.0 (2 x OCH_2), 59.2 (2 x OCH_3), 59.1 (OCH_3).

HRMS (TOF ES+): m/z $[M+Na]^+$= 499.2164 (Calculated: 499.2155).

IR ν_{max}(film)/cm^{-1}: 2926 (w), 2877 (br), 2823 (w), 1715 (m), 1586 (m), 1429 (m), 1200 (m), 1101 (s), 727 (m).

3,4,5-Trisubstituted benzyl alcohol - general procedure

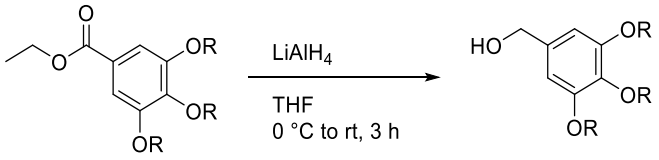

Known compounds prepared according to the literature procedure.[133] To a stirred suspension of $LiAlH_4$ (1.3 eq.) in dry THF was added a solution of the corresponding ethyl 3,4,5-trisubstituted benzoate (1 eq.) in dry THF at 0 °C under argon. The mixture was brought back to room temperature, stirred for 3 h and was then quenched by successive addition of isopropyl alcohol, cold water and a 30% aq. solution of sodium hydroxide. After filtration of the crude through a pad of Celite (eluent: EtOAc), the filtrate was washed with brine, dried over $MgSO_4$, and the solvent was evaporated *in vacuo*. The resulting benzyl alcohol was used in the next step with no further purification.

3,4,5-Tris(1,4,7-trioxaoctyl) benzyl alcohol (71a)

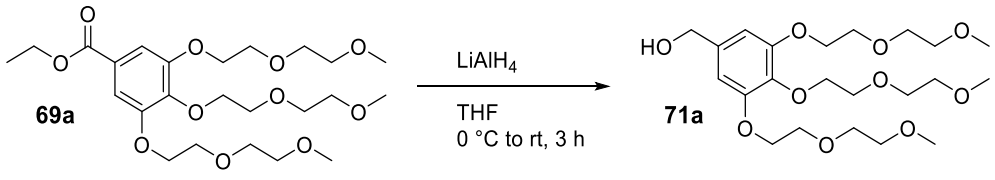

From a stirred suspension of $LiAlH_4$ (200 mg, 5.15 mmol) in dry THF (4 mL) and a solution of **69a** (2.00 g, 3.96 mmol) in dry THF (8 mL). The reaction mixture was quenched by successive addition of isopropyl alcohol (1 mL), cold water (3 mL) and a 30% aq. solution of sodium hydroxide (1 mL). **71a** was afforded as a light yellow oil (1.137 g, 62%).

^{1}H NMR (400 MHz, $CDCl_3$) δ 6.61 (s, 2H, CH_{Ar}), 4.57 (s, 2H, CH_2OH), 4.20-4.11 (m, 6H, OCH_2), 3.86-3.83 (m, 4H, CH_2), 3.82-3.77 (m, 2H, CH_2), 3.74-3.68 (m, 6H, CH_2), 3.58-3.53 (m, 6H, CH_2), 3.37 (s, 9H, OCH_3).

^{13}C NMR (101 MHz, $CDCl_3$) δ 152.9 (2 x C_{Ar}), 137.9 (C_{Ar}), 136.7 (C_{Ar}), 106.6 (CH_{Ar}), 72.5 (OCH_2), 72.2 (OCH_2), 72.1 (2 x OCH_2), 70.8 (2 x OCH_2), 70.7 (OCH_2), 70.6 (OCH_2), 70.0 (2 x OCH_2), 69.0 (2 x OCH_2), 65.5 (CH_2OH), 59.2 (3 x OCH_3).

HRMS (TOF ES+): m/z $[M+Na]^+$= 485.2368 (Calculated: 485.2363).

IR ν_{max}(film)/cm^{-1}: 3453 (br), 2926 (w), 2874 (br), 2823 (w), 1589 (w), 1435 (m), 1299 (w), 1101 (br, s).

3,4,5-Tris(hexahexyloxy)benzyl alcohol (71b)

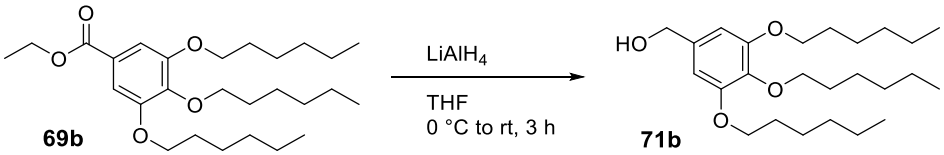

From a stirred suspension of $LiAlH_4$ (110 mg, 2.89 mmol) in dry THF (2 mL) and a solution of **69b** (1.00 g, 2.22 mmol) in dry THF (4 mL). The reaction mixture was quenched by successive addition of isopropyl alcohol (1 mL), cold water (3 mL) and a 30% aq. solution of sodium hydroxide (1 mL). **71b** was obtained as a light yellow solid (746 mg, 82%).

^{1}H NMR (400 MHz, $CDCl_3$) δ 6.55 (s, 2H, CH_{Ar}), 4.59 (s, 2H, C**H**$_2$OH), 4.00-3.90 (m, 6H, OCH_2), 1.84-1.69 (m, 6H, CH_2), 1.52-1.41 (m, 6H, CH_2), 1.38-1.28 (m, 12H, CH_2), 0.93-0.87 (m, 9H, CH_3).

^{13}C NMR (101 MHz, $CDCl_3$) δ 153.4 (2 x C_{Ar}), 137.7 (C_{Ar}), 136.2 (C_{Ar}), 105.5 (2 x CH_{Ar}), 73.6 (OCH_2), 69.3 (2 x OCH_2), 65.8 (CH_2OH), 31.9 (CH_2), 31.7 (2 x CH_2), 30.4 (CH_2), 29.5 (2 x CH_2), 25.9 (3 x CH_2), 22.8 (CH_2), 22.8 (2 x CH_2), 14.2 (CH_3), 14.2 (2 x CH_3).

HRMS (TOF ES+): m/z $[M+Na]^+$= 431.3138 (Calculated: 431.3137).

IR ν_{max}(film)/cm^{-1}: 3307 (br, w), 2956 (m), 2930 (m), 2873 (m), 2858 (m), 1590 (m), 1505 (m), 1437 (s), 1391 (m), 1333 (m), 1224 (m), 1127 (s), 1110 (s), 1012 (m), 811 (m).

3,4,5-Tris(1,4,7-trioxaoctyl) benzyl chloride (72)

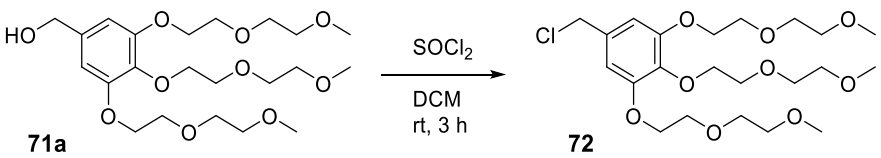

A known compound prepared according to the literature procedure.[133] To a solution of **71a** (200 mg, 0.43 mmol) in dry DCM (25 mL) at room temperature was added dropwise a solution

of $SOCl_2$ (320 µL, 4.3 mmol) in dry DCM (10 mL). The solution was stirred at room temperature for 3 h. The solvent was evaporated *in vacuo*, affording **72** in a quantitative yield.

^{1}H NMR (400 MHz, $CDCl_3$) δ 6.62 (s, 2H, CH_{Ar}), 4.48 (s, 2H, CH_2Cl), 4.21-4.12 (m, 6H, OCH_2), 3.89-3.83 (m, 4H, CH_2), 3.82-3.77 (m, 2H, CH_2), 3.74-3.69 (m, 6H, CH_2), 3.60-3.52 (m, 6H, CH_2), 3.38 (s, 6H, CH_3), 3.37 (s, 3H, CH_3).

^{13}C NMR (101 MHz, $CDCl_3$) δ 152.8 (2 x C_{Ar}), 138.7 (C_{Ar}), 132.9 (C_{Ar}), 108.4 (2 x CH_{Ar}), 72.5 (OCH_2), 72.2 (OCH_2), 72.2 (2 x OCH_2), 70.9 (2 x OCH_2), 70.7 (OCH_2), 70.6 (OCH_2), 69.9 (2 x OCH_2), 69.1 (2 x OCH_2), 59.2 (3 x OCH_3), 46.7 (CH_2Cl).

HRMS (TOF ES+): m/z $[M+Na]^+$= 503.2005 (Calculated: 503.2024).

IR ν_{max}(film)/cm^{-1}: 2925 (w), 2876 (br), 2823 (w), 1591 (m), 1504 (w), 1437 (m), 1333 (m), 1101 (s).

2-(6-Bromohexyloxy)-3,6,7,10,11-pentahexyloxytriphenylene (73)

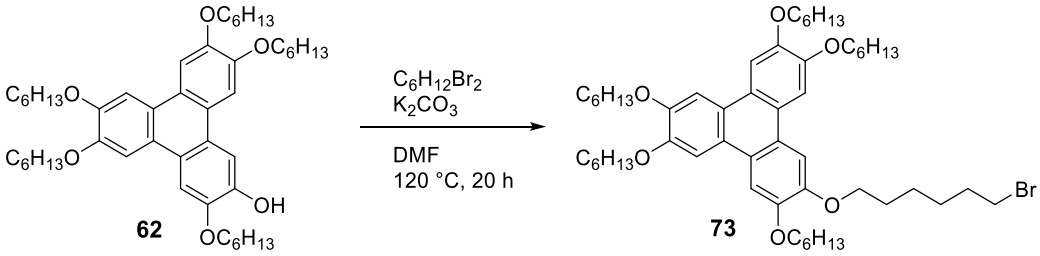

A known compound prepared according to a modified literature procedure.[215] A solution of **62** (192 mg, 0.27 mmo), K_2CO_3 (75 mg, 0.54 mmol) and 1,6-dibromohexane (200 µL, 1.34 mmol) in degassed DMF (1 mL) was stirred at 120 °C for 20 h under argon. DMF was then evaporated *in vacuo* and the resulting dough was filtrated through a pad of Celite (eluent: DCM). The solvent was evaporated *in vacuo* and the resulting solid was recrystallised from ethanol to afford **73** as an off-white solid (140.3 mg, 57%).

^{1}H NMR (400 MHz, $CDCl_3$) δ 7.83 (s, 6H, CH_{Ar}), 4.23 (t, J = 6.6 Hz, 12H, OCH_2), 3.45 (t, J = 6.8 Hz, 2H, CH_2Br), 2.00-1.86 (m, 14H, CH_2), 1.68-1.50 (m, 14H, CH_2), 1.49-1.30 (m, 20H, CH_2), 1.00-0.87 (m, 15H, CH_3).

^{13}C NMR (101 MHz, $CDCl_3$) δ 149.2 (C_{Ar}), 123.7 (C_{Ar}), 107.5 (CH_{Ar}), 69.8 (OCH_2), 33.9 (CH_2Br), 32.9 (CH_2), 31.8 (CH_2), 29.6 (CH_2), 29.5 (CH_2), 28.1 (CH_2), 26.0 (CH_2), 25.6 (CH_2), 22.8 (CH_2), 14.2 (CH_3). The carbons could not be attributed due to overlapping peaks.

HRMS (TOF ES+): m/z $[M+H]^+$= 909.5374 (Calculated: 909.5373).

2-(6-(3-Hydroxyphenyloxy)hexyloxy)-3,6,7,10,11-pentahexyloxytriphenylene (77)

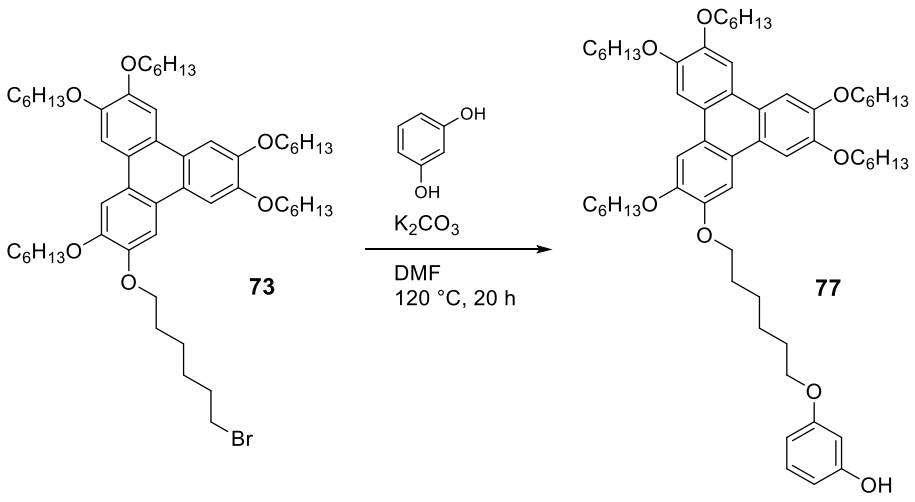

A novel compound. A solution of **73** (246.1 mg, 0.27 mmol), resorcinol (149 mg, 1.35 mmol) and K_2CO_3 (75 mg, 0.54 mmol) in DMF (4 mL) was stirred at 120 °C and the reaction monitored by TLC (hexane:DCM = 3:6). After 20 h stirring, the reaction mixture was cooled down to room temperature and acidified with a 1 M aq. HCl solution. The solution was extracted with EtOAc (x3). The combined organic phases were washed with brine, dried over $MgSO_4$ and the solvent was evaporated *in vacuo*. The crude orange solid was purified by column chromatography (SiO_2, DCM). **77** was obtained as a white solid (105.9 mg, 42%).

^{1}H NMR (400 MHz, $CDCl_3$) δ 7.84 (s, 6H, $CH_{Ar\text{-}triphenylene}$), 7.10 (t, J = 8.4 Hz, 1H, $CH_{Ar\text{-}resorsinol}$), 6.50-6.44 (m, 1H, $CH_{Ar\text{-}resorcinol}$), 6.43-6.37 (m, 2H, $CH_{Ar\text{-}resorcinol}$), 4.99 (s, 1H, OH), 4.23 (t, J = 6.6 Hz, 12H, OCH_2), 3.95 (t, J = 6.4 Hz, 2H, OCH_2), 2.02-1.88 (m, 12H, CH_2), 1.88-1.77 (m, 2H, CH_2), 1.67-1.51 (m, 14H, CH_2), 1.47-1.32 (m, 20H, CH_2), 1.01-0.86 (m, 15H, CH_3).

^{13}C NMR (101 MHz, $CDCl_3$) δ 160.6 (C_{Ar}), 156.9 (C_{Ar}), 149.2 (C_{Ar}), 149.1 (C_{Ar}), 149.1 (C_{Ar}), 149.1 (C_{Ar}), 130.2 ($CH_{Ar\text{-}resorcinol}$), 123.9 ($C_{Ar}$), 123.9 ($C_{Ar}$), 123.8 ($C_{Ar}$), 107.8 ($CH_{Ar\text{-}resorcinol}$), 107.6 ($CH_{Ar\text{-}triphenylene}$), 107.1 ($CH_{Ar\text{-}resorcinol}$), 102.2 ($CH_{Ar\text{-}resorcinol}$), 69.9 ($OCH_2$), 68.0 ($OCH_2$), 31.8 ($CH_2$), 29.6 ($CH_2$), 29.3 ($CH_2$), 26.1 ($CH_2$), 26.0 ($CH_2$), 14.2 ($CH_3$). The carbons could not be attributed due to overlapping peaks.

HRMS (TOF ES+): m/z [M]= 936.6451 (Calculated: 936.6479).

IR ν_{max}(film)/cm^{-1}: 3467 (m), 2926 (m), 2857 (m), 1615 (m), 1508 (m), 1433 (s), 1255 (s), 1165 (s), 1148 (s), 1037 (s), 838 (m).

TP6Gall (78)

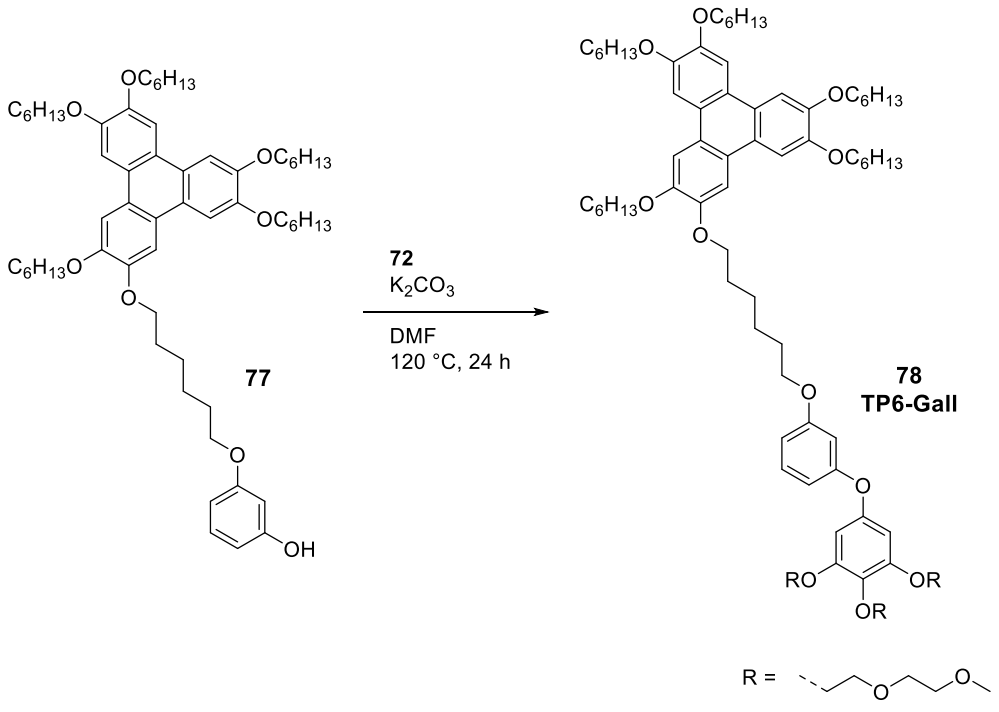

A novel compound. A solution of **72** (163 mg, 0.339 mmol), **77** (105.9 mg, 0.113 mg) and K_2CO_3 (47 mg, 0.339 mmol) in degassed DMF (5 mL) was stirred under argon at 120 °C for 24 h. The reaction mixture was diluted with water and extracted with EtOAc (x3). The combined organic phases were washed with brine, dried over $MgSO_4$ and the solvent was evaporated *in vacuo*. Purification by column chromatography (SiO_2, neat DCM to DCM:MeOH = 97.5:2.5) afforded **78** - TP6Gall as an off-white solid in a 87% yield (136 mg).

^{1}H NMR (400 MHz, $CDCl_3$) δ 7.83 (s, 6H, $CH_{Ar\text{-}Triphenylene}$), 7.19-7.13 (m, 1H, $CH_{Ar\text{-}Resorcinol}$), 6.65 (s, 2H,$CH_{Ar\text{-}Gallate}$), 6.56-6.50 (m, 3H, $CH_{Ar\text{-}Resorcinol}$), 4.90 (s, 2H, $OCH_{2\text{-}Benzylic}$), 4.23 (t, *J* = 6.5 Hz, 12H, OCH_2), 4.20-4.13 (m, 6H, OCH_2), 3.97 (t, *J* = 6.5 Hz, 2H, OCH_2), 3.88-3.83 (m, 4H, OCH_2), 3.83-3.78 (m, 2H, OCH_2), 3.74-3.68 (m, 6H, OCH_2), 3.58-3.53 (m, 6H, OCH_2), 3.38 (s, 3H, OCH_3), 3.37 (s, 6H, OCH_3), 2.01-1.89 (m, 12H, CH_2), 1.89-1.81 (m, 2H, CH_2), 1.63-1.53 (m, 12H, CH_2), 1.44-1.33 (m, 22H, CH_2), 0.97-0.89 (m, 15H, CH_3).

^{13}C NMR (101 MHz, $CDCl_3$) δ 160.5 (C_{Ar}), 160.1 (C_{Ar}), 152.9 (C_{Ar}), 149.2 (C_{Ar}), 132.6 (CH_{Ar}), 130.0 (CH_{Ar}), 123.8 (C_{Ar}), 107.6 (CH_{Ar}), 107.4 (CH_{Ar}), 107.3 (CH_{Ar}), 107.0 (CH_{Ar}), 102.0 (CH_{Ar}), 77.4 ($CH_{resorcinol}$), 72.5 (OCH_2), 72.2 (OCH_2), 72.2 (OCH_2), 70.9 (OCH_2), 70.7 (OCH_2), 70.6 (OCH_2), 70.2 (OCH_2), 69.9 ($OCH_{2\text{-Triphenylene}}$), 69.0 ($OCH_2$), 68.1 ($OCH_2$), 59.2 ($OCH_3$), 31.8 ($CH_2$), 29.6 ($CH_2$), 26.0 ($CH_2$), 22.81 ($CH_2$), 14.20 ($CH_3$). The carbons could not be attributed due to overlapping peaks.

HRMS (TOF ES+): m/z $[M+Na]^+$= 1403.8754 (Calculated: 1403.8736).

IR ν_{max}(film)/cm^{-1}: 2826 (m), 2857 (m), 1615 (m), 1591 (m), 1516 (m), 1435 (s), 1386 (m), 1260 (s), 1172 (s), 1048 (br), 1026 (m), 837 (m).

7.4 Experimental procedures and analytical data for chapter four

(4-Dodecylphenyl)magnesium bromide (114a)

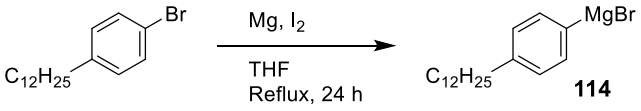

To a solution of magnesium turnings (320 mg, 13.2 mmol) and iodine (catalytic amount) in dry THF (6 mL) under argon was added dropwise a solution of 4-bromododecylbenzene (2.93 g, 9 mmol) in THF (15 mL). The mixture was stirred at reflux under argon for 6 h. A greenish solution was obtained and was used in the next step with no further purification.

(4-methoxyphenyl)magnesium bromide (114b)

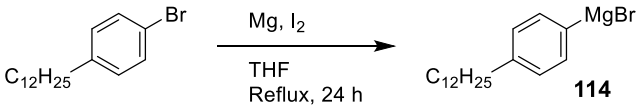

To a solution of magnesium turnings (213 mg, 8.78 mmol) and iodine (catalytic amount) in dry THF (4 mL) under argon was added dropwise a solution of 4-bromododecylbenzene (1.26 g,

6.75 mmol) in THF (11 mL). The mixture was stirred at reflux under argon for 6 h. A greenish solution was obtained and was used in the next step with no further purification.

Bis(4-n-dodecylbiphenyl)acetylene (115)

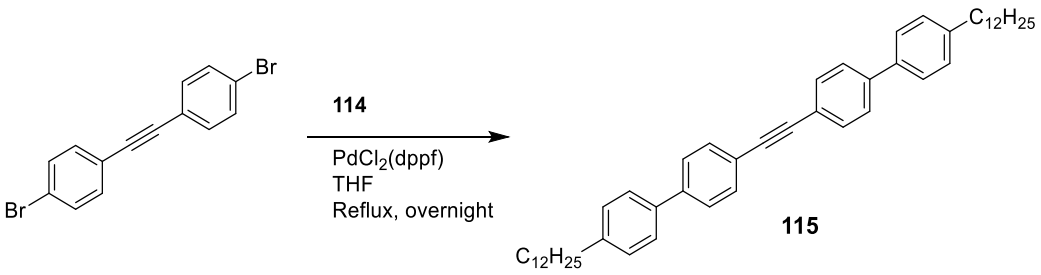

A known compound prepared according to literature procedure.[175] To a solution of di(4-bromophenyl)acetylene (719 mg, 2.14 mmol) in dry THF (60 mL) was added the freshly prepared solution (*ca.* 0.4 M) of (4-dodecylphenyl)magnesium bromide **114a** (20 mL, 8.57 mmol) under argon. $PdCl_2$(dppf) (138 mg, 0.17 mmol) was then added and the reaction mixture was stirred at reflux overnight under argon. The reaction mixture was cooled down to room temperature. The obtained white precipitate was filtered and washed with methanol and petroleum ether. **115** was obtained as an off-white solid (1.1672 g, 82%).

^{1}H NMR (400 MHz, $C_2D_2Cl_4$, 70 °C) δ 7.64 (s, 8H, CH_{Ar}), 7.57 (d, *J* = 8.2 Hz, 4H, CH_{Ar}), 7.31 (d, *J* = 8.2 Hz, 4H, CH_{Ar}), 2.75-2.66 (m, 4H, CH_{Ar}), 1.77-1.64 (m, 4H, CH_2), 1.49-1.24 (m, 36H, CH_2), 0.94 (t, *J* = 6.8 Hz, 6H, CH_3).

^{13}C NMR (101 MHz, $C_2D_2Cl_4$, 70 °C) δ 142.5 (2 x C_{Ar}), 140.7 (2 x C_{Ar}), 137.3 (2 x C_{Ar}), 131.9 (4 x CH_{Ar}), 128.8 (4 x CH_{Ar}), 126.6 (4 x CH_{Ar}), 126.5 (4 x CH_{Ar}), 121.8 (2 x C_{Ar}), 90.0 (C≡C), 35.4 (2 x CH_2), 31.7 (2 x CH_2), 31.0 (2 x CH_2), 29.5 (4 x CH_2), 29.4 (2 x CH_2), 29.3 (2 x CH_2), 29.3 (2 x CH_2), 29.2 (2 x CH_2), 29.1 (2 x CH_2), 22.5 (2 x CH_2), 13.9 (2 x CH_3).

MS (AP+, 700 °C): m/z$[M+H]^+$= 667.6.

IR ν_{max}(film)/cm^{-1}: 2959 (m), 2916 (m), 1283 (m), 2948 (m), 1717 (s), 1171 (m) 805 (m).

Hexa(4-*n*-dodecylbiphenyl)benzene (116)

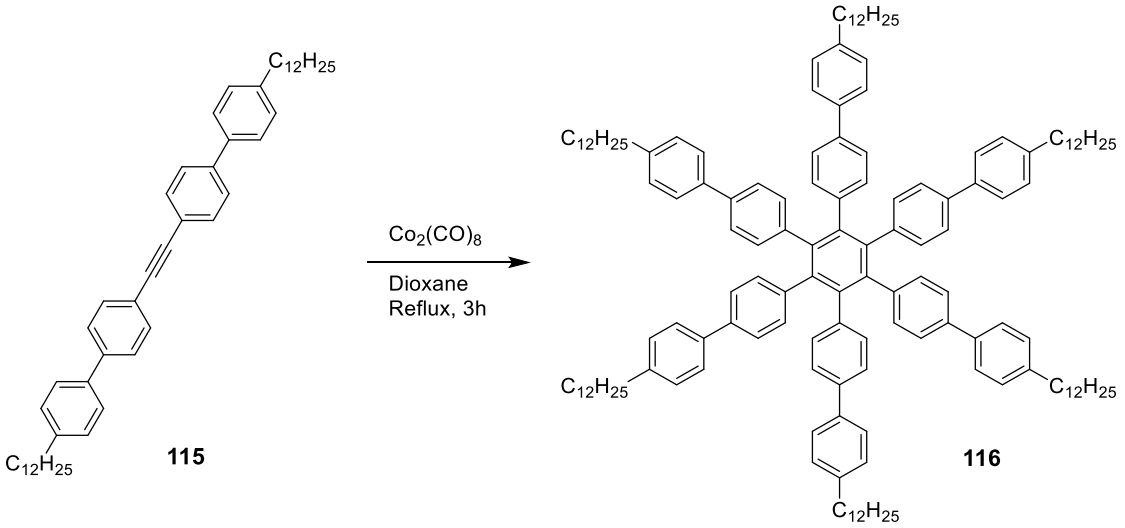

A known compound prepared according to the literature procedure.[175] A suspension of **115** (600 mg, 0.9 mmol), $Co_2(CO)_8$ (31 mg, 0.09 mmol) in dry and degassed dioxane (9 mL) was refluxed for 3 h under argon. The solvent was evaporated *in vacuo* and the resulting solid was purified by column chromatography (SiO_2, DCM:PE = 2:8) affording **116** in a 55% yield (990 mg).

^{1}H NMR (400 MHz, $CDCl_3$) δ 7.34 (d, *J* = 8.2 Hz, 12H, CH_{Ar}), 7.12 (t, *J* = 8.3 Hz, 24H, CH_{Ar}), 6.93 (d, *J* = 8.3 Hz, 12H, CH_{Ar}), 2.56 (t, J = 7.5 Hz, 12H, CH_2), 1.62-1.51 (m, 12H, CH_2), 1.34-1.18 (m, 108H, CH_2), 0.88 (t, *J* = 6.9 Hz, 18H, CH_3).

^{13}C NMR (101 MHz, $CDCl_3$) δ 141.8 (6 x C_{Ar}), 140.4 (6 x C_{Ar}), 139.6 (6 x C_{Ar}), 138.2 (6 x C_{Ar}), 137.6 (6 x C_{Ar}), 132.1 (12 x CH_{Ar}), 128.7 (12 x CH_{Ar}), 126.7 (12 xCH_{Ar}), 125.2 (12 x CH_{Ar}), 35.7 (6 x CH_2), 32.1 (6 x CH_2), 31.7 (6 x CH_2), 29.8 (12 x CH_2), 29.8 (6 x CH_2), 29.7 (6 x CH_2), 29.7 (6 x CH_2), 29.5 (6 x CH_2), 29.5 (6 x CH_2), 22.8 (6 x CH_2), 14.3 (6 x CH_3).

HRMS (TOF LD+, retinoic acid): m/z$[M+H]^+$= 2001.0.

1,4,7,10,13,16-Hexakis(4'-dodecylphenyl)hexa-*peri*-hexabenzocoronene - HBC-PhC$_{12}$ (117)

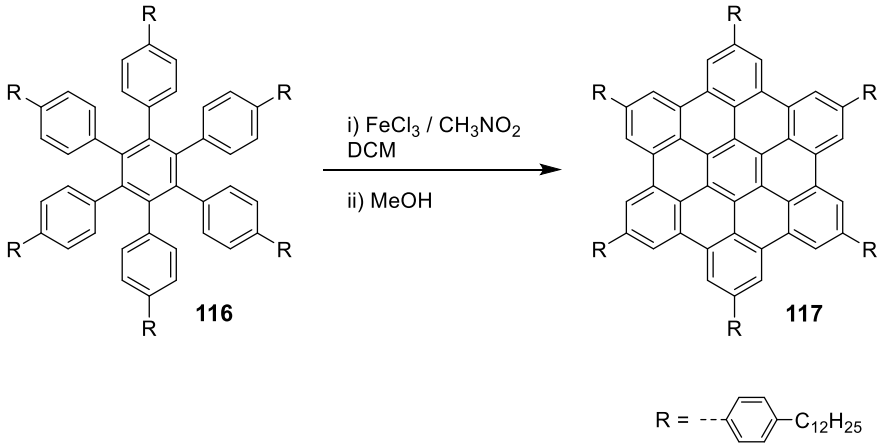

A known compound prepared according to literature procedure.[175] To a solution of **116** (612 mg, 0.31 mmol) in anhydrous DCM (400 mL) and under constant bubbling of argon was added a solution of anhydrous $FeCl_3$ (2.23 g, 13.8 mmol) in CH_3NO_2 (50 mL). The reaction mixture was stirred under constant bubbling of argon at 21 °C for 2 h. After a reductive work-up by adding methanol (400 mL) the precipitate was filtered *in vacuo* and washed with methanol. The dark brown precipitate was dissolved in the minimum amount of DCM and precipitated out again by adding methanol to remove any residual iron chloride. **117** was obtained as a yellow solid (405 mg, 74%).

^{1}H NMR (600 MHz, *p*-$C_6D_4Cl_2$, 85 °C) δ 8.51 (br, 12H, CH_{Ar}), 7.83 (br, 12H, CH_{Ar}), 7.61 (br, 12H, CH_{Ar}), 3.25 (br, 12H, CH_2), 2.31 (br, 12H, CH_2), 1.99 (br, 12H, CH_2), 1.92 (br, 12H, CH_2), 1.87-1.54 (m, 84H, CH_2), 1.26-1.13 (m, 18H, CH_3). The broadness of the peaks is due to the aggregation of HBC-PhC12 in *p*-$C_6D_4Cl_2$.

^{13}C NMR (151 MHz, *p*-$C_6D_4Cl_2$, 85 °C) δ 129.3 (12 x CH_{Ar}), 128.3 (12 x CH_{Ar}), 120.0 (12 x CH_{Ar}), 36.6 (6 x CH_2), 32.4 (12 x CH_2), 30.5 (6 x CH_2), 30.5 (6 x CH_2), 30.4 (6 x CH_2), 30.4 (6 x CH_2), 30.3 (6 x CH_2), 30.2 (6 x CH_2), 29.9 (6 x CH_2), 23.0 (6 x CH_2), 14.3 (6 x CH_3). None of the quaternary carbon were observed due to overlapping with the solvent and due to aggregation.

MS (LD+, retinoic acid): m/z$[M+H]^+$ = 1988.1.

IR ν_{max}(film)/cm^{-1}: 2923 (s), 2851 (s), 1683 (m), 1604 (m), 1464 (m), 1006 (m), 821 (m).

Bromination of oligoethylene glycol monomethyl ether – general procedure:

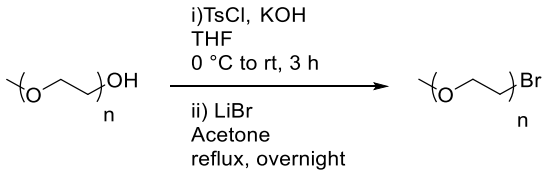

Known compounds prepared according to the literature procedure.[216] To a solution of oligoethylene glycol monomethyl ether in THF at 0 °C was added a 6 M aq. KOH solution (2.5 eq.). A solution of tosyl chloride (1.7 eq.) in THF was then added dropwise. The mixture was stirred at 0 °C for 1 h, then brought to room temperature and further stirred for 1 h. Water was added and the reaction mixture was extracted with diethyl ether (x3). The combined organic phases were washed with a 1 M aq. KOH solution, water, brine and dried over $MgSO_4$. The desired tosyl derivatives were used in the next step with no further purification.

To the crude tosylate derivative in acetone, LiBr (10 eq.) was slowly added. The mixture was stirred at reflux overnight. Water was added and the reaction mixture was extracted with DCM (x3). The combined organic phases were washed with brine, dried over $MgSO_4$ and the solvent was evaporated *in vacuo*. The 1-bromo derivative compound was afforded as a pale yellow oil and was used in the next step with no further purification.

1-Bromo-3,6,9-trioxadecane (119a)

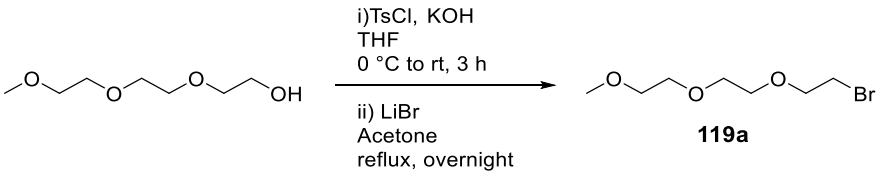

From triethylene glycol monomethyl ether (15 g, 91.4 mmol) in THF (50 mL), tosyl chloride (30.04 g, 157.6 mmol) in THF (44 mL) and KOH (13.27 g,, 237.1 mmol) in H_2O (40 mL). The crude tosylate was reacted with lithium bromide (79 g, 914 mmol) in acetone (250 mL). **119a** was obtained as a light yellow oil in a quantitative yield (20.8 mg).

^{1}H NMR (400 MHz, $CDCl_3$) δ 3.81 (t, *J* = 6.3 Hz, 2H, O**C**H_2CH_2Br), 3.70-3.63 (m, 6H, OCH_2), 3.57-3.53 (m, 2H, OCH_2), 3.47 (t, *J* = 6.3 Hz, 2H, CH_2Br), 3.38 (s, 3H).

^{13}C NMR (101 MHz, $CDCl_3$) δ 72.1 (OCH_2), 71.3 (O**C**H_2CH_2Br), 70.7 (2 x OCH_2), 70.7 (OCH_2), 59.2 (OCH_3), 30.4 (CH_2Br).

HRMS (TOF ES+): m/z[M+Na]$^+$= 249.0100 (Calculated: 249.0102).

IR ν_{max}(film)/cm^{-1}: 2874 (br), 1454 (w), 1101 (s).

1-Bromo-3,6,9,12-tetraoxatridecane (119b)

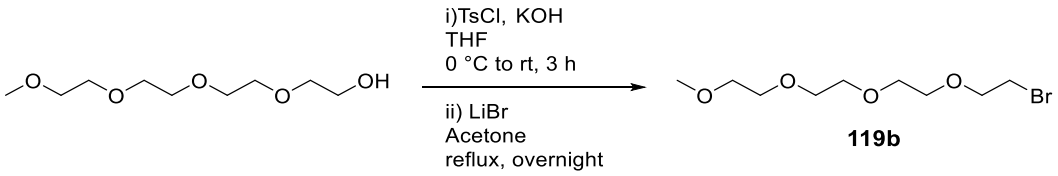

From tetraethylene glycol monomethyl ether (5 g, 24 mmol) in THF (13 mL), tosyl chloride (8.8 g, 45.9 mmol) in THF (10 mL) and KOH (3.36 g, 60 mmol) in H_2O (10 mL). The crude tosylate was reacted with lithium bromide lithium bromide (20.8 g, 240 mmol) in acetone (100 mL). **119b** was obtained as a light yellow oil in a quantitative yield (6.5 g).

^{1}H NMR (400 MHz, $CDCl_3$) δ 3.80 (t, *J* = 6.3 Hz, 2H, O**C**H_2CH_2Br), 3.69-3.62 (m, 10H), 3.56-3.52 (m, 2H), 3.46 (t, *J* = 6.3 Hz, 2H, CH_2Br), 3.37 (s, 3H, CH_3).

^{13}C NMR (101 MHz, $CDCl_3$) δ 72.0 (OCH_2), 71.3 (O**C**H_2CH_2Br), 70.7 (br, 3 x OCH_2), 70.6 (2 x OCH_2), 59.2 (OCH_3), 30.4 (CH_2Br).

HRMS (TOF ES+): m/z$[M+Na]^+$= 293.0369 (Calculated: 293.0364).

IR ν_{max}(film)/cm^{-1}: 2869 (br), 1454 (w), 1100 (s).

Phthalimidation of the 1-bromooligoethylene glycol monomethyl ether - general procedure:

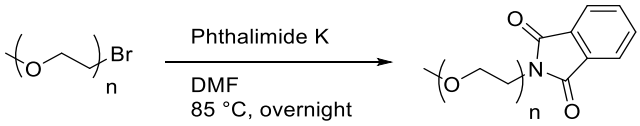

Known compounds prepared according to a modified literature procedure.[217] A solution of 1-bromooligoethylene glycol monomethyl ether (1 eq.) and phthalimide potassium salt (2 eq.) in DMF was stirred overnight at 85 °C. The mixture was then filtered and the filtrate was evaporated *in vacuo*. Purification by column chromatography (SiO_2) afforded the compound as a light yellow oil.

1-Phthalimido-3,6,9-trioxadecane (120a)

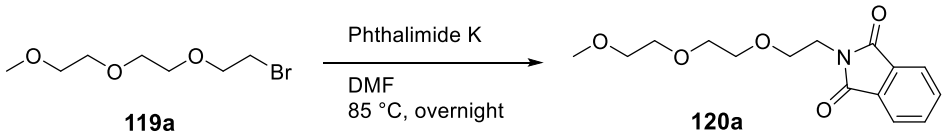

119a **120a**

From **119a** (5.0 g, 22.02 mmol) and phthalimide potassium salt (8.16 g, 44.04 mmol) in DMF (125 mL). Purification by column chromatography (SiO_2, EtOAc:Hexane = 1:1) afforded **120a** as a light yellow oil (4.19 g, 65%).

^{1}H NMR (400 MHz, $CDCl_3$) δ 7.79-7.73 (m, 2H, CH_{NPhth}), 7.66-7.60 (m, 2H, CH_{NPhth}), 3.82 (t, *J* = 5.8 Hz, 2H, CH_2NPhth), 3.66 (t, *J* = 5.8 Hz, 2H, O**CH_2**CH_2NPhth), 3.60-3.56 (m, 2H), 3.54-3.48 (m, 4H), 3.41-3.37 (m, 2H), 3.25 (s, 3H, OCH_3).

^{13}C NMR (101 MHz, $CDCl_3$) δ 168.4 (2 x C=O), 134.0 (2 x CH_{NPhth}), 132.3 (2 x C_{Nphth}), 123.3 (2 x CH_{NPhth}), 72.0 (OCH_2), 70.7 (OCH_2), 70.7 (OCH_2), 70.2 (OCH_2), 68.0 (O**C**$H_2$$CH_2NPhth$), 59.1 ($OCH_3$), 37.4 ($CH_2NPhth$).

HRMS (TOF ES+): m/z$[M+H]^+$= 294.1350 (Calculated: 294.1341).

IR ν_{max}(film)/cm^{-1}: 2873 (br), 1773 (w), 1706 (s), 1392 (m), 1101 (m), 1024 (m), 718 (s).

1-Phthalimido-3,6,9,12-tetraoxatridecane (120b)

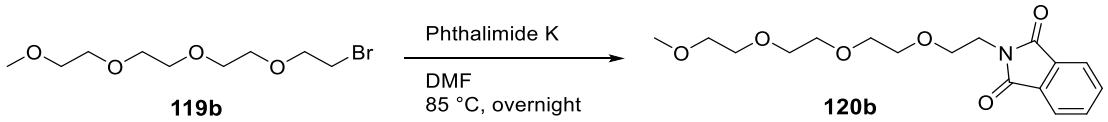

119b **120b**

From **119b** (6.5 g, 24 mmol) and phthalimide potassium salt (8.89 g, 48 mmol) in DMF (100 mL). Purification by column chromatography (SiO_2, EtOAc) afforded **120b** as a light yellow oil (5.76 g, 71%).

^{1}H NMR (400 MHz, $CDCl_3$) δ 7.87-7.80 (m, 2H, CH_{NPpth}), 7.73-7.67 (m, 2H, CH_{NPhth}), 3.89 (t, *J* = 5.8 Hz, 2H, CH_2NPhth), 3.73 (t, *J* = 5.2 Hz, 2H, O**C**$H_2$$CH_2NPhTh$), 3.66-3.49 (m, 12H, OCH_2), 3.36 (s, 3H, OCH_3).

^{13}C NMR (101 MHz, $CDCl_3$) δ 168.4 (2 x C=O), 134.0 (2 x CH_{NPhth}), 132.3 (2 x C_{NPhth}), 123.3 (2 x CH_{NPhth}), 72.0 (OCH_2), 70.7 (OCH_2), 70.7 (2 x OCH_2), 70.6 (OCH_2), 70.2 (OCH_2), 68.0 (O**C**$H_2$$CH_2NPhTh$), 59.1 ($OCH_3$), 37.4 ($CH_2NPhth$).

HRMS (TOF ES+): m/z$[M+Na]^+$= 360.1418 (Calculated: 360.1423).

IR ν_{max}(film)/cm^{-1}: 2869 (br), 1773 (w), 1707 (s), 1392 (m), 1100 (br, m), 1024(m), 718 (s).

Amination of 1-phthalimido oligoethylene glycol-general procedure:

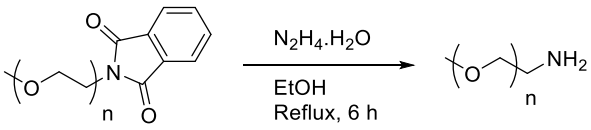

Known compounds prepared according to a modified literature procedure.[217] To a solution of 1-phthalimidooligoethylene glycol monomethyl ether (1 eq.) in ethanol was added a solution of hydrazine hydrate (78-82% aqueous solution, 2 eq.). The mixture was stirred at reflux for 6 h. Filtration through a pad of Celite (eluent: DCM) and evaporation of the solvent afforded a brown oil. Diethyl ether was added and the solution was sonicated for 10 min. Filtration through a pad of Celite (Eluent: DCM) followed by evaporation of the solvent afforded the 1-amino derivatives as light yellow oils.

1-Amino-3,6,9-trioxadecane (121a)

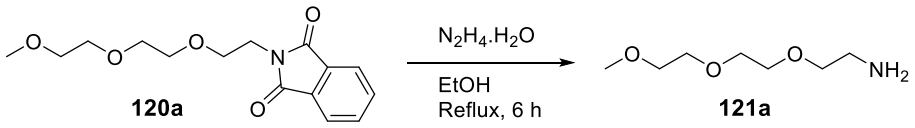

120a **121a**

From **120a** (4,00 g, 13.65 mmol) and a 78-82% aq. solution hydrazine (1.7 mL) in ethanol (140 mL). **121a** was afforded in a 91% yield (2.07 g).

^{1}H NMR (400 MHz, $CDCl_3$) δ 3.85 (br, 2H, OCH_2), 3.66 (br, 6H, OCH_2), 3.55 (br, 2H, OCH_2), 3.39 (s, 3H, OCH_3), 3.23 (br, 2H, C**H$_2$**NH_2). None of the exchangeable protons were observed.

^{13}C NMR (101 MHz, $CDCl_3$) δ 71.8 (OCH_2), 70.3 (OCH_2), 70.3 (OCH_2), 70.2 (OCH_2), 66.9 (OCH_2), 59.2 (OCH_3), 40.0 (**C**H_2NH_2).

HRMS (TOF ES+): m/z$[M+H]^+$= 164.1288 (Calculated: 164.1287).

IR ν_{max}(film)/cm^{-1}: 3369 (br), 2874 (br), 1658 (w), 1456 (w), 1095 (s).

1-Amino-3,6,9,12-tetraoxatridecane (121b)

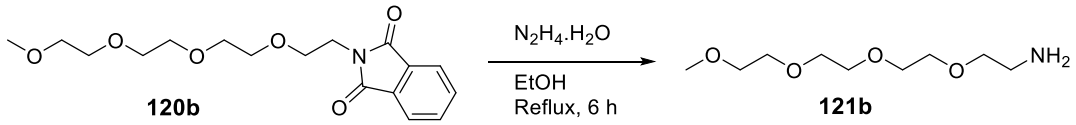

From **120b** (5.00 g, 14.82 mmol) and a 78-82% aq. solution of hydrazine (1.9 mL, 29.64 mmol) in ethanol (100 mL). **121b** was afforded in a 95% yield (2.92 g).

^{1}H NMR (400 MHz, $CDCl_3$) δ 3.67-3.60 (m, 10H, OCH_2), 3.56-3.52 (m, 2H, OCH_2), 3.50 (t, *J* = 5.2 Hz, 2H, OCH_2), 3.37 (s, 3H, OCH_3), 2.86 (t, *J* = 5.3 Hz, 2H, C**H**$_2$NH$_2$), 1.93 (br, 2H, NH_2).

^{13}C NMR (101 MHz, $CDCl_3$) δ 73.3 (OCH_2), 71.9 (OCH_2), 70.6 (3 x OCH_2), 70.5 (OCH_2), 70.3 (OCH_2), 59.0 (OCH_3), 41.7 (**C**H$_2$NH$_2$) .

HRMS (TOF ES+): m/z$[M+H]^+$= 208.1548 (Calculated: 208.1549).

IR ν_{max}(film)/cm^{-1}: 2876 (br), 1457 (w), 1094 (br, s), 1027 (w), 730 (m).

Synthesis of N,N'-Di(oligoethylene glycol) perylene diimide: general procedure

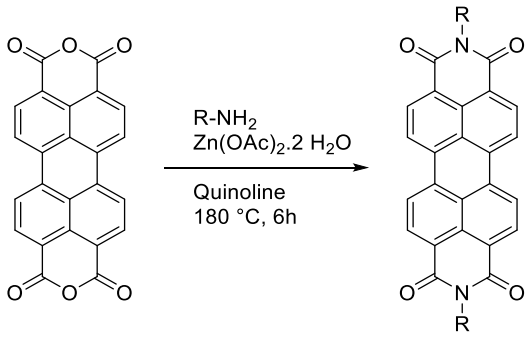

Known compounds prepared according to a modified literature procedure.[218] A solution of PTCDA (1 eq.), zinc acetate dihydrate (1 eq.) and the corresponding 1-amino chains (3 eq.) in quinoline was stirred at 180 °C for 6 h under argon. The solution was then cooled to room temperature and poured into a 1 M aq. HCl solution. The dark red precipitate was filtered and washed with successively a 1 M HCl solution, water and methanol and dried *in vacuo*.

N,N'-Di(3,6,9-trioxadecane)-3,4,9,10-tetracarboxy diimide (122a)

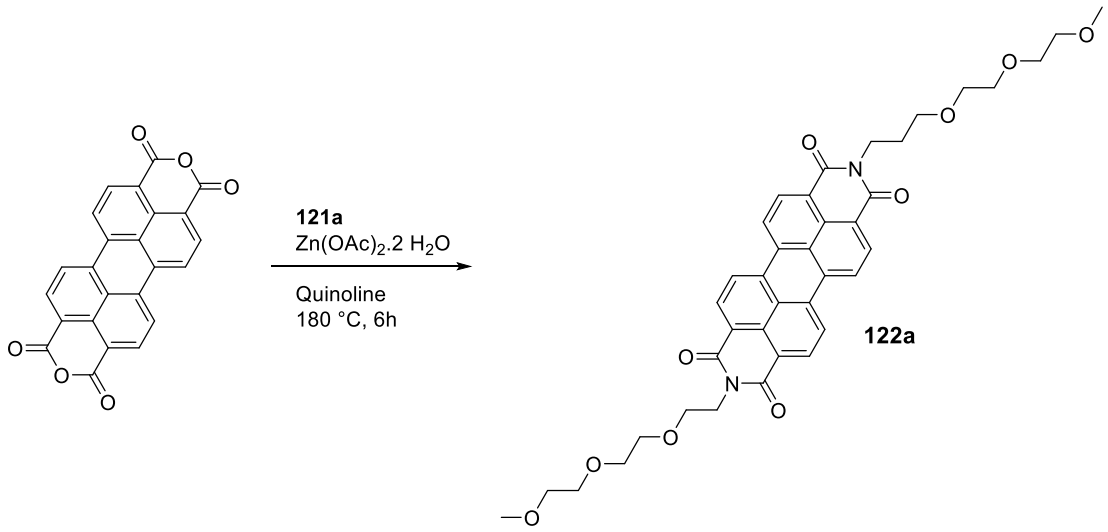

From PTCDA (100 mg, 0.25 mmol), zinc acetate dihydrate (46 mg, 0.25 mmol) and **121a** (122 mg, 0.75 mmol) in quinoline (3 mL). **122a** was afforded as a dark red solid in a 81% yield.

^{1}H NMR (400 MHz, $CDCl_3$) δ 8.52 (d, *J* = 8.0 Hz, 4H, CH_{Ar}), 8.37 (d, *J* = 8.1 Hz, 4H, CH_{Ar}), 4.46 (t, *J* = 6.0 Hz, 4H, CH_2NPhth), 3.88 (t, *J* = 6.0 Hz, 4H, OC**H**$_2$$CH_2$NPhth), 3.78-3.74 (m, 4H, OCH_2), 3.69-3.63 (m, 4H, OCH_2), 3.63-3.59 (m, 4H, OCH_2), 3.51-3.45 (m, 4H), 3.32 (s, 6H, OCH_3).

^{13}C NMR (101 MHz, $CDCl_3$) δ 163.4 (4 x C=O), 134.4 (4 x C_{Ar}), 131.3 (4 x CH_{Ar}), 129.3 (2 x C_{Ar}), 126.2 (2 x C_{Ar}), 123.3 (4 x C_{Ar}), 123.1 (4 x CH_{Ar}), 72.1 (2 x OCH_2), 70.8 (2 x OCH_2), 70.7 (2 x OCH_2), 70.3 (2 x OCH_2), 68.1 (2 x O**C**H_2CH_2NPhth), 59.2 (2 x OCH_3), 39.5 (2 x CH_2N).

HRMS (TOF ES+): m/z$[M+Na]^+$= 705.2420 (Calculated: 705.2424).

IR ν_{max}(film)/cm^{-1}: 2882 (br), 1689 (m), 1653 (m), 1591 (s), 1372 (w), 1110 (br), 857 (m), 810 (m), 744 (s).

m.p. = 320 °C.

N,N'-Di(3,6,9,12-tetraoxatridecane)-3,4,9,10-tetracarboxy diimide (122b)

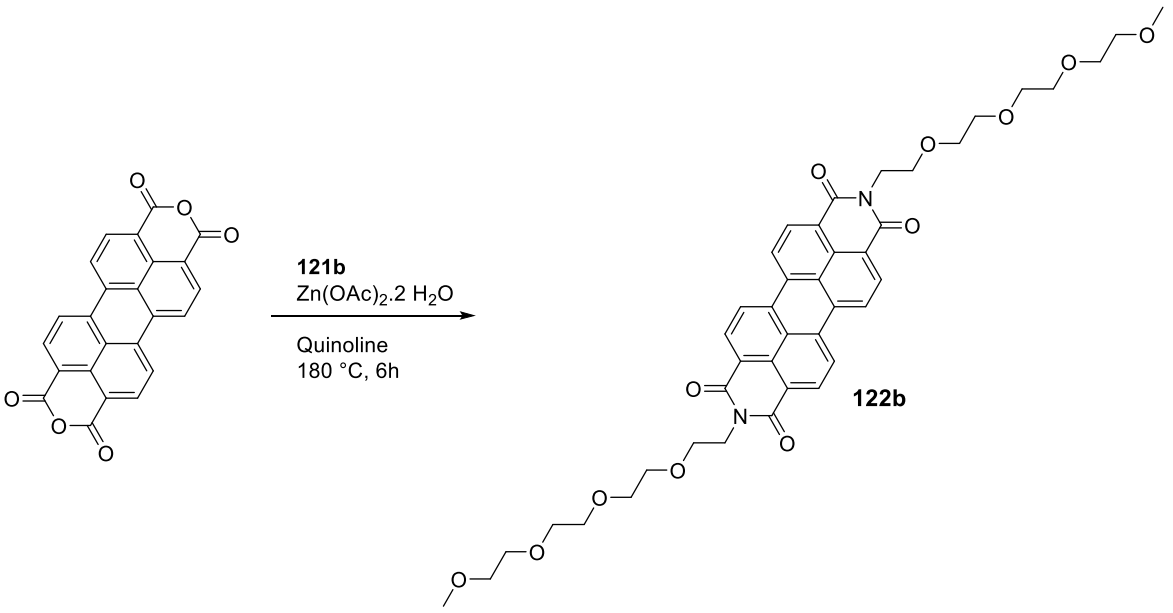

From PTCDA (100 mg, 0.25 mmol), zinc acetate dihydrate (46 mg, 0.25 mmol) and **121b** (155 mg, 0.75 mmol) in quinoline (3 mL). **122b** was afforded as a dark red solid in a 71% yield.

^{1}H NMR (400 MHz, $CDCl_3$) δ 8.26 (d, *J* = 7.9 Hz, 4H, CH_{Ar}), 8.01 (d, *J* = 8.1 Hz, 4H, CH_{Ar}), 4.40 (t, *J* = 6.0 Hz, 4H, CH_2NPhth), 3.86 (t, *J* = 6.0 Hz, 4H, OC**H**$_2$$CH_2$NPhth), 3.78-3.72 (m, 4H, OCH_2), 3.68-3.61 (m, 8H, OCH_2), 3.61-3.56 (m, 8H, OCH_2), 3.52-3.47 (m, 4H, OCH_2), 3.32 (s, 6H, OCH_3).

^{13}C NMR (101 MHz, $CDCl_3$) δ 163.0 (4 x C=O), 133.8 (4 x C_{Ar}), 130.9 (4 x CH_{Ar}), 128.8 (2 x C_{Ar}), 125.5 (2 x C_{Ar}), 122.9 (4 x C_{Ar}), 122.7 (4 x CH_{Ar}), 72.0 (2 x OCH_2), 70.7 (2 x OCH_2), 70.7 (4 x OCH_2), 70.6 (2 x OCH_2), 70.2 (2 x OCH_2), 68.0 (2 x O**C**H_2CH_2NPhth), 59.1 (2 x OCH_3), 39.4 (2 x CH_2N).

HRMS (TOF ES+): m/z$[M+Na]^+$= 793.2949 (Calculated: 793.2948).

IR ν_{max} (film)/cm^{-1}: 2878 (br), 1689 (s), 1655 (s), 1591 (s), 1580 (m), 1337 (s), 1241 (m), 1111 (br, s), 854 (m), 809 (m), 745 (m).

m.p. = 300 °C.

Tetrabutyl perylene-3,4,9,10-tetracarboxylate (105)

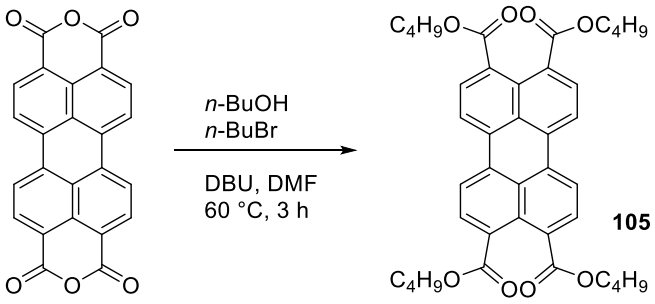

A known compound prepared according to the literature procedure.[219] To a solution of perylene-3,4,9,10-tetracarboxylic dianhydride (2.5 g, 6.37 mmol) in DMF (32 mL), *n*-BuOH (4.7 mL) and DBU (3.8 mL) was added. The mixture was stirred at 60 °C for 0.5 h. A solution of 1-bromobutane (5.5 mL, 51 mmol) in DMF (20 mL) was then added and the reaction mixture was further stirred at 60 °C for 3h. The solution was cooled down to room temperature and water (250 mL) was added. The resulting red precipitate was filtered and washed with water. Purification by column chromatography (SiO_2, DCM) afforded **105** as a light orange solid (3.60 g, 87%).

^{1}H NMR (400 MHz, $CDCl_3$) δ 7.97 (d, *J* = 8.0 Hz, 4H, CH_{Ar}), 7.86 (d, *J* = 7.9 Hz, 4H, CH_{Ar}), 4.35 (t, *J* = 6.9 Hz, 8H, OCH_2), 1.81 (q, *J* = 6.9 Hz, 8H, CH_2), 1.52 (q, J =7.6 Hz, 8H, CH_2), 1.02 (t, *J* = 7.4 Hz, 12H, CH_3).

^{13}C NMR (101 MHz, $CDCl_3$) δ 168.7 (4 x C=O), 132.8 (4 x C_{Ar}), 130.4 (4 x CH_{Ar}), 128.8 (2 x C_{Ar}), 128.6 (2 x C_{Ar}), 121.4 (4 x CH_{Ar} + 4 x C_{Ar}), 65.4 (4 x OCH_2), 30.8 (4 x CH_2), 19.4 (4 x CH_2), 14.0 (4 x CH_3).

HRMS (TOF ES+): m/z$[M+H]^+$= 652.3038 (Calculated: 652.3036).

IR ν_{max}(film)/cm^{-1}: 2959 (w), 2933 (w), 2872 (w), 1717 (s), 1130 (br).

Mesogenic properties: Cr 161 Col 242 I

Tetrabutyl 1,7-Dibromoperylene-3,4,9,10-tetracarboxylate (106)

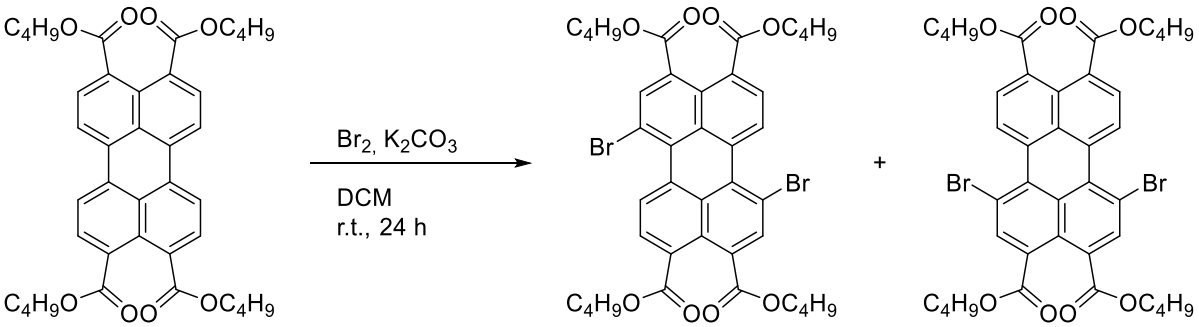

105 **106** **107**

A known compound prepared according to the literature procedure.[163] To a solution of **105** (3.0 g, 4.60 mmol) and potassium carbonate (1.58 g, 11.5 mmol) in DCM (40 mL), bromine (3.1 mL, 59.8 mmol) was slowly added. The reaction mixture was stirred at room temperature for 24 h. A 1 M aq. solution of sodium dithionite was then added dropwise. The organic phase was washed with water, brine and dried over $MgSO_4$ and the solvent was evaporated *in vacuo*. The red solid, composed of a 4:1 mixture of **106**:**107** was obtained. The crude was dissolved in the minimum amount of DCM and recrystallized from ACN. This operation was repeated three times and the regioisomerically pure 1,7-dibromoperylene-3,4,9,10-tetracarboxylate **106** was obtained as an orange solid (1.8 g, 47%).

^{1}H NMR (400 MHz, $CDCl_3$) δ 8.92 (d, *J* = 7.9 Hz, 2H, CH_{Ar}), 8.28 (s, 2H, CH_{Ar}), 8.08 (d, *J* = 7.9 Hz, 2H, CH_{Ar}), 4.34 (td, *J* = 6.9, 1.7 Hz, 8H, OCH_2), 1.83-1.74 (m, 8H, CH_2), 1.55-1.43 (m, 8H, CH_2), 1.00 (t, *J* = 7.4 Hz, 12H, CH_3).

^{13}C NMR (101 MHz, $CDCl_3$) δ 168.1 (2 x C=O), 167.3 (2 x C=O), 136.8 (2 x CH_{Ar}), 131.9 (2 x C_{Ar}), 131.9 (2 x C_{Ar}), 131.3 (2 x C_{Ar}), 130.6 (2 x C_{Ar}), 130.6 (2 x C_{Ar}), 129.2 (2 x CH_{Ar}), 127.8 (2 x CH_{Ar}), 126.6 (2 x C_{Ar}), 118.9 (2 x C_{Ar}Br), 66.0 (2 x OCH_2), 65.8 (2 x OCH_2), 30.8 (2 x CH_2), 30.7 (2 x CH_2), 19.4 (2 x CH_2), 19.4 (2 x CH_2), 13.9 (4 x CH_3).

HRMS (TOF ES+): m/z[M+Na]$^{+}$= 833.1122 (Calculated for $C_{40}H_{42}O_8Na^{79}Br^{81}Br$: 833.1124).

IR ν_{max}(film)/cm^{-1}: 2959 (w), 2933 (w), 2872 (w), 1718 (w), 1171 (w).

mp = 129 °C.

1,7-Dibromoperylene-3,4,9,10-tetracarboxylic dianhydride (103)

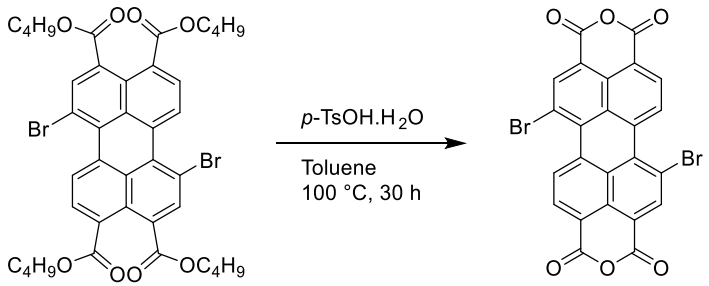

106 **103**

A known compound prepared according to the literature procedure.[163] A solution of **106** (1.0 g, 1.23 mmol) and TsOH.H_2O (1.17 g, 6.17 mmol) in toluene (35 mL) was stirred at 100 °C for 41 h. The dark red reaction mixture was cooled down to room temperature and the precipitate was filtered and washed with successively water and methanol. After drying the residue i*n vacuo*, **103** was afforded in a 74% yield (501.7 mg) as an insoluble dark red solid, which was used in the next step with no further purification.

NMR spectra could not be recorded do to the insolubility of **103** in common solvents.

MS (AP+): m/z[M+H]$^{+}$= 550.8.

IR ν_{max}(film)/cm^{-1}: 2966 (w), 1767 (s), 1737 (s), 1721 (w), 1590 (s), 1501 (m), 1375 (m), 1305 (m), 1284 (m), 1137 (m), 804 (s).

mp > 350 °C

N,N'-bis(3,6,9-trioxadecyl)-1,7-dibromoperylene-3,4,9,10-tetracarboxy diimide (123)

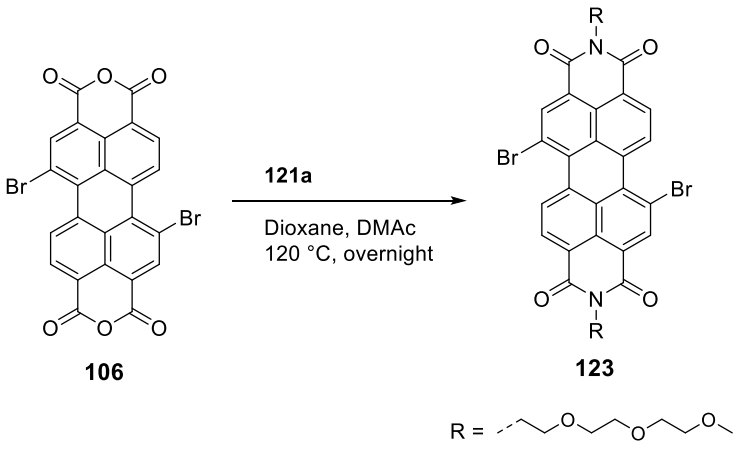

A known compound prepared according to a modified literature procedure.[220] A solution of **106** (250 mg, 0.45 mmol) and 3,6,9-trioxadecylamine **121a** (162 mg, 0.99 mmol) in a 1:1 mixture of anhydrous DMAc and anhydrous dioxane (10 mL) was stirred overnight at 120 °C under argon. The reaction mixture was cooled down to room temperature, diluted with water and extracted with chloroform (x3). The combined organic phases were washed with water, brine, dried on $MgSO_4$ and the solvent was evaporated *in vacuo*. The crude solid was recrystallised from MeOH and **123** was obtained as a dark red solid in a 51% yield (191 mg).

^{1}H NMR (400 MHz, $CDCl_3$) δ 9.42 (d, *J* = 8.2 Hz, 2H, CH_{Ar}), 8.86 (s, 2H, CH_{Ar}), 8.64 (d, *J* = 8.2 Hz, 2H, CH_{Ar}), 4.47 (t, *J* = 5.9 Hz, 4H, NCH_2), 3.85 (t, *J* = 5.9 Hz, 4H, OCH_2), 3.75-3.69 (m, 4H, OCH_2), 3.66-3.57 (m, 8H, OCH_2), 3.50-3.45 (m, 4H, OCH_2), 3.31 (s, 6H, CH_3).

^{13}C NMR (101 MHz, $CDCl_3$) δ 163.0 (2 x C=O), 162.5 (2 x C=O), 138.1 (2 x CH_{Ar}), 133.1 (2 x C_{Ar}), 132.9 (2 x C_{Ar}), 130.1 (2 x CH_{Ar}), 129.3 (2 x C_{Ar}), 128.6 (2 x CH_{Ar}), 127.1 (2 x C_{Ar}), 123.2 (2 x C_{Ar}), 122.8 (2 x C_{Ar}), 120.9 (2 x $C_{Ar}Br$), 72.0 (2 x OCH_2), 70.8 (2 x OCH_2), 70.8 (2 x OCH_2), 70.3 (2 x OCH_2), 68.0 (2 x OCH_2), 59.2 (2 x OCH_3), 39.6 (2 x CH_2N).

IR ν_{max}(film)/cm^{-1}: 2870 (br), 1686 (s), 1654 (s), 1589 (s), 1101 (br).

HRMS (TOF ES+): m/z$[M+Na]^+$= 863.0613 (Calculated for $C_{38}H_{36}O_{10}Na^{79}Br^{81}Br$: 863.0614).

2,5,8,12,15,18-Hexaoxa-nonadecan-10-ol (128)

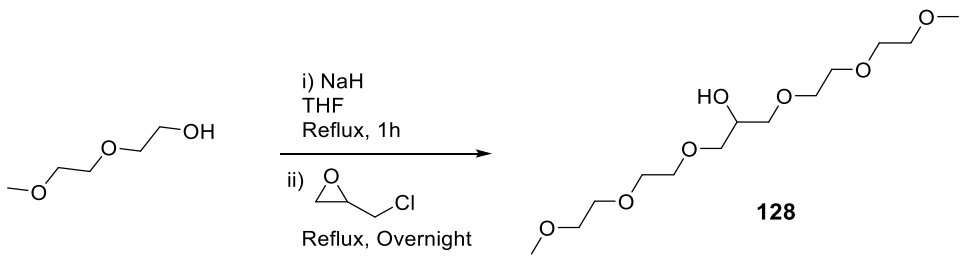

A known compound prepared according to a modified literature procedure.[183] A solution of sodium hydride (60% in mineral oil, 12.24 g, 510 mmol) in dry THF (80 mL) was stirred at reflux under argon. A solution of diethylene glycol monomethyl ether (30.6 g, 255 mmol) in dry THF (20 mL) was then added dropwise over a period of 30 min. The reaction mixture was further stirred at reflux for 1 h. Epichlorhydrin (4.72 g, 51 mmol) was then added dropwise. After stirring at reflux for 24 h, the mixture was cooled down to room temperature and water was slowly added. The reaction mixture was extracted with DCM (x3). The combined organic phases were washed with brine, dried over $MgSO_4$ and the solvent was evaporated *in vacuo*. High vacuum distillation (T = 150 °C) afforded **128** as a light yellow oil (11.07 g, 74%).

^{1}H NMR (400 MHz, $CDCl_3$) δ 4.02-3.93 (m, 1H, CH), 3.70-3.61 (m, 12H, CH_2), 3.59-3.46 (m, 8H, CH_2), 3.40-3.35 (m, 6H, CH_3).

^{13}C NMR (101 MHz, $CDCl_3$) δ 72.3 (2 x OCH_2), 71.6 (2 x OCH_2), 70.4 (2 x OCH_2), 70.1 (4 x OCH_2), 69.0 (CHOH), 58.6 (2 x CH_3).

HRMS (TOF ES+): m/z$[M+Na]^+$= 319.1735 (Calculated: 319.1733).

IR ν_{max}(film)/cm^{-1}: 2955 (m), 2921 (s), 2853 (m), 1459 (m), 1378 (m).

10-(6-Bromo-1,4-dioxahexyl)-2,5,8,12,15,18-hexaoxa-nonadecane (129)

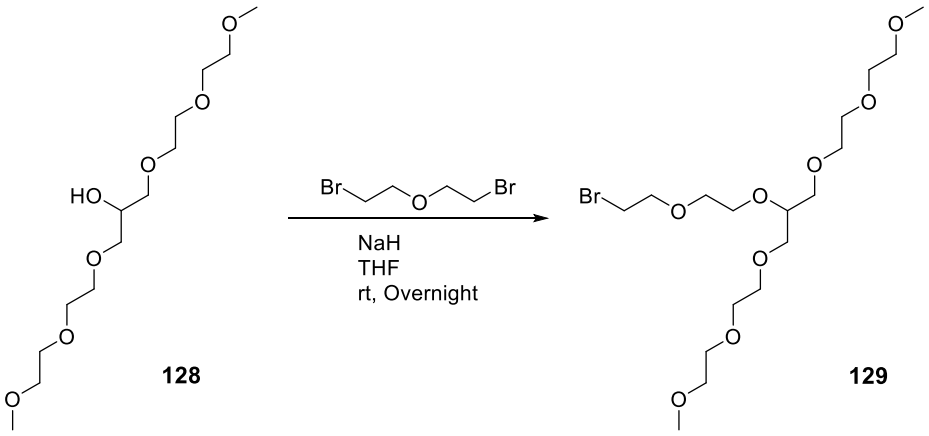

128 **129**

A novel compound. A solution of sodium hydride (60% in mineral oil, 310 mg, 7.76 mmol) in dry THF (70 mL) was stirred at room temperature for 15 min under argon. **128** (1.15 g, 3.88 mmol) was added and the reaction mixture was stirred at room temperature for 30 min. Bis(2-bromoethyl)ether (4.5 g, 19.4 mmol) was added dropwise and the reaction mixture was stirred overnight at room temperature. The reaction mixture was quenched with isopropanol (3 mL) and filtrated though a pad of Celite (eluent: DCM). The filtrate was evaporated *in vacuo* and the resulting light brown oil was purified by column chromatography (SiO_2, neat ACN) to afford **129** as a light brown oil (891 mg, 51%).

^{1}H NMR (400 MHz, $CDCl_3$) δ 3.85-3.74 (m, 4H, CH_2), 3.71-3.67 (m, 1H, CH), 3.64 (m, 14H, CH_2), 3.60-3.50 (m, 8H, CH_2), 3.46 (t, J = 6.3 Hz, 2H, CH_2Br), 3.38 (s, 6H, CH_3).

^{13}C NMR (101 MHz, $CDCl_3$) δ 78.4 (OCH), 72.0 (2 x OCH_2), 71.4 (2 x OCH_2), 71.2 (OCH_2), 70.8 (2 x OCH_2), 70.7 (OCH_2), 70.6 (2 x OCH_2), 70.6 (2 x OCH_2), 69.9 (OCH_2), 59.1 (2 x OCH_3), 30.5 (CH_2-Br).

HRMS (TOF ES+): m/z$[M+Na]^+$= 469.1415 (Calculated: 469.1413); $[M+K]^+$= 487.1.

IR ν_{max}(film)/cm^{-1}: 2868 (br), 1457 (w), 1353 (w), 1099 (s).

10-(6-Phthalimido-1,4-dioxahexyl)-2,5,8,12,15,18-hexaoxa-nonadecane (130)

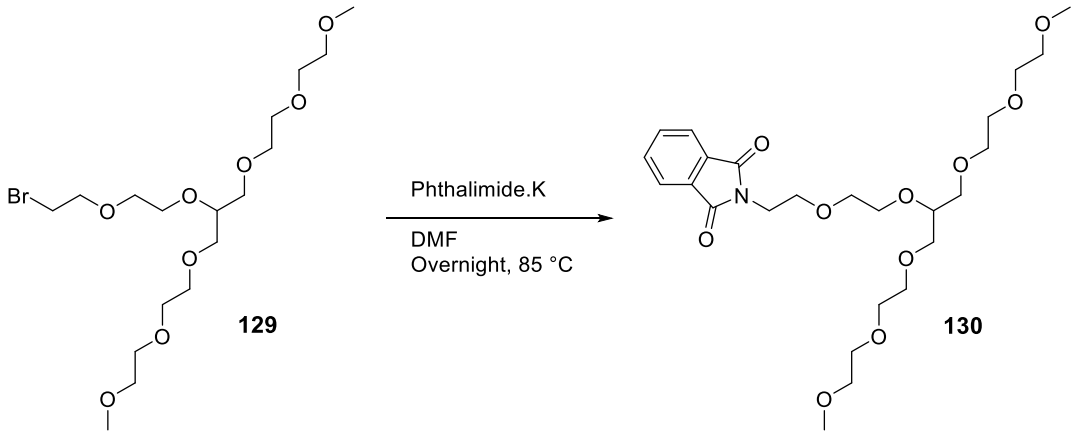

A novel compound. A solution of **129** (149 mg, 0.33 mmol) and potassium phthalimide (122 mg, 0.66 mmol) in DMF (2 mL) was stirred overnight at 85 °C. After cooling to room temperature, the mixture was filtrated through a pad of Celite (eluent: DCM) and the filtrate was evaporated *in vacuo*. Purification by column chromatography (SiO_2, EtOAc:MeOH = 95:5) afforded **130** as a light yellow oil (114 mg, 67%).

^{1}H NMR (400 MHz, $CDCl_3$) δ 7.84 (dd, J = 5.5, 3.0 Hz, 2H, CH_{Ar}), 7.71 (dd, J = 5.5 Hz, 3.0 Hz, 2H, CH_{Ar}), 3.88 (t, J = 5.8 Hz, 2H, CH_2-NPhth), 3.75-3.68 (m, 4H), 3.66-3.58 (m, 15H, CH_2 + CH), 3.56-3.44 (m, 8H, CH_2), 3.37 (s, 6H, CH_3).

^{13}C NMR (101 MHz, $CDCl_3$) δ 168.4 (2 x C=O), 134.0 (2 x CH_{Ar}), 132.3 (2 x C_{Ar}), 123.4 (2 x CH_{Ar}), 78.5 (CH), 72.1 (2 x OCH_2), 71.4 (2 x OCH_2), 71.0 (2 x OCH_2), 70.7 (4 x OCH_2), 70.5 (OCH_2), 69.9 (OCH_2), 68.0 (OCH_2), 59.2 (2 x OCH_3), 37.5 (CH_2-NPhTh).

HRMS (TOF ES+): m/z$[M+Na]^+$= 536.2474 (Calculated: 536.2472); $[M+K]^+$= 552.2.

IR ν_{max}(film)/cm^{-1}: 2874 (br), 1774 (w), 1709 (s), 1392 (m), 1100 (s), 1024 (m), 721 (s).

10-(6-Amino-1,4-dioxahexyl)-2,5,8,12,15,18-hexaoxa-nonadecane *(*131)

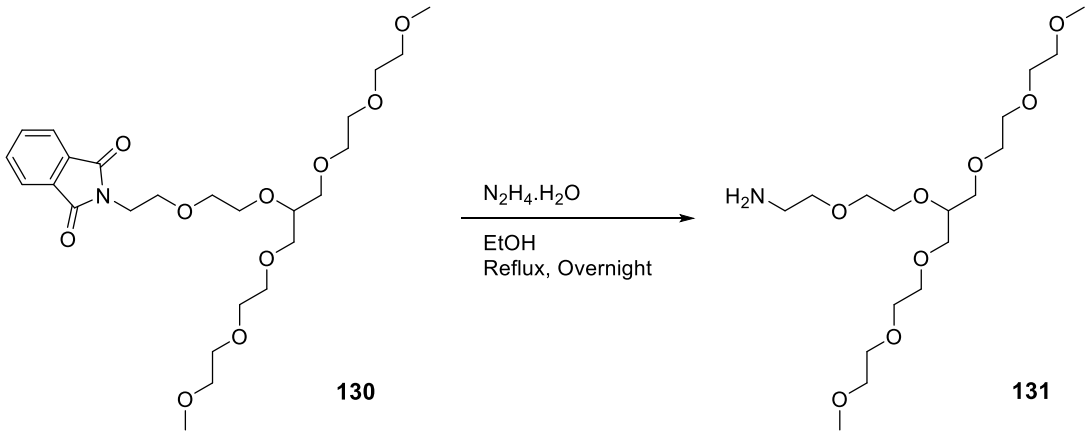

A novel compound. A solution of **130** (353 mg, 0.687 mmol) and hydrazine hydrate (0.1 mL) in ethanol (12 mL) was stirred overnight at reflux. The resulting dough was filtrated though a pad of Celite (eluent: MeOH). The solvent was evaporated, diethyl ether was added and the solution was sonicated for 10 min. Filtration though a pad of Celite (eluent: diethyl ether) afforded **131** as a yellow oil (220 mg, 84%).

^{1}H NMR (400 MHz, $CDCl_3$) δ 3.72-3.67 (m, 2H, CH_2), 3.65-3.60 (m, 1H, CH), 3.60-3.42 (m, 26H, CH_2), 3.30 (s, 6H, CH_3), 2.80 (br, 2H, NH_2).

^{13}C NMR (101 MHz, $CDCl_3$) δ 78.3 (CH), 72.8 (OCH_2), 71.9 (2 x OCH_2), 71.3 (2 x OCH_2), 70.8 (2 x OCH_2), 70.6 (2 x OCH_2), 70.5 (3 x OCH_2), 69.6 (OCH_2), 59.0 (2 x OCH_3), 41.6 (CH_2NH_2).

HRMS (TOF ES+): m/z$[M+H]^+$= 384.2596 (Calculated: 384.2597).

IR ν_{max}(film)/cm^{-1}: 2872 (br), 1633 (w), 1454 (w), 1353 (w), 1246 (w), 1078 (s, br), 976 (m), 864 (m), 692 (w).

N,N'-Bis(7-(2,5,8-trioxanonyl)-3,6,9,12,15-pentaoxahexadecyl)-3,4,9,1-perylene tetracarboxylic diimide (132 - BPDI)

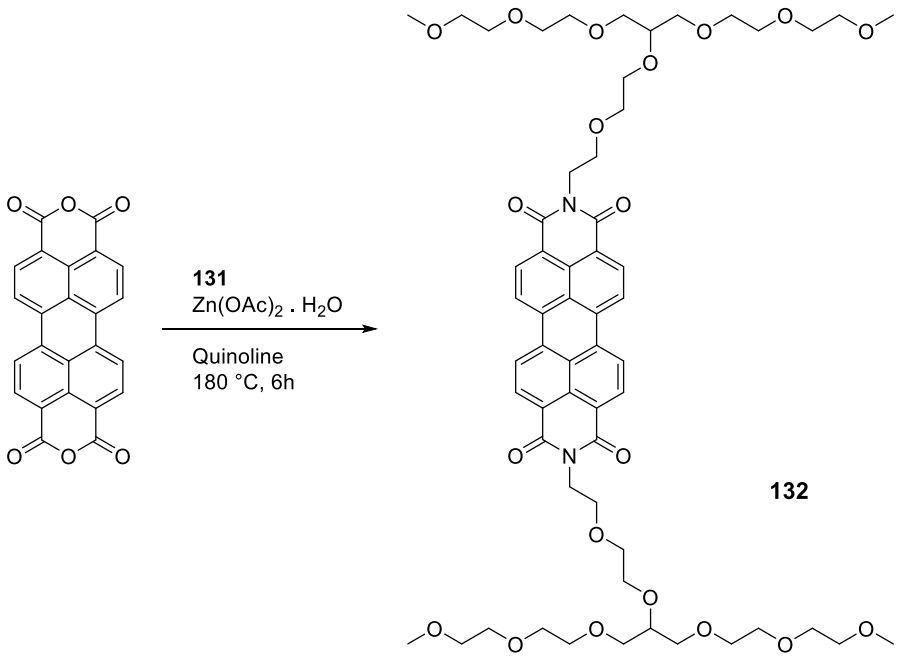

A novel compound. A solution of 3,4,9,10-perylenetetracarboxylic dianhydride (75 mg, 0.192 mmol), zinc acetate (35 mg, 0.192 mmol) and **131** (220 mg, 0.575 mmol) in quinoline (3 mL) was stirred at 180 °C for 6 h under argon. After cooling down to room temperature chloroform was added and the organic phase was washed with a 1 M aqueous solution of HCl (x4), brine, dried over $MgSO_4$ and the solvent was evaporated *in vacuo*. The crude was purified by preparative HPLC (C_{18}, Isocratic ACN:H_2O = 1:1) and **132** (BDPI) was obtained as a red solid in a 51% yield (109 mg).

^{1}H NMR (400 MHz, $CDCl_3$) δ 8.56 (d, *J* = 8.0 Hz, 4H, CH_{Ar}), 8.44 (d, *J* = 8.1 Hz, 4H, CH_{Ar}), 4.45 (t, *J* = 6.0 Hz, 4H, NCH_2), 3.85 (t, *J* = 6.0 Hz, 4H, CH_2), 3.78-3.72 (m, 8H, CH_2), 3.72-3.57 (m, 26H, CH_2), 3.57-3.45 (m, 16H, CH_2 +CH), 3.36 (s, 12H, OCH_3).

^{13}C NMR (101 MHz, $CDCl_3$) δ 163.4 (4 x C=O), 134.5 (4 x C_{Ar}), 131.4 (4 x CH_{Ar}), 129.4 (2 x C_{Ar}), 126.3 (2 x C_{Ar}), 123.3 (4 x C_{Ar}), 123.1 (4 x CH_{Ar}), 78.5 (2 x CH), 72.1 (4 x OCH_2), 71.4 (4 x OCH_2),

70.9 (4 x OCH_2), 70.7 (2 x OCH_2), 70.5 (2 x OCH_2), 69.9 (2 x OCH_2), 68.0 (2 x OCH_2), 59.2 (4 x OCH_3), 39.5 (2 x CH_2N).

MS (TOF ES+): m/z$[M+Na]^+$= 1145.46.

IR ν_{max}(film)/cm^{-1}: 2870 (br), 1693 (s), 1655 (s), 1593 (s), 1338 (m), 1100 (s), 810 (m), 746 (m).

7.5 Experimental procedures and analytical data for chapter five

Perylene-3,4,9,10-tetracarboxylic acid monoanhydride monopotassium carboxylate (102)

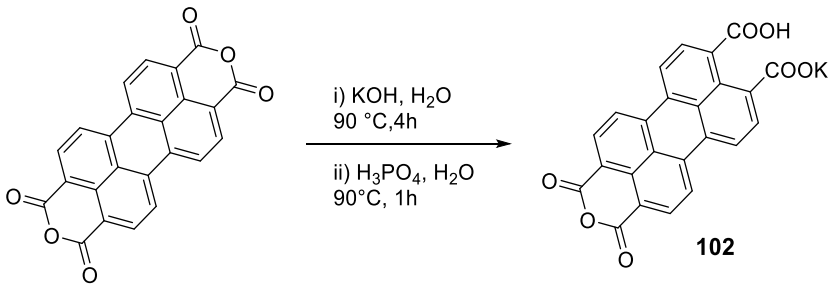

A known compound prepared according to the literature procedure.[198,221] A solution of perylene-3,4,9,10-tetracarboxylic anhydride (3.00 g, 7.65 mmol) in a 5% aq. KOH solution (35 mL) was heated at 90 °C for 4 h. After cooling down the reaction mixture to room temperature, a 10% aq. H_3PO_4 solution (12.5 mL) was added and stirred for 1 h at 90 °C. The resulting precipitate was filtrated and washed with water. The dark red solid was dried at 80 °C overnight. **097** was obtained in a 96% yield (3.29 g) and was used in the next step without further purification.

NMR spectra could not be recorded do to the insolubility of **102** in common solvents.

A mass spectra could not be obtained using MS ES+, ES-, LD+ or - (dithranol), AP + or - as the ionisation methods.

IR ν_{max}(film)/cm^{-1}: 3126 (w), 3066 (w), 1755 (br), 1721 (br), 1590 (s), 1507 (m), 1371 (w), 1300 (m), 1002 (m).

3,4,9,10-Perylenetetracarboxylic-3,4-anhydride-9,10-imide (133)

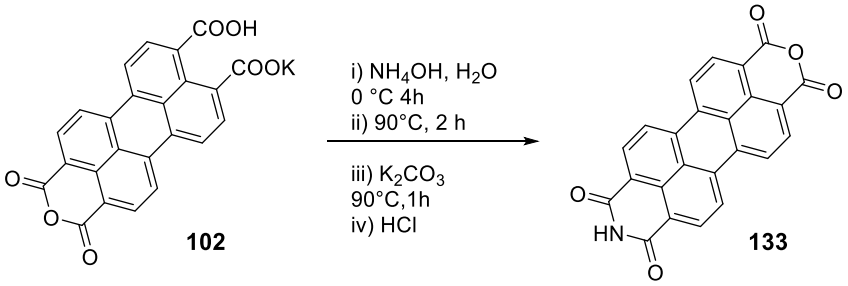

102 **133**

A known compound prepared according to the literature procedure.[198,221] A solution of **102** (2.00 g, 4.46 mmol) and a 35% ammonium hydroxide solution (2.5 mL) in water (100 mL) was stirred at 0-5 °C for 4 h. The reaction mixture was then stirred at 90 °C for another 2 h. A 25% aq. potassium carbonate solution (25 mL) was then added and the solution was further stirred for 1 h at 90 °C. After cooling it down to room temperature, the obtained precipitate was filtrated and washed with a 2% aq. potassium carbonate solution until the filtrate was colourless (*ca.* 150 mL). The residue was dissolved in a hot 3.5% aq. KOH solution and the reaction mixture was stirred at 70 °C for 5 min. After filtration *in vacuo*, the filtrate was acidified with a 10% aq. HCl solution until pH = 1. The precipitate was filtered *in vacuo* and washed with water. The dark red residue was dried in the oven (T = 80 °C) overnight and **133** was obtained as a dark red powder in a 18% yield (308 mg).

NMR spectra could not be recorded do to the insolubility of **133** in common solvents.

MS(LD-, dithranol): m/z[M-H]$^-$= 389.9.

IR ν_{max}(film)/cm^{-1}: 3536 (w, br), 3162 (w), 3034 (w, br), 2856 (w), 1680 (br), 1580 (br), 1315 (m), 1008 (br), 847 (m), 730 (m).

N-(3,6-dioxahexyl)-3,4,9,10-perylene-tetracarboxylic diimide (134)

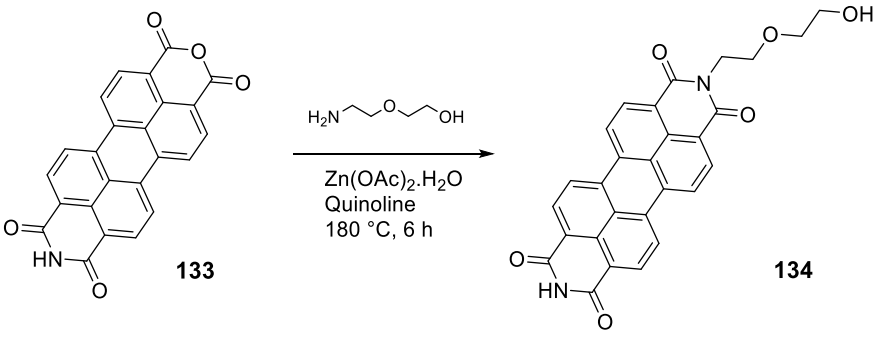

A novel compound. A solution of **133** (250 mg, 0.639 mmol), zinc diacetate monohydrate (59 mg, 0.320 mmol) and 2-(2-aminoethoxy)ethanol (95 µL, 0.959 mmol) in quinoline (4 mL) was heated at 180 °C for 6 h. After cooling down to room temperature, a 1 M aq. HCl solution was added and the solution was filtered *in vacuo*. The residue was washed with a 3.5% aq. KOH solution (to remove any residual starting material) and with water. After drying the residue overnight in an oven (T = 100 °C), **134** was afforded as a dark red powder (236 mg, 77%).

NMR spectra could not be recorded do to the insolubility of **134** in common solvents.

MS(LD-, dithranol): m/z[M-H]$^-$= 476.7.

IR ν_{max}(film)/cm^{-1}: 3503 (br), 3463 (br), 3150 (w), 3097 (w), 3032 (w), 2856 (w), 1685 (s), 1673 (s), 1650 (s), 1589 (s), 1574 (s), 1361 (m), 1332 (m), 1272 (m), 1117 (w), 1056 (w), 850 (br), 740 (w).

N-(3,6-dioxahexyl)-N'-[7-(2,5,8-trioxanonyl)-3,6,9,12,15-pentaoxahexadecyl]-3,4,9,10-perylene-tetracarboxylic diimide (135)

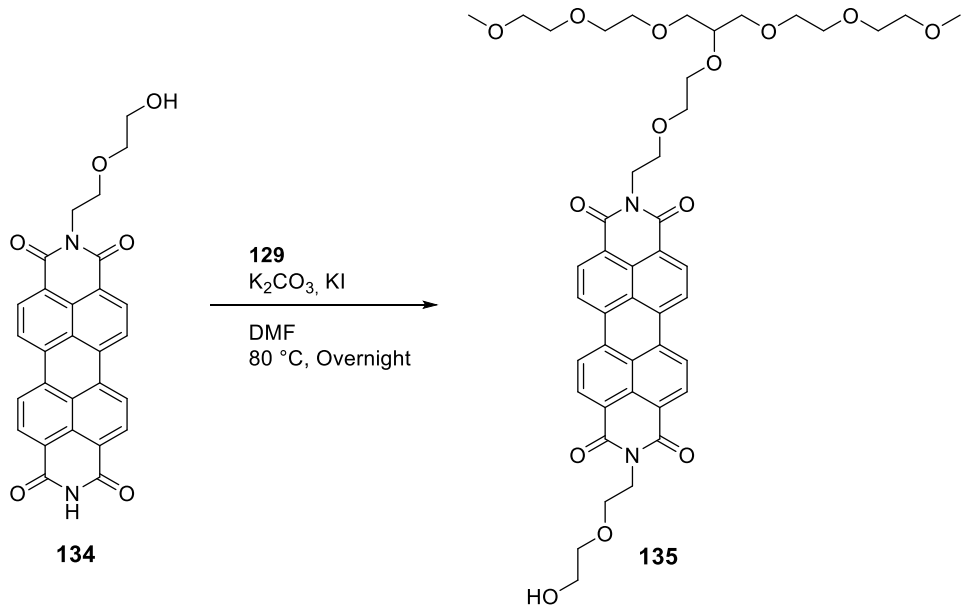

A new compound prepared according to a modified literature procedure.[161] A solution of **134** (200 mg, 0.42 mmol), **129** (374 mg, 0.84 mmol), K_2CO_3 (116 mg, 0.84 mmol) and KI (14 mg, 84 µmol) in dry DMF (10 mL) was stirred at 80 °C for 3 days under argon. Filtration through a pad of Celite (eluent: DCM) followed by precipitation from hexane afforded **135** as a dark red solid (185 mg, 58%). **135** was further purified by preparative HPLC (C_{18}, isocratic ACN:H_2O = 1:1).

^{1}H NMR (400 MHz, $CDCl_3$) δ 8.21 (br, 4H, CH_{Ar}), 7.90 (br, 4H, CH_{Ar}), 4.44-4.35 (m, 4H, OCH_2), 3.93 (t, *J* = 5.4 Hz, 2H, OCH_2), 3.85 (t, *J* = 6.0 Hz, 2H, OCH_2), 3.80-3.69 (m, 8H, OCH_2), 3.68-3.46 (m, 22H, OCH + OCH_2 + OH), 3.35 (s, 6H, OCH_3).

^{13}C NMR (101 MHz, $CDCl_3$) δ 163.2 (2 x C=O), 162.9 (2 x C=O), 133.8 (4 x C_{Ar}), 133.5 (4 x C_{Ar}), 130.9 (4 x CH_{Ar}), 128.7 (2 x C_{Ar}), 125.4 (2 x C_{Ar}), 122.7 (4 x CH_{Ar}), 78.5 (OCH), 72.5 (OCH_2), 72.1 (2 x OCH_2), 71.4 (2 x OCH_2), 70.9 (2 x OCH_2), 70.7 (2 x OCH_2), 70.6 (2 x OCH_2), 70.5 (OCH_2), 69.9 (OCH_2), 68.4 (OCH_2), 67.9 (OCH_2), 62.0 (OCH_2), 59.1 (2 x OCH_3), 39.9 (CH_2N), 39.5 (CH_2N).

HRMS (MS ES+): m/z[M+Na]$^+$= 867.3322 (Calculated: 867.3316).

IR ν_{max}(film)/cm^{-1}: 2869 (br), 1692 (s), 1646 (s), 1593 (s), 1439 (m), 1402 (m), 1362 (m), 1344 (m), 1247 (m), 1093 (br), 809 (s), 744 (s).

4,4'-Bis(4-dodecylphenyl)benzyl (136a)

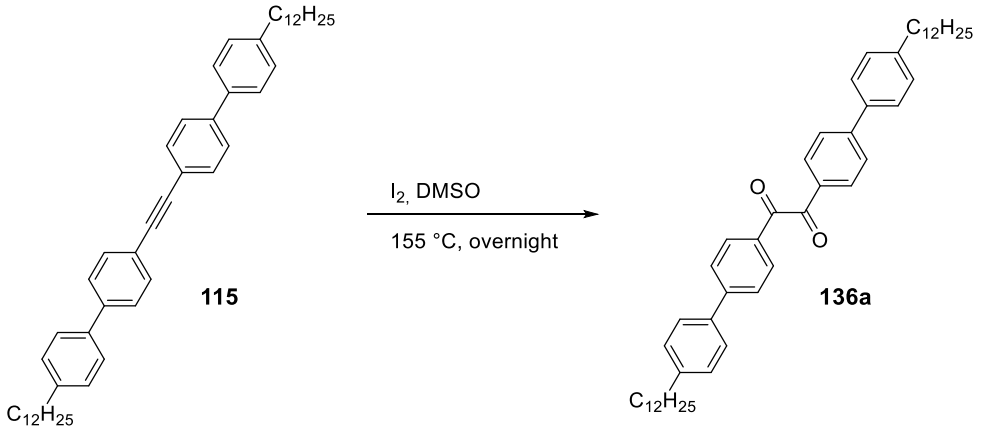

A novel compound prepared according to a literature procedure.[142] A solution of **115** (300 mg, 0.45 mmol) and I_2 (57 mg, 0.225 mmol) in DMSO (3 mL) was stirred overnight at 155 °C under argon. A 4% aq. solution of $NaSO_3$ was then added and the reaction mixture was stirred at room temperature for 0.5 h. The solution was extracted with petroleum ether (x3). The combined organic phases were washed with water (x3), brine, dried over $MgSO_4$ and the solvent was evaporated *in vacuo*. **136a** was obtained as a yellow solid (241 mg, 77%).

^{1}H NMR (400 MHz, $CDCl_3$) δ 8.07 (d, *J* = 8.5 Hz, 4H, CH_{Ar}), 7.74 (d, *J* = 8.5 Hz, 4H, CH_{Ar}), 7.56 (d, *J* = 8.3 Hz, 4H, CH_{Ar}), 7.30 (d, *J* = 8.2 Hz, 4H, CH_{Ar}), 2.66 (m, 4H, CH_2), 1.72-1.60 (m, 4H, CH_2), 1.47-1.21 (m, 36H, CH_2), 0.89 (t, *J* = 6.7 Hz, 6H, CH_3).

^{13}C NMR (101 MHz, $CDCl_3$) δ 194.3 (2 x C=O), 147.7 (2 x C_{Ar}), 143.9 (2 x C_{Ar}), 136.9 (2 x C_{Ar}), 131.6 (2 x C_{Ar}), 130.6 (4 x CH_{Ar}), 129.2 (4 x CH_{Ar}), 127.5 (4 x CH_{Ar}), 127.3 (4 x CH_{Ar}), 35.8 (2 x CH_2),

32.1 (2 x CH_2), 31.5 (2 x CH_2), 29.8 (4 x CH_2), 29.8 (2 x CH_2), 29.7 (2 x CH_2), 29.6 (2 x CH_2), 29.5 (4 x CH_2), 22.8 (2 x CH_2), 14.3 (2 x CH_3).

HRMS (TOF ES+): m/z$[M+Na]^+$= 721.4974 (Calculated: 721.4961).

IR ν_{max}(film)/cm^{-1}: 2919 (s), 2850 (s), 1659 (s), 1601 (s), 1467 (m), 1220 (m), 1181 (s), 1004 (m), 881 (m).

4,4'-Dibromobenzil (136b)

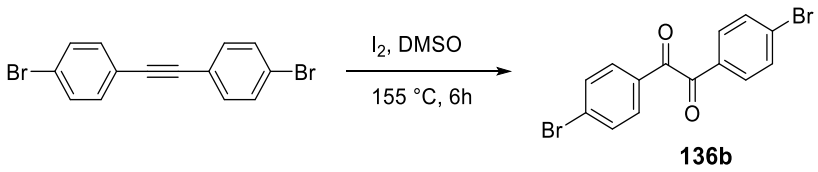

136b

A known compound prepared according to the literature procedure.[222] A solution of bis(4-bromophenyl)acetylene (1.500 g, 4.46 mmol), and iodine (566 mg, 2.23 mmol) in DMSO (7.5 mL) was stirred at 155 °C for 6 h. The reaction mixture was then cooled down to room temperature and a 1% aq. solution of $Na_2S_2O_4$ (100 mL) was added. The resulting yellow crystals were filtrated and washed with water. Recrystallisation from dioxane afforded **136b** as yellow crystals (1.06 g, 65%).

^{1}H NMR (400 MHz, $CDCl_3$) δ 7.90-7.78 (m, 4H, CH_{Ar}), 7.76-7.63 (m, 4H, CH_{Ar}).

^{13}C NMR (101 MHz, $CDCl_3$) δ 192.7 (2 x C=O), 132.7 (4 x CH_{Ar}), 131.7 (2 x C_{Ar}), 131.4 (4 x CH_{Ar}), 130.9 (2 x C_{Ar}).

HRMS (MS AP+): m/z$[M+H]^+$= 368.8946 (Calculated: 368.8949 for $C_{14}H_9O_2{}^{79}Br^{81}Br$).

IR ν_{max}(film)/cm^{-1}: 3093 (w), 1660 (s), 1585 (s), 1568 (s), 1482 (m), 1397 (m), 1207 (m), 1172 (m), 1069 (m), 1007 (m), 830 (s).

1,3-Bis(4-bromophenyl)propan-2-one (137)

137

A known compound prepared according to the literature procedure.[223] A solution of *p*-bromophenylacetic acid (5.00 g, 23.3 mmol) in dry DCM (50 mL) was added to a solution of DCC (4.8 g, 23.3 mmol) and DMAP (709 mg, 5.8 mmol) in dry DCM (50 mL) under argon. The reaction mixture was stirred at room temperature for 24 h under argon. The resulting precipitate was removed by filtration and the filtrate was evaporated *in vacuo*. The solid was recrystallized from methanol to afford **137** as a light orange solid (1.94 g, 45%).

^{1}H NMR (400 MHz, $CDCl_3$) δ 7.45 (d, *J* = 8.4 Hz, 4H, CH_{Ar}), 7.01 (d, *J* = 8.3 Hz, 4H, CH_{Ar}), 3.68 (s, 4H, CH_2).

^{13}C NMR (101 MHz, $CDCl_3$) δ 204.4 (C=O), 132.7 (2 x C_{Ar}), 132.0 (4 x CH_{Ar}), 131.3 (4 x CH_{Ar}), 121.4 (2 x C_{Ar}), 48.6 (2 x CH_2).

HRMS (TOF ES+): m/z$[M+Na]^+$= 390.9122 (Calculated: 390.9132).

IR ν_{max}(film)/cm^{-1}: 2886 (w), 1716 (s),1487 (s), 1056 (s), 1011 (s), 791 (m).

2,2-Bis(4-Bromophenylmethyl)dioxolane (138)

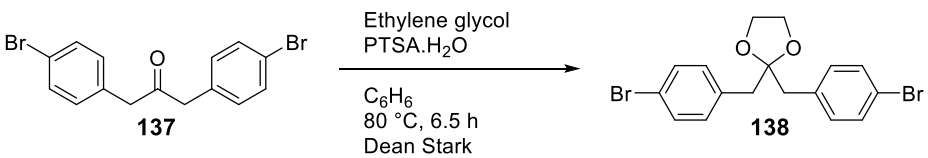

137 **138**

A known compound prepared according to a modified literature procedure.[142] A solution of **137** (534 mg, 1.45 mmol) and *p*-toluenesulfonic acid monohydrate (55 mg, 0.29 mmol, 20 mol%) in benzene (25 mL) was heated at reflux using a Dean Stark apparatus for 6.5 h. After

cooling down the reaction mixture to room temperature, the solvent was evaporated *in vacuo*. Chloroform was added, and the organic phase was washed with water, brine, dried over $MgSO_4$ and the solvent was evaporated *in vacuo*. **138** was obtained as white crystals (538 mg, 90%).

^{1}H NMR (400 MHz, $CDCl_3$) δ 7.41-7.37 (m, 4H, CH_{Ar}), 7.15-7.11 (m, 4H, CH_{Ar}), 3.44 (s, 4H, CH_2), 2.86 (s, 4H, CH_2).

^{13}C NMR (101 MHz, $CDCl_3$) δ 135.5 (2 x C_{Ar}), 132.6 (4 x CH_{Ar}), 131.1 (4 x CH_{Ar}), 120.7 (2 x C_{Ar}), 110.5 (C_{Ar}), 65.7 (2 x CH_2), 44.2 (2 x CH_2).

HRMS (MS AP+): m/z$[M+H]^+$= 410.9593 (Calculated: 410.9595).

IR ν_{max}(film)/cm^{-1}: 1486 (s), 1180 (s), 1041 (s), 1012 (s), 955 (m), 832 (m), 819 (m), 786 (s), 729 (m), 658 (m).

2,2-Bis[(4'-dodecylbiphenyl-4-yl)methyl]dioxolane (139)

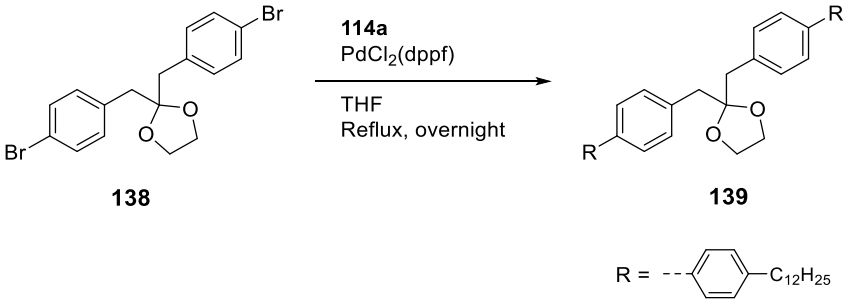

A novel compound prepared according to a literature procedure.[142] 4-Dodecylphenylmagnesium bromide **114a** (freshly prepared, 0.44 M, 8 mL) was added to a solution of **138** (1.14 g, 3.51 mmol) in dry THF (7 mL) under argon. $PdCl_2$(dppf) (61 mg, 0.075 mmol) was added and the reaction mixture was stirred at reflux overnight under argon.

After evaporation of the solvent *in vacuo*, the crude was purified by column chromatography (SiO_2, Hexane:EtOAc = 95:5 to 90:10) to afford **139** as a light yellow solid (512 mg, 74%).

^{1}H NMR (400 MHz, $CDCl_3$) δ 7.43 (dd, *J* = 8.2, 2.0 Hz, 8H, CH_{Ar}), 7.26 (d, *J* = 8.1 Hz, 4H, CH_{Ar}), 7.14 (d, *J* = 8.1 Hz, 4H, CH_{Ar}), 3.42 (s, 4H, OCH_2), 2.91 (s, 4H, OCH_2), 2.54 (d, *J* = 7.5 Hz, 4H, CH_2), 1.59-1.50 (m, *J* = 14.5, 7.0 Hz, 4H, CH_2), 1.33-1.10 (m, 36H, CH_2), 0.80 (t, *J* = 6.8 Hz, 6H, CH_3).

^{13}C NMR (101 MHz, $CDCl_3$) δ 142.0 (2 x C_{Ar}), 139.2 (2 x C_{Ar}), 138.4 (2 x C_{Ar}), 135.5 (2 x C_{Ar}), 131.3 (4 x CH_{Ar}), 128.9 (4 x CH_{Ar}), 126.9 (4 x CH_{Ar}), 126.5 (4 x CH_{Ar}), 111.1 (C_{Ar}), 65.6 (2 x OCH_2), 44.4 (2 x OCH_2), 35.8 (2 x CH_2), 32.1 (2 x CH_2), 31.7 (2 x CH_2), 29.8 (4 x CH_2), 29.8 (2 x CH_2), 29.8 (2 x CH_2), 29.7 (2 x CH_2), 29.5 (4 x CH_2), 22.8 (2 x CH_2), 14.3 (2 x CH_3).

HRMS (MS AP+): m/z$[M+H]^+$= 743.7.

IR ν_{max}(film)/cm^{-1}: 2917 (s,br), 2848 (s), 1499 (m), 1468 (m), 1312 (m), 1179 (m), 1030 (m), 1005 (m), 832 (m), 784 (m), 719 (m).

1,3-Bis(4'-dodecylbiphenyl-4-yl)propan-2-one (140)

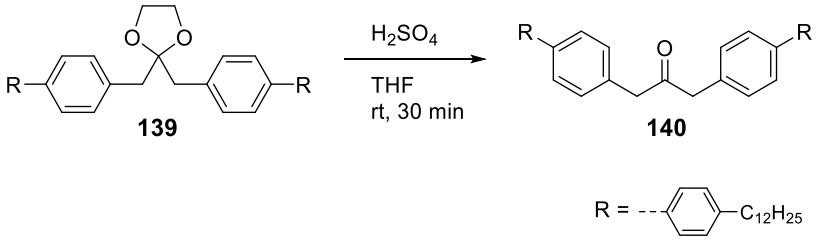

A novel compound prepared according to a modified literature procedure.[142] To a solution of **139** (198 mg, 0.266 mmol) in THF (5 mL) was added dropwise conc. sulphuric acid (4 mL). The mixture was vigorously stirred at room temperature. After 30 min, water was added to the dark orange solution. The reaction mixture was extracted with toluene (x3). The combined

organic phases were washed with water, brine, dried over $MgSO_4$ and the solvent was evaporated *in vacuo*. **140** was afforded as a light yellow solid (149 mg, 80%).

^{1}H NMR (400 MHz, $CDCl_3$) δ 7.54 (d, *J* = 8.2 Hz, 4H, CH_{Ar}), 7.50 (d, *J* = 8.2 Hz, 4H, CH_{Ar}), 7.28-7.19 (m, 8H, CH_{Ar}), 3.79 (s, 4H, CH_2CO), 2.64 (t, *J* = 7.7 Hz, 4H, CH_2), 1.73-1.59 (m, 4H, CH_2), 1.41-1.18 (m, 36H, CH_2), 0.88 (t, *J* = 6.7 Hz, 6H, CH_3).

^{13}C NMR (101 MHz, $CDCl_3$) δ 205.9 (C=O), 142.4 (2 x C_{Ar}), 140.2 (2 x C_{Ar}), 138.1 (2 x C_{Ar}), 132.8 (2 x C_{Ar}), 130.0 (4 x CH_{Ar}), 129.0 (4 x CH_{Ar}), 127.4 (4 x CH_{Ar}), 127.0 (4 x CH_{Ar}), 49.0 (2 x $CH_{2\text{-benzylic}}$), 35.8 (2 x CH_2), 32.1 (2 x CH_2), 31.7 (2 x CH_2), 29.8 (2 x CH_2), 29.8 (2 x CH_2), 29.8 (2 x CH_2), 29.7 (2 x CH_2), 29.5 (4 x CH_2), 22.9 (2 x CH_2), 14.3 (2 x CH_3).

2,3,4,5-tetrakis(4'-dodecylbiphenyl-4-yl)cyclopentadienone (141)

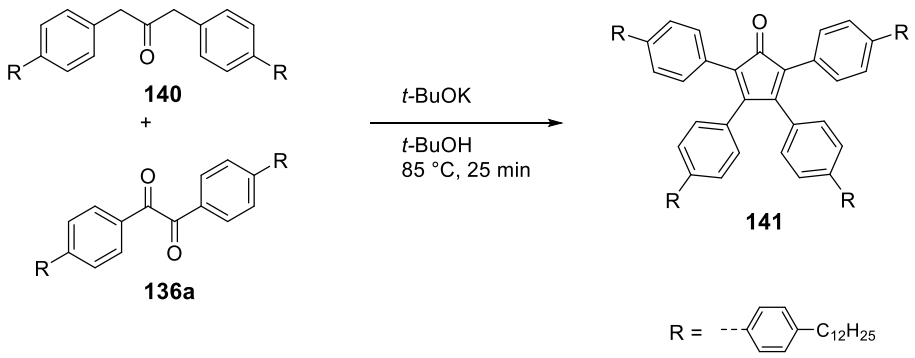

A novel compound. A solution of **140** (100 mg, 143 µmol), **136a** (100 mg, 143 µmol) and *t*-BuOK (16 mg, 143 µmol) in *t*-BuOH (10 mL) was stirred at 85 °C for 25 min under argon. The solvent was removed *in vacuo* and the crude was purified by column chromatography (SiO_2, hexane:DCM = 7:3) to afford **141** as a dark red powder (42 mg, 22%).

^{1}H NMR (400 MHz, $CDCl_3$) δ 7.54-7.44 (m, 16H, CH_{Ar}), 7.37 (d, *J* = 8.4 Hz, 4H, CH_{Ar}), 7.23 (d, *J* = 8.3 Hz, 8H, CH_{Ar}), 7.07 (d, *J* = 8.4 Hz, 4H, CH_{Ar}), 2.63 (t, *J* = 7.7 Hz, 8H, CH_2), 1.69-1.59 (m, 8H, CH_2), 1.45-1.07 (m, 72H, CH_2), 0.93-0.83 (m, 12H, CH_3).

^{13}C NMR (101 MHz, $CDCl_3$) δ 200.6 (C=O), 154.2 (2 x C_{Ar}), 142.8 (2 x C_{Ar}), 142.4 (2 x C_{Ar}), 141.1 (2 x C_{Ar}), 140.1 (2 x C_{Ar}), 138.1 (2 x C_{Ar}), 137.5 (2 x C_{Ar}), 131.9 (2 x C_{Ar}), 130.7 (4 x CH_{Ar}), 130.2 (4 x CH_{Ar}), 129.7 (2 x C_{Ar}), 129.1 (4 x CH_{Ar}), 129.0 (4 x CH_{Ar}), 126.9 (4 x CH_{Ar}), 126.9 (4 x CH_{Ar}), 126.7 (4 x CH_{Ar}), 126.4 (4 x CH_{Ar}), 125.2 (2 x C_{Ar}), 35.8 (4 x CH_2), 32.1 (4 x CH_2), 31.6 (4 x CH_2), 29.8 (8 x CH_2), 29.8 (4 x CH_2), 29.8 (4 x CH_2), 29.7 (4 x CH_2), 29.5 (4 x CH_2), 29.5 (4 x CH_2), 22.9 (4 x CH_2), 14.3 (4 x CH_3).

2,3,4,5-Tetrakis(4-bromophenyl)cyclopentadienone (142)

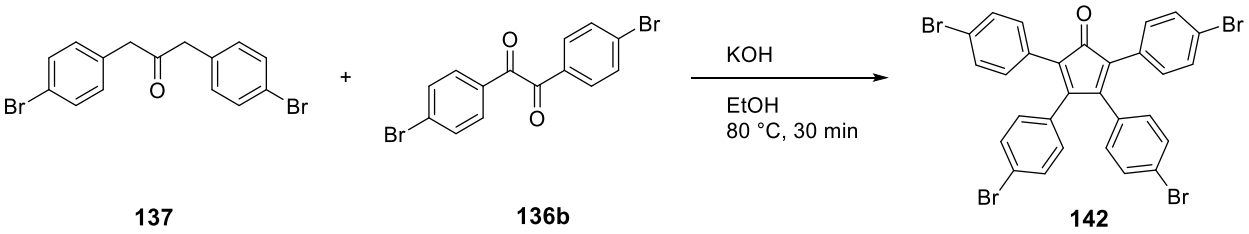

137 **136b** **142**

A known compound prepared according to the literature procedure.[224] To a solution of **137** (310 mg, 0.84 mmol) and **136b** (310 mg, 0.84 mmol) in ethanol (3 mL) was added a solution of KOH (47 mg, 0.84 mmol) in ethanol (0.5 mL). The reaction mixture was stirred at reflux for 40 min. The dark red solution was then cooled down to 0 °C. The resulting dark red precipitate was filtered and washed with cold ethanol, affording **142** as dark red crystals (365 mg, 62%).

^{1}H NMR (400 MHz, $CDCl_3$) δ 7.43-7.34 (m, 8H, CH), 7.09-7.03 (m, 4H, CH), 6.80-6.74 (m, 4H, CH).

^{13}C NMR (101 MHz, $CDCl_3$) δ 198.9 (C=O), 153.2 (2 x C_{Ar}), 131.9 (4 x CH_{Ar}), 131.7 (8 x CH_{Ar}), 131.3 (2 x C_{Ar}), 130.9 (4 x CH_{Ar}), 129.1 (2 x C_{Ar}), 125.1 (2 x C_{Ar}), 123.7 (2 x C_{Ar}), 122.6 (2 x C_{Ar}).

HRMS (MS AP+): m/z$[M+H]^+$= 700.7979 (Calculated: 700.7972 for $C_{29}H_{17}O^{79}Br_2{}^{81}Br_2$).

IR ν_{max}(film)/cm^{-1}: 1710 (s), 1583 (m), 1482 (m), 1073 (m), 1008 (s), 761 (s).

4-Bromo-4'-hexyloxybiphenyl (143)

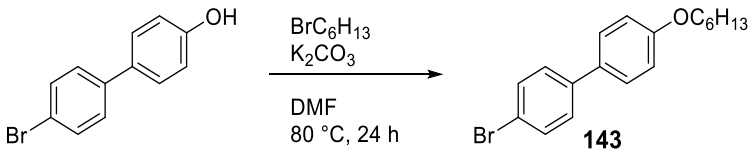

A solution of 4-bromo-4'-hydroxybiphenyl (2.00g, 8.03 mmol), K_2CO_3 (2.22 g, 16.06 mmol) and 1-bromohexane (1.55 g, 9.3 mmol) in DMF (50 mL) was stirred at 80 °C for 24 h. The solvent was evaporated *in vacuo* and the resulting dough filtrated though a pad of Celite (eluent = DCM). After evaporation of the solvent *in vacuo*, the light brown solid was recrystallised from methanol and **143** was afforded as an off-white solid (2.12 g, 79%).

^{1}H NMR (400 MHz, $CDCl_3$) δ 7.55-7.50 (m, 2H, CH_{Ar}), 7.50-7.45 (m, 2H, CH_{Ar}), 7.44-7.39 (m, 2H, CH_{Ar}), 7.00-6.92 (m, 2H, CH_{Ar}), 3.99 (t, *J* = 6.6 Hz, 2H, OCH_2), 1.87-1.73 (m, 2H, CH_2), 1.54-1.42 (m, 2H, CH_2), 1.42-1.29 (m, 4H, CH_2), 0.97-0.86 (m, 3H, CH_3).

^{13}C NMR (101 MHz, $CDCl_3$) δ 159.1 (C_{Ar}), 140.0 (C_{Ar}), 132.4 (C_{Ar}), 131.9 (2 x CH_{Ar}), 128.4 (2 x CH_{Ar}), 128.1 (2 x CH_{Ar}), 120.8 (C_{Ar}), 115.0 (2 x CH_{Ar}), 68.3 (OCH_2), 31.8 (CH_2), 29.4 (CH_2), 25.9 (CH_2), 22.8 (CH_2), 14.2 (CH_3).

HRMS (MS AP+): m/z$[M+H]^+$= 333.0820 (Calculated: 333.0854 for $C_{18}H_{22}O^{79}Br$).

IR ν_{max}(film)/cm^{-1}: 2955 (m), 2928 (br, m), 2868 (m), 1604 (m), 1521 (w), 1481 (m), 1473 (m), 1393 (w), 1286 (m), 1251 (m), 1197 (m), 1030 (m), 996 (m),803 (br, s).

Bis(4-methoxybiphen-4'-yl)acetylene (145)

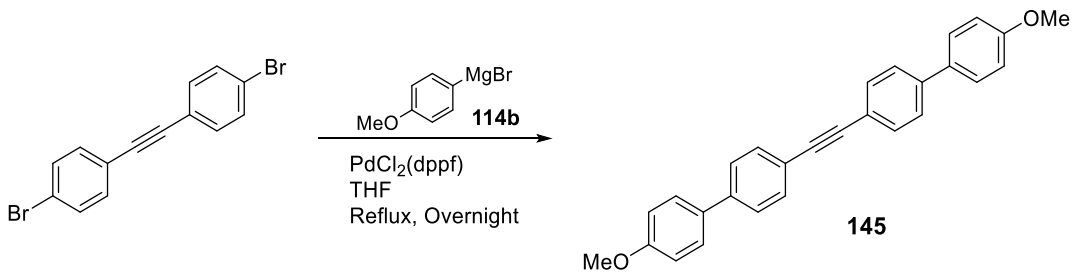

A known compound prepared according to a modified literature procedure.[175] To a solution of bis(4-bromophenyl)acetylene (567 mg, 1.69 mmol) in dry THF (40 mL) was added a freshly prepared solution of 4-methoxyphenylmagnesium bromide **114b** (6.8 mmol) in dry THF (15 mL). $PdCl_2$(dppf) (110 mg, 0.14 mmol) was then added and the reaction mixture was stirred at reflux overnight under argon. The solution was then cooled to room temperature. The resulting white precipitate was then filtered *in vacuo* and washed with methanol and petroleum ether. **145** was obtained as an off-white solid (528 mg, 80%).

^{1}H NMR (400 MHz, $C_2Cl_4D_2$, 80 °C) δ 7.67 – 7.57 (m, 12H), 7.08 – 7.00 (m, 4H), 3.90 (s, 6H).

^{13}C NMR (101 MHz, $C_2Cl_4D_2$, 80 °C) δ 159.5 (2 x C_{Ar}), 140.4 (2 x C_{Ar}), 132.7 (2 x C_{Ar}), 131.9 (4 x CH_{Ar}), 127.9 (4 x CH_{Ar}), 126.3 (4 x CH_{Ar}), 121.5 (2 x C_{Ar}), 114.5 (4 x CH_{Ar}), 90.0 (C≡C), 55.3 (2 x OCH_3).

MS (MS AP+): m/z$[M+H]^+$= 391.1.

IR ν_{max}(film)/cm^{-1}: 3042 (w), 2961 (w), 2840 (w), 2047 (w), 1924 (w), 1893 (w), 1602 (m), 1499 (m), 1288 (m), 1250 (m), 1163 (m), 1036 (m), 823 (s), 814 (s), 797 (m), 669 (m).

1,2,3,4-Tetrakis(4'-bromophenyl)-5,6-di(4'-methoxybiphenyl-4-yl)benzene (149)

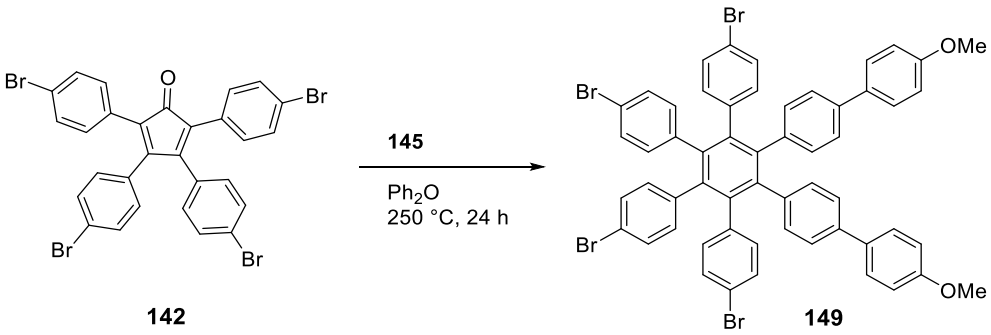

A new compound prepared according to a modified literature procedure.[205] A solution of **142** (179 mg, 0.256 mmol) and **145** (127 mg, 0.325 mmol) in degassed diphenyl ether (0.75 mL) was stirred at 250 °C for 24 h under argon. The crude was purified by column chromatography (SiO_2, dry load, Hexane:EtOAc = 8:2) to afford **149** as a pale yellow solid (193 mg, 71%).

^{1}H NMR (400 MHz, $CDCl_3$) δ 7.37 (d, *J* = 8.8 Hz, 4H, CH_{Ar}), 7.13-7.01 (m, 12H, CH_{Ar}), 6.87 (d, *J* = 8.8 Hz, 4H, CH_{Ar}), 6.80 (d, *J* = 8.3 Hz, 4H, CH_{Ar}), 6.70-6.63 (m, 8H, CH_{Ar}), 3.80 (s, 6H, OCH_3).

^{13}C NMR (101 MHz, $CDCl_3$) δ 159.2 (2 x C_{Ar}), 140.9 (2 x C_{Ar}), 139.7 (2 x C_{Ar}), 139.2 (4 x C_{Ar}), 139.0 (2 x C_{Ar}), 138.3 (2 x C_{Ar}), 137.8 (2 x C_{Ar}), 133.1 (2 x C_{Ar}), 132.9 (4 x CH_{Ar}), 132.8 (4 x CH_{Ar}), 131.7 (4 x CH_{Ar}), 130.5 (4 x CH_{Ar}), 130.4 (4 x CH_{Ar}), 127.9 (4 x CH_{Ar}), 125.2 (4 x CH_{Ar}), 120.3 (2 x C_{Ar}), 120.1 (2 x C_{Ar}), 114.2 (4 x CH_{Ar}), 55.5 (2 x OCH_3).

IR ν_{max}(film)/cm^{-1}: 3037 (w), 2835 (w), 1900 (w), 1608 (m), 1492 (s), 4687 (m), 1289 (m), 1245 (s), 1176 (m), 1011 (s), 821 (s), 762 (s), 715 (m).

MS (MS ES+): m/z$[M+Na]^+$= 1080.9.

1,2,3,4-(4'-Dodecylphenyl)-5,6-(4'-methoxyphenyl)benzene (150)

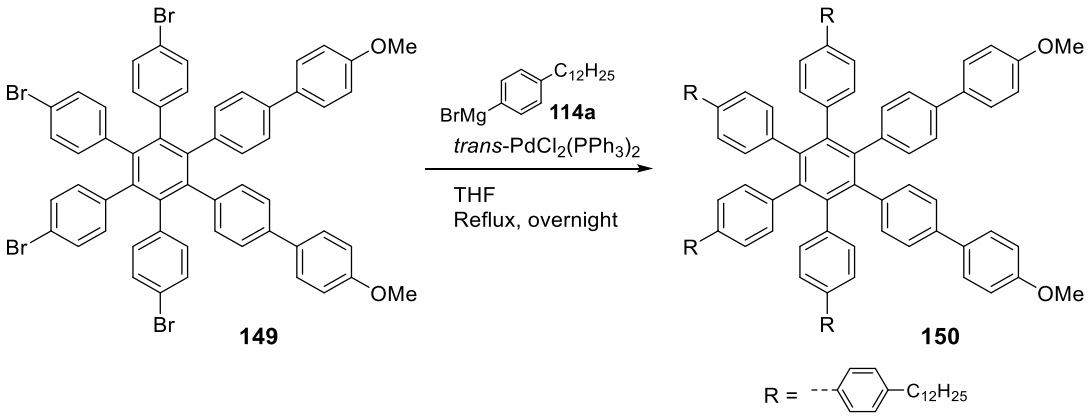

A new compound prepared according to a modified literature procedure.[225] To a solution of **149** (400 mg, 0.376 mmol) and *trans*-$PdCl_2(PPh_3)_2$ (11 mg, 15 µmol) in dry THF (7 mL) was added a freshly prepared solution of 4-dodecylbenzene magnesium bromide **114a** (3.76 mmol) in dry THF (8 mL). The reaction mixture was stirred at reflux overnight under argon. After evaporation of the solvent *in vacuo*, the crude was dissolved in the minimum amount of DCM and methanol was added. The resulting precipitate was filtered and washed with methanol. Purification by column chromatography (SiO_2, dry load, hexane:EtOAc = 9:1) afforded **150** as a waxy yellow solid (281 mg, 43%).

^{1}H NMR (400 MHz, $CDCl_3$) δ 7.41-7.33 (m, 12H, CH_{Ar}), 7.21-7.10 (m, 20H, CH_{Ar}), 7.00-6.94 (m, 12H, CH_{Ar}), 6.86 (d, *J* = 8.9 Hz, 4H, CH_{Ar}), 3.80 (s, 6H, OCH_3), 2.59 (t, *J* = 7.7 Hz, 8H, CH_2), 1.60 (t, *J* = 7.5 Hz, 8H, CH_2), 1.39-1.21 (m, 72H, CH_2), 0.91 (t, *J* = 6.8 Hz, 12H, CH_3).

^{13}C NMR (101 MHz, $CDCl_3$) δ 159.0 (2 x C_{Ar}OMe), 141.8 (4 x C_{Ar}), 140.5 (6 x C_{Ar}), 139.6 (2x C_{Ar}), 139.6 (2 x C_{Ar}), 139.3 (2 x C_{Ar}), 138.1 (4 x C_{Ar}), 137.6 (4 x C_{Ar}), 137.3 (2 x C_{Ar}), 133.5 (2 x C_{Ar}), 132.1 (12 x CH_{Ar}), 128.7 (8 x CH_{Ar}), 127.9 (4 x CH_{Ar}), 126.7 (8 x CH_{Ar}), 125.2 (8 x CH_{Ar}), 125.0 (4 x CH_{Ar}), 114.1 (4 x CH_{Ar}), 55.4 (2 x OCH_3), 35.7 (4 x CH_2), 32.9 (4 x CH_2), 31.7 (4 x CH_2), 29.8

(4 x CH_2), 29.8 (8 x CH_2), 29.8 (4 x CH_2), 29.7 (4 x CH_2), 29.5 (4 x CH_2), 29.5 (4 x CH_2), 22.9 (4 x CH_2), 14.3 (4 x CH_3).

MS (LD+, Nicotinic acid): m/z$[M+H]^+$= 1724.0; $[M+Na]^+$= 1747.1.

IR ν_{max}(film)/cm^{-1}: 3026 (w), 2921(s), 2854 (s), 1608 (m), 1499 (s), 1465 (m), 1289 (m), 1247 (s), 1177 (m), 1005 (m), 822 (s, br), 774 (s).

1,4,7,10-Tetrakis(4'-dodecylphenyl)-13,16-bis(4'-methoxyphenyl)hexa-*peri*-hexabenzocoronene (152)

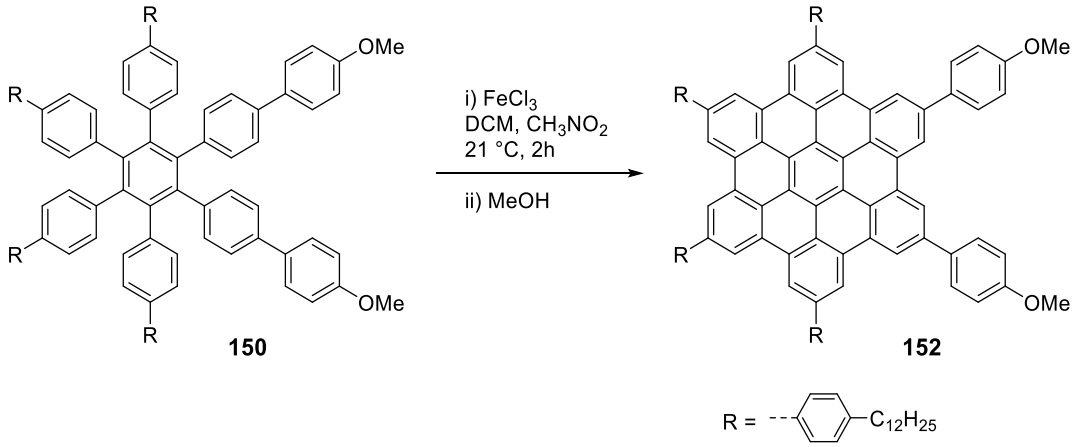

A new compound prepared according to a modified literature procedure.[175] To a solution of **150** (175 mg, 101 µmol) in anhydrous DCM (140 mL) and under a constant flux of argon was added a solution of anhydrous $FeCl_3$ (737 mg, 4.5 mmol) in CH_3NO_2 (18 mL). The reaction mixture was stirred at 21 °C for 2 h under a constant flux of argon. Methanol (150 mL) was then added to quench the reaction. The white precipitate was filtrated *in vacuo* and washed with methanol. **152** was obtained as a yellow solid in a 96% yield (166 mg) and was used in the next step without further purification.

NMR spectra could not be recorded do to the aggregation of **152**.

MS (LD+, Nicotinic acid): m/z$[M+H]^+$= 1712.0.

IR ν_{max}(film)/cm^{-1}: 2921 (s), 2851 (s), 1608 (m), 1513 (s), 1463 (m), 1371 (m), 1281 (w), 1245 (s), 1177 (m), 1037 (m), 872 (m), 827 (s, br), 720 (m).

1,4,7,10-Tetrakis(4'-dodecylphenyl)-13,16-bis(4'-hydroxyphenyl)hexa-*peri*-hexabenzocoronene (153)

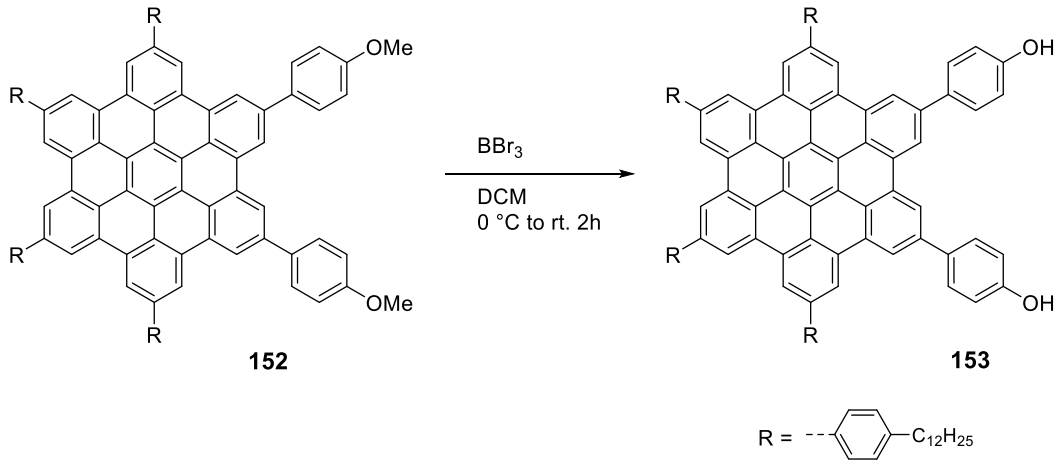

A new compound prepared according to a modified literature procedure.[225] To a solution of **105** (50 mg, 29 µmol) in anhydrous DCM (2 mL) was added 2 drops of BBr_3 at 0 °C. The reaction mixture was stirred for 1 h at 0 °C under argon. The black solution was brought back to room temperature and stirred overnight. Water was added to quench the residual BBr_3 and the reaction mixture was poured into methanol. The resulting precipitate was filtrated *in vacuo* and washed with methanol. **106** was obtained as a yellow solid in a quantitative yield and was used in the next step with no further purification.

NMR spectra could not be recorded do to the aggregation of **153**.

MS (LD+, retinoic acid): m/z$[M]^+$= 1683.0.

154

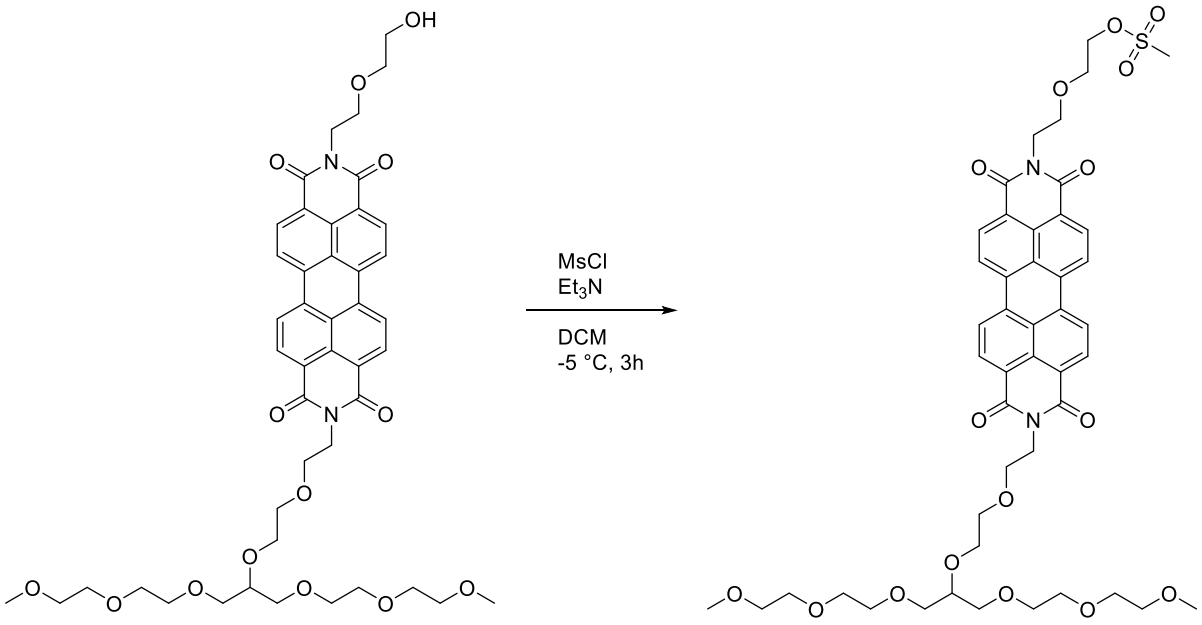

To a solution of **135** (101 mg, 119 µmol) and triethylamine (120 mg, 1.18 mmol) in DCM (2 mL) was added a solution of mesyl chloride (96 mg, 838 µmol) in DCM (2 mL) at -5 °C. After 3 h stirring, the dark red solution was washed with water, brine, dried over $MgSO_4$ and the solvent was evaporated *in vacuo*. The resulting oil was used in the next step with no further purification.

HBC-BPDI (155)

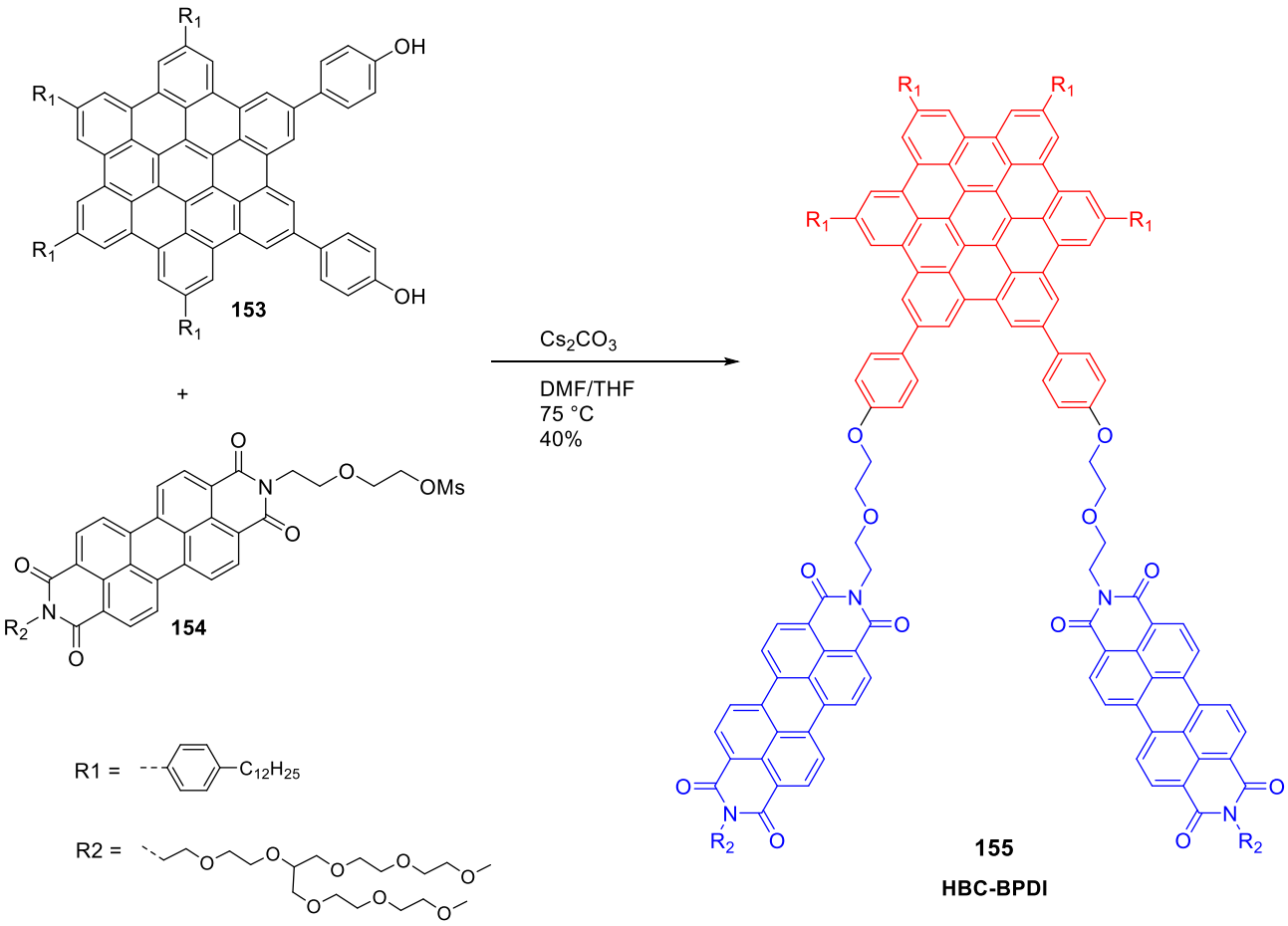

A solution of **153** (50 mg, 30 µmol), the freshly prepared **154** (119 µmol) and Cs_2CO_3 (39 mg, 119 µmol) in DMF:THF = 1:4 (5 mL) was stirred at 75 °C for 2.5 days under argon. The reaction mixture was further stirred at 90 °C for additional 24 h. DCM and water were added and the reaction mixture was extracted with DCM (x3). The combined organic phases were washed with water (x2), brine, dried over $MgSO_4$ and the solvent was evaporated *in vacuo*. The resulting dark red solid was purified by column chromatography (Sephadex LH-20, THF:MeOH = 9:1). The solvent was evaporated *in vacuo*. The solid was dissolved in the minimum amount of THF and recrystallised from ACN, affording **155** as a dark red solid (40 mg, 40%).

NMR characterisation in $CDCl_3$ (ambient temperature) or *p*-$C_6D_4Cl_2$ (85 °C) of **155** showed very broad peaks which could not be attributed and are due to the strong aggregation of HBC-BPDI.

MS (LD+, dithranol): m/z$[M+Na]^+$= 3358.4.

IR ν_{max}(film)/cm^{-1}: 2922 (s), 2852 (s), 1694 (s), 1657 (s), 1607 (m), 1594 (s), 1514 (s), 1439 (m), 1403 (w), 1364 (m), 1343 (m), 1248 (w), 1175 (w), 1094 (br), 1018 (br), 874 (w), 830 (w), 808 (m), 745 (m).

7.6 HLPC traces

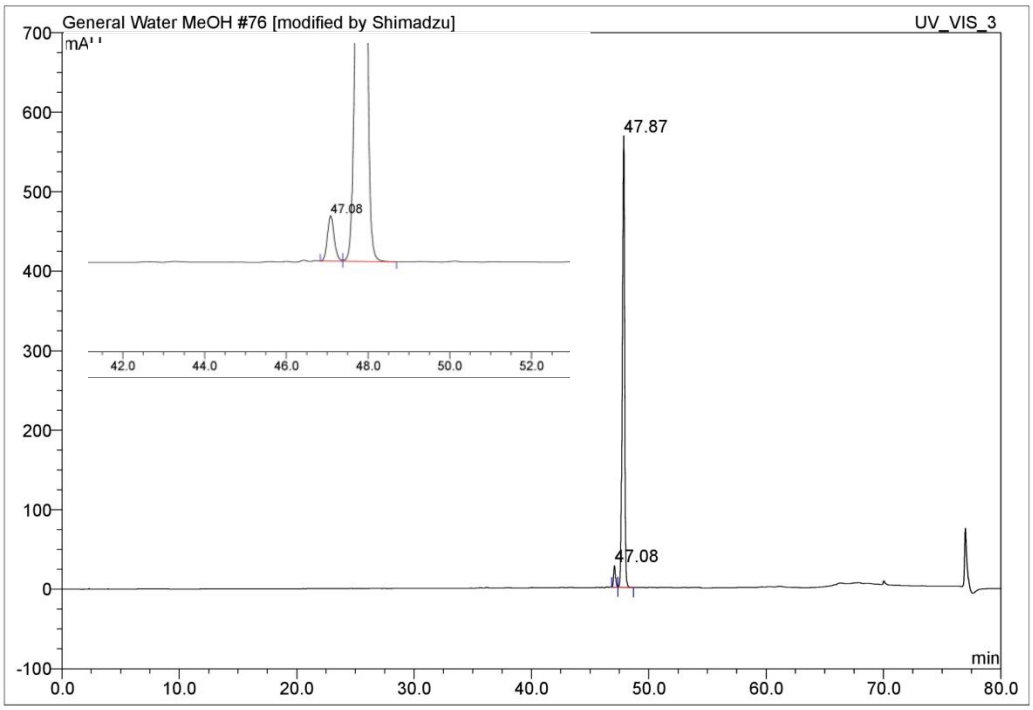

No.	Ret.Time min	Peak Name	Height mAU	Area mAU*min	Rel.Area %	Amount	Type
1	47.08	n.a.	27.065	5.195	3.70	n.a.	BM
2	47.87	n.a.	567.675	135.071	96.30	n.a.	MB
Total:			594.740	140.266	100.00	0.000	

Figure 7.1: Analytical reverse phase C18 HPLC chromatograph of technical grade TP6EO2M (retention time : 47.9 min) using H_2O/MeOH gradient (0-70 % MeOH over 40 min, plateau for 10 min and 70-100 % MeOH over 10min).

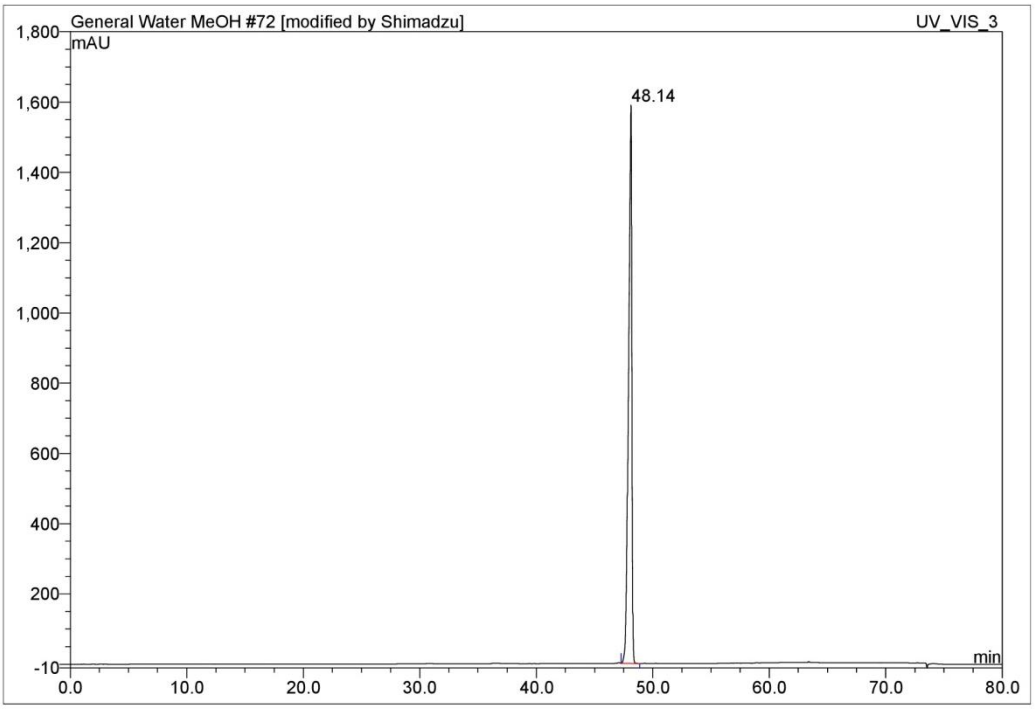

No.	Ret.Time min	Peak Name	Height mAU	Area mAU*min	Rel.Area %	Amount	Type
1	48.14	n.a.	1588.874	525.741	100.00	n.a.	BMB
Total:			1588.874	525.741	100.00	0.000	

Figure 7.2: Analytical reverse phase C18 HPLC chromatograph of TP6EO2M (retention time : 48.1 min) using H_2O/MeOH gradient (0-70% MeOH over 40 min, plateau for 10 min and 70-100% MeOH over 10min).

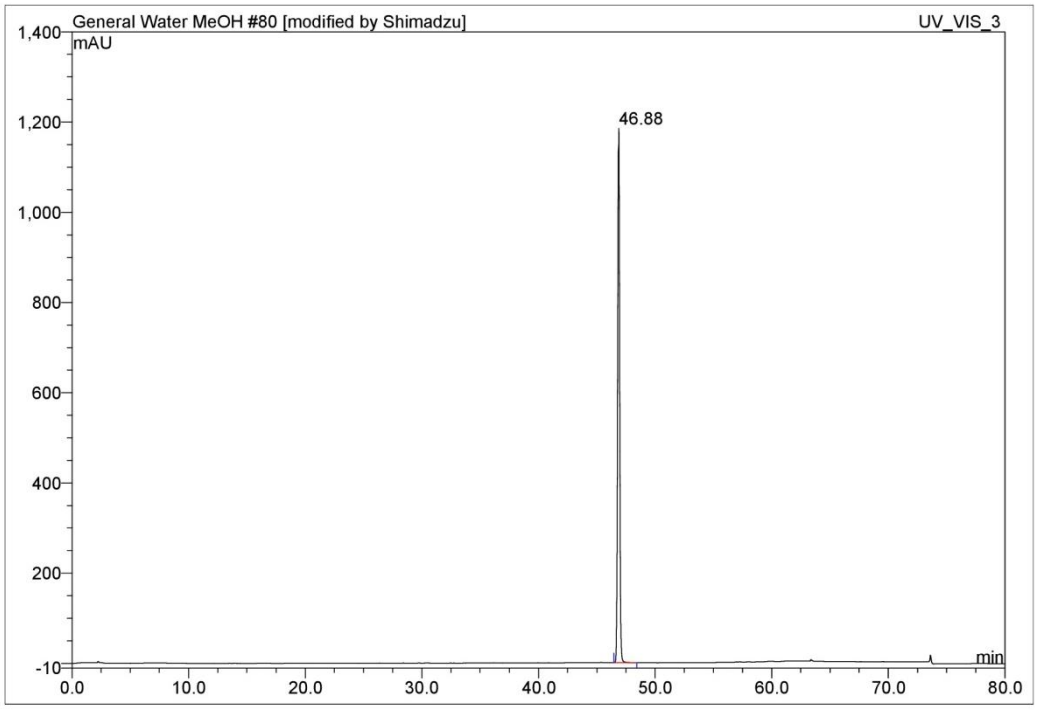

No.	Ret.Time min	Peak Name	Height mAU	Area mAU*min	Rel.Area %	Amount	Type
1	46.88	n.a.	1184.760	225.383	100.00	n.a.	BMB
Total:			1184.760	225.383	100.00	0.000	

Figure 7.3: Analytical reverse phase C18 HPLC chromatograph of TP6EO3M (retention time: 46.9 min) using H_2O/MeOH gradient (0-70% MeOH over 40 min, plateau for 10 min and 70-100% MeOH over 10 min).

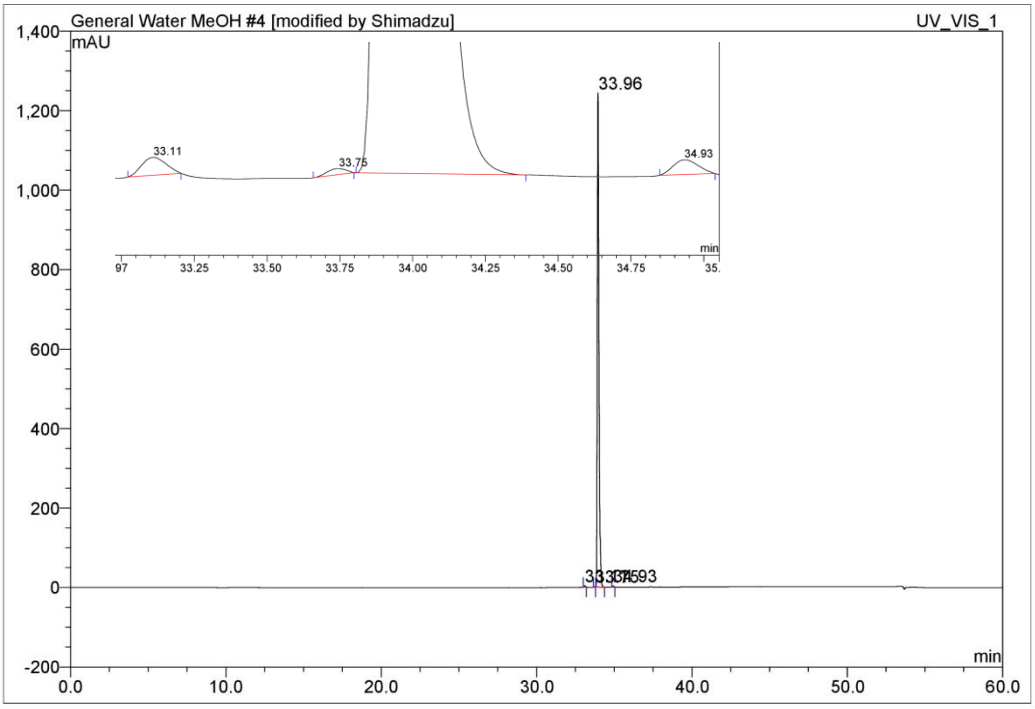

No.	Ret.Time min	Peak Name	Height mAU	Area mAU*min	Rel.Area %	Amount	Type
1	33.11	n.a.	3.237	0.311	0.20	n.a.	BMB*
2	33.75	n.a.	1.075	0.084	0.05	n.a.	BMB*
3	33.96	n.a.	1242.817	158.665	99.59	n.a.	BMB
4	34.93	n.a.	2.658	0.263	0.16	n.a.	BMB*
Total:			1249.787	159.322	100.00	0.000	

Figure 7.4 : Analytical reverse phase C18 HPLC chromatograph of TP6EO4M (retention time: 34.0 min) using H_2O/MeOH gradient (0-100 % MeOH over 40 min).

8 Appendix: Theory of aggregation

The theory of aggregation described by Israelachvili[54] is applicable under the following conditions:

- The system is in equilibrium
- The aggregation is isodesmic and all the components in the aggregate have the same chemical potential
- This theory does not take the interaction between the aggregates and can be therefore applied only on diluted systems.

In equilibrium, all chemical potentials of each molecule in different aggregate is identical. The chemical potential of each molecule in the system can be expressed as follows:

$$\mu = \mu_1^0 + k_B T ln(X_1) = \mu_2^0 + \frac{1}{2} k_B T ln\left(\frac{1}{2} X_2\right) = \cdots = \mu_N^0 + \frac{1}{N} k_B T ln\left(\frac{1}{N} X_N\right) \quad (1)$$

With: X_N = Volume fraction of the molecules in aggregates composed of N monomer, k_B = Boltzman constant, an T the temperature.

The energy of the aggregate composed of N molecules is therefore $N\mu_N^0$.

By using the law of mass action, and based on the association of monomer to aggregates or the dissociation of aggregates to monomers, the following equations be can expressed:

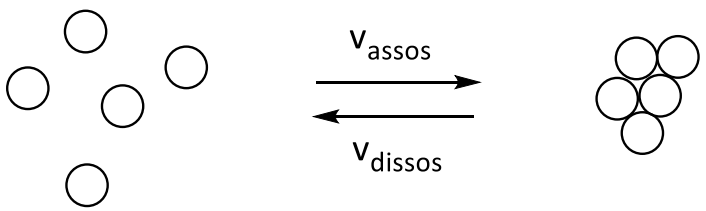

$$v_{assoc} = k_1 X_1^N$$

$$v_{dissoc} = k_N \frac{X_N}{N}$$

At the equilibrium, the rate of association and dissociation are equals:

$$v_{assoc} = v_{dissoc}$$

$$k_1 X_1^N = k_N \frac{X_N}{N}$$

$$\frac{k_1}{k_n} = \frac{X_N}{N X_1^N}$$

The equilibrium constant K can be expressed as follows

$$K = e^{\frac{-\Delta G}{k_B T}} = \frac{k_{assoc}}{k_{dissoc}} = \frac{k_1}{k_n}$$

The volume fraction of the molecules in an aggregate of size N is therefore:

$$X_N = N X_1^N e^{\frac{(\mu_1^0 - \mu_N^0)N}{k_B T}} = N X_1^N e^{\frac{-N\mu_N^0}{k_B T}} \qquad (2)$$

Is it worth noting that the chemical potential of a monomer is equal to zero, as the monomer has no interactions.

By considering that the energy between two molecules in the aggregate being $\alpha k_B T$, the total energy in the aggregate can be written as

$$N\mu_N^0 = -(N-1)\alpha \mathrm{k}_B \mathrm{T} \qquad (3)$$

with (N-1) representing the number of intermolecular bonds in the aggregate.

By combining (3) and (2), we obtain:

$$X_N = N(X_1 e^{\alpha})^N e^{-\alpha} \qquad (4)$$

The total aggregate volume fraction Φ of molecules in the solution is equal to the sum of each volume fraction of each aggregates:

$$\Phi = \sum_{N=1}^{N} X_N = X_1 + X_2 + \cdots + X_N$$

$$\Phi = \sum_{i=1}^{\infty} N(X_1 e^{\alpha})^N e^{-\alpha} = \frac{X_1}{(1 - X_1 e^{\alpha})^2}$$

This equation can be solved for X_1:

$$X_1 = \frac{(1 + 2\Phi e^{\alpha}) - \sqrt{1 + 4\Phi e^{\alpha}}}{2\Phi e^{2\alpha}} \qquad (5)$$

Knowing the density of the aggregated molecules ρ and the concentration of the solution C_M, ϕ=f(C_M) can be calculated:

$$C_M = \frac{\rho\Phi}{M(1 - \Phi)}$$

with M, the molecular mass of the molecule in grams/mol in the aggregate and the density expressed in grams/dm^3.

The absorption spectra in the case of chromophore such as Sunset Yellow FCF [51] or one-dimensional type aggregation compounds is dependent on the aggregation process and therefore on the concentration. This behaviour can be explained by the change of the electronic state of the molecules in the aggregate, due to interaction with close molecules.

The transition energy of an aggregate is therefore equal to the transition energy E_0 of one molecule plus a de*via*tion. It has been proved that the more molecule in the aggregate, the less the impact of an additional molecule on the absorption spectra. The energy eigenstates can be mathematically modelled as followed:

$$E_M = E_0 + 2\beta\cos\left(\frac{m\pi}{N+1}\right)$$

with β constant and m the energy eigenstate index. As the transition energy is proportional to the absorption coefficient of a molecule in the aggregate a_n at a given wavelength, the same behaviour as the transition energy can be assumed for a_n:

$$a_N = a_1 + 2\beta\cos\left(\frac{\pi}{N+1}\right) \qquad (6)$$

with a_1 absorption coefficient of an isolated molecule. This equation gives the absorption coefficient of an aggregate of size N. The absorption coefficient of a distribution of aggregates of N molecules can therefore be calculated using the following relation:

$$\varepsilon_\lambda = \sum_{N=1}^{50} a_N \frac{X_N}{\Phi} \qquad (7)$$

By using the relation (7) is it assumed that the aggregates composed of more than 50 monomers does not participate substantially to the absorption coefficient. By replacing a_N by the equation (6) and X_N by the relation (4) it is therefore possible to obtain ε=f(α,β,a_1). Using the least square fitting method, the constants α, β, and a_1 can be calculated from experimental molar extinction coefficients.

(1) REN 21. *Renewables 2016. Global status report*; 2016.

(2) Becquerel, A. E. *Compt. Rend.* **1839**, *6*, 561–567.

(3) Smith, W. *Nature* **1873**, *7* (173), 303–303.

(4) Adams, W. G.; Day, R. E. *Proc. R. Soc. London* **1876**, *25* (171–178), 113–117.

(5) Chapin, D. M.; Fuller, C. S.; Pearson, G. L. *J. Appl. Phys.* **1954**, *25* (5), 676.

(6) Green, M. A.; Emery, K.; Hishikawa, Y.; Warta, W.; Dunlop, E. D. *Prog. Photovoltaics Res. Appl.* **2016**, *24* (7), 905–913.

(7) Spanggaard, H.; Krebs, F. C. *Sol. Energy Mater. Sol. Cells* **2004**, *83* (2–3), 125–146.

(8) Chamberlain, G. A. *Sol. Cells* **1983**, *8* (1), 47–83.

(9) Tang, C. W. *Appl. Phys. Lett.* **1986**, *48* (2), 183.

(10) Roncali, J.; Leriche, P.; Blanchard, P. *Adv. Mater.* **2014**, *26* (23), 3821–3838.

(11) Hudhomme, P. *EPJ Photovoltaics* **2013**, *4*, 40401.

(12) Nielsen, C. B.; Holliday, S.; Chen, H.; Cryer, S. J.; McCulloch, I. *Acc. Chem. Res.* **2015**, *48* (11), 2803–2812.

(13) Sergeyev, S.; Pisula, W.; Geerts, Y. H. *Chem. Soc. Rev.* **2007**, *36* (12), 1902–1929.

(14) Halls, J. J. M.; Walsh, C. A.; Greenham, N.; C.; Marseglia, E. A.; Friend, R.; H.; Moratti, S. C.; Holmes, A.; B. *Nature* **1995**, *376* (6540), 498–500.

(15) Yu, G.; Gao, J.; Hummelen, J. C.; Wudl, F.; Heeger, A. J. *Science* **1995**, *270* (5243), 1789–1791.

(16) Mikhnenko, O. V; Blom, P. W. M.; Nguyen, T.-Q. *Energy Environ. Sci.* **2015**, *8* (7), 1867–1888.

(17) Watkins, P. K.; Walker, A. B.; Verschoor, G. L. B. *Nano Lett.* **2005**, *5* (9), 1814–1818.

(18) Huang, Y.; Kramer, E. J.; Heeger, A. J.; Bazan, G. C. *Chem. Rev.* **2014**, *114* (14), 7006–7043.

(19) Cheng, P.; Zhan, X. *Chem. Soc. Rev.* **2016**, *45*, 2544–2582.

(20) Diao, Y.; Shaw, L.; Bao, Z.; Mannsfeld, S. C. B. *Energy Environ. Sci.* **2014**, *7*, 2145–2159.

(21) Dang, M. T.; Wantz, G.; Bejbouji, H.; Urien, M.; Dautel, O. J.; Vignau, L.; Hirsch, L. *Sol. Energy Mater. Sol. Cells* **2011**, *95* (12), 3408–3418.

(22) Liu, C.-Y.; Bard, A. J. *Chem. Mater.* **2000**, *12* (8), 2353–2362.

(23) Treat, N. D.; Brady, M. A.; Smith, G.; Toney, M. F.; Kramer, E. J.; Hawker, C. J.; Chabinyc, M. L. *Adv. Energy Mater.* **2011**, *1* (1), 82–89.

(24) Hegde, R.; Henry, N.; Whittle, B.; Zang, H.; Hu, B.; Chen, J.; Xiao, K.; Dadmun, M. *Sol. Energy Mater. Sol. Cells* **2012**, *107*, 112–124.

(25) Lu, L.; Kelly, M. A.; You, W.; Yu, L. *Nat. Photonics* **2015**, *9* (8), 491–500.

(26) Goubard, F.; Wantz, G. *Polym. Int.* **2014**, *63* (8), 1362–1367.

(27) Farahat, M. E.; Patra, D.; Lee, C.-H.; Chu, C.-W. *ACS Appl. Mater. Interfaces* **2015**, *7* (40), 22542–22550.

(28) Qin, D.; Li, G.; Quan, W.; Chen, L.; Liu, J.; Zhang, J.; Yan, D. *Sci. China Physics, Mech. Astron.* **2013**, *56* (3), 530–534.

(29) Rajesh, K. R.; Paudel, K.; Johnson, B.; Hallani, R.; Anthony, J.; Ostroverkhova, O. *J. Photonics Energy* **2015**, *5* (1), 57208.

(30) Khlyabich, P. P.; Burkhart, B.; Thompson, B. C. *J. Am. Chem. Soc.* **2011**, *133* (37), 14534–14537.

(31) Huang, T.-Y.; Patra, D.; Hsiao, Y.-S.; Chang, S. H.; Wu, C.-G.; Ho, K.-C.; Chu, C.-W. *J. Mater. Chem. A* **2015**, *3* (19), 10512–10518.

(32) Kumazawa, K.; Yoshizawa, M.; Liu, H.-B.; Kamikawa, Y.; Moriyama, M.; Kato, T.; Fujita, M. *Chem. Eur. J.* **2005**, *11* (8), 2519–2524.

(33) Cheng, P.; Zhan, X. *Mater. Horiz.* **2015**, *2* (5), 462–485.

(34) Arca, F.; Loch, M.; Lugli, P. *IEEE J. Photovoltaics* **2014**, *4* (6), 1560–1565.

(35) Salim, T.; Wong, L. H.; Bräuer, B.; Kukreja, R.; Foo, Y. L.; Bao, Z.; Lam, Y. M. *J. Mater. Chem.* **2011**, *21* (1), 242–250.

(36) Kim, C. S.; Tinker, L. L.; DiSalle, B. F.; Gomez, E. D.; Lee, S.; Bernhard, S.; Loo, Y.-L. *Adv. Mater.* **2009**, *21* (30), 3110–3115.

(37) Renaud, C.; Mougnier, S.-J.; Pavlopoulou, E.; Brochon, C.; Fleury, G.; Deribew, D.; Portale, G.; Cloutet, E.; Chambon, S.; Vignau, L.; Hadziioannou, G. *Adv. Mater.* **2012**, *24* (16), 2196–2201.

(38) Yuan, K.; Chen, L.; Chen, Y. W. *J. Mater. Chem. C* **2014**, *2*, 3835–3845.

(39) Yang, C.; Lee, J. K.; Heeger, A. J.; Wudl, F. *J. Mater. Chem.* **2009**, *19* (30), 5416–5423.

(40) Kim, J. B.; Allen, K.; Oh, S. J.; Lee, S.; Toney, M. F.; Kim, Y. S.; Kagan, C. R.; Nuckolls, C.;

Loo, Y.-L. *Chem. Mater.* **2010**, *22* (20), 5762–5773.

(41) Raja, R.; Liu, W.-S.; Hsiow, C.-Y.; Hsieh, Y.-J.; Rwei, S.-P.; Chiu, W.-Y.; Wang, L. *Org. Electron.* **2014**, *15*, 2223–2233.

(42) Li, L.; Xiao, L.; Qin, H.; Gao, K.; Peng, J.; Cao, Y.; Liu, F.; Russell, T. P.; Peng, X. *ACS Appl. Mater. Interfaces* **2015**, *7* (38), 21495–21502.

(43) Qin, H.; Li, L.; Guo, F.; Su, S.; Peng, J.; Cao, Y.; Peng, X. *Energy Environ. Sci.* **2014**, *7* (4), 1397.

(44) Sun, Y.; Welch, G. C.; Leong, W. L.; Takacs, C. J.; Bazan, G. C.; Heeger, A. J. *Nat. Mater.* **2011**, *11* (1), 44–48.

(45) Van der Poll, T. S.; Love, J. A.; Nguyen, T.-Q.; Bazan, G. C. *Adv. Mater.* **2012**, *24* (27), 3646–3649.

(46) Kyaw, A. K. K.; Wang, D. H.; Gupta, V.; Leong, W. L.; Ke, L.; Bazan, G. C.; Heeger, A. J. *ACS Nano* **2013**, *7* (5), 4569–4577.

(47) Reinitzer, F. *Monatshefte für Chemie* **1888**, *9* (1), 421–441.

(48) Lydon, J. *Liq. Cryst.* **2011**, *38* (11–12), 1663–1681.

(49) Lydon, J. *J. Mater. Chem.* **2010**, *20* (45), 10071.

(50) Heilmeier, G. H.; Zanoni, L. A.; Barton, L. A. *Proc. IEEE* **1968**, *56* (7), 1162–1171.

(51) Chandrasekhar, S.; Sadashiva, B. K.; Suresh, K. A. *Pramana* **1977**, *9* (5), 471–480.

(52) Wöhrle, T.; Wurzbach, I.; Kirres, J.; Kostidou, A.; Kapernaum, N.; Litterscheidt, J.; Haenle, J. C.; Staffeld, P.; Baro, A.; Giesselmann, F.; Laschat, S. *Chem. Rev.* **2016**, *116* (3),

1139–1241.

(53) Laschat, S.; Baro, A.; Steinke, N.; Giesselmann, F.; Hägele, C.; Scalia, G.; Judele, R.; Kapatsina, E.; Sauer, S.; Schreivogel, A.; Tosoni, M. *Angew. Chemie Int. Ed.* **2007**, *46* (26), 4832–4887.

(54) Israelachvili, J. N. In *Intermolecular and Surface Forces*; Elsevier, 2011; pp 503–534.

(55) Horowitz, V.; Janowitz, L.; Modic, A.; Heiney, P.; Collings, P. *Phys. Rev. E* **2005**, *72* (4), 1–10.

(56) Kouwer, P. H. J.; Mehl, G. H. *J. Am. Chem. Soc.* **2003**, *125* (37), 11172–11173.

(57) Kouwer, P. H. J.; Mehl, G. H. *Mol. Cryst. Liq. Cryst.* **2003**, *397* (1), 1–16.

(58) Kouwer, P. H. J.; Welch, C. J.; McRobbie, G.; Dodds, B. J.; Priest, L.; Mehl, G. H. *J. Mater. Chem.* **2004**, *14* (12), 1798–1803.

(59) Apreutesei, D.; Mehl, G. *Mol. Cryst. Liq. Cryst.* **2006**, *449* (1), 107–115.

(60) Apreutesei, D.; Mehl, G. H. *Chem. Comm.* **2006**, No. 6, 609–611.

(61) Kouwer, P. H. J.; Mehl, G. H. *J. Mater. Chem.* **2009**, *19* (11), 1564.

(62) Date, R. W.; Bruce, D. W. *J. Am. Chem. Soc.* **2003**, *125* (30), 9012–9013.

(63) Schmidt, H.; Schultz, G. *Justus Liebig's Ann. der Chemie* **1880**, *203* (1–2), 118–137.

(64) Mannich, C.; Berlin, U. *Chem. Ber.* **1907**, 153–158.

(65) Motoyanagi, J.; Yamamoto, Y.; Saeki, A.; Alam, M. A.; Kimoto, A.; Kosaka, A.; Fukushima, T.; Seki, S.; Tagawa, S.; Aida, T. *Chem. Asian J.* **2009**, *4* (6), 876–880.

(66) Van de Craats, A. M.; Siebbeles, L. D. A.; Bleyl, I.; Haarer, D.; Berlin, Y. A.; Zharikov, A. A.; Warman, J. M. *J. Phys. Chem. B* **1998**, *102* (48), 9625–9634.

(67) Bacher, A.; Bleyl, I.; Erdelen, C. H.; Haarer, D.; Paulus, W.; Schmidt, H.-W. *Adv. Mater.* **1997**, *9* (13), 1031–1035.

(68) Wendorff, J. H.; Christ, T.; Glüsen, B.; Greiner, A.; Kettner, A.; Sander, R.; Stümpflen, V.; Tsukruk, V. V. *Adv. Mater.* **1997**, *9* (1), 48–52.

(69) Seguy, I.; Destruel, P.; Bock, H. *Synth. Met.* **2000**, *111–112*, 15–18.

(70) Clements, J.; Boden, N.; Gibson, T. D.; Chandler, R. C.; Hulbert, J. N.; Ruck-Keene, E. A. *Sensors Actuators B Chem.* **1998**, *47* (1–3), 37–42.

(71) Gong, Y.; Huang, Y.; Jiang, L.; Lu, T. *Inorg. Chem.* **2014**, *53* (18), 9457–9459.

(72) Chen, X.; Chen, L.; Chen, Y. *RSC Adv.* **2014**, *4* (7), 3627–3632.

(73) Allinson, H.; Boden, N.; Bushby, R. J.; Evans, S. D.; Martin, P. S. *Mol. Cryst. Liq. Cryst. Sci. Technol. Sect. A. Mol. Cryst. Liq. Cryst.* **1997**, *303* (1), 273–278.

(74) Kumar, S. *Liq. Cryst.* **2004**, *31* (8), 1037–1059.

(75) Kumar, S. *Liq. Cryst.* **2005**, *32* (9), 1089–1113.

(76) Pal, S. K.; Setia, S.; Avinash, B. S.; Kumar, S. *Liq. Cryst.* **2013**, *40* (12), 1769–1816.

(77) Kumar, S.; Manickam, M.; Varshney, S. K.; Shankar Rao, D. S.; Krishna Prasad, S. *J. Mater. Chem.* **2000**, *10* (11), 2483–2489.

(78) Boden, N.; Bushby, R. J.; Cammidge, A. N. *J. Chem. Soc. Chem. Commun.* **1994**, No. 4, 465.

(79) Pérez, D.; Guitián, E. *Chem. Soc. Rev.* **2004**, *33* (5), 274–283.

(80) Sarhan, A. A. O.; Bolm, C. *Chem. Soc. Rev.* **2009**, *38* (9), 2730.

(81) Kumar, S.; Varshney, S. K. *Liq. Cryst.* **1999**, *26* (12), 1841–1843.

(82) Kumar, S.; Manickam, M. *Chem. Comm.* **1997**, 1615–1616.

(83) Srinivasa HT, S. K. *Org. Chem. Curr. Res.* **2013**, *2* (2), 2–4.

(84) Matheson, I. M.; Musgrave, O. C.; Webster, C. J. *Chem. Commun.* **1965**, No. 13, 278–279.

(85) Rathore, R.; Shukla, R.; Zhai, L. *Org. Lett.* **2009**, *11* (15), 3474–3477.

(86) Cho, H. Y.; Scott, L. T. *Tetrahedron Lett.* **2015**, *56* (23), 3458–3462.

(87) Grzybowski, M.; Skonieczny, K.; Butenschön, H.; Gryko, D. T. *Angew. Chemie Int. Ed.* **2013**, *52* (38), 9900–9930.

(88) Zhai, L.; Shukla, R.; Wadumethrige, S. H.; Rathore, R. *J. Org. Chem.* **2010**, *75* (14), 4748–4760.

(89) Rempala, P.; Kroulík, J.; King, B. T. *J. Am. Chem. Soc.* **2004**, *126* (46), 15002–15003.

(90) Rempala, P.; Kroulík, J.; King, B. T. *J. Org. Chem.* **2006**, *71* (14), 5067–5081.

(91) King, B. T.; Kroulík, J.; Robertson, C. R.; Rempala, P.; Hilton, C. L.; Korinek, J. D.; Gortari, L. M. *J. Org. Chem.* **2007**, *72* (7), 2279–2288.

(92) Borner, R. C.; Boden, N.; Bushby, R. J.; Borner, R. C.; Cammidge, A. N.; Bushby, R. J.; Cammidge, A. N.; Jesudason, M. V. *Liq. Cryst.* **2006**, *33* (11–12), 1439–1448.

(93) Kavitha, C.; Avinash, B. S.; Kumar, S.; Lakshminarayanan, V. *Mater. Chem. Phys.* **2012**, *133* (2–3), 635–641.

(94) Haverkate, L. A.; Zbiri, M.; Johnson, M. R.; Deme, B.; Mulder, F. M.; Kearley, G. J. *J. Phys. Chem. B* **2011**, *115* (47), 13809–13816.

(95) Klivansky, L. M.; Hanifi, D.; Koshkakaryan, G.; Holycross, D. R.; Gorski, E. K.; Wu, Q.; Chai, M.; Liu, Y. *Chem. Sci.* **2012**, *3* (6), 2009.

(96) Terasawa, N.; Monobe, H.; Kiyohara, K. *J. Fluor. Chem.* **2006**, *127* (7), 954–961.

(97) Terasawa, N.; Tanigaki, N.; Monobe, H.; Kiyohara, K. *J. Fluor. Chem.* **2006**, *127* (8), 1096–1104.

(98) Koshkakaryan, G.; Jiang, P.; Altoe, V.; Cao, D.; Klivansky, L. M.; Zhang, Y.; Chung, S.; Katan, A.; Martin, F.; Salmeron, M.; Ma, B.; Aloni, S.; Liu, Y. *Chem. Comm.* **2010**, *46* (45), 8579–8581.

(99) Arikainen, E. O.; Boden, N.; Bushby, R. J.; Clements, J.; Movaghar, B.; Wood, A. *J. Mater. Chem.* **1995**, *5* (12), 2161.

(100) Boden, N.; Bushby, R. J.; Clements, J.; Luo, R. *J. Mater. Chem.* **1995**, *5* (10), 1741–1748.

(101) Zhao, B.; Liu, B.; Png, R. Q.; Zhang, K.; Lim, K. A.; Luo, J.; Shao, J.; Ho, P. K. H.; Chi, C.; Wu, J. *Chem. Mater.* **2010**, *22* (2), 435–449.

(102) Boden, N.; Bushby, R. J.; Lu, Z.; Lozman, O. R. *Liq. Cryst.* **2001**, *28* (5), 657–661.

(103) Boden, N.; Bushby, R. J.; Jesudason, M. V.; Sheldrick, B. *J. Chem. Soc. Chem. Commun.* **1988**, No. 19, 1342.

(104) Herbaut, A.; Baranoff, E. *Chimia* **2015**, *69* (9), 520–523.

(105) Hughes, R. E.; Hart, S. P.; Smith, D. A.; Movaghar, B.; Bushby, R. J.; Boden, N. *J. Phys. Chem. B* **2002**, *106* (26), 6638–6645.

(106) Akinshina, A.; Walker, M.; Wilson, M. R.; Tiddy, G. J. T.; Masters, A. J.; Carbone, P. *Soft Matter* **2015**, *11* (4), 680–691.

(107) Al-Lawati, Z. H.; Alkhairalla, B.; Bramble, J. P.; Henderson, J. R.; Bushby, R. J.; Evans, S. D. *J. Phys. Chem. C* **2012**, *116* (23), 12627–12635.

(108) Bast, T.; Hentschke, R. *J. Phys. Chem.* **1996**, *100* (30), 12162–12171.

(109) Boden, N.; Bushby, R. J.; Hardy, C. *J. Phys. Lettres* **1985**, *46* (7), 325–328.

(110) Boden, N.; Bushby, R. J.; Hardy, C.; Sixl, F. *Chem. Phys. Lett.* **1986**, *123* (5), 359–364.

(111) Boden, N.; Bushby, R. J.; Hubbard, J. F. *Mol. Cryst. Liq. Cryst. Sci. Technol. Sect. A. Mol. Cryst. Liq. Cryst.* **1997**, *304* (1), 195–200.

(112) Hentschke, R.; Edwards, P. J. B.; Boden, N.; Bushby, R. J. *Macromol. Symp.* **1994**, *81* (1), 361–367.

(113) Hughes, R.; Smith, A.; Bushby, R.; Movaghar, B.; Boden, N. *Mol. Cryst. Liq. Cryst.* **1999**, *332*, 547–557.

(114) Hubbard, J. F. The phase behaviour of one-dimensional self-assembling molecular aggregates, University of Leeds, 1997, Vol. 1.

(115) Padia, F. N.; Yaseen, M.; Gore, B.; Rogers, S.; Bell, G.; Lu, J. R. *J. Phys. Chem. B* **2014**, *118* (1), 179–188.

(116) Berthod, A.; Tomer, S.; Dorsey, J. G. *Talanta* **2001**, *55* (1), 69–83.

(117) Tamura, T.; Yoshida, K.; Hachida, T.; Tsuchiya, M.; Nakamura, M.; Kazue, Y.; Tachikawa, N.; Dokko, K.; Watanabe, M. *Chem. Lett.* **2010**, *39* (7), 753–755.

(118) Bushby, R. J.; Lu, Z. *Synthesis* **2001**, No. 5, 763–767.

(119) Buchanan, G. W.; Rastegar, M. F.; Yap, G. P. *Can. J. Chem.* **2001**, *79* (2), 195–200.

(120) Buchanan, G. W.; Azad, M.; Yap, G. P. A. *J. Mol. Struct.* **2001**, *598* (2–3), 145–151.

(121) Lu, Y.; Moore, J. S. *Tetrahedron Lett.* **2009**, *50* (28), 4071–4077.

(122) Hansch, C.; Leo, A.; Taft, R. W. *Chem. Rev.* **1991**, *91* (2), 165–195.

(123) Orlando, J. J. *Phys. Chem. Chem. Phys.* **2007**, *9* (31), 4189.

(124) Di Tommaso, S.; Rotureau, P.; Crescenzi, O.; Adamo, C. *Phys. Chem. Chem. Phys.* **2011**, *13* (32), 14636.

(125) Tripathi, U. N.; Siddiqui, A.; Ahmad, M. S.; Singh, K. *J. Coord. Chem.* **2010**, *63* (5), 894–905.

(126) Rabek, J. F.; Lindén, L. .; Kaczmarek, H.; Qu, B. J.; Shi, W. F. *Polym. Degrad. Stab.* **1992**, *37* (1), 33–40.

(127) Rabek, J. F.; Lucki, J.; Qu, B. J.; Shi, W. F. *Macromolecules* **1991**, *24* (4), 836–843.

(128) Zhai, L.; Shukla, R.; Rathore, R. *Org. Lett.* **2009**, *11* (15), 3474–3477.

(129) Weissman, S. A.; Zewge, D. *Tetrahedron* **2005**, *61* (33), 7833–7863.

(130) Closs, F.; Häußling, L.; Henderson, P.; Ringsdorf, H.; Schuhmacher, P. *J. Chem. Soc.,*

Perkin Trans. 1 **1995**, No. 7, 829–837.

(131) Kumar, S.; Manickam, M. *Synthesis* **1998**, *1998* (8), 1119–1122.

(132) Herbaut, A. J.; Baranoff, E. *RSC Adv.* **2016**, *6* (13), 10655–10661.

(133) Percec, V.; Wilson, D. a; Leowanawat, P.; Al., E. *Science* **2010**, *328* (5981), 1009–1014.

(134) Wang, X.; Wang, D. Z. *Tetrahedron* **2011**, *67* (19), 3406–3411.

(135) Wang, X.; Zhang, B.; Wang, D. Z. *J. Am. Chem. Soc.* **2011**, *133* (13), 5160–5160.

(136) Lewis, G. E. *J. Org. Chem.* **1965**, *30* (7), 2433–2436.

(137) Ohta, S.; Tachi, T.; Okamoto, M. *Synthesis* **1983**, *1983* (4), 291–293.

(138) Clar, E.; Ironside, C. T.; Zander, M. *J. Chem. Soc.* **1959**, No. 142, 142.

(139) Halleux, A.; Martin, R. H.; King, G. S. D. *Helv. Chim. Acta* **1958**, *41* (5), 1177–1183.

(140) Herwig, P.; Kayser, C. W.; Müllen, K.; Spiess, H. W. *Adv. Mater.* **1996**, *8* (6), 510–513.

(141) Stabel, A.; Herwig, P.; Müllen, K.; Rabe, J. P. *Angew. Chemie Int. Ed. English* **1995**, *34* (15), 1609–1611.

(142) Fechtenkötter, A.; Tchebotareva, N.; Watson, M.; Müllen, K. *Tetrahedron* **2001**, *57* (17), 3769–3783.

(143) Yang, X.; Dou, X.; Müllen, K. *Chem. – An Asian J.* **2008**, *3* (4), 759–766.

(144) Feng, X. C3-Symmetric Discotic Liquid Crystalline Materials for Molecular Electronics: Versatile Synthesis and Self-organization, Johannes Gutenberg-Universität, Mainz, 2008.

(145) Koch, N.; Heimel, G.; Wu, J.; Zojer, E.; Johnson, R. L.; Brédas, J.-L.; Müllen, K.; Rabe, J. P. *Chem. Phys. Lett.* **2005**, *413* (4–6), 390–395.

(146) Wang, Z.; Dötz, F.; Enkelmann, V.; Müllen, K. *Angew. Chemie Int. Ed.* **2005**, *44* (8), 1247–1250.

(147) Goddard, R.; Haenel, M. W.; Herndon, W. C.; Krueger, C.; Zander, M. *J. Am. Chem. Soc.* **1995**, *117* (1), 30–41.

(148) Van de Craats, A. M.; Warman, J. M.; Fechtenkötter, A.; Brand, J. D.; Harbison, M. A.; Müllen, K. *Adv. Mater.* **1999**, *11* (17), 1469–1472.

(149) Keil, M.; Samorí, P.; dos Santos, D. A.; Birgerson, J.; Friedlein, R.; Dkhissi, A.; Watson, M.; Müllen, K.; Brédas, J. L.; Rabe, J. P.; Salaneck, W. R. *J. Chem. Phys.* **2002**, *116* (24), 10854.

(150) Mukai, K.; Harada, M.; Kikuzawa, Y.; Mori, T.; Sugiyama, J. *Electrochem. Solid-State Lett.* **2011**, *14* (4), A52.

(151) Zilberman, Y.; Tisch, U.; Pisula, W.; Feng, X.; Müllen, K.; Haick, H. *Langmuir* **2009**, *25* (9), 5411–5416.

(152) Zilberman, Y.; Tisch, U.; Shuster, G.; Pisula, W.; Feng, X.; Müllen, K.; Haick, H. *Adv. Mater.* **2010**, *22* (38), 4317–4320.

(153) Schmidt-Mende, L. *Science* **2001**, *293* (5532), 1119–1122.

(154) Kardos, M. Verfahren zur Darstellung eines Küpenfarbstoffes der Naphtalinreihe, DE276357, 1913.

(155) Herbst, W.; Hunger, K.; Wilker, G.; Ohleier, H.; Winter, R. *Industrial Organic Pigments*; Wiley-VCH Verlag GmbH & Co. KGaA: Weinheim, FRG, 2004; Vol. Third Edit.

(156) Würthner, F. *Chem. Commun.* **2004**, No. 14, 1564–1579.

(157) Huang, C.; Barlow, S.; Marder, S. R. *J. Org. Chem.* **2011**, *76* (8), 2386–2407.

(158) Li, C.; Wonneberger, H. *Adv. Mater.* **2012**, *24* (5), 613–636.

(159) Würthner, F.; Saha-Möller, C. R.; Fimmel, B.; Ogi, S.; Leowanawat, P.; Schmidt, D. *Chem. Rev.* **2016**, *116* (3), 962–1052.

(160) Kozma, E.; Catellani, M. *Dye. Pigment.* **2013**, *98* (1), 160–179.

(161) Wicklein, A.; Lang, A.; Muth, M.; Thelakkat, M. *J. Am. Chem. Soc.* **2009**, *131* (40), 14442–14453.

(162) Würthner, F.; Stepanenko, V.; Chen, Z.; Saha-Möller, C. R.; Kocher, N.; Stalke, D. *J. Org. Chem.* **2004**, *69* (23), 7933–7939.

(163) Sengupta, S.; Dubey, R. K.; Hoek, R. W. M.; van Eeden, S. P. P.; Gunbas, D. D.; Grozema, F. C.; Sudhölter, E. J. R.; Jager, W. F. *J. Org. Chem.* **2014**, *79* (14), 6655–6662.

(164) Perrin, L.; Hudhomme, P. *European J. Org. Chem. 2011* (28), 5427–5440.

(165) Nakazono, S.; Imazaki, Y.; Yoo, H.; Yang, J.; Sasamori, T.; Tokitoh, N.; Cédric, T.; Kageyama, H.; Kim, D.; Shinokubo, H.; Osuka, A. *Chem. - A Eur. J.* **2009**, *15* (31), 7530–7533.

(166) Nakazono, S.; Easwaramoorthi, S.; Kim, D.; Shinokubo, H.; Osuka, A. *Org. Lett.* **2009**, *11* (23), 5426–5429.

(167) Marciniak, H.; Li, X.-Q.; Würthner, F.; Lochbrunner, S. *J. Phys. Chem. A* **2011**, *115* (5), 648–654.

(168) Sadrai, M.; Bird, G. R. *Opt. Commun.* **1984**, *51* (1), 62–64.

(169) Ford, W. E.; Kamat, P. V. *J. Phys. Chem.* **1987**, *91* (25), 6373–6380.

(170) Li, G.; Zhao, Y.; Li, J.; Cao, J.; Zhu, J.; Sun, X. W.; Zhang, Q. *J. Org. Chem.* **2015**, *80* (1), 196–203.

(171) Zang, L.; Liu, R.; Holman, M. W.; Nguyen, K. T.; Adams, D. M. *J. Am. Chem. Soc.* **2002**, *124* (36), 10640–10641.

(172) Baumstark, D.; Wagenknecht, H.-A. *Angew. Chemie Int. Ed.* **2008**, *47* (14), 2612–2614.

(173) Segura, J. L.; Herrera, H.; Bäuerle, P. *J. Mater. Chem.* **2012**, *22* (18), 8717.

(174) Schmidt-Mende, L.; Fechtenkötter, A.; Müllen, K.; Moons, E.; Friend, R. H.; MacKenzie, J. D. *Science* **2001**, *293* (5532), 1119–1122.

(175) Fechtenkötter, A.; Saalwächter, K.; Harbison, M. A.; Müllen, K.; Spiess, H. W. *Angew. Chemie Int. Ed.* **1999**, *38* (20), 3039–3042.

(176) Tomović, Ž. New Discotic Liquid Crystals Based on Large Polycyclic Aromatic Hydrocarbons as Materials for Molecular Electronics, Johannes Gutemberg-Universität Mainz, 2004.

(177) Fleming, A. J.; Coleman, J. N.; Dalton, A. B.; Fechtenkötter, A.; Watson, M. D.; Müllen, K.; Byrne, H. J.; Blau, W. J. *J. Phys. Chem. B* **2003**, *107* (1), 37–43.

(178) Im, C.; Tian, W.; Bässler, H.; Fechtenkötter, A.; Watson, M. D.; Müllen, K. *J. Chem. Phys.*

2003, *119* (7), 3952.

(179) Fechtenkötter, A. Liquid Crystalline Hexabenzocoronenes as Organic Molecular Materials – Synthesis, Characterization and Application, Johannes Gutenberg-Universität, Mainz, 2001.

(180) Dubey, R. K.; Efimov, A.; Lemmetyinen, H. *Chem. Mater.* **2011**, *23* (3), 778–788.

(181) Zhang, L.; Wang, L.; Zhang, G.; Yu, J.; Cai, X.; Teng, M.; Wu, Y. *Chinese J. Chem.* **2012**, *30* (12), 2823–2826.

(182) Cormier, R. A.; Gregg, B. A. *Chem. Mater.* **1998**, *10* (5), 1309–1319.

(183) Simon, J.; Vacus, J. *Adv. Mater.* **1995**, *7* (9), 797–800.

(184) Imm, S.; Bähn, S.; Neubert, L.; Neumann, H.; Beller, M. *Angew. Chemie Int. Ed.* **2010**, *49* (44), 8126–8129.

(185) Shimizu, K. I.; Kon, K.; Onodera, W.; Yamazaki, H.; Kondo, J. N. *ACS Catal.* **2013**, *3* (1), 112–117.

(186) Sugandhi, E. W.; Falkinham III, J. O.; Gandour, R. D. *Bioorg. Med. Chem.* **2007**, *15* (11), 3842–3853.

(187) Nemoto, H.; Cai, J.; Iwamoto, S.; Yamamoto, Y. *J. Med. Chem.* **1995**, *38* (10), 1673–1678.

(188) Mizoshita, N.; Tani, T.; Inagaki, S. *Chem. Commun.* **2012**, *48* (87), 10772.

(189) Neuteboom, E. E.; Meskers, S. C. J.; Meijer, E. W.; Janssen, R. A. J. *Macromol. Chem. Phys.* **2004**, *205* (2), 217–222.

(190) De Witte, P. A. J.; Hernando, J.; Neuteboom, E. E.; Van Dijk, E. M. H. P.; Meskers, S. C.

J.; Janssen, R. A. J.; Van Hulst, N. F.; Nolte, R. J. M.; García-Parajó, M. F.; Rowan, A. E. *J. Phys. Chem. B* **2006**, *110* (15), 7803–7812.

(191) Nilsson, A.; Goodwin, R. J. A.; Swales, J. G.; Gallagher, R.; Shankaran, H.; Sathe, A.; Pradeepan, S.; Xue, A.; Keirstead, N.; Sasaki, J. C.; Andren, P. E.; Gupta, A. *Chem. Res. Toxicol.* **2015**, *28* (9), 1823–1830.

(192) Swales, J. G.; Tucker, J. W.; Spreadborough, M. J.; Iverson, S. L.; Clench, M. R.; Webborn, P. J. H.; Goodwin, R. J. A. *Anal. Chem.* **2015**, *87* (19), 10146–10152.

(193) Griffiths, R. L.; Creese, A. J.; Race, A. M.; Bunch, J.; Cooper, H. J. *Anal. Chem.* **2016**, *88* (13), 6758–6766.

(194) Dössel, L. F.; Kamm, V.; Howard, I. a; Laquai, F.; Pisula, W.; Feng, X.; Li, C.; Takase, M.; Kudernac, T.; De Feyter, S.; Müllen, K. *J. Am. Chem. Soc.* **2012**, *134* (13), 5876–5886.

(195) Wang, S.; Dössel, L.; Mavrinskiy, A.; Gao, P.; Feng, X.; Pisula, W.; Müllen, K. *Small* **2011**, *7* (20), 2841–2846.

(196) Mativetsky, J. M.; Kastler, M.; Savage, R. C.; Gentilini, D.; Palma, M.; Pisula, W.; Müllen, K.; Samorì, P. *Adv. Funct. Mater.* **2009**, *19* (15), 2486–2494.

(197) Samorì, P.; Fechtenkötter, A.; Reuther, E.; Watson, M. D.; Severin, N.; Müllen, K.; Rabe, J. P. *Adv. Mater.* **2006**, *18* (10), 1317–1321.

(198) Pasaogullari, N.; Icil, H.; Demuth, M. *Dye. Pigment.* **2006**, *69* (3), 118–127.

(199) Cesari, C.; Sambri, L.; Zacchini, S.; Zanotti, V.; Mazzoni, R. *Organometallics* **2014**, *33* (11), 2814–2819.

(200) Bernhardt, S.; Kastler, M.; Enkelmann, V.; Baumgarten, M.; Müllen, K. *Chem. - A Eur. J.* **2006**, *12* (23), 6117–6128.

(201) Dötz, F.; Brand, J. D.; Ito, S.; Gherghel, L.; Müllen, K. *J. Am. Chem. Soc.* **2000**, *122*, 7707–7717.

(202) Chinchilla, R.; Nájera, C. *Chem. Rev.* **2007**, *107* (3), 874–922.

(203) Mio, M. J.; Kopel, L. C.; Braun, J. B.; Gadzikwa, T. L.; Hull, K. L.; Brisbois, R. G.; Markworth, C. J.; Grieco, P. A. *Org. Lett.* **2002**, *4* (19), 3199–3202.

(204) Ogliaruso, M. A.; Romanelli, M. G.; Becker, E. I. *Chem. Rev.* **1965**, *65* (3), 261–367.

(205) Takematsu, K.; Takanori, F.; Takuzo, A. JP2008266152A, 2008.

(206) Thiemann, T.; Iniesta, J.; Walton, D. J. *J. Chem. Res.* **2008**, *2008* (3), 173–180.

(207) Jin, W.; Fukushima, T.; Kosaka, A.; Niki, M.; Ishii, N.; Aida, T. *J. Am. Chem. Soc.* **2005**, *127* (23), 8284–8285.

(208) De Luca, G.; Liscio, A.; Melucci, M.; Schnitzler, T.; Pisula, W.; Clark, C. G.; Scolaro, L. M.; Palermo, V.; Müllen, K.; Samorì, P. *J. Mater. Chem.* **2010**, *20* (1), 71.

(209) Henderson, C. *J. Histotechnol.* **1989**, *12* (2), 123–124.

(210) Percec, V.; Imam, M. R.; Peterca, M.; Wilson, D. a; Graf, R.; Spiess, H. W.; Balagurusamy, V. S. K.; Heiney, P. a. *J. Am. Chem. Soc.* **2009**, *131* (22), 7662–7677.

(211) Goodby, J. W.; Hird, M.; Toyne, K. J.; Watson, T. *J. Chem. Soc. Chem. Commun.* **1994**, No. 14, 1701.

(212) Stewart, D.; Mchattie, G. S.; Imrie, C. T. *J. Mater. Chem.* **1998**, *8* (0), 47–51.

(213) Boden, N.; Bushby, R. J.; Cammidge, A. N. *J. Am. Chem. Soc.* **1995**, *117* (3), 924–927.

(214) Kong, X.; He, Z.; Gopee, H.; Jing, X.; Cammidge, A. N. *Tetrahedron Lett.* **2011**, *52* (1), 77–79.

(215) Yu, W.-H.; Chen, C.; Hu, P.; Wang, B.-Q.; Redshaw, C.; Zhao, K.-Q. *RSC Adv.* **2013**, *3* (33), 14099.

(216) Northrop, B. H.; Glöckner, A.; Stang, P. J. *J. Org. Chem.* **2008**, *73* (5), 1787–1794.

(217) Alonso, J. M.; Reichel, A.; Piehler, J.; del Campo, A. *Langmuir* **2008**, *24* (2), 448–457.

(218) Percec, V.; Sun, H. J.; Leowanawat, P.; Peterca, M.; Graf, R.; Spiess, H. W.; Zeng, X.; Ungar, G.; Heiney, P. a. *J. Am. Chem. Soc.* **2013**, *135* (10), 4129–4148.

(219) Li, Y.; Wang, C.; Li, C.; Di Motta, S.; Negri, F.; Wang, Z. *Org. Lett.* **2012**, *14* (20), 5278–5281.

(220) Franceschin, M.; Borbone, N.; Oliviero, G.; Casagrande, V.; Scuotto, M.; Coppola, T.; Borioni, S.; Mayol, L.; Ortaggi, G.; Bianco, A.; Amato, J.; Varra, M. *Bioconjug. Chem.* **2011**, *22* (7), 1309–1319.

(221) Tröster, H. *Dye. Pigment.* **1983**, *4* (3), 171–177.

(222) Rusanov, A. L.; Keshtov, M. L.; Begretov, M. M.; Khotina, I. A.; Mikitaev, A. K. *Russ. Chem. Bull.* **1996**, *45* (5), 1169–1175.

(223) Keshtov, M. L.; Mal, E. I.; Marochkin, D. V; Muranov, A. V; Khokhlov, A. R. *Polym. Sci. Ser. B* **2012**, *54* (5–6), 289–296.

(224) Vives, G.; Rapenne, G. *Tetrahedron* **2008**, *64* (50), 11462–11468.

(225) Rathore, R.; Burns, C. L.; Deselnicu, M. I. *Org. Lett.* **2001**, *3* (18), 2887–2890.